Characterization of the Behaviour of Solution-Responsive Polymers by Fluorescence

by

Michael Andrew Theodore Fowler

A thesis

presented to the University of Waterloo

in fulfillment of the

thesis requirement for the degree of

Doctor of Philosophy

in

Chemistry

Waterloo, Ontario, Canada, 2014

This thesis consists of material all of which I authored or co-authored: see Statement of Contributions included in the thesis. This is a true copy of the thesis, including any required final revisions, as
accepted by my examiners.

I understand that my thesis may be made electronically available to the public.

Statement of Contributions:

Chapter 2: Effect of Sequence on the Ionization Behaviour of a Series of Amphiphilic Polypeptides

Contributor:	Contribution:
Fowler, M. A.	Manuscript writing, experimental design and execution, data analysis
Siddique, B.	Sample synthesis
Duhamel, J.	Manuscript editing, aided in experimental design and data analysis

Chapter 5: Studying Pyrene-Labelled Macromolecules with the Model Free Analysis

Contributor:	Contribution:
Fowler, M. A.	Manuscript writing, experimental design and execution, data analysis
Duhamel, J.	Manuscript editing, aided in experimental design and data analysis
Bahun, G. J.	Provided samples for analysis
Adronov, A.	Provided samples for analysis
Zaragoza-Galán, G.	Provided samples for analysis
Rivera, E.	Provided samples for analysis

Abstract

Two families of amphiphilic polymers were characterized with respect to their ability to respond to changing solution conditions using steady-state and time-resolved fluorescence. Firstly, a series of 5 sequential amphiphilic polypeptides consisting of hydrophilic and ionizable aspartic acid (Asp) and hydrophobic phenylalanine (Phe) in varying sequence $(Asp_xPhe_y)_n$ were studied. The effect of pH on the collapse and aggregation behaviour of the samples was investigated using light scattering which determined that the samples became insoluble when the fraction of ionized amino acids decreased below 0.2. Pyrene fluorescence measurments demonstrated that hydrophobic aggregate formation was the cause of this behaviour. The fluorescence and light scattering experiments yielded a detailed description of how pH affects the collapse and aggregation behaviour of amphiphilic polypeptides.

Secondly, a series of poly(N-isopropylacrylamide) chains in aqueous solution, varying in length and end-labelled with pyrene (Py$_2$-PNIPAM), were studied with respect to their temperature dependent solubility using turbidimetry, light scattering, and fluorescence. The cloud point temperature (T_c) of the Py$_2$-PNIPAM samples was found to increase with increasing chain length. Steady-state fluorescence spectra yielded the ratio of excimer intensity to that of monomer intensity, or $(I_E/I_M)^{SS}$, which reached a maximum at T_c. Time-resolved fluorescence decays were analyzed using Model-Free Analysis (MFA). The MFA yielded the average rate constant of excimer formation $<k>$, and the parameters f_{agg}, f_{diff} and f_{free}, which reflect the molar fractions of pyrenes that form excimer from pre-formed aggregates, form excimer by diffusion, and do not form excimer, respectively. Increasing the temperature above T_c caused a strong decrease in $<k>$ and f_{free}, and a sharp rise in f_{diff}, which is consistent with the formation of

mesoglobules. Increasing the temperature above the dehydration temperature of unlabelled PNIPAM ($T_m = 34\ ^oC$) caused the distribution of pyrene to stabilize.

The third study focused on aqueous mixtures of Py$_2$-PNIPAM and unlabelled PNIPAM, and their ability to mix when the temperature was raised above T_m. Using turbidimetry, separate transitions for Py$_2$-PNIPAM and unlabelled PNIPAM were identified. Steady-state fluorescence of the labelled chains demonstrated separate $(I_E/I_M)^{SS}$ transitions for the labelled and unlabelled chains as well. The MFA of the time-resolved fluorescence decays yielded no transition in $\langle k \rangle$ at T_m, while f_{agg}, f_{diff} and f_{free} showed transitions consistent with unlabelled PNIPAM entering the Py$_2$-PNIPAM mesoglobules. This led to the conclusion that the two polymers are able to mix at and above T_m, and that the mesoglobules are not frozen and vitreous.

Fourthly, a variety of pyrene-labelled polymers in organic solution were studied using steady-state and time-resolved fluorescence, where the results of Birks' Scheme and the Fluorescence Blob Model (FBM) were compared to the results of the MFA. The MFA was found to be able to faithfully reproduce the results of the other, more established, models. In addition, the MFA allowed the calculation of $(I_E/I_M)^{SPC}$, the ratio of excimer to monomer intensity as determined by time-resolved fluorescence, which scaled linearly with both $(I_E/I_M)^{SS}$ and $\langle k \rangle$. From this it was concluded that the MFA is able to fit the decays of pyrene-labelled polymers with any architecture studied thus far, but also provides an absolute measure of I_E/I_M which can be reproduced in any lab.

Acknowledgements

I would first like to thank my supervisor Jean Duhamel for his support and guidance throughout the process of creating this thesis, it has certainly been a learning experience. I would also like to thank my committee members: Mario Gauthier, Michael Palmer and Pu Chen.

I would like to thank all of my colleagues in both the Duhamel and Gauthier lab groups both current and former, for all of the help they've offered me over the years as well as all the memorable experiences while working with them.

I would like to thank my parents for always encouraging the pursuit of higher education.

Most importantly I would like to thank my wife Jess, for her love, her support, and especially her patience while I completed my graduate studies.

To my loving wife, Jess.

Table of Contents

List of Figures

List of Tables

List of Schemes

List of Abbreviations

$<k>$, $<k^{MF}>$	Average rate constant for excimer formation, model-free analysis
$<\tau_N>$	Number-average lifetime
$<\tau_N>_E$	Number-average lifetime of the pyrene monomer
$<\tau_N>_M$	Number-average lifetime of the pyrene excimer
$<\tau_w>$	Weight-average lifetime
$(Asp_xPhe_y)_n$	Sequential polypeptides composed of a repeating unit of x aspartic acid and y phenylalanine residues
$[Asp^-]$	Concentration of ionized aspartic acid residues
$[Asp]_{total}$	Total concentration of aspartic acid residues, regardless of ionization state
α	Degree of ionization of a polyelectrolyte
a_{E-}/a_{E+}	Ratio of negative to positive pre-exponential factors in the excimer decay
a_L	Pre-exponential factor for the long pyrene lifetime
An	Anthracene
a_W	Pre-exponential factor for the lifetime of pyrene in water
AP	Amphiphilic polymer
APE	Amphiphilic polyelectrolyte
Asp	Aspartic Acid
C&A	Collapse and aggregation
Cl^-	Chloride ion
CGT	Coil-to-globule transition
CoAm-PS-MPy	Polystyrene randomly labelled with pyrenemethyamine via an amide linkage
CoEs-PS-BuPy	Polystyrene randomly labelled with pyrenebutanol via an ester linkage
CoEt-PS-BuPy	Polystyrene randomly labelled with pyrenebutanol via an ether

	linkage
CoEt-PS-MPy	Polystyrene randomly labelled with pyrenemethanol via an ether linkage
DMF	N,N-Dimethylformamide
DMSO	Dimethylsulfoxide
ε	Molar extinction coefficient
ε_m	Massic extinction coefficient
$E0^*$	Pyrenes which form excimer from ground-state dimers
EL^*	Pyrenes which form long-lived excimer from ground-state dimers
EEC	End-to-end cyclization
f_{agg}	Molar fraction of aggregated pyrene
f_{diff}	Molar fraction of pyrene forming excimer by diffusion
f_{free}	Molar fraction of pyrene which is incapable of forming excimer
FBM	Fluorescence blob model
H_3O^+	Hydronium ion
HASE	Hydrophobically modified alkali swellable emulsion
I_1/I_3	Ratio of the first and third fluorescence peak intensity for the pyrene monomer
$(I_E/I_M)^{SPC}$	Ratio of excimer to monomer fluorescence intensity, determined by time-resoved fluorescence
$(I_E/I_M)^{SPC}_{ffree=0}$	Ratio of excimer to monomer fluorescence intensity, determined by time-resoved fluorescence, excluding the contribution of free pyrene
$(I_E/I_M)^{SS}$	Ratio of excimer to monomer fluorescence intensity, determined by steady-state fluorescence
IRF	Instrument response function
k_1	Rate constant for excimer formation, Birks' Scheme
k_{-1}	Rate constant for excimer dissociation, Birks' Scheme
k_{blob}	Rate constant for excimer formation within a blob

k_{cy}	Rate constant for end-to-end cyclization
k_r	Radiative rate constant for an excited fluorophore
k_{nr}	Non-radiative rate constant for an excited fluorophore
LCST	Lower critical solution temperature
lip$_2$-PNIPAM	Poly(N-isopropylacrylamide) end-labelled with octadecyl groups
λ_{max}	Maximum excimer fluorescence wavelength
λ_{Py}	Pyrene content of a polymer
LS	Light Scattering
Lys	Lysine
MFA	Model free analysis
M_n	Number-average molecular weight
MWD	Molecular weight distribution
N	Chain length, number of monomers
N_{blob}	Number of monomer units within a blob
NRET	Non-radiative energy transfer
PA	Polyaryl Fréchet-type dendron
PDI	Polydispersity index
PEO	Poly(ethylene oxide)
PEO-MPy$_2$	Poly(ethylene oxide) end-labelled with pyrenemethanol
Phe	Phenylalanine
Phen	Phenanthrene
$pK_a{}^{app}$	Apparent pK_a of ionizable groups on a polyelectrolyte
PLM	Pyrene-labelled macromolecule
PNIPAM	Poly(N-isopropylacrylamide)
PP	Polypropionic acid dendron
PS	Polystyrene
PS-BuPy$_2$	Polystyrene end-labelled with pyrenebutanol
Py-PNIPAM	Pyrene labelled poly(N-isopropylacrylamide)
Py^*_{diff}	Pyrenes which form excimer by diffusion

Py^*_{free}	Pyrenes which are incapable of forming excimer
SDS	Sodium dodecyl sulfate
SMA	Styrene-maleic anhydride copolymer
SPC	Single photon counting, a time-resolved fluorescence method
SS, SSF	Steady-state fluorescence
T_c	Cloud point temperature
T_m	Stable mesoglobule temperature
τ_E	Excimer lifetime
τ_{E0}	Excimer lifetime
τ_{EL}	Long-lived excimer lifetime
τ_{ES}	Short-lived lifetime in the excimer decay
τ_M	Monomer lifetime

Chapter 1:

Literature Review

The purpose of this chapter is to provide an overview of solution-responsive polymers and the fundamental principles behind the techniques used to characterize them. The first part of this chapter will focus on amphiphilic polymers in aqueous solution, as their solubility in water can be adjusted by changing the solution conditions. In particular, the properties of hydrophobically modified poly(N-isopropylacrylamide) (PNIPAM) and a polypeptide composed of well-defined sequences of x aspartic acids and y phenylalanines ($Asp_xPhe_y)_n$, two specific examples of solution responsive polymers, will be discussed. A description of the fundamentals of fluorescence will then be given, followed by a review of the various models used to analyze fluorescence data obtained from pyrene-labelled macromolecules. Finally, a summary of the project objectives for this thesis as well as a thesis outline will be provided.

1.1 Solution Responsive Polymers

1.1.1 Amphiphilic polymers

Amphiphilic polymers (APs) are macromolecules which contain at least two different types of chemical units, one of which is soluble in an organic solvent and the other in water. These units can be incorporated into the polymer by copolymerizing hydrophilic and hydrophobic monomers or by covalently attaching a limited number of hydrophobic groups to a hydrophilic polymer. In aqueous solution, the hydrophobic groups associate with one another to avoid contact with the solvent, while the hydrophilic polymer segments extend out into the solution, allowing the chain to remain solvated. The combination of soluble and insoluble segments on the same polymer chain causes APs to associate with one another in aqueous solution, since hydrophobic interactions occur between as well as within molecules. Intermolecular hydrophobic attraction leads to AP self-assembly, which can result in the formation of polymeric networks if the association follows an open mechanism. If the association occurs according to a closed

2

mechanism, polymeric aggregates with well-defined structures such as micelles, cylinders, vesicles, and lamellae can form instead.[1-12] The specific shape adopted by the macromolecular aggregates depends on the polymer composition, architecture, and concentration as well as the solvent being used. Schematic depictions of these structures are shown in Figure 1.1.
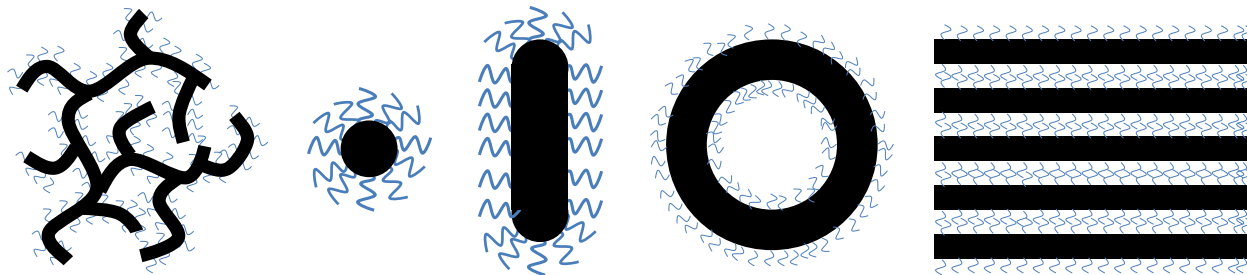
Figure 1.1: Self-assembled structures formed by amphiphilic polymers in aqueous solution. From left to right: Networks, micelles, rods, vesicles, and lamellae. Black domains denote aggregated hydrophobic chain segments, while blue domains denote hydrophilic segments.

Intermolecular hydrophobic associations in aqueous solution can also occur even if the number of hydrophobes attached to the hydrophilic chain is very low, resulting in smaller aggregates which can act as physical cross-links between AP chains. The aggregates thus formed are relatively easy to disrupt by applying shear to the AP solution. Consequently, APs have found applications as associative thickeners or colloidal stabilizers.[2] APs have also been used for advanced oil recovery,[12] as colloidal stabilizers,[8] and as encapsulating vectors to deliver therapeutic agents.[4,11] The broad range of applications for APs is a result of the wide variety of monomers from which they can be synthesized, but also the variety of synthetic methods that can be applied to control their architecture. Amphiphilic block copolymers are composed of discrete regions of hydrophilic or hydrophobic monomers, respectively, with the relative length of each block having a strong effect on the conformation adopted by the chains in solution and the shape

3

of the resulting polymeric aggregate.[8] In order to obtain a well-defined polymer molecular weight (M_n) and molecular weight distribution (MWD), amphiphilic block copolymers are commonly synthesized by anionic or controlled radical polymerization.[3,5,6,8,10,11] Amphiphilic random copolymers, also referred to as statistical copolymers, require much less careful control of both M_n and the MWD and therefore are often synthesized by radical copolymerization.[2,9,12] Amphiphilic alternating copolymers, with a regular repeating pattern of alternating monomers, may also be synthesized by radical copolymerization if one chooses monomers whose electron donor-acceptor character are opposite from one another, such as styrene and maleic anhydride.[13] Finally sequential polymers, which contain a repeating pattern of a carefully controlled monomer sequence, may be synthesized by condensation polymerization of a macromonomer with a well-defined sequence.[14] The arrangement of hydrophobic and hydrophilic subunits in the various architectures just discussed is shown in Figure 1.2.

The placement of different monomers along a polymer has a strong effect on its solution properties; a block copolymer is not expected to possess the same solution properties as a random copolymer. The technique used to synthesize the polymer will determine the amount of control one possesses over the exact monomer composition of the polymer, as well as the location of each monomer within the chain. Sequential polymers offer the highest level of control for both parameters, but unfortunately the synthesis of polymers with specific sequences is inherently difficult.[15] Consequently, experiments using sequential polymers are relatively rare even though theoretical predictions have indicated that the sequence of monomers within a polymer dictates the solution properties of APs,[15-17] and therefore sequential polymer synthesis should in principle allow one to achieve the desired properties in a rational manner. Due to the

wide variety of structures and applications found for APs, it is not surprising that APs have been the subject of several reviews.[1-12]

a)

b)

c)

d)
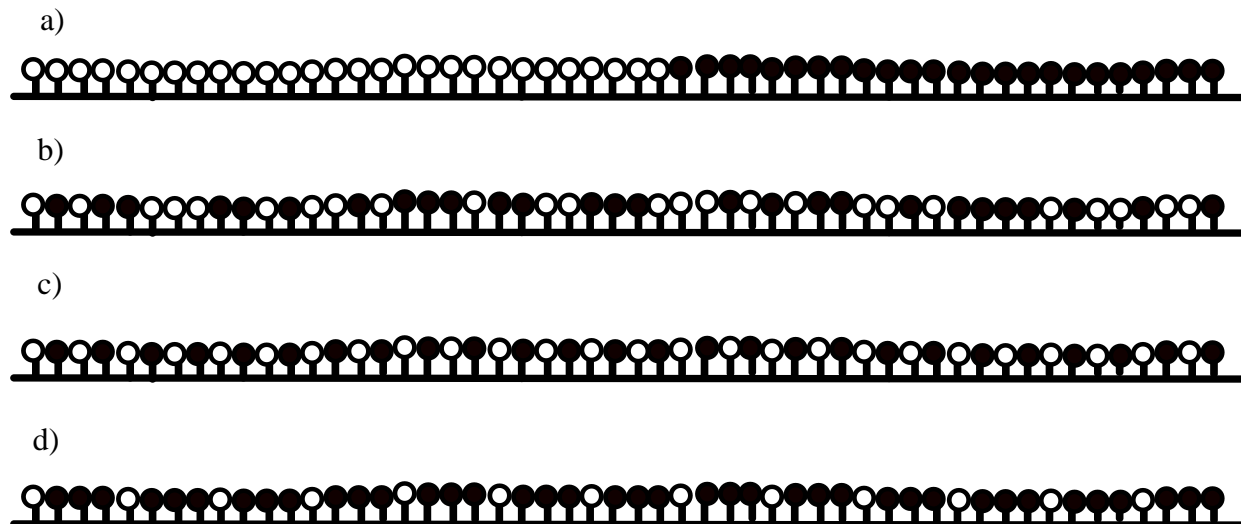
Figure 1.2: Representative monomer sequences for a) block copolymers, b) random copolymers, c) alternating copolymers, and d) sequential copolymers. ○ hydrophilic monomers. ● hydrophobic monomers.

1.1.2 Amphiphilic Polyelectrolytes

A specific class of APs referred to as amphiphilic polyelectrolytes (APEs) possess an ionizable functional group as their hydrophilic monomers. APEs whose ionizable groups remain ionized regardless of pH, such as polysulfonic acids, are referred to as strong polyelectrolytes.[18,19] If the ionizable group of an APE is a weak acid or base it is referred to as a weak polyelectrolyte, and its ionization level will vary with solution pH. The charges along the backbone of both weak and strong polyelectrolytes repel one another, and the strength of this repulsion increases as the distance between charges decreases, favouring an extended coil conformation. Attractive forces between the hydrophobic groups present on the chain favour a collapsed globule conformation. Thus, the distribution of an APE between an extended coil or collapsed globule conformation

depends on the balance between hydrophobicity and ionization,[20] a balance that depends on the solution pH for weak APEs. A representative diagram of this phenomenon is shown in Figure 1.3. The solution behaviour of a weak APE is further complicated by the fact that the ionization behaviour of polymeric acid functional groups can depart significantly from what is expected for small molecule organic acids. The apparent pK_a (pK_a^{app}) of a polyacid is affected by the interactions between the negative charges located on the ionized acid groups.[21-23] The negative charges already present along the backbone create an energy barrier to further ionization, as the creation of an additional negative charge will increase the local charge concentration and thus the strength of mutual electrostatic repulsion. This energy barrier can be overcome by increasing the chemical potential of the solution through the addition of a base.
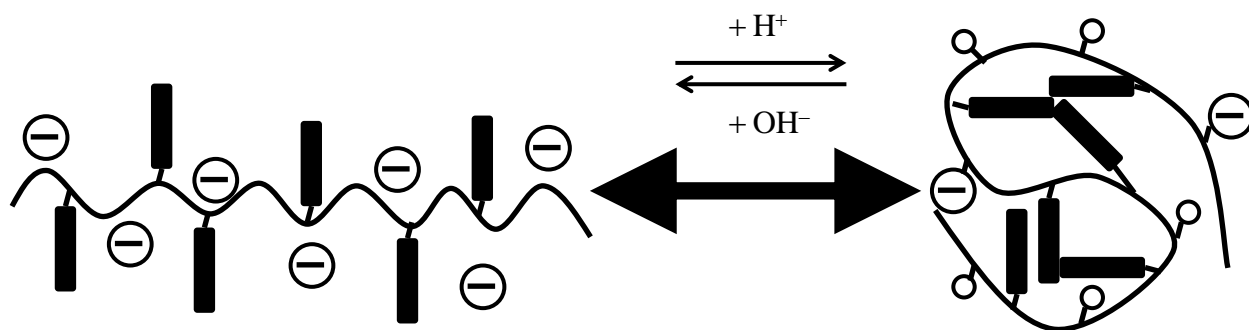
Figure 1.3: Effect of electrostatic interactions on polymer conformation. Left: Extended coil. Right: Collapsed globule.

1.1.3 Sequential Amphiphilic Polypeptides.

Sequential polypeptides composed of polymerized amino acids are of particular interest for the study of APEs as they are the synthetic counterpart to natural proteins, which are the prime example of sequential polymers with a well-defined monomer sequence and tightly controlled MWD. Among the twenty standard amino acids, there are multiple examples of both

hydrophobic and weak ionizable monomers, making them viable candidates for the synthesis of a wide variety of amphiphilic polyelectrolytes. Phenylalanine (Phe) is useful because it possesses an aromatic ring which not only makes it strongly hydrophobic but also absorbs in the UV region;[24] this makes the determination of the concentration of a Phe-containing polymer in solution relatively straightforward. Aspartic acid (Asp) is interesting because it is a weak acid, and its incorporation into a polypeptide yields a weak polyelectrolyte. In addition, polymeric Asp in the absence of electrostatic repulsive effects has been well characterized previously, with a pK_a being reported between 3.6 and 3.8 depending on whether the residue is surrounded by hydrophilic amino acid residues[25,26] or exposed to water.[27] If Asp is adjacent to a hydrophobic amino acid residue, its pK_a has been found to increase by up to six pH units.[25,28,29]

Since the ionization of Asp is affected by the proximity of both Phe and other Asp residues, sequential polymers containing these two residues allow the effect that one monomer has on the other to be determined. The second chapter of this thesis reports such a study. The sequential polypeptides examined contained Asp and Phe in varying proportions; the general nomenclature for the polymer is $(Asp_xPhe_y)_n$ with the subscripts x and y denoting the number of Asp and Phe residues, respectively, in the repeating unit of the polymer. The sample containing a sequence of one Asp residue followed by three Phe residues is thus referred to as $(Asp_1Phe_3)_n$, the structure of which is shown in Figure 1.4 for basic solutions, where Asp is expected to be ionized. The variation in the pK_a of the Asp residues and its dependence on the nature of the neighbouring amino acids can be investigated using the $(Asp_xPhe_y)_n$ samples, since their well-defined sequences mean that the exact locations of Asp and Phe are known. This is of particular interest since, in addition to its hydrophobic character, Phe also separates the Asp residues from one another. A charge on a polyelectrolyte is only able to affect residues up to half a Debye

length away,[30] equivalent to approximately one and a half nanometers or four residues for polypeptides in a 10 mM aqueous solution of sodium chloride. As a result, the presence of Phe residues along the polypeptide chain reduces the effect of the degree of ionization (α) on pK_a^{app} by increasing the distance between Asp residues.
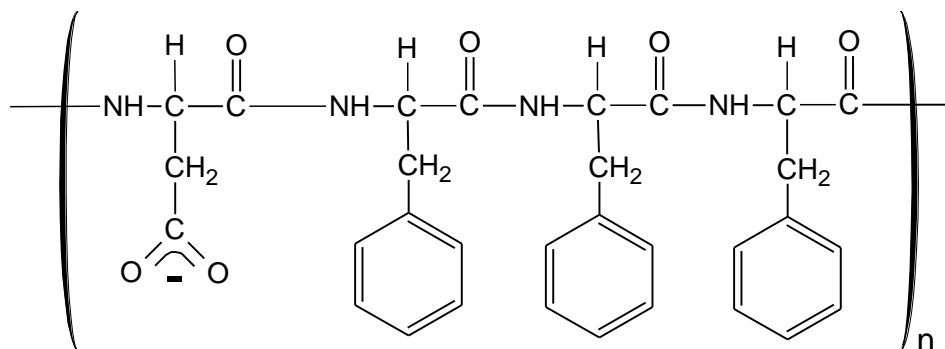
Figure 1.4: Structure of the $(Asp_1Phe_3)_n$ repeating unit.

1.1.4 Thermo-responsive Polymers

In addition to pH and ionic strength, the solubility of a polymer is also affected by temperature, making temperature another parameter one can use to elicit a change in solution behaviour. One example of this type of solution response is the temperature-dependence of the solubility of aqueous poly(*N*-isopropylacrylamide) (PNIPAM), which was first reported in the late 1960s.[31] It was observed that PNIPAM remained water-soluble at low temperature, but became insoluble as the temperature was increased above a cloud point temperature (T_c). This change in solubility occurs because the PNIPAM chains undergo a coil-to-globule transition (CGT) at T_c as the PNIPAM chains dehydrate.[32,33] The CGT occurs over a narrow temperature range due to the fact that hydration and dehydration of PNIPAM is cooperative,[34,35] a property which also causes PNIPAM chains to adopt a pearl necklace conformation when solvated.[36] The solution behaviour

8

of PNIPAM has been characterized by a variety of techniques including viscometry,[37-39] turbidimetry,[38,40-43] light scattering,[39,43,44] fluorescence,[41,44-48] and small angle neutron scattering.[34,36,49] These studies have confirmed that at T_c the PNIPAM chains dehydrate and undergo a CGT, before aggregating into mesoglobules.[32,33,50,51] For a given PNIPAM solution the value of T_c is dependent on M_n, the nature of any additional functional groups present on the chain, and the polymer concentration if it is less than 1 g/L.[43] Since the discovery of the thermo-responsive solubility of PNIPAM, extensive studies have been carried out on the interaction of PNIPAM with various hydrophobic groups and molecules, such as small molecule surfactants,[38,52] hydrophobically modified non-PNIPAM polymers,[37,41] or hydrophobes covalently attached onto the PNIPAM chain itself.[34,36,40,42,44,45,47,49] These studies have shown that hydrophobic aggregates disrupt the thermally induced aggregation of PNIPAM and affect T_c, while the CGT of PNIPAM at T_c has also been shown to disrupt hydrophobic aggregates.[37]

The effect of M_n on the value of T_c for telechelic (doubly end-labelled) PNIPAM is particularly strong, where T_c increases with increasing M_n for hydrophobic end-groups,[42] while hydrophilic end groups cause the opposite trend. Since telechelic polymers always contain two functional end-groups, increasing the chain length between the two end-groups causes a decrease in the local concentration of functional groups which dampens their effect on T_c. The cooperative nature of PNIPAM dehydration causes the dehydration of the monomers adjacent to any hydrophobe covalently attached to the polymer, which usually affects their solution behaviour. Additionally these hydrophobic end groups cause intermolecular interactions in water, even at polymer concentrations in the μM range,[45] which leads to micelle formation.

The structure of a hydrophobically modified PNIPAM sample, whose study was the subject of two chapters in this thesis, is shown in Figure 1.5. Studies of PNIPAM end-capped

9

with lipophilic octadecyl groups (lip$_2$-PNIPAM) by Winnik et al. have led to the development of a model predicting the conformational changes undergone by lip$_2$-PNIPAM as it responds to changes in solution temperature.[34,36,44,49] According to this model, there are three distinct temperature regimes that determine the conformation of lip$_2$-PNIPAM chains. Regime I describes the polymer solution at temperatures below T_c, where the hydrophobic end-groups of lip$_2$-PNIPAM self-assemble to form polymeric rosette micelles. Regime II corresponds to the temperature range above T_c but below T_m, where T_m is the temperature where PNIPAM undergoes its CGT, which is found to occur at 34 $^{\circ}$C.[44] In Regime II the micelles aggregate into mesoglobules, whose size increases and water content decreases as the temperature increases. Above T_m is Regime III, where the mesoglobules are stable and do not experience any changes in size or composition. A more detailed discussion of the exact changes which take place in each Regime will be provided in Chapter 3.
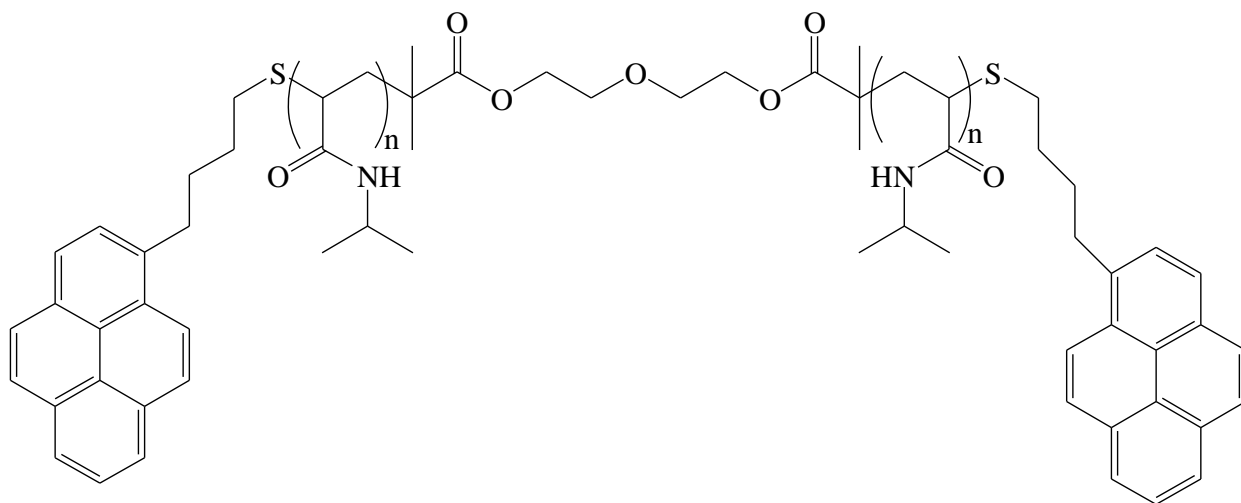
Figure 1.5: Structure of telechelic hydrophobically modified PNIPAM, with pyrene as the hydrophobic group.

Regardless of the nature of the phenomena which causes a change in solution behaviour, fluorescence is typically a useful tool to characterize solution-responsive polymers and will be discussed hereafter.

1.2 Using Pyrene Fluorescence to Study Solution-responsive Polymers

1.2.1 Fluorescence

When a fluorescent molecule, or fluorophore, absorbs a photon of light, it becomes electronically excited in a process which occurs on a femtosecond time scale. The electronic and vibrational energy level of the resulting excited state will vary depending on the wavelength of light absorbed; however, the fluorophore will relax to the lowest vibrational level of the singlet excited state S_1 via a process called Internal Conversion which occurs on a picosecond time scale. The molecule may then return to the ground-state via the fluorescence radiative process, which is accompanied by the emission of a photon. The rate of fluorescence emission varies depending on the fluorophore; however fluorescence typically occurs on a nanosecond timescale. Since there are multiple vibrational levels of the electronic ground-state to return to, there are multiple fluorescence peaks in the emission spectrum. However the fluorescence spectrum does not depend on the wavelength of the light absorbed, as the Internal Conversion process ensures that fluorescence always occurs from the lowest vibrational level of the S_1 excited state. When in the excited state, it is also possible for a fluorophore to return to the ground state via a nonradiative process. Finally, the fluorophore may also undergo intersystem crossing and enter an excited triplet state, which can eventually return to the ground-state via a radiative phosphorescence process. The relationships between these transitions and the energy levels involved are best described by a Jablonski diagram[53] shown in Figure 1.6.

11
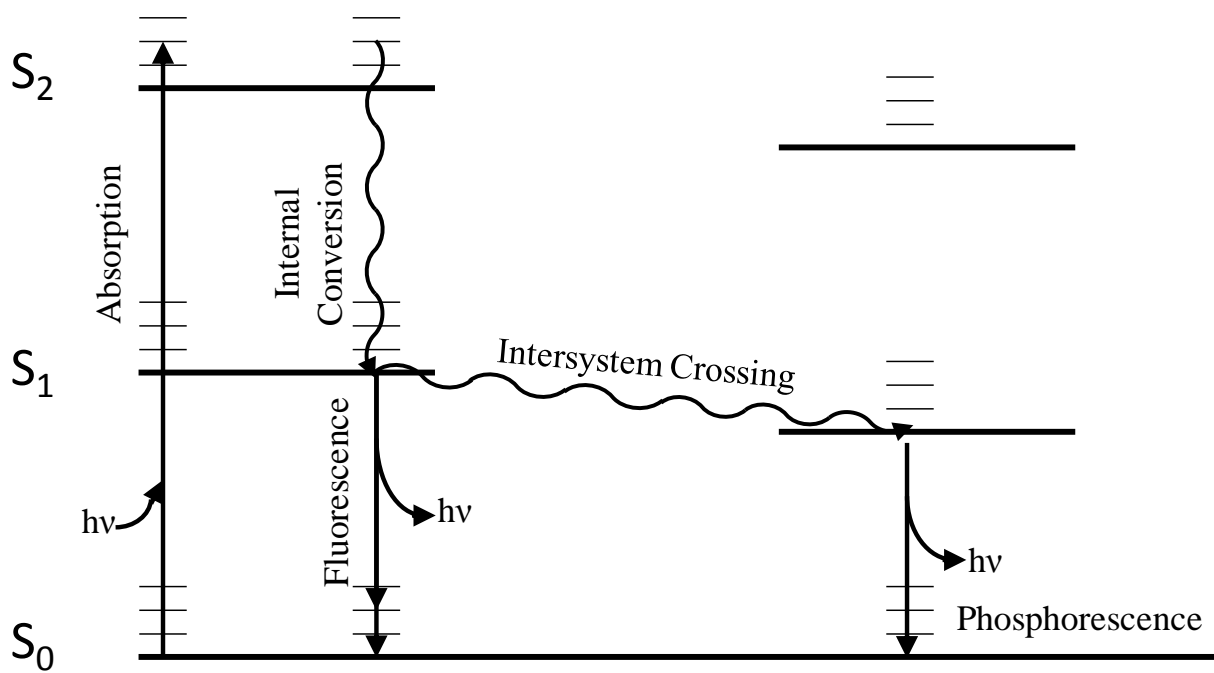
Figure 1.6: Jablonksi diagram of the absorbance, fluorescence, and phosphorescence emission processes, and the relative energy levels involved. Electronic and vibrational energy levels are denoted by thick and thin horizontal lines, respectively.

The time scale over which fluorescence emission occurs depends on the lifetime (τ) of the fluorophore, which itself is a function of the radiative and nonradiative rate constants as shown in Equation 1.1.

$$\tau = \frac{1}{k_r + k_{nr}} \tag{1.1}$$

In Equation 1.1, k_r refers to the radiative rate constant that describes the relaxation of the excited fluorophore to the ground-state via the emission of a photon and is intrinsic to the fluorophore. k_{nr} represents the sum of all the rate constants associated with processes that return the excited

chromophore to the ground-state in a radiationless manner. These radiationless relaxation processes result from interactions of the excited chromophore with the solvent or from collisional quenching. Collisional quenching occurs when a diffusional encounter between an excited fluorophore and another molecule results in the fluorophore returning to the ground-state via a nonradiative process. Any photophysical process which decreases the fluorescence intensity is referred to as fluorescence quenching. Fluorescence quenching may be observed in steady-state measurements as a decrease in intensity. In time-resolved measurements, quenching causes a decrease in τ since it is associated with an increase in k_{nr} (see Eq. 1.1). Since a fluorophore only remains in the excited state for a limited amount of time, collisional quenching yields useful experimental information only when quenching occurs on a time scale that is similar to the lifetime of the fluorophore. One type of collisional quenching which has received a great deal of scientific attention is the self-quenching of pyrene, as pyrene possesses a number of properties which make it particularly well-suited to the study of polymers in solution.

1.2.2 Pyrene Fluorescence

Fluorescent labels such as pyrene are used to characterize the solution behaviour of polymers as they report on the internal dynamics of macromolecules. Pyrene is an extremely effective fluorescent molecule when used for the characterization of polymers as it possesses a high quantum yield (0.32 in cyclohexane),[54] a high molar extinction coefficient, a long lifetime, and the ability to form an excited dimer or excimer for short. Pyrene absorbs UV light with a maximum of absorption around 340 nm. The fluorescence spectrum of the pyrene monomer has distinct peaks from 370 to 400 nm, while the pyrene excimer has a broad, featureless fluorescence spectrum centred at 480 nm. The ratio of the steady-state fluorescence intensity of

the excimer to that of the monomer, or $(I_E/I_M)^{SS}$, describes the efficiency of a pyrene labelled macromolecule at forming excimer, which is proportional to the likelihood of having a pyrene-pyrene encounter. Consequently, the amount of excimer formed, and by extension the $(I_E/I_M)^{SS}$ ratio, increases with both the concentration of pyrene[55] and the rate of pyrene excimer formation. The relationship between $(I_E/I_M)^{SS}$ and polymer solution behaviour will be further discussed in a later section.

The steady-state fluorescence spectrum of pyrene also yields information on the polarity of the local environment experienced by pyrene by determining the fluorescence intensity ratio of the first and third peaks of the monomer fluorescence spectrum, that is, the I_1/I_3 ratio. This ratio is low in apolar environments and high in polar environments.[56,57] As an example, the I_1/I_3 ratio is equal to 1.14 for pyrene in SDS micelles,[56] between 1.0 and 1.2 for pyrene in the hydrophobic microdomains of styrene-maleic anhydride copolymers,[58] and 1.80 for pyrene in water.[57] The relationship between solvent polarity and I_1/I_3 holds true for pyrene (used in Chapter 2) and any derivatives bearing a reactive linker where the four fused benzene rings of the pyrenyl group are separated from a heteroatom in the linker by a single methylene group. However replacing the methylene group with a butyl group causes the pyrene to lose its sensitivity to solvent polarity.[59] An example of the steady-state fluorescence spectrum of pyrene is shown in Figure 1.7.

While a great deal of information about the solution behaviour of pyrene-labelled polymers may be gained by measuring the relative fluorescence intensities of the pyrene monomer and excimer, steady-state fluorescence cannot distinguish between excimers formed by diffusional encounters between an excited and a ground-state pyrene, or by direct excitation of pre-associated ground-state pyrenes. Neither can it distinguish between monomers which can

participate in diffusional excimer formation from those which cannot, as they possess the same fluorescence emission spectrum. These species do, however, possess different fluorescence lifetimes (τ) and they may therefore be differentiated using time-resolved fluorescence.
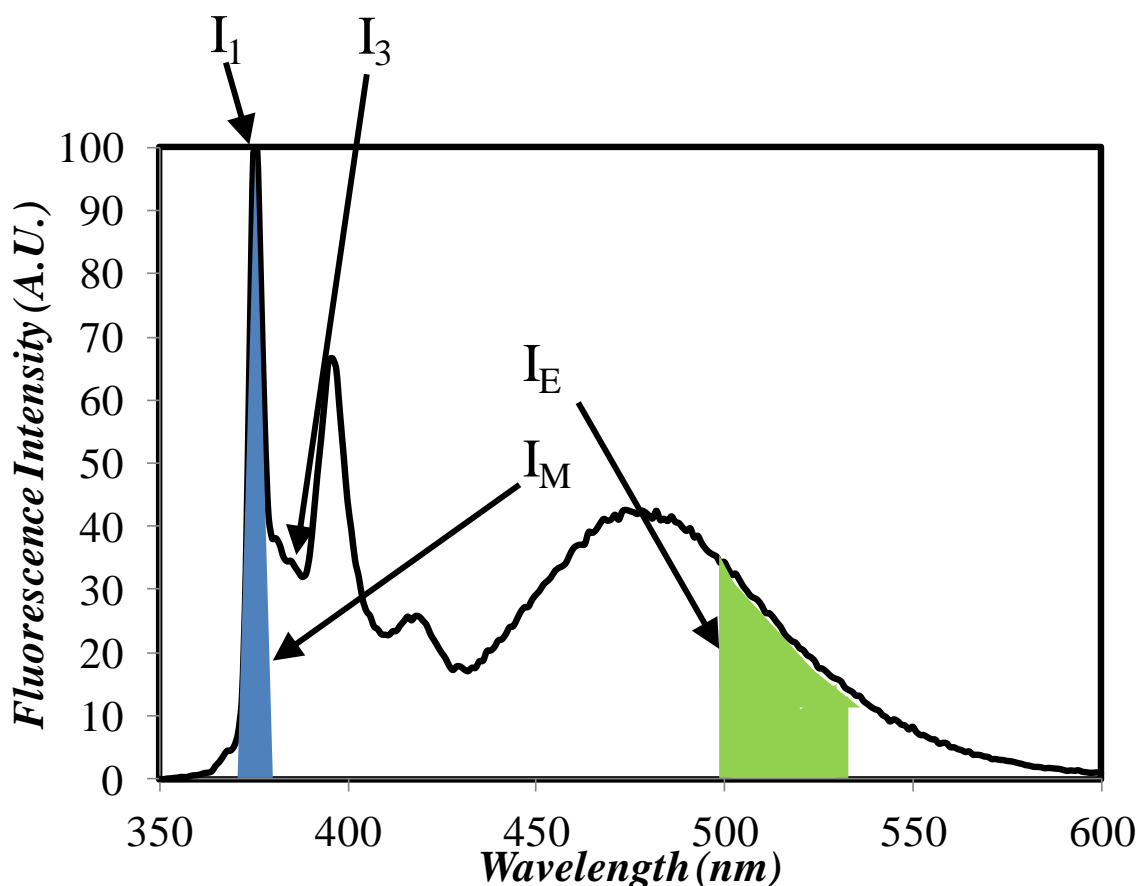
Figure 1.7: Steady-state fluorescence spectrum of pyrene for a 14 kg/mol end-labelled PNIPAM sample in water with a concentration of 0.02 g/L. $\lambda_{ex} = 342$ nm.

If molecular pyrene in solution is excited with a short pulse of light, its fluorescence will decay over time in a manner which is described by the Birks scheme, shown in Scheme 1.1.[55] In this scheme, a pyrene molecule absorbs a photon of light ($h\nu$) and becomes excited. This excited pyrene may then return to the ground-state with a rate constant equal to $1/\tau_M$, where τ_M is its

natural lifetime. Alternatively, pyrene may diffusionally encounter a ground-state pyrene with a rate constant k_1 and form an excited dimer, also called an excimer. The excimer may then return to the ground-state with a rate constant equal to the inverse of its lifetime $1/\tau_E$, or it may dissociate with a rate constant k_{-1}. The rate constant k_1 describes the rate of collisional quenching of the monomer via excimer formation. What is unusual in this quenching event is that it results in the creation of a distinct fluorescent species, namely an excimer.
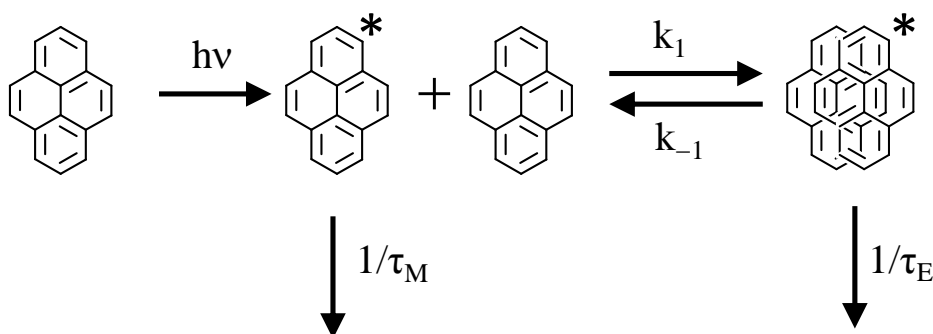
Scheme 1.1: Birks' Scheme for pyrene excimer formation.

The Birks Scheme allows a distinction to be made between pyrene monomers which will never form excimer and emit as if they were free in solution (Py_{free}) and pyrene monomers capable of forming excimer by diffusion (Py_{diff}), as these two pyrene species share the same fluorescence spectrum but have different lifetimes. This ability to gain detailed information about the behaviour of pyrene through the analysis of their time-resolved fluorescence decays has led to the use of pyrene to study the behaviour of hydrophobically modified polymers,[59-63] including pyrene-labelled PNIPAM in organic solvents and water,[45,46] and to target the hydrophobic pockets of PNIPAM in water.[41,44] It has not always been possible to obtain this level of detailed information on polymers using pyrene fluorescence, as the use of a model is

typically required to interpret time-resolved fluorescence decays. The Birks Scheme is one such model; however, it may only be applied to a specific class of pyrene-labelled polymers. One species which is not considered in the standard Birks' scheme is excimer generated through the direct excitation of pyrene dimers, which is found in aggregates of ground-state pyrenes (Py_{agg}). This situation is most often encountered with solutions of pyrene-labelled polymers where the polymer backbone is well solvated but the pyrene label is not. Over the years, numerous models have been developed which enable one to gain quantitative information on the solution behaviour of pyrene-labelled polymers. These models are described hereafter.

1.2.3 Modeling of Pyrene Excimer formation

Efforts to obtain information about the behaviour of polymers in solution by using pyrene fluorescence were initiated close to four decades ago. These studies began in 1976, when Zachariasse and Kuhnle used steady-state pyrene fluorescence to determine the conformation of pyrene end-labelled alkyl chains.[64] Shortly thereafter Perico and Cuniberti extended this method to probe the rate of end-to-end cyclization (EEC) for a series of pyrene end-labelled poly(ethylene oxide)s (PEO). They were the first to demonstrate that $(I_E/I_M)^{SS}$ decreased with increasing chain length N.[65] The study of polymers using pyrene fluorescence was extended beyond the analysis of steady-state fluorescence spectra in 1980, when Winnik et al. acquired the time-resolved fluorescence decays of a series of pyrene end-labelled polystyrenes (PS) and fitted them with the Birks Scheme[66] introduced in Scheme 1.1. This study represented the first example in the literature where the rate constant of EEC (k_{cy}) was determined quantitatively through the use of pyrene excimer formation. Two major conclusions were reached in this study. The first was that the ratio $(I_E/I_M)^{SS}$ was directly proportional to k_{cy}, and the second was that k_{cy}

scaled as $N^{-1.6}$ where N is the PS chain length. The effect of chain length on k_{cy} has been confirmed by numerous studies that used steady-state or time-resolved fluorescence to probe k_{cy} for pyrene end-labelled monodispersed linear chains[65-72] or alkyl chains.[64,73] Equations 1.2 and 1.3 were used to fit the pyrene monomer and excimer decays, respectively, according to the Birks Scheme. The parameters X, Y, τ_1^{-1}, and τ_2^{-1} are all calculated using k_{cy}, and k_{-cy}, the rate constants for excimer formation and dissociation, respectively, as well as τ_M and τ_E which are the monomer and excimer decay times, respectively.

$$\left[Py^* \right] = \frac{\left[Py^*_{diff} \right]_0}{\sqrt{(X-Y)^2 + 4k_{cy}k_{-cy}}}\left(\left(X - \tau_2^{-1}\right) \times \exp\left(-t/\tau_1\right) - \left(X - \tau_1^{-1}\right) \times \exp\left(-t/\tau_2\right)\right)$$
$$+ \left[Py^*_{free} \right]_0 \times \exp\left(-t/\tau_M\right) \tag{1.2}$$

$$\left[E^* \right] = \frac{k_{cy}\left[Py^*_{diff} \right]_0}{\sqrt{(X-Y)^2 + 4k_{cy}k_{-cy}}}\left(-\exp\left(-t/\tau_1\right) + \exp\left(-t/\tau_2\right)\right) \tag{1.3}$$

While the Birks Scheme has been widely applied to describe pyrene excimer formation in solutions of monodispersed polymers end-labelled with pyrene, it does suffer from a number of limitations. Notably, since Birks' Scheme uses a single rate constant k_{cy} (equivalent to k_1 in Scheme 1.1) which depends strongly on chain length,[67] macromolecules labelled with only two pyrenes separated by a single chain length must be used since only these macromolecules will yield a single rate constant for excimer formation. Macromolecules labelled with more than two pyrenes will generate a distribution of chain lengths between pyrene pairs and thus, due to the dependence of k_{cy} on chain length, would give rise to a distribution of rate constants. In order to obtain accurate fits, k_{cy} must be large enough to allow differentiation between the corresponding

18

decay time $(k_{cy} + 1/\tau_M)^{-1}$ of pyrenes attached to doubly-labelled chains, which are able to form excimer, and that of any singly labelled chains, which cannot form excimer and emit with the natural lifetime τ_M.

The fluorescence spectra of relatively flexible PEO chains have been successfully interpreted by applying the Birks Scheme for chains with up to 1350 chemical bonds along the backbone,[65] while the study of stiffer polystyrene (PS) chains have been limited to chains no longer than 530 chemical bonds.[66] These chain lengths correspond to polymer molecular weights of 20 and 27 kg/mol, respectively, and are significantly shorter than the chains typically used in industrial applications. Furthermore, since the labels are located at the chain-ends, these studies provide no information about the behaviour of the bulk of the chain.

In order to expand the study of macromolecules beyond short, end-labelled, and monodispersed linear chains, new approaches needed to be introduced. One of them aimed to characterize macromolecules randomly labelled chains with very low amounts of pyrene.[74,75] The purpose of this approach was to reduce the breadth of the distribution of rate constants to the point where the pyrene content was sufficiently low and the average distance between pyrenes was so large that the resulting decays could be fitted with the two exponentials used in the Birks Scheme. Surprisingly, the results of these fits yielded values for k_{-1} which were far larger than what is typically reported for end-labelled polymers, which was unexpected since the dissociation rate constant for a pyrene excimer should be a property intrinsic to the excited species and should not depend on how the pyrene is attached to a polymer. Atypically high values for k_{-1} have since been shown to reflect circumstances where too little excimer is being formed, resulting in the breakdown of the Birks Scheme.[71] Other attempts to fit the fluorescence decays of pyrene-labelled macromolecules that were not monodispersed end-labelled chains with

the Birks Scheme led to unsatisfactory results,[76,77] as more than the 2 exponentials required by the Birks Scheme[55,67] were needed.

1.2.4 The Dimer-Monomer-Dimer (DMD) Model

The lack of a model capable of fitting the complex fluorescence decays obtained from polymers with architectures more complex than pyrene end-labelled polymers led to the conclusion that only qualitative information could be obtained from these decays, as simply fitting the decays with a sum of exponentials is subject to significant uncertainties.[53,78]   This conclusion was challenged when the DMD model was introduced, which was the first model to account for more than one rate constant for excimer formation, developed to fit the decays of a highly constrained di-1,3-(1-pyrenyl)propane.[79]   The fundamental premise of this model is that the pyrene groups are capable of forming two different excimer species by diffusion, each species having its own lifetime and its own rate constants for formation and dissociation. A matrix-based method was used to solve the differential equations which resulted from the DMD model. Thus there was no explicit mathematical expression describing the decay of the monomer and excimer over time. The monomer and excimer decays could however be fitted with a sum of three exponentials, using the same decay times for the monomer and excimer fits but different pre-exponential factors, therefore a total of nine parameters were optimized. The DMD model was found to be quite successful if there were two distinct rate constants for excimer formation.[79-82] When it was applied to samples requiring more than two rate constants for excimer formation, problems such as the generation of physically impossible pre-exponential factors were found to occur.[74]   Other models capable of handling the decays of samples with a distribution of rate constants were therefore needed.

1.2.5 The Fluorescence Blob Model (FBM)

In 1999, the Fluorescence Blob Model (FBM) was proposed as a method capable of retrieving quantitative information from the complex fluorescence decays obtained from linear polymers randomly labelled with pyrene.[83] This model relies on the fundamental assumption that a pyrene label can only probe a finite volume referred to as a blob during a fluorescence experiment. Since an excited pyrene only remains in the excited state for a limited time, there is a limit to the distance it can travel before returning to the ground state. The process of pyrene excimer formation which would occur inside a fixed spherical volume had been considered previously by Tachyia for micellar systems,[84] and mathematical treatment was used to derive the equations which describe the process of excimer formation within randomly labelled polymers.[83] The only difference between a micelle and a blob is that a pyrene label is able to pass across the boundaries of blobs clustered within the volume defined by the polymer coil, but not through those of micelles which are well separated in aqueous solution. Therefore the FBM required an additional term to describe the rate at which the exchange of ground-state pyrenes from one blob to the next would occur, resulting in typically seven parameters to be optimized under constrained conditions. Once the FBM was confirmed as being able to fit the fluorescence decays of randomly labelled polymers,[83] it was then applied to aqueous solutions of hydrophobically modified alkali swellable emulsion (HASE) polymers.[85]

The equations used in the FBM directly describe the time dependence of the concentration of excited pyrenes. Consequently, they can be integrated to yield the fluorescence intensities of the monomer and excimer and used to calculate the quantity $(I_E/I_M)^{SPC}$, which is the ratio of the intensity of the excimer relative to that of the monomer as determined by the analysis of time-resolved fluorescence decays acquired with the single photon counting (SPC)

21

technique.[86] Calculation of $(I_E/I_M)^{SPC}$ provides further validation of the results obtained from the analysis of the fluorescence decays according to the FBM, as it should reproduce the trends obtained with $(I_E/I_M)^{SS}$. The contribution of each pyrene species to the decay is obtained using the FBM, which makes it possible to calculate the value of $(I_E/I_M)^{SPC}$ without the contribution from those pyrenes that cannot form excimer. This feature of the $(I_E/I_M)^{SPC}$ ratio represents a useful tool for determining the sensitivity of the fluorescence emitted by a solution of pyrene-labelled polymers to the presence of free pyrene.

While the FBM can handle significantly more complex decays than the Birks Scheme, it does also have limitations. One assumption made when deriving the FBM equations is that the pyrenes are randomly distributed among the blobs according to a Poisson distribution. As a result, the FBM is not able to accurately fit polymer samples which are not truly randomly labelled. Non-random labelling may be intentional, as is the case with dendrons that are end-labelled with pyrene, or unintentional such as when unforeseen clustering of pyrene occurs along the backbone during the labelling process. In addition, solution conditions can also cause a non-random distribution of the pyrene labels such as when excessive aggregation of the pyrene labels is induced. Consequently, it was deemed necessary to introduce a more broadly applicable model capable of fitting the fluorescence decays acquired with any type of pyrene-labelled macromolecule.

1.2.6 The Model-free Analysis

The Model-free Analysis (MFA) was first introduced in 2005, where it was applied to the analysis of fluorescence decays acquired from aqueous solutions of pyrene-labelled HASE and sodium dodecyl sulfate (SDS) and found to reproduce the results of the FBM analysis with regard to the fractions of pyrene species present in solution and the average rate constant of

excimer formation.[87] The fundamental assumption of the MFA is that the process of excimer formation by diffusion can be fitted by a sum of exponentials, typically 2 or 3, regardless of the nature of the physical processes which leads to excimer formation. Once a pyrene monomer absorbs a photon of light and becomes excited, it may either emit as a monomer with a lifetime τ_M or diffusionally encounter a ground-state pyrene at a rate that can be approximated by a sum of exponentials denoted as *f(t)*. The excimer may also be formed via the direct excitation of pyrenes which are associated in the ground-state and form excimer virtually instantaneously. Regardless of how the excimer is formed, it then emits with a lifetime τ_E. The process of excimer dissociation, whereby an excimer breaks apart to form an excited monomer and a ground-state monomer, occurs so slowly at room temperature relative to the rate of excimer fluorescence as to be insignificant and is therefore not considered in the analysis. The process of pyrene excimer formation according to the MFA is shown in Scheme 1.2.
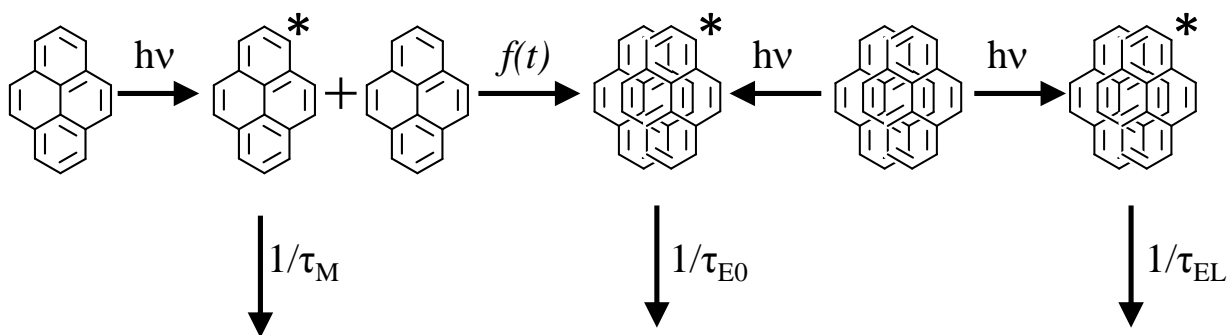
Scheme 1.2: Pyrene excimer formation according to the Model Free Analysis.

The fitting of the fluorescence decays with the MFA equations has been described in a number of papers.[87-90] The MFA assumes the presence of four pyrene species in solution, the first of which is Py^*_{diff}, which refers to pyrenes that form excimer by diffusion. The second is

Py^*_{free}, which refers to pyrenes that are incapable of forming excimer. The third and fourth

species are $E0^*$ and EL^*, which refer to well- and poorly stacked excimers generated by the

direct excitation of pyrenes which were associated in the ground-state. Equation 1.4 describes

the time dependent profile of the monomer, and is used to fit the time-resolved fluorescence

decays of the monomer. Equation 1.5 does the same for the excimer. The terms τ_M, τ_{E0}, and τ_{EL}

refer to the lifetimes of the free monomer, excimer, and long lived excimer species, respectively.

$$[Py^*]_{(t)} = [Py^*_{diff}]_{(t=0)} \sum_{i=1}^{n} a_i e^{-t/\tau_i} + [Py^*_{free}]_{(t=0)} e^{-t/\tau_M} \tag{1.4}$$

$$[E0^*]_{(t)} = -[Py^*_{diff}]_{(t=0)} \sum_{i=1}^{n} a_i \frac{\dfrac{1}{\tau_i} - \dfrac{1}{\tau_M}}{\dfrac{1}{\tau_i} - \dfrac{1}{\tau_{E0}}} e^{-t/\tau_i} +$$

$$\left([E0^*]_{(t=0)} + [Py^*_{diff}]_{(t=0)} \sum_{i=1}^{n} a_i \frac{\dfrac{1}{\tau_i} - \dfrac{1}{\tau_M}}{\dfrac{1}{\tau_i} - \dfrac{1}{\tau_{E0}}} \right) e^{-t/\tau_{E0}} + [EL^*]_{(t=0)} e^{-t/\tau_L} \tag{1.5}$$

While there are thirteen parameters in Equations 1.4 and 1.5 which must be optimized,

there are a number of constraints which limit the degrees of freedom in the optimization. The

lifetime τ_M is fixed in the analysis by using a value obtained from a model compound, and other

lifetimes such as τ_{E0} or τ_{EL} may also be fixed if suitable values may be obtained by independent

experiments. The lifetimes τ_i and pre-exponential factors a_i are the same in the monomer and

excimer decay, significantly reducing the number of parameters that need to be optimized.

Finally, the MFA parameters are optimized with constraints imposed by the kinetic parameters

which describe excimer formation. Consequently, values obtained from the MFA are physically

plausible.[61,91] An example of this type of restriction is that the exponential corresponding to the lifetime τ_M must possess a positive pre-exponential factor, as a negative value would mean that a fluorescence decay process is causing an increase in the amount of excited pyrene present in solution that does not form excimer, which is impossible. The lack of any assumption about the physical nature of $f(t)$ has led to the proposal that the MFA is able to handle any architecture of macromolecules which have been labelled with pyrene.[91]

The parameters obtained by the MFA can be used to calculate the fractional contributions of the various pyrene species to the decays.[92] When combined with their respective absorbance coefficients and radiative rate constants, these fractions can be used to calculate the molar fractions of pyrene species in solution. This highlights one important advantage of the MFA. It identifies the main features of the monomer and excimer time-resolved fluorescence decays and summarizes them with a small set of parameters, namely, the average rate constant of excimer formation $<k>$, the excimer lifetime τ_{E0}, and the fluorescence fractions f_{free}, f_{diff}, and f_{agg}. These parameters, along with Eqs. 1.6 and 1.7, can be used to calculate $(I_E/I_M)^{SPC}$, including $\left(I_E/I_M\right)^{SPC}_{ffree=0}$ with f_{free} set to equal zero, which was impossible when no such equations existed to fit complex fluorescence decays. The ability of the MFA to be applied to any polymer architecture and distill the fluorescence data into a few key parameters has led to its use in the study of a wide variety of pyrene-labelled constructs including dendrimers,[88,89] HASE,[87] surfactants,[90] aqueous aggregates of mono-labelled PEO,[93] and constructs composed of pyrene-labelled dendrimers covalently linked to a porphyrin.[92] The one major drawback of the MFA is that the kinetic parameter $<k>$ is an average of the rate constants of excimer formation.   This means that some detail is lost when compared to other models such as DMD, Birks' Scheme, and FBM in terms of providing a closer description of the kinetics of excimer formation. This is an

unfortunate but unavoidable consequence of the fact that the MFA makes no assumptions about the process of excimer formation. As a result, one cannot ascribe an individual component of *f(t)* to any particular excimer forming process, and only the average meaningfully reflects the kinetics of excimer formation.

$$\left(\frac{I_E}{I_M}\right)^{SPC} = \frac{f_{diff} \times \tau_{E0} \times <\tau> \times <k> + f_{E0} \times \tau_{E0} + f_{EL} \times \tau_{EL}}{f_{diff} \times <\tau> + f_{free} \times \tau_M} \tag{1.6}$$

$$\left(\frac{I_E}{I_M}\right)^{SPC}_{f_{free}=0} = \frac{f_{diff} \times \tau_{E0} \times <\tau> \times <k> + f_{E0} \times \tau_{E0} + f_{EL} \times \tau_{EL}}{f_{diff} \times <\tau>} \tag{1.7}$$

1.2.7 Summary

Pyrene fluorescence is an extremely useful tool for the characterization of polymers in solution since excimer formation is necessarily related to the movement of the polymer chains to which pyrene is attached. The process of pyrene excimer formation can be characterized by obtaining a rate constant through the application of a specific model to the analysis of fluorescence decays of end-labelled short alkyl chains (DMD model),[79] end-labelled polymers (Birks' Scheme),[55,67] randomly labelled polymers (FBM),[83,94] and end-labelled dendrimers (MFA).[61,88] Specifically, randomly labelled linear polymers allow the determination of the effect that the chemical structure of the monomer has on the internal dynamics of the resulting polymer,[46,72,83,94-97] while end-labelled dendrimers allow one to probe the dynamics of the chains ends as the generation number of the dendrimer increases.[88,98-102] The choice of the model used to fit the fluorescence decays of the pyrene labelled macromolecule depends on both the level of detail desired and the samples that are under study, as not all models are applicable to all sample types. This is visualized in Scheme 1.3.
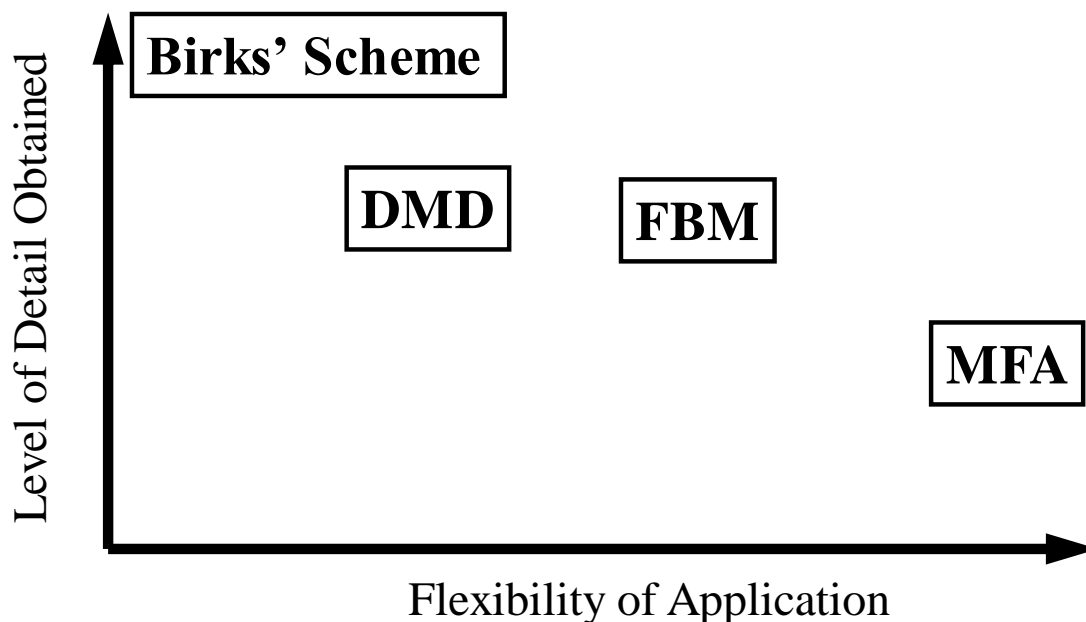
Scheme 1.3: Qualitative relationship between model applicability and level of detail obtained.

The four models discussed here all provide information on the excimer lifetime, and require knowledge of the lifetime of isolated pyrene monomers. The Birks Scheme provides the greatest level of detail with regard to the kinetics of excimer formation and polymer behaviour, yielding the rate of cyclization and excimer dissociation, as well as equations which directly describe the change in concentration of the excited species over time and allow the calculation of $(I_E/I_M)^{SPC}$. However, its applicability is severely restricted, as it can only be applied to pyrene end-labelled monodispersed polymer chains with relatively low molecular weights and no excessively strained geometry. The DMD model provides a measure of the same rates as the Birks Scheme, but its applicability to the study of pyrene-labelled macromolecules has been questioned.[103] It is, however, capable of fitting the decays acquired with short end-labelled alkyl chains with a constrained geometry.[79] The FBM provides information on the local pyrene

concentration as well as the rate of excimer formation, and the volume probed by a pyrene during its lifetime. The FBM equations can also be used to calculate $(I_E/I_M)^{SPC}$.[86] The only limitation of the FBM is that it cannot determine the rate of excimer dissociation, as it is assumed to be negligible in order to allow FBM analysis to be performed. The FBM is more widely applicable than either Birks' Scheme or the DMD Model, as it can handle the decays of randomly labelled polydispersed macromolecules. The MFA is the most widely applicable model, as all inquiries thus far have shown that it can handle any polymer architecture.[87-93,103] However it only yields an average rate constant for excimer formation, with no details about the exact processes leading to excimer formation. Thus one should choose a model based on both the samples it can analyze as well as the level of detail it provides.

1.3 Project Objectives

Since the mid 1970s, pyrene fluorescence has been used to gain detailed information on the behaviour of pyrene-labelled polymers in solution.[64,66,69,83] These studies have typically focused on homogeneous polymer solutions; the detailed information which can be obtained from fluorescence makes it an attractive tool for the characterization of solution-responsive polymers. The goal of this thesis is to use steady-state and time-resolved fluorescence to characterize the behaviour of solution-responsive polymers in aqueous solution to gain information on their aggregation behaviour, as well as their chain dynamics under conditions where they are either soluble or insoluble. Fluorescence analysis will be first applied to aqueous solutions of pH-responsive sequential amphiphilic polypeptides. While the ionization behaviour of polypeptide homopolymers has been studied for some time, the behaviour of polymers containing both ionizable and hydrophobic groups in a defined sequence, which more closely mimics the behaviour of biological polymers, has not been undertaken prior to this work. A series of

polypeptide samples with a wide range of hydrophilic-lipophilic balance will be characterized to determine their acid-base behaviour, their aggregation behaviour, and their ability to solubilize and protect hydrophobic compounds from aqueous solution. With regard to the latter, pyrene fluorescence is a technique ideally suited to the task as pyrene is strongly hydrophobic and it reports on its environment based on its steady-state and time-resolved fluorescence.

The study of the solution properties of aqueous hydrophobically modified PNIPAM is the subject of two of the research chapters presented in this thesis. They possess a lower critical solution temperature, which drastically reduces their solubility as the temperature is increased above this value. This is in contrast to the more commonly encountered upper critical solution temperature, where the solubility is reduced as the temperature is decreased below a critical value. These samples contain pyrene as their hydrophobe which makes them particularly well-suited to characterization by fluorescence. Solutions of Py_2-PNIPAM probe the changes which occur in the solution as the chains undergo a CGT at T_c, with the MFA allowing the specific changes in the rate of excimer formation and the distribution of pyrene species to be monitored. Solutions containing both Py_2-PNIPAM and unlabelled PNIPAM will be investigated as they allow the monitoring of the interactions between the two polymers by fluorescence, specifically focusing on the interactions which occur as the unlabelled PNIPAM becomes insoluble at 34 ^{o}C. The study of the neat Py_2-PNIPAM solutions and the mixtures of Py_2-PNIPAM and PNIPAM will provide a detailed description of the polymers as they undergo their CGTs which can be compared to a model proposed by F. M. Winnik et al.[34,36,44,49]

At this point of the thesis, the Model Free Analysis will have been applied to a number of polymer solutions, including the two studies presented in this thesis on Py_2-PNIPAM in aqueous solution with conformations other than those of solvated linear chains due to aggregation of the

polymer chains. The purpose of the final experimental chapter of this thesis is to investigate whether the MFA is able to analyze any possible polymer architecture by comparing the rate constants obtained by the MFA to those obtained by Birks' Scheme or the FBM, and also by comparing $(I_E/I_M)^{SPC}$ to $(I_E/I_M)^{SS}$ for no less than 30 pyrene-labelled macromolecular constructs with different architectures.

1.4 Thesis Outline

The layout of this thesis is as follows. Chapter 1 provided an overview of the properties of the solution-responsive polymers being studied, as well as giving information on the use of models to analyze fluorescence data. The response of a series of amphiphilic polypeptides to changes in *pH* is investigated in Chapter 2, focusing on both the acid/base and aggregation properties of the chains as well as the hydrophobic domains they form. Chapter 3 presents a study on the changes in behaviour which occur when pyrene-labelled PNIPAM in aqueous solutions undergoes a CGT as the solution temperature is increased. The behaviour of aqueous mixtures of pyrene-labelled PNIPAM and unlabelled PNIPAM, and the specific transition that occurs at 34 ^{o}C for these mixtures, is investigated in Chapter 4. The validity and applicability of the Model Free Analysis, which was widely used in the previous chapters, is investigated in Chapter 5. Chapter 6, which is the final chapter, contains a summary of the conclusions that were reached in this work, as well as suggestions for future work.

Chapter 2:

Effect of Sequence on the Ionization Behaviour of a Series of Amphiphilic Polypeptides

2.1 Overview

The pH-dependent behaviour of five polypeptides made of hydrophilic and pH-responsive aspartic acid (Asp) and hydrophobic phenylalanine (Phe), that had been prepared by stitching together short well-defined sequences of Asp and Phe, was studied. The effect of pH on these polypeptides referred to as $(Asp_3Phe_1)_n$, $(Asp_2Phe_1)_n$, $(Asp_1Phe_1)_n$, $(Asp_1Phe_2)_n$, and $(Asp_1Phe_3)_n$ varied dramatically depending on their constituting sequence. The more hydrophobic polypeptides $(Asp_1Phe_2)_n$ and $(Asp_1Phe_3)_n$ behaved as if the Asp's were isolated from each other and showed an apparent pK_a (pK_a^{app}) that remained constant with the level of ionization ($\alpha =$ [Asp$^-$]/[Asp]$_{total}$) and equalled 5.4 and 6.4, respectively. The more hydrophilic polypeptides $(Asp_3Phe_1)_n$ and $(Asp_2Phe_1)_n$ behaved like weak polyacids showing a linear increase in pK_a^{app} with increasing α. The pK_a^{app} of $(Asp_1Phe_1)_n$ showed a trend as a function of α intermediate between the Asp-rich and Phe-rich polypeptides, behaving as if the Asp were isolated at low α values (< 0.35) but acting as a weak polyacid for large α values (> 0.35). The effect that α and thus, the charge density of the polypeptides, had on the collapse and aggregation of the polypeptides was characterized by conducting static light scattering and fluorescence measurements. Static light scattering measurements demonstrated that all polypeptides precipitated and aggregated in aqueous solution at a critical charge density of 0.2. Fluorescence measurements with pyrene as aprobe indicated that this behaviour was due to the formation of Phe aggregates in water. Together, these experiments provide a complete description of how pH affects the behaviour of a series of unique amphiphilic polypeptides designed with a well-defined sequence.

2.2 Introduction

Amphiphilic polymers (APs) are a broad class of polymers able to self-assemble in aqueous solution to form networks, micelles, vesicles, or cylinders.[1-12] APs have found a wide variety of applications such as in the paint and paper coating industry as associative thickeners and/or colloidal stabilizers,[1,9] in the cosmetic and pharmaceutical industry to encapsulate, transport, and deliver in a controlled manner various therapeutic agents,[3,11] and in the oil industry for enhanced oil recovery.[12] Due to their broad realm of applications, APs have been and continue to be the focus of intense scientific scrutiny which has led to the publication of a vast number of reviews on their syntheses and properties.[1-12]

APs come in a variety of guises, but the forms of APs most commonly encountered in the literature consist of block, random, and alternating copolymers prepared from two monomers, one monomer being hydrophilic and the other hydrophobic. This relatively limited number of AP architectures parallels the number of highly efficient synthetic procedures that can produce these types of copolymers, typically by three chain polymerizations which are briefly described hereafter. First, the advent of controlled living polymerizations using initially an ionic and later a radical propagating center led to the easy preparation of block APs having well-defined molecular weight distributions (MWDs).[4-6,9,11] Second, statistical copolymers can be obtained by radical copolymerization of a hydrophobic and a hydrophilic monomer.[1,8,12] The third commonly used synthesis generates alternating APs by taking advantage of a pair of monomers whose reactivity ratios, when multiplied, yield a small value. This is usually achieved by selecting a pair of vinyl monomer bearing substituents with opposite electron donor-acceptor character such as with maleic anhydride and alkyl vinyl ethers.[13] While these chain polymerizations have allowed the efficient synthesis of block, random, and alternating

copolymers, which will behave as APs if the two monomers used in the copolymerization are hydrophilic and hydrophobic, it remains noticeable that none of these syntheses offers much control over the sequence in which the hydrophobic and hydrophilic monomers are being incorporated into the chain. This is unfortunate in view of recent theoretical developments which have exposed the importance of the sequence of hydrophobic and hydrophilic monomers in determining the properties of APs in solution.[14-16] This situation has led some to comment that "experimental efforts in this area have lagged behind computational efforts due to the synthetic challenges inherent in generating precise sequence-specific polymers in quantity."[16]

This study uses peptidic APs of well-defined sequences that were prepared by polymerizing short Asp_xPhe_y peptides with a definded sequence, where x and y varied from 1 to 3, into a series of five polypeptides $(Asp_xPhe_y)_n$. Under basic conditions at pH 9, aspartic acid (Asp) is negatively charged and highly water-soluble, whereas phenylalanine (Phe) is hydrophobic regardless of pH. The synthesis and solution properties at pH 9 of the polypeptides $(Asp_3Phe_1)_n$, $(Asp_2Phe_1)_n$, $(Asp_1Phe_1)_n$, $(Asp_1Phe_2)_n$, and $(Asp_1Phe_3)_n$ have been described in an earlier publication.[17] At pH 9, the more hydrophobic $(Asp_1Phe_2)_n$ and $(Asp_1Phe_3)_n$ polypeptides were shown to undergo some intermolecular association and were able to encapsulate the hydrophobic chromophore pyrene and protect it from the solvent. Herein we take advantage of the fact that the Asp residue of the $(Asp_xPhe_y)_n$ polypeptides is pH-sensitive to characterize the pH-dependent behaviour of these peptidic APs in aqueous solution via a combination of potentiometry, static light scattering, and fluorescence measurements. The results demonstrate the dramatic effect that the sequence of an AP containing weak carboxylic acids has on the apparent pK_a of the hydrophilic pH-sensitive monomer, and consequently, the pH-range where such an AP remains water-soluble and can be used effectively. This study highlights the

34

complications associated with predicting the level of ionization of APs whose hydrophilic groups are weak acids and whose hydrophobic pendants are incorporated in a statistical manner into the AP backbone. Since the interplay that exists between ionization and hydrophobicity affects whether an AP is present as an open coil or a collapsed globule,[18] the results presented herein should be relevant to scientists interested in studying the coil-to-globule collapse of polypeptides or designing APs that can be used as colloidal stabilizers, polymeric surfactants, or associative thickeners.

2.3 Experimental

Chemicals and Reagents: The synthesis and characterization of the polypeptides $(Asp_3Phe_1)_n$, $(Asp_2Phe_1)_n$, $(Asp_1Phe_1)_n$, $(Asp_1Phe_2)_n$, and $(Asp_1Phe_3)_n$ prepared with well-defined sequences has been described in detail in an earlier publication.[17] The notation used to represent the polypeptides describes the sequence of the peptide that was polymerized to prepare the polypeptide. Taking $(Asp_3Phe_1)_n$ as an example, this polypeptide was synthesized by preparing the tetrapeptide Asp_3Phe_1 which was then polymerized to yield $(Asp_3Phe_1)_n$. The five polypeptides had a similar M_w of $9,600 \pm 1,300$ g.mol^{-1}. Poly(aspartic acid) (Asp_n) with a weight average molecular weight (M_w) of 24 kg.mol^{-1} was purchased from Sigma-Aldrich. NaOH (BDH) and HCl (reagent ACS grade) were supplied by Fischer and sodium carbonate anhydrous (ACS grade) was obtained from EMD. Solvents of spectrograde quality (acetone, methanol, *N,N*-dimethylformamide (DMF) and dimethylsulfoxide (DMSO)) were bought from VWR or Caledon. All solvents were used as received unless otherwise stated. Milli-Q water with a resistivity of over 18 MΩ.cm was used to make all the aqueous solutions. Spectra/Por® 7

regenerated cellulose dialysis membranes having a cut-off value of 3,500 g/mol were used for dialysis.

Preparation of the polypeptide aqueous solutions: Polypeptide solutions used for potentiometry were prepared using the following protocol. A known amount of the polypeptide (~ 50 mg representing 90 and 300 μmol of Asp for $(Asp_1Phe_3)_n$ and $(Asp_3Phe_1)_n$, respectively) was dissolved in 7 mL of DMF. To this mixture 3 mL of an aqueous 0.1 M NaOH (300 μmol) was added at a rate of one drop every 4 s with vigorous stirring. The solution turned cloudy as the polypeptide precipitated into stable aggregates due to its poor solubility in the water/DMF mixture. The NaOH solution was used to ensure that all aspartic acids in the polypeptide were ionized. The resulting solution was placed in a dialysis bag with a molecular weight cutoff of 3500 g/mol and dialyzed against a solution of 0.01 M NaCl at pH 10.5 for 2 days, using a total of 4 L of dialysis solution replaced in 1 L changes. After dialysis was finished, the solutions were transparent and they were transferred to a round bottom flask capped with a rubber septum.

The absorption of carbon dioxide by basic aqueous solutions of the polypeptides was found to introduce an unacceptable amount of bicarbonate into the solutions which lowered the pH of the solution. To prevent this, the following steps were taken. An airtight container was used to perform the dialysis. All preparative steps (dialysis, titration) were conducted under a positive pressure of nitrogen. The basic aqueous solutions, against which the polypeptide solutions were dialyzed, were prepared by vigorously bubbling nitrogen through water overnight before adding NaOH. Solution changes during dialysis were performed using flexible tubing purged with nitrogen before transfer. Anecdotally, a vial containing 10 mL of stirred polypeptide solution prepared at pH 9 showed a visible drop in pH of up to 0.2 unit when one exhaled one's breath into it.

The polypeptide solutions used for the fluorescence and light scattering experiments were prepared according to a slightly modified protocol. A known amount of polypeptide (~ 50 mg) was dissolved in 7 mL of DMF, to which a known amount (~140 μL) of a 5.0 mM solution of pyrene in DMF was added. The solutions was then neutralized with 3 mL of 0.1 M NaOH and dialyzed in an airtight container against a 0.01 M NaCl solution which was saturated with pyrene beforehand and whose pH was adjusted to 10.5 with a few drops of a 10 M NaOH solution. Saturation of the 0.01 M NaCl solution at pH 10.5 with pyrene was achieved by adding a few pyrene crystals and allowing the solution to stand overnight. After dialysis, the polypeptide solutions were kept in a sealed container. Since the degree of Asp ionization is a function of pH only, the stringent procedure applied to ensure total CO_2 exclusion from the solutions used for potentiometry measurements was deemed unnecessary. The sealed container ensured that so little CO_2 could dissolve in the solutions that neither the ionic strength of the solution established by the presence of 0.01 M NaCl nor the pH would be affected.

UV-Vis absorption. The massic absorbance coefficient (ε_m expressed in $cm^{-1}.g^{-1}.L$) of the polypeptides was obtained by analysing the absorption spectra of the Phe residue acquired with a Hewlett Packard 8452A diode array spectrophotometer using a quartz cell (Hellma) with a 1 cm path length. The spectrophotometer measures the absorption as a function of wavelength in 2 nm increments. The absorption spectra needed to be corrected for light scattering. This was done by fitting the non-absorbing part of the absorption spectrum which reported on the light scattered by the solution with a 3rd order polynomial, extrapolating the polynomial to wavelengths where the sample absorbed, and subtracting the polynomial from the absorbance. A sample spectrum describes the procedure applied in Figure SI2.1 in Supporting Information (SI2). The ε_m values were employed at a later stage to determine the massic concentration in g/L of the polypeptide

37

solutions used for fluorescence by acquiring the absorption spectrum of these solutions with a Varian Cary 100 Bio UV-Vis spectrophotometer.

Massic absorbance coefficients of polypeptides. The determination of an absorbance coefficient requires that the concentration of the solution of the absorbing species be known accurately. Unfortunately, this information was not readily available as the polypeptide solutions were obtained by dialysis, which resulted in a decrease of the original concentration. To determine the polypeptide concentration in the solutions, three aliquots of a polypeptide stock solution and three similar aliquots of the 0.01 M NaCl solution adjusted to pH 10.5 with a few drops of 10 M NaOH solution and used to prepare the polypeptide solutions were dried in tared vials under a gentle flow of nitrogen before being kept in a vacuum oven at 60 $^{\circ}$C overnight. The vials were weighed and the average masses of the dried samples were obtained. The concentration of the polypeptide solution was determined by taking the difference between the solid contents of the polypeptide solution and that of the 0.01 M NaCl solution. The UV-Vis absorption spectrum of each polypeptide solution was acquired. A plot of absorbance at 258 nm vs. concentration was generated for each polypeptide, the slope of which was equal to the massic extinction coefficient ε_m.

Titration of polypeptide solutions. Carefully weighed volumes (~10 mL) of 0.6 − 1.0 g/L polypeptide aqueous solutions with 0.01 M NaCl were placed in a vial under a gentle flow of nitrogen. The pH of the polypeptide solutions after dialysis was close to 9.5. The solutions were titrated with 0.1 M HCl added in 10 µL increments using an Eppendorf pipettor (VWR). After each HCl addition, the solution was left to stir for 5 min. to allow it to equilibrate. The titration curves were conducted in triplicate for each $(Asp_xPhe_y)_n$ sample to assess the magnitude of the errors associated with the titration. One complication for error determination arises from the

different sets of degree of ionization (α) and pH values that are obtained in each titration (see Tables S2.1-5 in Supporting Information (SI2)) which makes the determination of average value and standard deviation difficult. This complication was addressed by applying a polynomial fit with no physical meaning to the three titration curves obtained for a given $(Asp_xPhe_y)_n$ polypeptide. The polynomial fits for the three titration curves were then used to generate three sets of pH and pK_a values obtained as a function of the same α values calculated with 0.01 increments. These three sets of pH and pK_a values were then used to average the pH and pK_a trends and the average and error of the trends were plotted. The titration of $(Asp)_n$ was performed once. A VWR Scientific pH meter model 8000 was used to determine the pH after each addition. The concentration of the polypeptide solutions in g/L was determined by UV-Vis absorbance using the ε_m values.

Steady-state fluorescence measurements. The steady-state fluorescence spectra were obtained using a Photon Technology International LS-100 steady-state fluorometer equipped with a continuous xenon lamp. A fluorescence cell (VWR) with an inner cross section of 10×10 mm^2 was used with right angle geometry and the solutions were kept aerated. The pyrene emission spectra were acquired by exciting the polypeptide solutions at 340 nm. Light scattering measurements were acquired by exciting the sample at 500 nm and monitoring the signal from 490 – 510 nm in 0.5 nm increments.

Time-resolved fluorescence measurements. The fluorescence decay profiles were obtained with a time-correlated single photon counter manufactured by IBH Ltd. using a NanoLED 340 nm diode as the excitation source. Samples were excited at 340 nm and the emission wavelength was set at 375 nm. The samples were placed in a 10×10 mm^2 fluorescence cell (VWR). All decays were collected with the right angle geometry over 1,000 channels with a minimum of

20,000 counts taken at the decay maximum to ensure a high signal-to-noise ratio. A light scattering standard was used to determine the instrument response function (IRF). Analysis of the decays was performed by convoluting the IRF with a sum of typically 3 exponentials as shown in Equation 2.1 and comparing the convolution result with the experimental decay.

$$i(t) = a_1\exp(-t/\tau_1) + a_2\exp(-t/\tau_2) + a_3\exp(-t/\tau_3) \tag{2.1}$$

The pre-exponential factors and decay times in Equation 2.1 were optimized using the Marquardt-Levenberg algorithm.[19] The quality of the fits was established from the χ^2 values ($<$ 1.30) and the random distribution around zero of the residuals and of the autocorrelation function of the residuals.

2.4 Results and Discussion

The preparation of the polypeptide solutions by dialysis induced a dilution of the polypeptide solution which necessitated the determination of the polypeptide concentration after dialysis using UV-Vis absorption. Phenylalanine has an absorption peak at 258 nm with a molar extinction coefficient $(\varepsilon)^{20}$ of 202 $M^{-1}.cm^{-1}$ which may be converted to a massic extinction coefficient (ε_m) of 1.37 $Lg^{-1}cm^{-1}$ by dividing ε by 147.17 g/mol, the residue mass of polymerized Phe (i.e. the molar mass of Phe minus that of water). Since the Phe content of the $(Asp_xPhe_y)_n$ samples varied significantly, the ε_m value was determined for each $(Asp_xPhe_y)_n$ sample. A stock polypeptide solution was used to prepare a concentration series of polypeptide solutions. Absorbance spectra of the polypeptide solutions were acquired and corrected for light scattering (see Experimental section for details). The corrected absorption spectra are shown in Figure

2.1A. A plot of the corrected absorbance at 258 nm versus the polypeptide concentration in g/L yielded a straight line whose slope equalled ε_m. The ε_m values were then used to determine the concentration of any new polypeptide solution prepared through dialysis.

Figure 2.1B shows a plot of the individual ε_m value of each polypeptide as a function of the Phe content of the polypeptides. A straight line was obtained that passes through zero. The slope of the line yields an ε_m value of 166 $M^{-1}cm^{-1}$ for a Phe residue in the polypeptide. The ε_m of molecular Phe equals 202 $M^{-1}cm^{-1}$ and is thus higher than predicted from Figure 2.1B obtained with the polypeptide solutions. This result is reasonable since the Phe residues present in the $(Asp_xPhe_y)_n$ polypeptides aggregate in aqueous solution and the Phe aggregates display a lower ε_m value compared to that of molecularly dissolved Phe as observed for aggregates of other aromatic molecules.[21,22]
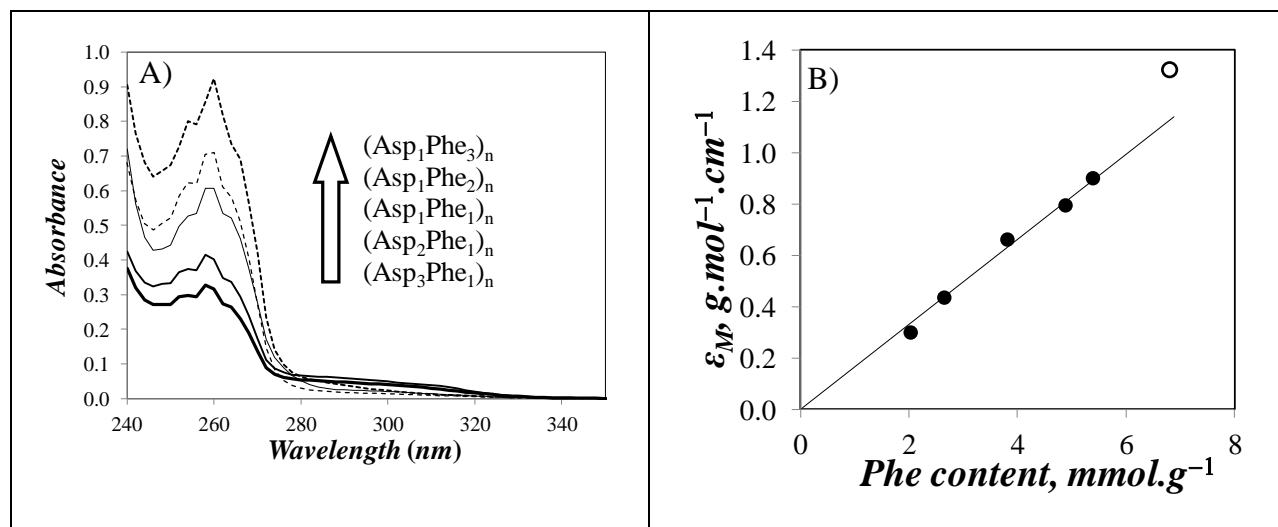
Figure 2.1. A) Absorbance spectra of the polypeptides solutions with a concentration of 1.0 g.L−1. B) Massic extinction coefficient determination for phenylalanine containing polymers. (●) Polypeptides in 0.01 M NaHCO3 solution at pH 9.0 and (○) phenylalanine in water.

In order to compare the ionization behaviour of the different polypeptides, basic aqueous solutions of the polypeptides in their aspartate form were titrated with HCl solution and the pH of the solution was plotted as a function of the degree of ionization α. As will be shown subsequently, the Phe content of the polypeptide samples drastically affects the relative acidity of the Asp residues. The calculation of α relies on the existence of a limited number of ionic species in solution during the titration. These species are the H_3O^+, OH^-, Cl^-, Asp^-, and Na^+ ions. The concentrations of H_3O^+ and OH^- can be derived from the solution pH, the Cl^- concentration is known from the amount of HCl titrant added, and that of Na^+ can be obtained from the concentrations of OH^- and Asp^- initially present. This leaves Asp^- as the only ion whose concentration is unknown, but which can be calculated using the electroneutrality equation for the solution given by Equation 2.2.

$$\left[OH^-\right]+\left[Cl^-\right]+\left[Asp^-\right]=\left[Na^+\right]+\left[H_3O^+\right]$$

(2.2)

Equation 2.2 can be easily rearranged to yield the concentration of ionized Asp residues, [Asp⁻]. Knowledge of [Asp⁻] enables the calculation of α using Equation 2.3, with [Asp$_{tot}$] being the total concentration of Asp residues, ionized or not.

$$\alpha = \frac{\left[Asp^-\right]}{\left[Asp_{tot}\right]}$$

(3)

Each point in the titration yields a set of α and pH values which result in plots of α versus pH shown for all polypeptides in Figure 2.2. It is noticeable in Figure 2.2 that the error on pH increased for α values smaller than 0.2 and larger than 0.9. This behaviour reflects the difficulty associated with the determination of $[Asp^-]$ from Equation 2.2 when the polypeptide is hardly $([Asp^-] << [Asp_{tot}]$ and $\alpha < 0.2)$ or fully $([Asp^-] \approx [Asp_{tot}]$ and $\alpha > 0.9)$ ionized. Consequently, the pH and pK_a values retrieved for α values smaller than 0.2 and greater than 0.9 were not considered in our discussion. These plots enable one to compare the response of these polypeptides to changes in the pH of the solution.
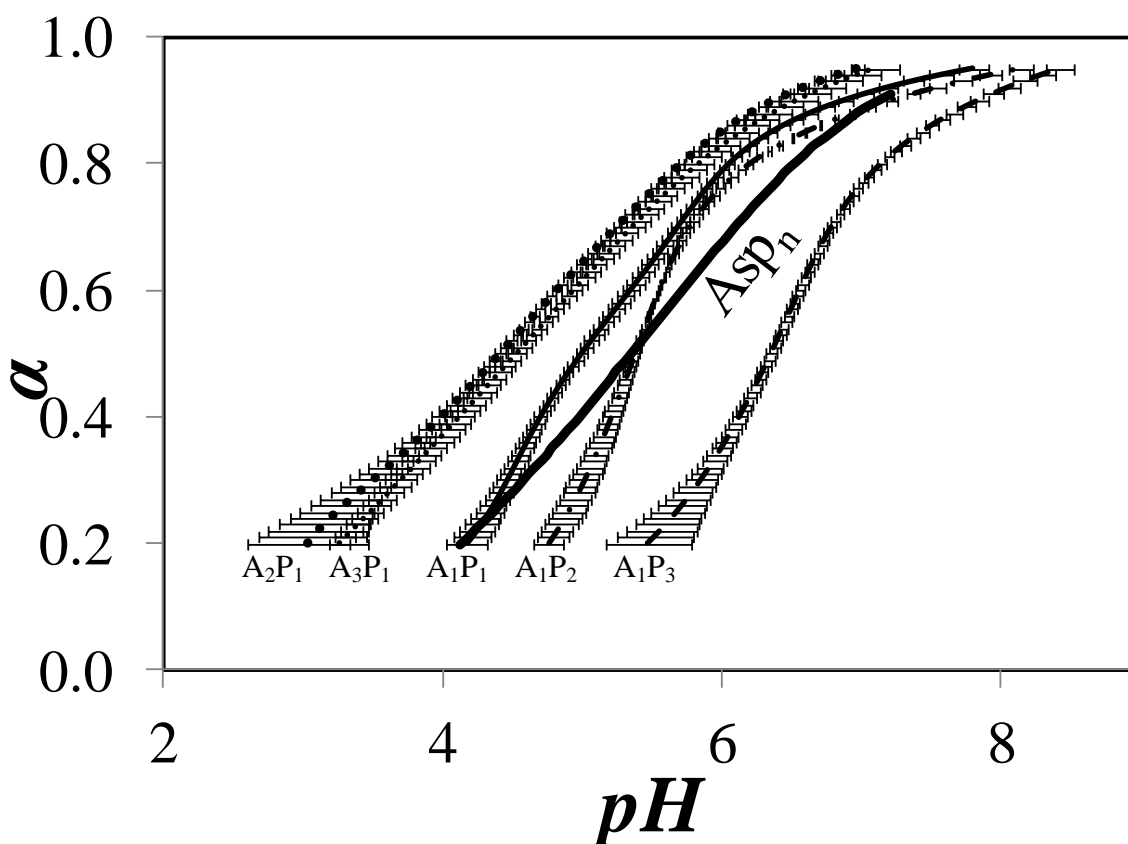
Figure 2.2. Titration curves of aqueous polypeptide solutions. Curves (right to left): $(Asp_1Phe_3)_n$, $(Asp_1Phe_2)_n$, $(Asp_1Phe_1)_n$, $(Asp_3Phe_1)_n$, $(Asp_2Phe_1)_n$; Asp_n (━)

43

On the one hand, the titration curves for the hydrophobic $(Asp_1Phe_3)_n$ and $(Asp_1Phe_2)_n$ polypeptides showed a rapid change in α value over a rather narrow range of pH, typical of monomeric acid titrations. In contrast, titration of the solutions of the more hydrophilic $(Asp_2Phe_1)_n$ and $(Asp_3Phe_1)_n$ samples showed a linear decrease in α with decreasing pH values, which is the behaviour expected of a weak polyacid.[23-25] These observations reflect the effect that the Phe content of the $(Asp_xPhe_y)_n$ polypeptides has on their respective acid-base behaviour.

To further refine these observations, the relative acidity of the Asp residues was determined by calculating the apparent pK_a of the polymer at each point in the titration. With α being the fraction of Asp residues in the basic (ionized) form, and $(1-\alpha)$ being the fraction of Asp residues in the acidic (neutral) form, the data sets shown in Figure 2.2 for the pH and degree of ionization were used to calculate the apparent pK_a of the Asp residues in the polymer at a given degree of ionization using the Henderson-Hasselbalch equation given in Equation 2.4.

$$pH = pK_a + \log\left(\frac{[A^-]}{[HA]}\right) = pK_a + \log\left(\frac{\alpha}{1-\alpha}\right)$$

(2.4)

The resulting plots of apparent pK_a ($pK_a{}^{app}$) versus α are shown in Figure 2.3A for all polypeptides. To ensure that the procedure used to prepare and titrate the polypeptide solutions was reliable, it was first applied to poly(aspartic acid) (Asp_n) which has been studied extensively by potentiometry.[23,24] The plot of $pK_a{}^{app}$ versus α obtained for Asp_n in Figure 2.3A exhibited the expected profile with a $pK_a{}^{app}$ value at $\alpha = 0.5$ ($pK_a{}^{app}[0.5]$) of 5.4 in perfect agreement with the literature.[23] Asp_n is a weak polyacid and its $pK_a{}^{app}$ increases linearly with increasing α as a result of the increased repulsion experienced by a hydroxide anion as it approaches the negatively

charged Asp_n. This control experiment led to the conclusion that the experimental protocol applied to the titration of the polypeptide solutions could be trusted. The results obtained in Figure 2.3A with the other polypeptides are now discussed.
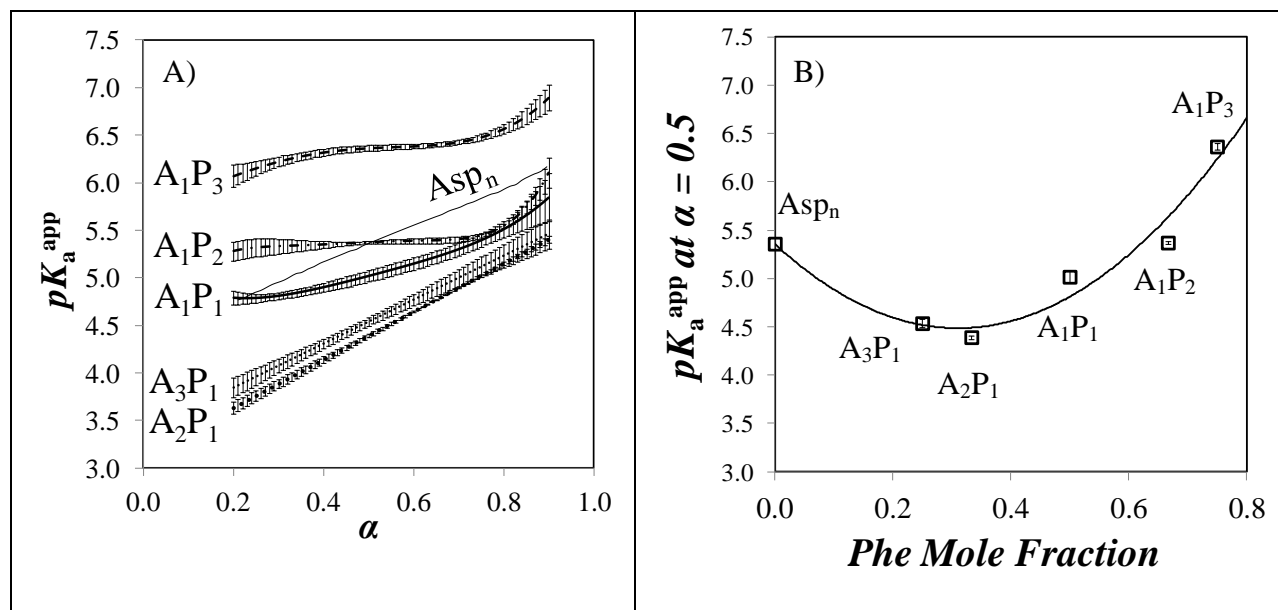
Figure 2.3. A) Apparent pK_a determination for aqueous solutions of $(Asp_1Phe_3)_n$ (━), $(Asp_1Phe_2)_n$ (━ •), $(Asp_1Phe_1)_n$ (━━), $(Asp_3Phe_1)_n$ (▪), $(Asp_2Phe_1)_n$ (●), and Asp_n (────) polypeptide. B) Apparent pK_a at $\alpha = 0.5$; the error bars are smaller than the symbols.

The Phe-rich and hydrophobic polymers $(Asp_1Phe_3)_n$ and $(Asp_1Phe_2)_n$ yielded largely constant pK_a^{app} values regardless of α in the same manner as a molecule bearing a single carboxylic acid would. It implies that the Phe residues isolate the ionized Asp residues and prevent them from inhibiting the neutralization of other neighboring Asp's. The Asp-rich hydrophilic polymers $(Asp_3Phe_1)_n$ and $(Asp_2Phe_1)_n$ showed a pK_a^{app} for the polymer that increased linearly with increasing degree of ionization, mimicking the behaviour of Asp_n. As for Asp_n, this α-dependent variation in pK_a is typical of weak polyacids as the ions present on the

backbone interact and inhibit further ionization. The $(Asp_1Phe_1)_n$ polymer showed a behaviour intermediate between the two types, behaving as a polyelectrolyte for $\alpha > 0.35$ and as a monomeric acid for $\alpha < 0.35$.

In addition to the effects on the slope of the pK_a curve, more information could be retrieved about the relative acidity of the Asp residues by further analyzing Figure 2.3A. For low α values, the hydrophilic polymers took pK_a^{app} values between 3.6 and 3.8, which agree with the reported pK_a value of 3.9 for isolated Asp residues surrounded by hydrophilic residues[26,27] or well-exposed to solvent.[28] Interestingly, the pK_a^{app} of $(Asp_3Phe_1)_n$ and $(Asp_2Phe_1)_n$ was smaller than that of Asp_n over the entire range of α values. This observation suggests that isolating short Asp_2 and Asp_3 sequences between two neutral Phe residues enhances the acidity of the Asp residues when compared to Asp_n. As the Phe content is increased, this effect continues until further incorporation of hydrophobic Phe inhibits the titration of the Asp residues. The hydrophobic polypeptides showed significantly higher $pK_a^{app}[0.5]$ values of 5.4 and 6.4 for $(Asp_1Phe_2)_n$ and $(Asp_1Phe_3)_n$, respectively. These large $pK_a^{app}[0.5]$ values for a carboxylic acid are due to the nearby presence of hydrophobic residues which hinder the ionization of the Asp residues.[26,29,30]

The combination of these two effects are summarized in Figure 2.3B where $pK_a^{app}[0.5]$ is plotted as a function of the Phe content of the polypeptide. $pK_a^{app}[0.5]$ first decreases with increasing Phe content due to a decrease of the Asp density along the polypeptide. Based on a recent report,[31] a charged residue on a polyelectrolyte affects residues located half a Debye length away, which in the case of a 10 mM NaCl solution would amount to 1.5 nm, or a 4 amino acids stretch on both sides of the charged residue for a polypeptide. Consequently, one charged Asp in Asp_n would affect 8 others resulting in an Asp/Asp^- ratio of 8/1. In the case of

$(Asp_3Phe_1)_n$ and $(Asp_2Phe_1)_n$, this ratio decreases to 6/1 and 5/1, respectively, due to the presence of neutral Phe residues that act as insulators. The decrease in the Asp/Asp^- ratio suggests that the Asp's of $(Asp_3Phe_1)_n$ and $(Asp_2Phe_1)_n$ are less affected by the negative charges created along the polymer when α increases and that these polypeptides are more acidic than Asp_n as observed experimentally in Figures 2.3A and 2.3B. They also exhibit similar Asp/Asp^- ratios and were found to behave similarly in Figure 2.3. As the Phe content of the polypeptide is increased further a second effect comes into play, where the introduction of hydrophobic Phe inhibits the ionization of Asp, resulting in the increase in $pK_a^{app}[0.5]$ observed with increasing Phe content in Figure 3B.[26,29,30]

During the course of the $(Asp_xPhe_y)_n$ titrations, it was observed that for all but the $(Asp_3Phe_1)_n$ sample, the solutions would turn turbid at some point as the pH decreased. This turbidity was clearly the result of the aggregation of the $(Asp_xPhe_y)_n$ chains induced by the hydrophobic Phe residues no longer being stabilized by the neutralized Asp residues. This observation suggested that light scattering could be used to determine the onset pH where aggregation occurred. To this end, the right angle light scattering intensity of pyrene loaded $(Asp_xPhe_y)_n$ solutions was measured with the steady-state fluorometer as the pH was varied. It was plotted as a function of α in Figure 2.4A from which a clear trend emerges. The light scattering intensity begins to increase due to the formation of insoluble polypeptide aggregates at a lower α value with decreasing Phe content. Out of all the polypeptides, $(Asp_3Phe_1)_n$ failed to precipitate over the entire range of α values studied between 0.2 and 1.0, that is the region for which α could be accurately calculated. In addition, the more hydrophobic polypeptides showed a relatively smooth transition from soluble to insoluble, while the more hydrophilic samples showed much sharper transitions.

In Figure 2.4A, there is a characteristic α value for each polymer below which there is a significant increase in light scattering intensity. Furthermore, it can be observed that this characteristic α value decreases with increasing Asp content and suggests that the solubility of the polypeptides depends on the linear density of negatively charged Asp along the chain, $(Asp_1Phe_3)_n$ having the lowest possible charge density of one Asp^- per four amino acids whereas $(Asp_3Phe_1)_n$ having the highest of three Asp^- per four amino acids. Since α is the number of charges present per Asp residue, it is trivial to convert these values to the number of charges per amino acid (Asp or Phe). The result of changing the x-axis from the ionization level α in Figure 2.4A to the linear density of negative charge per residue is shown in Figure 2.4B.

When the overall charge density was used to compare the light scattering profile in Figure 2.4B, the light scattering intensity for all polypeptide solutions but that for $(Asp_3Phe_1)_n$ was found to increase rapidly with decreasing charge density when the charge density decreased below 0.2. The polypeptide $(Asp_3Phe_1)_n$ remained water-soluble even when most Asp were in the acid form. The trend shown in Figure 2.4B indicates the existence of a critical charge density below which the four more hydrophobic polypeptides aggregate. This result suggests that electrostatic forces control the aggregation behaviour of these samples rather than their Phe content.

The existence of hydrophobic microdomains generated by polypeptide aggregates can be determined using a hydrophobic fluorophore that is able to interact with the hydrophobic microdomains, and whose emission will respond to a change in the polarity of its local environment. Pyrene is such a fluorophore, and its fluorescence was employed to probe the polypeptide solutions as a function of polypeptide sequence and degree of ionization. The fluorescence spectra of the polypeptide solutions loaded with pyrene were acquired and some
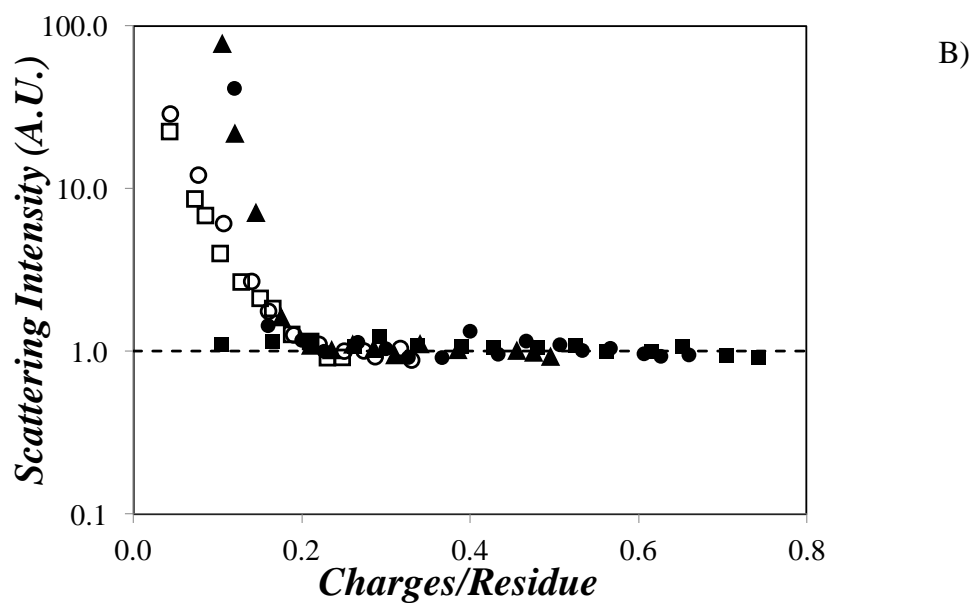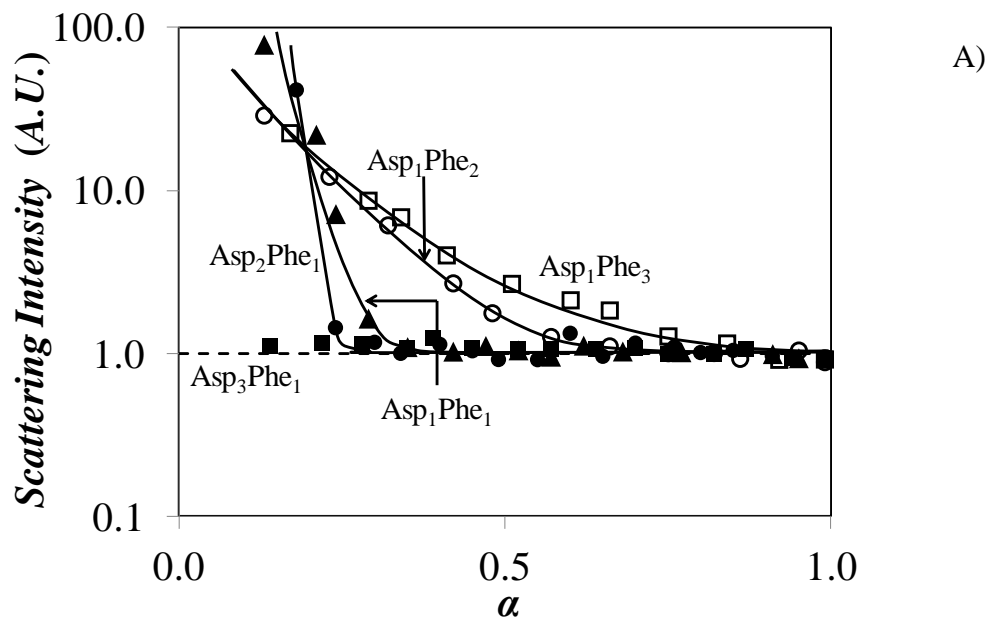
Figure 2.4. Right angle light scattering intensity of aqueous polypeptide solutions as a function of A) the degree of ionization of Asp residues and B) the density of negative charge along the backbone. $(Asp_1Phe_3)_n$ (□), $(Asp_1Phe_2)_n$ (○), $(Asp_1Phe_1)_n$ (▲), $(Asp_2Phe_1)_n$ (●), $(Asp_3Phe_1)_n$ (■).

representative spectra obtained for an α value of 0.5 are shown in Figure SI2.2 in SI2. The fluorescence spectra were used to calculate the I_1/I_3 ratio of pyrene which reflects the polarity of the microenvironment of pyrene.[32-34] A higher I_1/I_3 ratio reflects a more polar environment. A plot of I_1/I_3 versus α is shown in Figure 2.5. The three more hydrophobic polypeptides, namely $(Asp_1Phe_3)_n$, $(Asp_1Phe_2)_n$, and $(Asp_1Phe_1)_n$, showed a low and constant I_1/I_3 ratio of 1.20 ± 0.02. An I_1/I_3 ratio of 1.20 is typical of pyrene being incorporated inside hydrophobic microdomains, probably generated by the Phe residues. For instance, the I_1/I_3 ratio of pyrene has been reported to equal 1.14 in micelles of sodium dodecyl sulfate $(SDS)^{32}$ or between 1.0 and 1.2 in the hydrophobic microdomains generated by different maleic anhydride-styrene (SMA) copolymers.[35] These I_1/I_3 ratios are much lower than that of 1.80 reported for pyrene in water.[33,34]

Although pH-induced aggregation occurs at α values of 0.4, 0.6, and 0.8 for, respectively, $(Asp_1Phe_1)_n$, $(Asp_1Phe_2)_n$, and $(Asp_1Phe_3)_n$ in Figure 2.4A, no change in the I_1/I_3 ratio was observed at these α values in Figure 2.5 for these polypeptides. The absence of transition is due to the presence of intramolecular hydrophobic domains which are generated by the Phe residues of the polypeptides even at high α values, under conditions where the polypeptides are little or not aggregated. These hydrophobic microdomains host pyrene regardless of whether the polypeptides are soluble or fully aggregated above or below the critical charge density of 0.2, respectively. Since the environment experienced by pyrene did not change its polarity as the polypeptides became less ionized and eventually aggregated, the I_1/I_3 ratio remained constant in Figure 2.5 over the entire range of α values. The I_1/I_3 values shown by the

most hydrophilic polypeptides increased to 1.46 ± 0.06 and 1.67 ± 0.06 for $(Asp_3Phe_1)_n$ and $(Asp_2Phe_1)_n$, respectively. The I_1/I_3 ratio of 1.67 for $(Asp_2Phe_1)_n$ approaches that of pyrene in water found to equal 1.77 ± 0.05.[33,34] That the I_1/I_3 ratio be consistently lower and equal to 1.46 for the more hydrophilic polypeptide $(Asp_3Phe_1)_n$ is attributed to the existence of pyrene microcrystals whose presence was inferred from Figure SI2.2.E. Nevertheless, the noticeably higher I_1/I_3 ratios obtained for $(Asp_3Phe_1)_n$ and $(Asp_2Phe_1)_n$ reflect the fact that little (for $(Asp_3Phe_1)_n$) to no (for $(Asp_2Phe_1)_n$) hydrophobic microdomains are present in these samples and that if pyrene was associated with the polypeptide, it was also exposed to water.
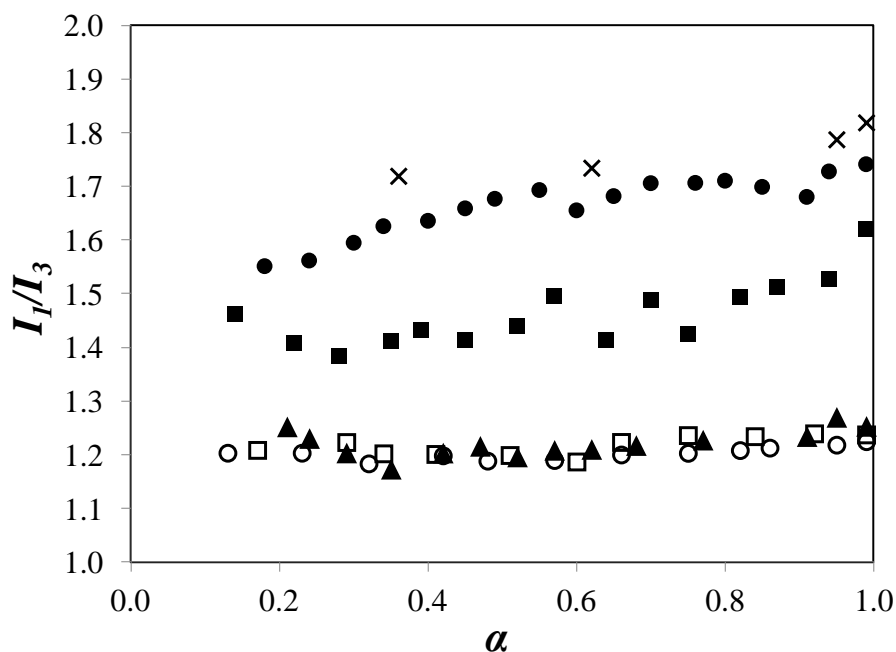
Figure 2.5. I_1/I_3 ratio of pyrene in the $(Asp_xPhe_y)_n$ aqueous solutions. $(Asp_1Phe_3)_n$ (□), $(Asp_1Phe_2)_n$ (○), $(Asp_1Phe_1)_n$ (▲), $(Asp_2Phe_1)_n$ (●), $(Asp_3Phe_1)_n$ (■), and pyrene in water (✗).

The pyrene-loaded polypeptide solutions were prepared without outgassing oxygen. Since oxygen is a powerful quencher of pyrene fluorescence, its presence in the polypeptide

aqueous solutions was utilized to probe the accessibility of the hydrophobic microdomains hosting a pyrene molecule to oxygen. To this end, the time-resolved fluorescence decays of the polypeptide solutions were acquired and fitted with a triexponential function. The pre-exponential factors and decay times retrieved from this analysis are listed in Table SI2.8. All solutions yielded a strong pre-exponential contribution for a decay time of 124 ± 13 ns which will be referred to as τ_W in the following discussion. The decay time τ_W matches that of pyrene in 0.01 M NaCl aqueous solution found to equal 127 ± 1 ns depending on pH. The pre-exponential contribution for τ_W reflects the presence of pyrene molecules that are either exposed to or dissolved in water. Whereas τ_W represented the longest decay time retrieved for the $(Asp_3Phe_1)_n$ and $(Asp_2Phe_1)_n$ solutions, a much longer decay time τ_L of 307 ± 15 ns was obtained for the $(Asp_1Phe_1)_n$, $(Asp_1Phe_2)_n$, and $(Asp_1Phe_3)_n$ solutions. Such a long decay time, more than twice longer than τ_W, indicates that some pyrene molecules are protected from quenching by oxygen dissolved in water. Decay times τ_L around 300 ns have been observed for pyrene located in the hydrophobic microdomains generated by other hydrophobically modified water-soluble polymers.[18,35,36] In the case of the polypeptides, these pyrene molecules are hosted inside the hydrophobic microdomains generated by $(Asp_1Phe_1)_n$, $(Asp_1Phe_2)_n$, and $(Asp_1Phe_3)_n$ where their exposure to the solvent is strongly reduced. The decay times τ_W and τ_L did not change much with pH as shown in Figure 2.6A where they are plotted as a function of α for all polypeptide solutions. All the decays analyzed exhibited one or two short decay times of 2-70 ns. The short decay times between 2 and 20 ns were due to light scattering that made its way through the detection system of the time-resolved fluorometer, despite the use of a cut-off filter for the acquisition of the fluorescence decays. The longer decay times between 20 and 70 ns which contributed to less than 20% of the total pre-exponential weight were attributed to residual

pyrene excimer formation due, in part, to the presence of pyrene microcrystals and/or quenching of the excited pyrene by the aromatic residues or the terminal amines of the polypeptides. Considering the pre-exponential factors a_W and a_L of the longer decay times τ_W and τ_L, the ratio $a_L/(a_W+a_L)$ was plotted as a function of α in Figure 2.6B. The ratio $a_L/(a_W+a_L)$ equalled zero for $(Asp_3Phe_1)_n$ and $(Asp_2Phe_1)_n$ as pyrene is exposed to water in these samples, is efficiently quenched by oxygen dissolved in water, and no contribution with a long decay times τ_L could be detected in these samples.
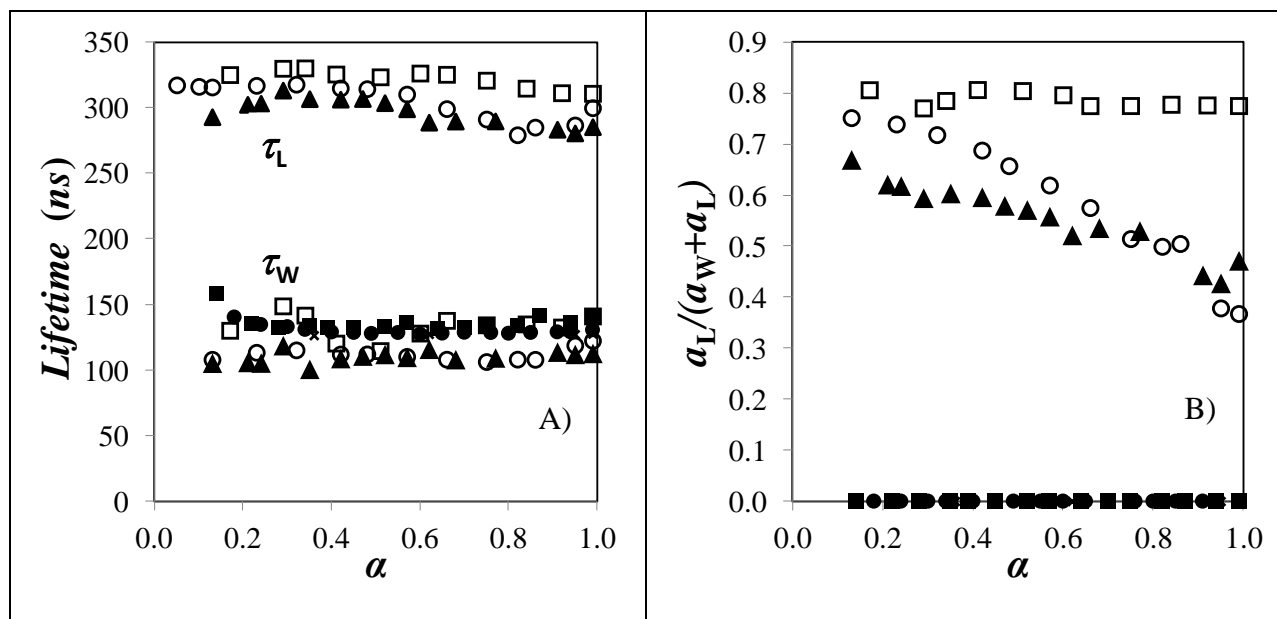
Figure 2.6. A) Decay times τ_W and τ_L and B) pre-exponential ratio $a_L/(a_W+a_L)$ of pyrene in $(Asp_xPhe_y)_n$ aqueous solutions as a function of α. $(Asp_1Phe_3)_n$ ($\square$), $(Asp_1Phe_2)_n$ ($\circ$), $(Asp_1Phe_1)_n$ ($\blacktriangle$), $(Asp_2Phe_1)_n$ ($\bullet$), $(Asp_3Phe_1)_n$ ($\blacksquare$).

The ratio $a_L/(a_W+a_L)$ remained constant with α and equaled 0.79 ± 0.01 for $(Asp_1Phe_3)_n$. It represents the largest $a_L/(a_W+a_L)$ value obtained with all polypeptides which reflects the more hydrophobic character of this sample. Interestingly, $a_L/(a_W+a_L)$ increased with decreasing α for the $(Asp_1Phe_1)_n$ and $(Asp_1Phe_2)_n$ samples. As the pH of the solution is lowered, more

carboxylate anions become protonated which increases the hydrophobic character of the polypeptide and induces a transfer of pyrene from the aqueous phase to the polypeptide. As pyrene is hosted by the hydrophobic microdomains that are created along the polypeptide when α decreases, it emits with a long decay time τ_L. For small α values, $a_L/(a_W+a_L)$ for $(Asp_1Phe_2)_n$ reached a value of 0.75, close to that of 0.79 ± 0.01 obtained with $(Asp_1Phe_3)_n$ at any α value. In summary, the plots shown in Figure 2.6 demonstrate first, that the $(Asp_3Phe_1)_n$ and $(Asp_2Phe_1)_n$ polypeptides are too hydrophilic to provide any protection to a hydrophobic molecule like pyrene from the solvent at any pH since $a_L/(a_W+a_L)$ in Figure 2.6B equals zero for all α values; second, that the $(Asp_1Phe_3)_n$ polypeptide is too hydrophobic to release pyrene to the solvent at any pH since $a_L/(a_W+a_L)$ in Figure 2.6B remains constant and equal to 0.79 ± 0.01 for all α values; and third, that only the $(Asp_1Phe_1)_n$ and $(Asp_1Phe_2)_n$ polypeptides show a change in the $a_L/(a_W+a_L)$ ratio as a function of α increasing from $\sim 0.4 - 0.5$ for α values greater than 0.9 to $\sim 0.65 - 0.75$ for α values smaller than 0.3. This latter behaviour demonstrates that these polypeptides are pH-responsive, protecting the hydrophobic pyrene molecule from the solvent at low pH values and releasing the pyrene molecules to the solvent at high pH values. The design of the polypeptides with their well-defined repeating sequences together with their study using the hydrophobic chromophore pyrene established that polypeptide sequences with Phe-to-Asp ratios between 1 and 2 result in pH-responsive polypeptides. A lower Phe-to-Asp ratio yields polypeptides that are too water-soluble whereas a higher Phe-to-Asp ratio yields polypeptides that are too hydrophobic.

Due to their poor solubility in pure water, the fully ionized polypeptides ($\alpha \approx 1.0$) were prepared in basic aqueous solution at pH 10.5. The ionized polypeptides were then titrated with 0.1 M HCl to probe the behavior of the polypeptides as a function of α down to an α value of

0.2. These titration experiments established that the $(Asp_1Phe_1)_n$ and $(Asp_1Phe_2)_n$ polypeptides responded to pH changes (see Figure 2.6). The reversibility of the process described above where the polypeptides expose pyrene to the solution at high pH but protects it from the solution at low pH was investigated for $(Asp_1Phe_1)_n$. A $(Asp_1Phe_1)_n$ solution with pyrene was prepared at pH 10.5. The solution was titrated with 0.1 M HCl to an α value of 0.2, before being back-titrated with a 0.1 M NaOH solution up to an α value of 1.0. The fluorescence decays of pyrene were acquired as a function of α and analyzed with a sum of exponentials. The results of this analysis are shown in Figure 2.7. For decreasing α values, a constant long (τ_L) and short (τ_W) decay times of, respectively, 310 ± 8 and 128 ± 9 ns were obtained and the contribution $a_L/(a_W+a_L)$ from τ_L increased from 0.50 to 0.70. These trends agree with those reported in Figure 2.6 for $(Asp_1Phe_1)_n$. Back-titration of the polypeptide solution yielded a constant τ_W of 114 ± 13 ns and a τ_L value that decreased from 320 ns at $\alpha = 0.2$ to 270 ± 12 ns for α values greater than 0.55. Again all τ_L values retrieved from the analysis of the fluorescence decays were more than twice larger than τ_W indicating that a fraction $a_L/(a_W+a_L)$ of pyrene molecules were protected from the solution. The fraction $a_L/(a_W+a_L)$ decreased from 0.70 to 0.40 when α increased from 0.2 to 0.9 indicating that exposure of pyrene to the solution increased upon increasing the pH of the solution. This result demonstrates reversibility of the protection afforded to pyrene by the polypeptide upon decreasing the solution pH.

Although the trends shown in Figure 2.7 indicate that the protection provided by the polypeptide upon decreasing the solution pH was reversible, the trends obtained for the $a_L/(a_W+a_L)$ ratio upon decreasing and increasing the α value did not overlap in Figure 2.7B. The different $a_L/(a_W+a_L)$ trends observed in Figure 2.7 are somewhat unexpected based on the known aversion of the polypeptides to create a negatively charged aspartate anion surrounded by

55

hydrophobic Phe residues. Consequently, titration of the fully ionized $(Asp_1Phe_1)_n$ polypeptide with 0.1 M HCl should be favored due to the disappearance of the negatively charged aspartate anions, while the reverse titration of the partially ionized $(Asp_1Phe_1)_n$ polypeptide with 0.1 M NaOH should be more difficult. Following this reasoning, exposure of pyrene to the solvent would be expected to occur at a higher α value during the reverse titration which is contrary to the trend found in Figure 2.7.
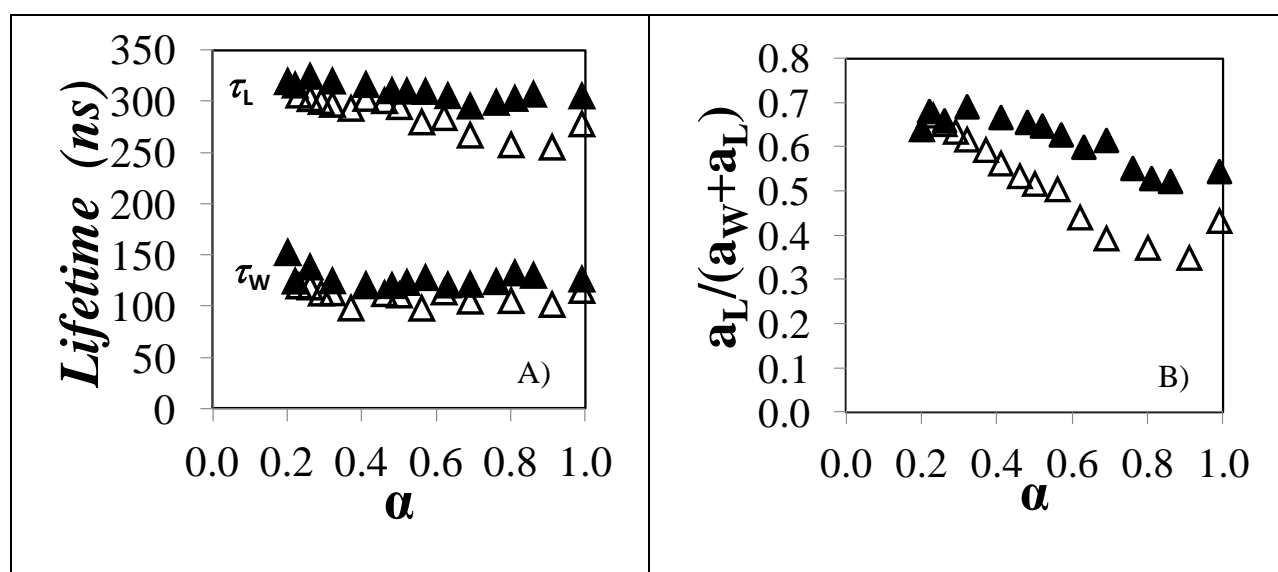
Figure 2.7. A) Decay times τ_W and τ_L and B) pre-exponential ratio $a_L/(a_W+a_L)$ of pyrene in $(Asp_1Phe_1)_n$ aqueous solutions as a function of α for decreasing (▲) and increasing (Δ) α values.

The difference in the trends obtained with the forward and reverse titrations in Figure 2.7 might be a consequence of the location of pyrene in the polypeptide aggregates. As more hydrophobic domains were created in the solution upon decreasing the pH, those pyrenes that had originally targeted the most hydrophobic domains present in the solution[17] diffused out of their original location and distributed themselves into the newly created hydrophobic domains.

In turn, those newly created hydrophobic domains were the first to decompose during the reverse titration, resulting in an enhanced exposure of pyrene to the solvent.

Such differences also suggest that polypeptide aggregation upon decreasing the pH and decomposition of the polypeptide aggregates upon raising the pH take place under non-equilibrium conditions using the protocol applied in this study. Indeed, preparation of the initial polypeptide solutions took two days because of the dialysis step required, allowing the solutions to approach equilibrium conditions. By comparison, each data point in Figure 2.7 took 15 min. to obtain, accounting for a 5 min. wait time to allow the solution to stir after each acid or base addition. Consequently, another likely reason for the hysteresis found in Figure 2.7 is that the data points were obtained under non-equilibrium conditions. Regardless of these considerations, the data presented in Figure 2.7 demonstrate unambiguously that the process of pyrene encapsulation by $(Asp_1Phe_1)_n$ upon decreasing the solution pH can be reversed by increasing the solution pH.

2.5 Conclusions

Since ionization and hydrophobicity are two major factors affecting the collapse and aggregation (C&A) of polymers in aqueous solution,[18] this study on polypeptides exhibiting well-defined sequences of Asp and Phe residues provided a unique opportunity to probe the effect that the sequence of the hydrophobic and ionizable monomers has on the behaviour of the amphiphilic polymer (AP) in aqueous solution. The apparent pK_a's (pK_a^{app}) of the polypeptides determined by potentiometry reflected how strongly the neutralisation of the Asp residues was affected by the sequence of the hydrophobic and ionisable residues. Flanking one Asp with at least two hydrophobic Phe's on both sides was found, firstly, to isolate an Asp efficiently and secondly, to

reduce its acidity substantially. Contrary to polyacids like poly(acrylic acid)[25] or poly(aspartic acid)[23] for which pK_a^{app} increases linearly with increasing degree of ionization (α), pK_a^{app} remained more or less constant with α for $(Asp_1Phe_2)_n$ and $(Asp_1Phe_3)_n$ (see Figure 2.3A). Since this behaviour is usually expected from small organic molecules bearing a single carboxylic acid, the Asp residues of the two more hydrophobic polypeptides are isolated from each other thanks to the two or three Phe flanking them on either side. Although the Asp residues of $(Asp_1Phe_2)_n$ and $(Asp_1Phe_3)_n$ are isolated, their acidity decreases by a full pK_a unit with increasing number of Phe in the sequence from two to three (see Figure 2.3B) due to the difficulty of generating a negatively charged carboxylate anion in a hydrophobic microdomain constituted of aggregated Phe's.[26,29,30]

The weak polyacid behaviour[23-25] that was recovered for $(Asp_3Phe_1)_n$ and $(Asp_2Phe_1)_n$ where two or three Asp residues were grouped in the polypeptide sequence and pK_a^{app} was found to increase linearly with increasing α for these samples. Interestingly, pK_a^{app} for $(Asp_3Phe_1)_n$ and $(Asp_2Phe_1)_n$ was one pK_a unit lower than for Asp_n (see Figures 2.3A and 2.3B). This stronger acidic character can be attributed to the presence of Phe residues which helped reduce the overall charge density of the ionized polyacid compared to Asp_n.

These experimental results illustrate the complexity associated with the study of the C&A of APs bearing pH-sensitive residues. Substantial variation of pK_a^{app} behaviours can be expected from these pH-sensitive residues, depending on how many are incorporated sequentially into an AP, and on the hydrophobicity of their immediate neighbors. Since the ionization level of an AP affects its conformation in solution, which will be either coiled or collapsed at high or low ionization levels, respectively,[18] this study suggests that conclusions about the C&A of an AP in solution drawn from APs prepared by random incorporation of hydrophobic and pH-sensitive

hydrophilic monomers are the outcome of a complex mixture of pK_a^{app} behaviours. This study also bears the promise that it might be possible to characterize the behaviour of any possible primary sequence of hydrophobic and pH-sensitive hydrophilic monomers and use this knowledge to predict the C&A of an AP whose sequence is a combination of all these primary sequences.

After having characterized the pK_a^{app} as a function of α for all polypeptides, the stability of the amphiphilic polypeptides was studied by static light scattering in aqueous solution. For all polypeptides except the more hydrophilic $(Asp_3Phe_1)_n$ that never precipitated, a minimum charge density of 0.2 was found to prevent the massive collapse of the polypeptide coils followed by precipitation (see Figure 2.4B). Aggregation of the polypeptides was induced by the hydrophobic association of the Phe residues that generated intra- and intermolecular hydrophobic microdomains in aqueous solution. These hydrophobic microdomains were efficiently targeted by molecular pyrene, whose fluorescence spectrum showed the responses typical of a change in the polarity of its local environment, as is evident from the I_1/I_3 ratios reported in Figure 2.5. Time-resolved fluorescence decay measurements showed that these hydrophobic microdomains protected pyrene efficiently from its surroundings, allowing pyrene to emit with an extremely long lifetime of 307 ns (see Figure 2.6A). The fluorescence experiments conducted with pyrene showed that the polypeptides $(Asp_1Phe_1)_n$ and $(Asp_1Phe_2)_n$ were pH-responsive, affording protection from the aqueous solution to pyrene under acidic conditions while exposing pyrene to the solution under basic conditions. The protection was found to be reversible in the case of $(Asp_1Phe_1)_n$ as increasing pH led to decomposition of the polypeptide aggregates and increased exposure of pyrene to the solvent.

The combination of potentiometry, static light scattering, and fluorescence measurements carried out with a series of amphiphilic polypeptides of well-defined sequence provided a detailed description of the factors that play a role in controlling the C&A of an AP. This study represents one of the very few examples in the current literature which characterized the effect that the sequence of hydrophilic and hydrophobic monomers has on the C&A of an amphiphilic macromolecule. The ability to synthesize polypeptides having well-defined repeating sequences of hydrophobic and hydrophilic monomers appears to open new scientific venues to probe these effects.

Chapter 3:

Temperature Response of Aqueous Solutions of Pyrene End-Labeled Poly(*N*-isopropylacrylamide)s Probed by Fluorescence

3.1 Overview

A series of pyrene end-labelled poly(*N*-isopropylacrylamide)s (Py-PNIPAMs) with well-defined molecular weights were dissolved in aqueous solution and studied using turbidimetry, light scattering, and fluorescence. The lower critical solution temperature (T_c) determined using turbidimetry or light scattering was found to increase with the number-average molecular weight (M_n) of the polymer. Pyrene excimer formation was studied by fluorescence. The steady-state fluorescence spectra yielded the ratio of the fluorescence intensity of the excimer over that of the monomer, namely the $(I_E/I_M)^{SS}$ ratio, which was found to go through a maximum at T_c, as did the polydispersity index of the time-resolved monomer fluorescence decays. The average decay times of the monomer and excimer as well as the ratio a_{E-}/a_{E+} which reflects the rise time in the excimer decays, all increased sharply at T_c. Global analysis of the time-resolved fluorescence decays of the pyrene monomer and excimer according to model-free analysis (MFA) allowed the calculation of the average rate constant of excimer formation ($<k>$) as well as the three fluorescence fractions f_{free}, f_{diff}, and f_{agg} describing the distribution of the pyrene labels in solution as pyrene labels which do not form excimer, form excimer by diffusion, and are aggregated, respectively. Increasing the solution temperature above T_c was found to cause a sharp decrease in $<k>$ and f_{free} but a sharp increase in f_{diff}. These changes were consistent with mesoglobule formation. Once the solution temperature was raised to the dehydration temperature T_m of the PNIPAM backbone, which is equal to 34 °C, the distribution of the pyrene pendants in solution stabilized and remained unchanged above this temperature. These results are consistent with the model proposed for telechelic PNIPAM by F. M. Winnik et al.

3.2 Introduction

Aqueous solutions of poly(*N*-isopropyl acrylamide) (PNIPAM) have been the subject of major interest for over 50 years,[1] and have been studied using a variety of techniques including viscometry,[2-4] turbidimetry,[3,5-8] light scattering,[4,8,9] fluorescence,[6,9-13] and neutron scattering.[14-16] The origin of this interest resides in the fact that PNIPAM possesses a lower critical solution temperature (LCST), also known as its cloud point (T_c), which is typically reported as 32 ^{o}C and is relatively insensitive to polymer concentration so long as the concentration is above 1 g/L.[17-21] At T_c, PNIPAM transitions from soluble coils to dehydrated globules, which form larger aggregates called mesoglobules.[17,22-24] The transition at T_c, also referred to as the coil-to-globule transition (CGT), is very sharp because the process of hydration/dehydration is cooperative[14,25] and results in chains that adopt a pearl necklace conformation in solution.[16] The value of T_c for a given PNIPAM solution depends on a number of factors that include the nature of any functional groups incorporated randomly along the chain or at the chain ends, the polymer molecular weight, and the polymer concentration[8] if the solution is in the dilute region. The nature of the end-groups has a particularly significant effect on telechelic PNIPAM, where hydrophobic end-groups cause T_c to decrease with decreasing molecular weight[7] while hydrophilic end groups result in the opposite trend.

Since PNIPAM turns water-insoluble above T_c, a number of studies have examined the interactions that exist between PNIPAM and either small molecule surfactants[3,26] or hydrophobically modified water-soluble polymers which are not PNIPAM.[2,6] They have shown that the presence of hydrophobic aggregates in solution affects the dehydration-induced aggregation of PNIPAM causing changes in T_c, while PNIPAM is also capable of disrupting hydrophobic aggregates when it undergoes its CGT.[2] These effects are due to the dehydration of

PNIPAM that occurs above T_c and results in the formation of less hydrophilic microdomains capable of interacting with hydrophobic groups. When the hydrophobic groups (referred to as *lip*) are covalently attached to PNIPAM, as is the case for telechelic lip$_2$-PNIPAM, the PNIPAM monomers closest to the hydrophobes are dehydrated below T_c. Accordingly, the PNIPAM chains in solution can be viewed as being composed of three distinct regions: The hydrophobes constitue the first region, the stretches of dehydrated monomers adjacent to the hydrophobes represent the second region, whereas the third region is made of stretches of hydrated monomers.

Like many amphiphilic molecules, lip$_2$-PNIPAM forms micellar aggregates when dissolved in water due to intermolecular hydrophobic interactions. These interactions have been shown to occur even at µM concentrations.[10] A model has been proposed by F.M. Winnik et al. to describe the behaviour of aqueous solutions of lip$_2$-PNIPAM as the temperature increases. This model is based on observations obtained with light scattering, neutron scattering, fluorescence[9,14-16] and other techniques. The key points of the model are presented hereafter.

Below 20 ^{o}C, lip$_2$-PNIPAM forms stable micelles with a three layered onion-like structure. The innermost core is composed of the hydrophobes, the outermost shell is composed of hydrated PNIPAM loops, and the middle region between the two consists of a mixture of water and dehydrated PNIPAM segments. As the temperature increases above 20 ^{o}C, the lip$_2$-PNIPAM solution enters the thermodynamic Regime I, where segments of the PNIPAM loops in the shell begin to dehydrate and collapse into the middle region. Water is expelled from the middle region as the dehydrating chains of the shell collapse into it, leading to a constant volume for the middle region and a decrease in the volume of the shell.[15] As dehydrated PNIPAM chain segments also enter the hydrophobic core, the core becomes more hydrophilic.[9] This behaviour continues until T_c is reached, reported as 31 ^{o}C for the polymer used in these studies.

At T_c, the lip$_2$-PNIPAM solution enters Regime II where the micelles begin to associate with one another to form larger aggregates called mesoglobules. The apparent M_n of PNIPAM mesoglobules increases significantly, while the internal fluidity of the mesoglobules decreases.[9,12] As the temperature approaches the stable mesoglobule temperature of 34 ^{o}C (T_m),[9] the mesoglobules increase in size, while the hydrophobic cores of the micelles within the mesoglobules begin to dissolve and disperse throughout the mesoglobule. At the same time, additional water is expelled from the mesoglobules.[15] Above T_m, the lip$_2$-PNIPAM solution enters Regime III, where mesoglobules stabilize and do not grow any further. At this stage, the mesoglobules are thought to be vitreous in nature.[15] In all three regimes, any structures formed, either micelles or mesoglobules, do not interact with one another if the polymer concentration is below 1 g/L.[14-16] While the solutions of lip$_2$-PNIPAM show a M_n dependence for T_c, T_m is always found to equal 34 ^{o}C regardless of M_n.

The hydrophobic groups present in lip$_2$-PNIPAM, and the manner in which they interact, affect the rheological behaviour of aqueous solutions of this polymer, which makes the determination of the association level and the time scale of interaction between these groups particularly interesting. For a variety of polymers, this has been accomplished by monitoring the fluorescence of pyrene labels covalently attached onto them.[27-30] Fluorescence studies have also been conducted in organic and aqueous solutions[10,11] on a series of pyrene end-labelled PNIPAM samples, referred to as Py$_2$-PNIPAM, where the octadecyl groups used in previous studies[9,15,16,31] were replaced with 1-pyrenebutyl groups. Pyrene was chosen for these studies because it is not only a highly useful fluorescent probe for studying hydrophobically modified polymers,[29,32-35] but it is also strongly hydrophobic. As a result, its presence at the chain-ends of PNIPAM chains

should cause minimal deviation from the typical behaviour observed with lip_2-PNIPAM in aqueous solution.

The study of pyrene-labelled polymers relies on the fluorescence of pyrene, a process which begins when a pyrene molecule absorbs a photon of UV light, leading to its excitation. As this excited pyrene is not interacting with other molecules at the time of excitation, it is referred to as a pyrene monomer. The pyrene monomer has a fluorescence emission spectrum with well-defined peaks in the 370-450 nm region and it fluoresces with a natural lifetime τ_M. If an excited pyrene monomer encounters another pyrene molecule in the ground-state, they are able to form an excited dimer or excimer which possesses its own lifetime τ_{E0} and exhibits a broad featureless fluorescence spectrum between 450 and 550 nm. Excimer may be formed either from pyrenes that encounter one another via diffusion during the time that the pyrene monomer is excited, or it may be formed virtually instantaneously from pyrenes which are associated in the ground-state. The relative amount of hydrophobic associations occurring in a solution of Py_2-PNIPAM can be easily estimated from steady-state fluorescence measurements by comparing the fluorescence intensity of the excimer relative to that of the monomer, although the proportion of excimer formed by diffusion versus the direct excitation of ground-state aggregates cannot be determined from the analysis of the steady-state fluorescence spectra.

The two types of excimer may, however, be differentiated by acquiring the time-resolved fluorescence decay of the excimer. Excimer formation via diffusion takes time, as the two molecules must diffuse towards one another, resulting in a rise time in the excimer decay. By contrast, ground-state dimers generate excimer instantaneously upon excitation, which reduces the importance of the rise time in the excimer decay. Consequently analysis of the rise time in the excimer fluorescence decay provides a quantitative measure of the molar fraction of those

pyrenes that form excimer by diffusion and those pyrenes that are aggregated. The pyrene monomer also consists of two populations: those pyrenes which are capable of forming excimer by diffusion, and those which are isolated and cannot form excimer. These monomer types may also be differentiated in the fluorescence decays, as isolated monomers emit with the single long lifetime of pyrene τ_M while monomers forming excimer by diffusion decay with shorter decay times. The accelerated decay of these latter monomers will be reflected also in the rise time of the excimer decays, since it is the same process which leads to the disappearance of the excited monomer and the creation of the excimer. Once the process of pyrene excimer formation by diffusion has been quantified, its rate constant may be determined to characterize the time scale over which pyrene-pyrene encounters take place.

The present study applies the Model Free Analysis (MFA) to fit the fluorescence decays acquired with a series of Py$_2$-PNIPAM samples as a function of temperature. The parameters retrieved from the MFA of the decays enable the characterization of the behaviour of the Py$_2$-PNIPAM samples in aqueous solution as they pass through T_c and T_m. In turn, the trends obtained through this analysis are interpreted within the framework provided by the model proposed by F.M. Winnik et al.[9,15] to investigate the extent of its validity.

3.3 Experimental

The synthesis of the pyrene-labelled PNIPAM polymers has been described in earlier publications.[11] The number-average molecular weight (M_n) of the samples used in this study can be found in Table 3.1. Py$_1$-PNIPAM refers to the chains singly-labelled with pyrene, while Py$_2$-PNIPAM refers to the doubly-labelled chains. The number in brackets denotes the M_n of the PNIPAM backbone. Unlabelled PNIPAM with a weight-average molecular weight of 20-25

kg/mol, averaged to 22K, was purchased from Sigma-Aldrich and used as received. Ethanol (HPLC grade reagent alcohol) was supplied by Fischer Scientific. Milli-Q water with a resistivity of over 18 MΩ·cm was used to prepare all aqueous solutions.

Table 3.1: Number-average molecular weight (M_n) and polydispersity index (PDI) of the PNIPAM samples and their concentrations for the fluorescence experiments.

Sample	M_n (kg/mol)	Polydispersity Index	Polymer Concentration for Light Scattering and Fluorescence Experiments (g/L)
Py$_2$-PNIPAM(14K)	13.7	1.10	0.017
Py$_2$-PNIPAM(25K)	25.4	1.07	0.032
Py$_2$-PNIPAM(45K)	44.5	1.10	0.056
Py$_1$-PNIPAM(7K)	7.7	1.02	0.018
Py$_1$-PNIPAM(12K)	12.3	1.02	0.030
Py$_1$-PNIPAM(25K)	23.5	1.09	0.059
PNIPAM(22K)	20-25		

Aqueous solutions of the Py$_n$-PNIPAM samples with $n = 1$ or 2 were prepared by dissolving the polymer in ethanol, determining the concentration using the absorbance of the pyrene labels at 344 nm and comparing it to the molar absorbance coefficients of 1-pyrenebutanol in ethanol ($\varepsilon_{Py} = 42250$ mol^{-1}Lcm^{-1}), then transferring a sufficient quantity of this solution into a vial to yield the desired concentration in water. A pyrene concentration of 2.5 μM, equivalent to an absorbance of 0.1, was targeted. This resulted in varying polymer concentration, as shown in Table 3.1. The ethanol was evaporated under a stream of nitrogen before adding the required amount of water to the vial. The solution was vortexed before being allowed to stand for a minimum of 30 minutes at 4 °C. The unlabelled PNIPAM solution was prepared by dissolving a known mass of polymer directly in water and adjusting the concentration via successive dilutions.

Turbidimetry measurements were performed on 0.5 g/L Py-PNIPAM solutions using a Varian Cary 100 Bio UV-Vis spectrophotometer to monitor the absorption at 500 nm as the temperature of the solution was raised at a heating rate of 0.5 $^\circ$C per minute.

Polymer solutions for light scattering and fluorescence experiments used a constant pyrene concentration of 2.5 μM. The corresponding polymer concentrations in g/L are reported in Table 3.1

Light scattering intensity and steady-state fluorescence measurements were conducted using a Photon Technology International LS-100 steady-state fluorometer equipped with a continuous xenon lamp. A fluorescence cell (VWR) with an inner cross section of 10×10 mm^2 was used with right angle geometry, and the solutions were kept aerated. Light scattering measurements were performed by irradiating the sample at 500 nm and monitoring the signal from 490 to 510 nm in 0.5 nm increments. The pyrene fluorescence spectra were acquired by exciting the polymer solutions at 342 nm.

The fluorescence spectrum of the excimer was isolated from the fluorescence spectrum of the monomer using the following procedure: The fluorescence spectrum of the Py$_1$-PNIPAM(25K) sample was used as a "pure" monomer spectrum as its emission intensity between 500 and 530 nm is less than 0.3% of the I_1 peak intensity at 375 nm. All spectra, including the monomer spectra, were normalized to their I_1 peak intensity. The normalized monomer spectrum at the appropriate temperature was subtracted from the corresponding Py$_2$-PNIPAM fluorescence spectrum to yield the excimer fluorescence spectrum. The normalized monomer fluorescence spectra of Py$_1$-PNIPAM(25K) were integrated across their entire wavelength range and the excimer spectra were integrated from 420 to 600 nm to yield I_M and I_E, respectively. The integrated I_M and I_E values were used to calculate the $(I_E/I_M)^{SS}$ ratio. The

isolated excimer fluorescence spectrum was fitted with a polynomial between 435 and 535 nm to determine the wavelength of the fluorescence intensity maximum. Figure S1 in Supporting Information (SI) provides a step-by-step description of the procedure applied to the separation of the fluorescence spectra of the pyrene monomer and excimer.

The fluorescence decay profiles were obtained with a time-correlated single photon counter manufactured by IBH Ltd. using a NanoLED 340 nm diode as the excitation source. Samples were excited at 342 nm, and the emission wavelength was set at 375 nm and 510 nm for the pyrene monomer and excimer, respectively. The samples were placed in a 10×10 mm^2 fluorescence cell (VWR). All decays were collected with the right angle geometry over 1,000 channels with a minimum of 20,000 counts taken at the decay maximum to ensure a high signal-to-noise ratio. A light scattering standard was used to determine the instrument response function (IRF). Analysis of the decays was performed by convoluting the IRF with a sum of typically three exponentials as shown in Eq. 3.1 and comparing the convolution result with the experimental decay. To ensure the reproducibility of the fluorescence decay analysis, decays were acquired in triplicate.

$$i(t) = a_1 \exp(-t/\tau_1) + a_2 \exp(-t/\tau_2) + a_3 \exp(-t/\tau_3) \qquad (3.1)$$

The pre-exponential factors and decay times used in Eq. 3.1 were optimized using the Marquardt−Levenberg algorithm.[36] The quality of the fits was established from the χ^2 values (<1.30) and the random distribution around zero of the residuals and of the autocorrelation function of the residuals.

The number-average ($<\tau_N>$) and weight-average ($<\tau_W>$) lifetimes of the pyrene monomer

fluorescence decays were calculated using Eqs. 3.2 and 3.3, and the polydispersity index (PDI)

of the monomer decays was taken as the ratio $<\tau_W>/<\tau_N>$.

$$\left\langle \tau_N \right\rangle = \frac{\sum a_i \tau_i}{\sum a_i} \tag{3.2}$$

$$\left\langle \tau_W \right\rangle = \frac{\sum a_i \tau_i^2}{\sum a_i \tau_i} \tag{3.3}$$

The parameters a_i and τ_i refer to, respectively, the ith pre-exponential factor and decay time

obtained from the multi-exponential fit of the decays with Eq. 3.1. The number-average lifetime

of the excimer was also obtained by applying Eq. 3.2 to those decay times with positive pre-

exponential factors.

Representative pyrene monomer fluorescence decays and the corresponding fluorescence

spectra are shown in Figure 3.1A and Figure 3.1B, respectively. The relationship between the

PDI and the shape of the monomer decay may be observed in Figure 3.1A, where the upper

decay has a PDI of 1.06 and is thus difficult to differentiate from a monoexponential decay. The

lower decay has a PDI of 1.30 and shows visible curvature in the early portion of the decay. The

magnitude of the curvature reflects the efficiency of excimer formation. The Py_2-PNIPAM(14K)

sample with a more pronounced curvature, and thus a larger PDI, forms more excimer than Py_2-

PNIPAM(25K). This is due to its shorter chain that brings the pyrene end-groups closer

together. This conclusion is confirmed by the fluorescence spectrum of Py_2-PNIPAM(25K)

71

shown in Figure 3.1B that demonstrates that the excimer emission intensity between 450 and 550 nm is strongly reduced for the larger chain as it holds the pyrene labels apart from one another.
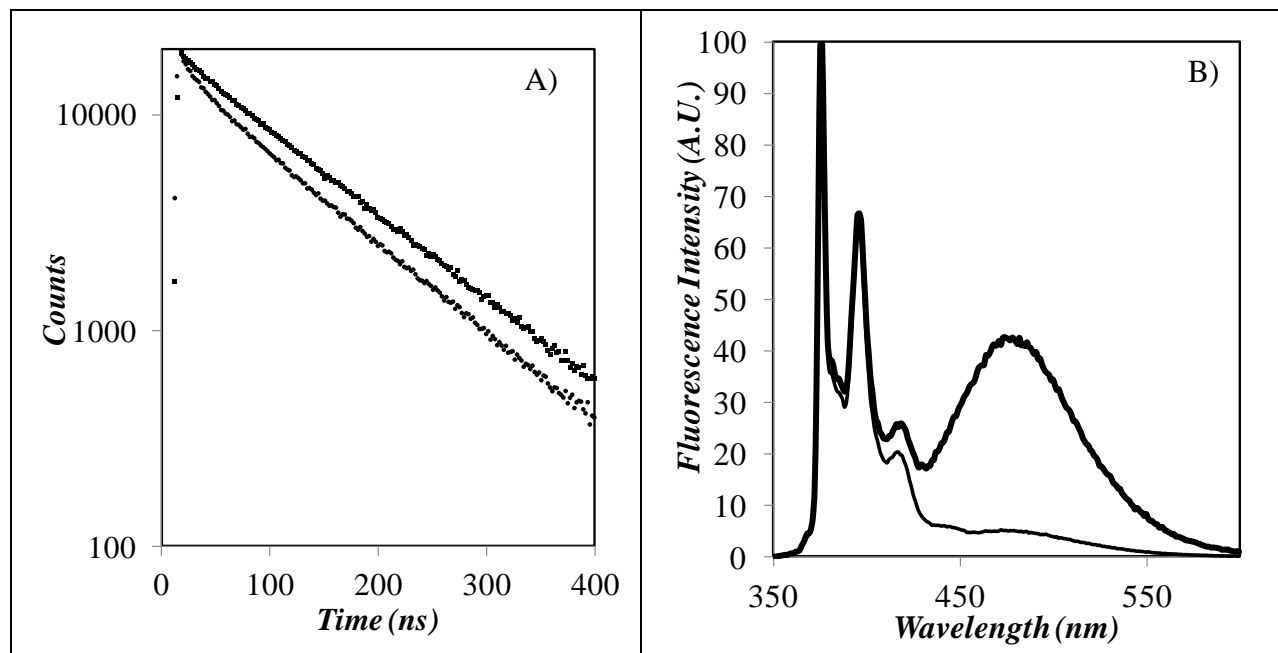
Figure 3.1: Pyrene monomer fluorescence decays and steady-state emission spectra. A) Upper decay: Py$_2$-PNIPAM(14K). Lower decay: Py$_2$-PNIPAM(25K) B) Upper Spectrum: Py$_2$-PNIPAM(14K). Lower spectrum: Py$_2$-PNIPAM(25K)

All decays were fitted using the MFA, which has been described in a number of articles.[37-40] The monomer and excimer decays were fitted with Eqs. 3.4 and 3.5, respectively. In those equations, Py^*_{free} refers to the pyrenes which are unable to form excimer and emit with a lifetime τ_M, Py^*_{diff} refers to the pyrenes which form excimer by diffusion, $E0^*$ refers to the pyrenes which are well stacked in the ground-state, form excimers pseudo-instantaneously upon excitation, and emit with a lifetime τ_{E0}, and EL^* and ES^* refer to pyrenes which are poorly stacked in the

ground-state and form excimers with long (τ_{EL}) and short (τ_{ES}) lifetimes, respectively. The ES^* species was only needed to analyze the excimer decays of the Py$_2$-PNIPAM(25K) sample above T_c.

$$[Py^*]_{(t)} = [Py^*_{diff}]_{(t=0)} \times \sum_{i=1}^{n} a_i \times \exp(-t/\tau_i) + [Py^*_{free}]_{(t=0)} \times \exp(-t/\tau_M) \qquad (3.4)$$

$$
\begin{aligned}
[E^*]_{(t)} = &-[Py^*_{diff}]_{(t=0)} \times \sum_{i=1}^{n} a_i \frac{\dfrac{1}{\tau_i} - \dfrac{1}{\tau_M}}{\dfrac{1}{\tau_i} - \dfrac{1}{\tau_{E0}}} \exp(-t/\tau_i) \\
&+ \left([E0^*]_{(t=0)} + [Py^*_{diff}]_{(t=0)} \times \sum_{i=1}^{n} a_i \frac{\dfrac{1}{\tau_i} - \dfrac{1}{\tau_M}}{\dfrac{1}{\tau_i} - \dfrac{1}{\tau_{E0}}} \right) \times \exp(-t/\tau_{E0}) \\
&+ [EL^*]_{(t=0)} \times \exp(-t/\tau_{EL}) + [ES^*]_{(t=0)} \times \exp(-t/\tau_{ES})
\end{aligned}
\qquad (3.5)
$$

The pre-exponential factors a_i in Eqs. 4 and 5 were normalized such that their sum equals 1, and the analysis was applied globally such that both the decay times τ_i and pre-exponential factors a_i were the same in both equations. The decay times and pre-exponential factors retrieved from the MFA were used to calculate the fluorescence fractions of each species, namely f_{free}, f_{diff}, and f_{agg}. The fraction f_{agg} is equal to the sum of f_{E0} and f_{EL}. The equations used to calculate these fractions can be found in a previous publication.[37] The average rate constant of excimer formation $<k>$ is calculated with Equation 3.6 where $<\tau_N>_M$ is the number average lifetime of the pyrene monomer.

$$< k >= \frac{1}{\langle \tau_N \rangle_M} - \frac{1}{\tau_M} \qquad\qquad (3.6)$$

3.4 Results and Discussion

The solution behaviour of the Py-PNIPAM samples was characterized first by performing turbidimetry measurements on aqueous solutions of Py_2-PNIPAM in order to determine T_c for each polymer solution. The value of T_c for these samples was taken as the temperature at which transmittance crossed the 50% transmittance mark in the traces shown in Figure 3.2A. It was reported in Table 3.2. The value of T_c obtained from the turbidimetry measurements conducted with a polymer concentration of 0.5 g/L was found to increase with increasing M_n as shown in Figure 3.2B and all samples showed effectively complete blockage of the light beam above their respective T_c values. T_c increases with increasing M_n and is a result of the reduction in the content of hydrophobic pyrene associated with an increase in M_n, although T_c appears to plateau. The trends observed in Figure 3.2 are consistent with previous studies.[7,9]

Fluorescence measurements were performed on the Py_2-PNIPAM samples with a pyrene concentration of 2.5 μM. This concentration results in solutions having an absorbance below 0.1 at 342 nm, the absorbance maximum of pyrene, which ensures that fluorescence intensities measured by steady-state fluorescence are proportional to the concentration of the fluorophores in solution. At a nominal pyrene absorbance of 0.1, the aqueous solutions of Py_2-PNIPAM(14K), Py_2-PNIPAM(25K), and Py_2-PNIPAM(45K) have polymer concentrations of 0.03 g/L, 0.06 g/L and 0.11 g/L, respectively. Since the aggregation behaviour of PNIPAM is affected by the concentration of polymer in solution,[8] any conclusions about the LCST of the Py_n-PNIPAM samples drawn from fluorescence experiments would need to be compared to T_c

values obtained by turbidimetry measurements made at the same concentration. Unfortunately, turbidimetry was found to be ineffective at determining T_c for these lower concentration solutions as the change in transmittance was not large enough for a clear determination.
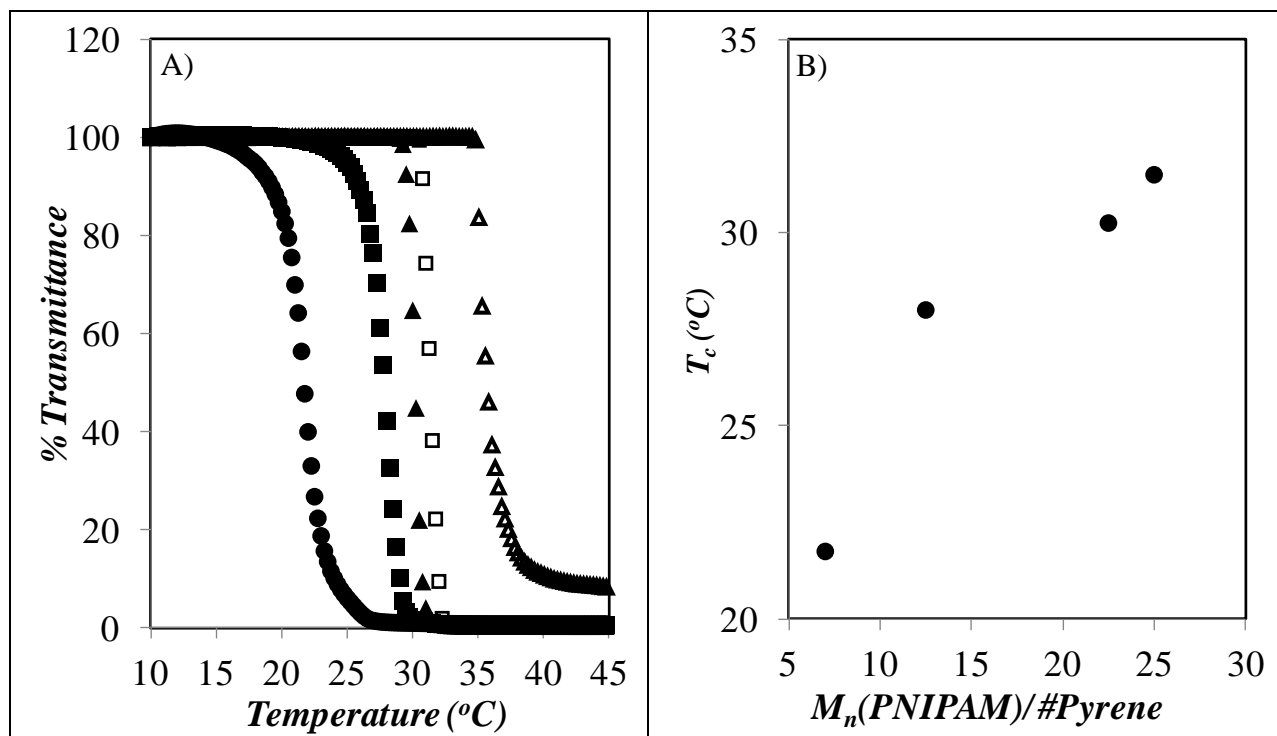
Figure 3.2: Turbidimetry measurements for 0.5 g/L Pyrene-Labeled PNIPAM samples. A: (●) Py$_2$-PNIPAM(14K), (■) Py$_2$-PNIPAM(25K), (▲) Py$_2$-PNIPAM(45K), (□) Py$_1$-PNIPAM(25K), and (△) PNIPAM(22K). B: T_c as a function of the ratio of M_n for the Py-PNIPAM samples over their respective number of pyrenes.

Right-angle light scattering intensity, measured in a steady-state fluorometer at 500 nm where pyrene does not absorb, was used instead to determine the temperature at which aggregation occurs in the solutions used for the fluorescence experiments. The change in light scattering (LS) intensity for aqueous solutions of the Py$_2$-PNIPAM samples is shown in Figure

3.3. For all Py$_2$-PNIPAM samples, the LS intensity is found to increase sharply at a set temperature. The temperature where the LS intensity increases abruptly was taken as the T_c value as done in a previous publication.[31] To this end, lines were drawn through the data points below and above the sharp increase and their intersection point was found. T_c was found to equal 24, 28, and 28 °C for Py$_2$-PNIPAM(14K), Py$_2$-PNIPAM(25K), and Py$_2$-PNIPAM(45K), respectively.
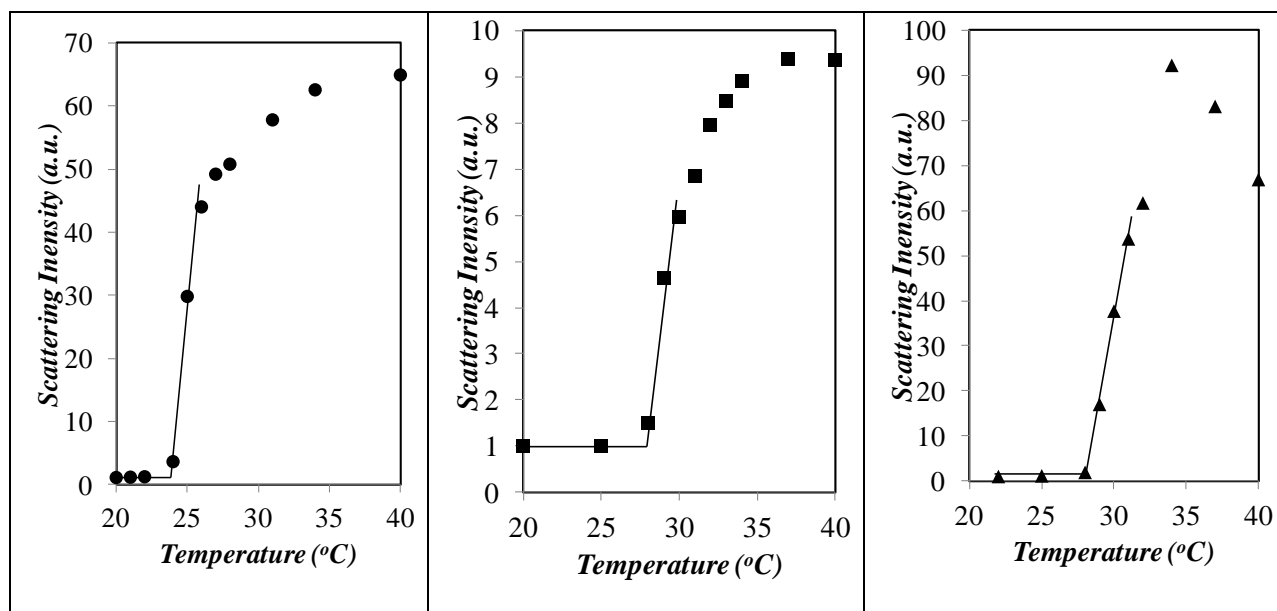
Figure 3.3: Normalized light scattering intensity of Py$_2$-PNIPAM samples as a function of temperature, Abs(342nm) = 0.1. (●) Py$_2$-PNIPAM(14K), (■) Py$_2$-PNIPAM(25K), and (▲)Py$_2$-PNIPAM(45K).

These results led to the conclusion that under dilute conditions, the pyrene content affects the value of T_c for pyrene-labeled PNIPAM, but the relationship is not clearly proportional to M_n contrary to what was observed in Figure 3.2B and Table 3.2 for the more concentrated solutions characterized by turbidimetry measurements.

Having determined the temperatures at which dilute solutions of Py_2-PNIPAM samples went through their cloud point, steady-state fluorescence spectra of the solutions were acquired for each sample. A light scattering correction was applied by subtracting the spectrum obtained from the light scattered by a non-fluorescently labelled PNIPAM(22K) solution at the same polymer concentration, scaled for intensity, from the fluorescence spectrum of the Py_2-PNIPAM solution. The spectra obtained for the Py_2-PNIPAM(14K) solution, normalized to the intensity of the I_1 peak of the pyrene monomer at 375 nm, are presented in Figure 3.4. The intensity of the excimer increases as the temperature increases until T_c is reached, at which point the excimer intensity decreases and its wavelength maximum undergoes a blue shift.

Table 3.2: Comparison of the T_c values determined by turbidimetry and light scattering.

Sample	T_c (^{o}C) (Turbidimetry)	T_c (^{o}C) (Light Scattering)
Py_2-PNIPAM(14K)	21.75	24
Py_2-PNIPAM(25K)	28.00	28
Py_2-PNIPAM(45K)	30.25	28
Py_1-PNIPAM(25K)	31.50	
PNIPAM(22K)	35.75	

The relationship between temperature and excimer intensity was further investigated by the determination of the ratio of the fluorescence intensity of the excimer over that of the monomer, namely the $(I_E/I_M)^{SS}$ ratio. The position of the excimer fluorescence maximum (λ_{max}) was also determined. Both $(I_E/I_M)^{SS}$ and λ_{max} are shown in Figure 3.5.

The changes observed in the fluorescence spectra of the Py_2-PNIPAM samples are of interest, as they provide an additional test of the behaviour predicted by the model proposed by F.M. Winnik et al. for lip_2-PNIPAM.[9,14-16] According to this model, the hydrophobic end-groups of lip_2-PNIPAM associate below T_c and the chains form flower-like micelles. As the solution

transitions through Regime I, these micelles undergo a number of conformational changes including a decrease in volume,[15] which in the case of Py$_2$-PNIPAM should result in a higher local pyrene concentration and thus the possibility of faster kinetics of excimer formation.
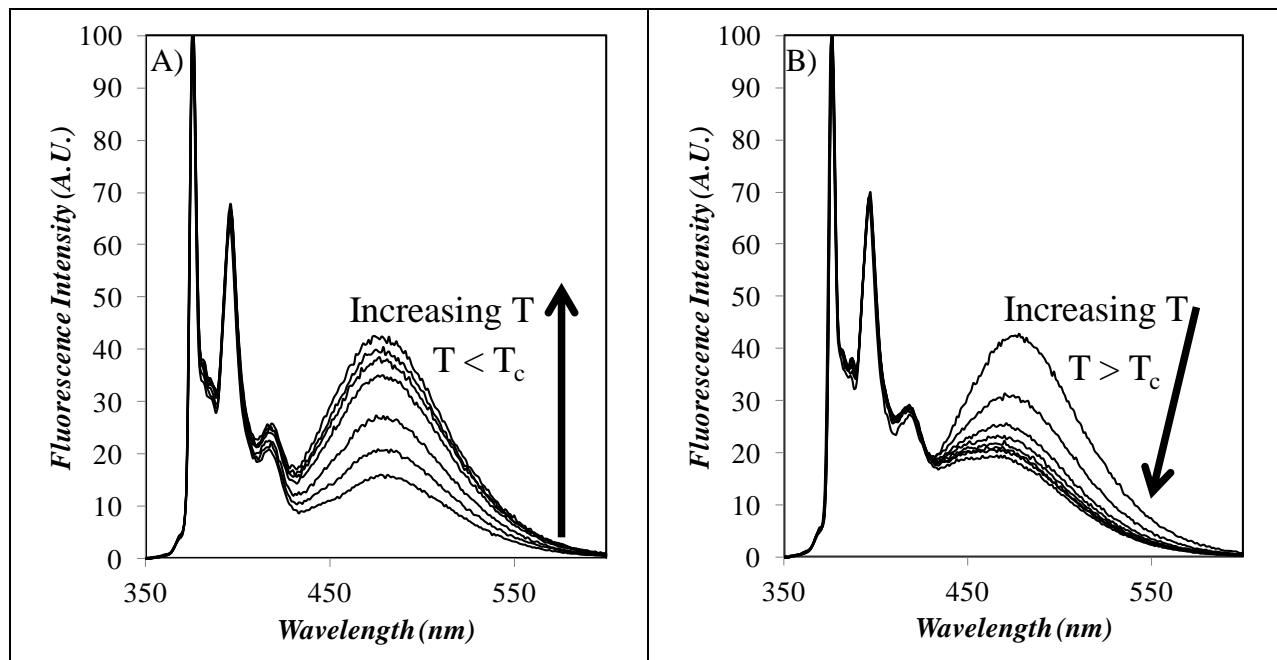
Figure 3.4: Steady-state fluorescence spectra for Py$_2$-PNIPAM(14K) at different temperatures. A) T increases from 15 to 23 $^{\circ}$C. B) T increases from 24 to 40 $^{\circ}$C.

All Py$_2$-PNIPAM samples showed a maximum in $(I_E/I_M)^{SS}$ at the same temperature where a sharp transition was observed in Figure 3.3 by light scattering. Although the value of $(I_E/I_M)^{SS}$ increases with increasing temperature in Regime I, no significant increase in light scattering was observed over the same temperature range (see Figure 3.3). The maximum of the broad structureless emission of the excimer shifted to lower wavelength once the samples were above T_c in Region II, as seen in the inset of Figure 3.5. The blue shift in the excimer emission wavelength in Region II indicates an increase in the relative amount of aggregated pyrene[41,42] as the polymer undergoes its cloud point transition. The drop in $(I_E/I_M)^{SS}$ above T_c might be due to

78

a change in the amount of pyrene excimer being generated from diffusive encounters between pyrene labels relative to the amount of excimer formed from the direct excitation of ground-state pyrene aggregates. The decrease in $(I_E/I_M)^{SS}$ could also be caused by a decrease in the rate constant of excimer formation, or some combination of both of these phenomena. These two phenomena are expected to occur when the hydrated PNIPAM coils pass through their cloud point and collapse to form stiffer domains composed of dehydrated PNIPAM chains that hinder diffusive encounters between the pyrene labels and favor their aggregation.
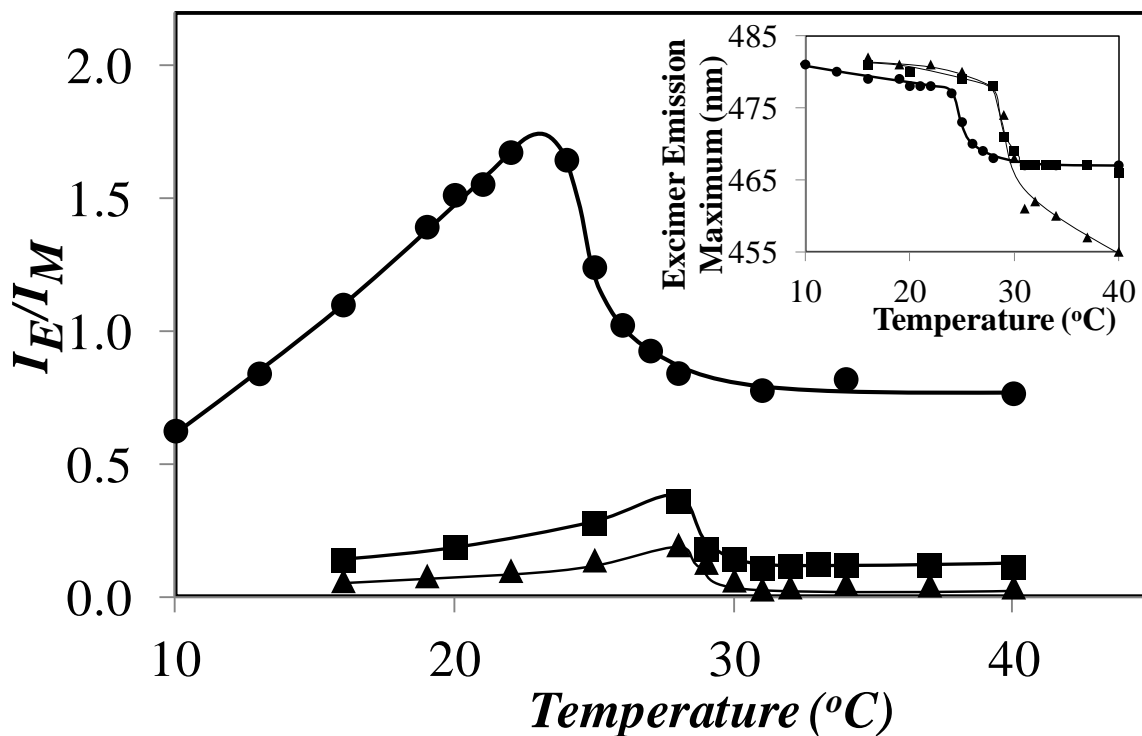
Figure 3.5: $(I_E/I_M)^{SS}$ ratio for PNIPAM in water as a function of temperature. Inset: Wavelength at the excimer intensity maximum. (●) Py$_2$-PNIPAM(14K), (■) Py$_2$-PNIPAM(25K), and (▲) Py$_2$-PNIPAM(45K).

While the steady-state fluorescence and light scattering measurements provided useful information on the aggregation behavior of the Py$_2$-PNIPAM samples, they did not give direct information on the kinetics describing the interactions between the hydrophobes. Time-resolved fluorescence decays of the pyrene monomer and excimer emission of Py$_2$-PNIPAM aqueous solutions were acquired, and they were first analyzed by performing a tri-exponential fit with Eq. 3.1. The PDI and number-average lifetime, $\langle\tau_N\rangle_M$, of the pyrene monomer decay were plotted as a function of temperature in Figure 3.6. The determination of T_c from the trends obtained with $\langle\tau_N\rangle_M$ was carried out according to the same protocol which was used for LS. A detailed error analysis of the value of T_c was prevented by the small number of data points in the linear region above T_c, leading to an unrealistic propagated error of up to 10 ^{o}C. The resolution of the temperature controller was 1 ^{o}C. Therefore, the error in the value of T_c based on trends obtained with $\langle\tau_N\rangle_M$ in Figure 3.6 should not be significantly larger than 1 ^{o}C.

At temperatures lower than T_c, $\langle\tau_N\rangle_M$ was found to decrease with increasing temperature for the Py$_2$-PNIPAM(14K), Py$_2$-PNIPAM(25K), and Py$_2$-PNIPAM(45K) samples. Above their respective T_c of 25 ^{o}C, 28 ^{o}C, and 29 ^{o}C, $\langle\tau_N\rangle_M$ increased with increasing temperature. The T_c values determined using $\langle\tau_N\rangle_M$ are slightly higher than those obtained with $(I_E/I_M)^{SS}$ or light scattering, which implies that the parameters retrieved from the pyrene monomer fluorescence decays may be less sensitive to the changes occurring in solution than parameters derived from steady-state fluorescence spectra. The polydispersity index (PDI) of the monomer decays was obtained by taking the ratio $\langle\tau_W\rangle_M/\langle\tau_N\rangle_M$. The PDI reflects the deviation of the monomer decay from monoexponential behaviour. The PDI of the decay showed a temperature dependence that is inverted when compared to that of $\langle\tau_N\rangle_M$. In fact, the PDI trends in Figure 3.6B paralleled closely those obtained with $(I_E/I_M)^{SS}$ in Figure 3.5. The decrease in $\langle\tau_N\rangle_M$ as the

temperature approaches T_c may be reasonably explained by an increase in the amount of excimer being formed by diffusion. This is supported by the increase in PDI reflecting greater curvature of the decay also resulting from excimer formation.
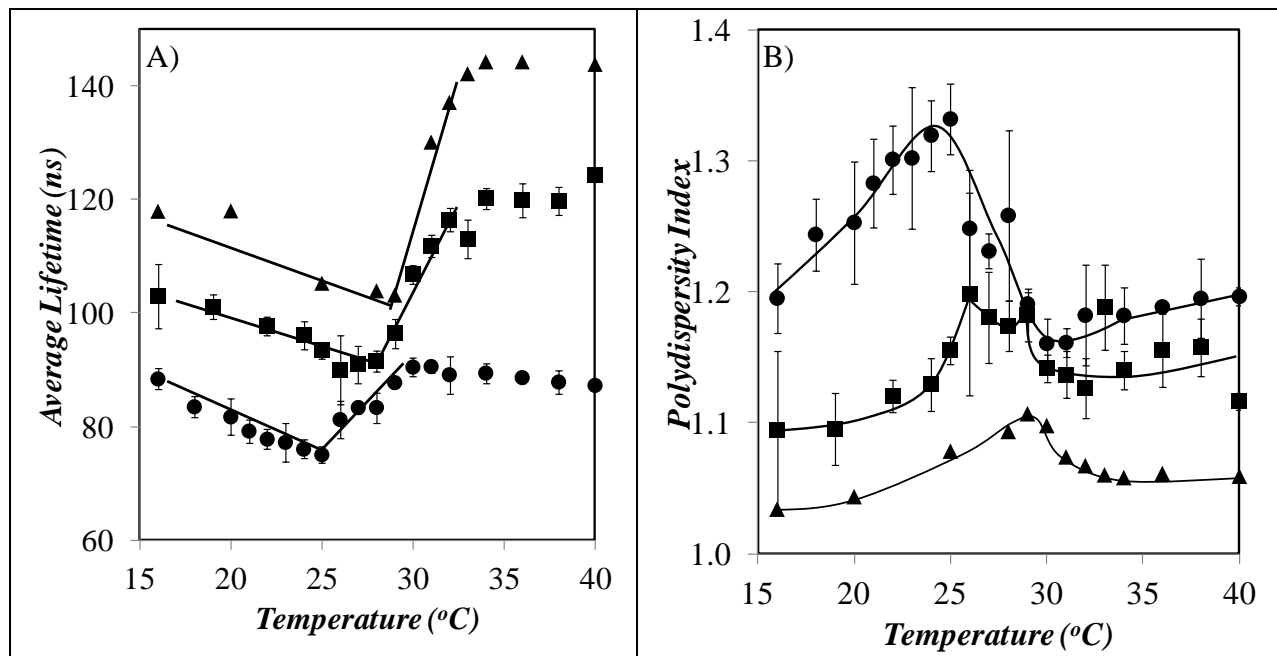
Figure 3.6: A) Number-average lifetime of the pyrene monomer decays for the pyrene labelled PNIPAM samples in water as a function of temperature. B) Polydispersity index of the pyrene monomer decays as a function of temperature. ($\bullet$) Py$_2$-PNIPAM(14K), ($\blacksquare$) Py$_2$-PNIPAM(25K), and ($\blacktriangle$) Py$_2$-PNIPAM(45K).

Above T_c, the monomer lifetime increases significantly due to a decrease in both the quenching efficiency of oxygen and the rate of excimer formation due to the decrease in local mobility associated with the collapse of the dehydrated PNIPAM. The decrease in PDI observed above T_c also supports a reduction in diffusional excimer formation. All of these results are in agreement with the steady-state fluorescence data, showing a maximum level of excimer formation around T_c. Accordingly, both $<\tau_N>_M$ and PDI can be viable tools for determining the

T_c value of Py$_2$-PNIPAM solutions, although it seems that PDI assigns the onset of the CGT to a higher temperature than was observed by LS (see Table 3.2). Above 34 ^{o}C, both $<\tau_N>_M$ and PDI remained constant within experimental error.

Having accounted for the trends obtained from the analysis of the monomer decays, we will now consider the trends obtained with the excimer decays. Thus multi-exponential fits of the excimer decays were also performed, and the average lifetime of the excimer $<\tau_N>_E$ and the ratio a_{E-}/a_{E+} were plotted as a function of solution temperature in Figure 3.7. The ratio a_{E-}/a_{E+}, equal to the sum of the negative pre-exponential factors over the sum of the positive pre-exponential factors retrieved from the fit of the excimer decay with Equation 3.1, is a measure of the amount of excimer formed by diffusion. A value of 0 for a_{E-}/a_{E+} indicates full aggregation while a value of -1 indicates purely diffusion-controlled excimer formation.

The $<\tau_N>_E$ values for Py$_2$-PNIPAM in Figure 3.7A show a significant increase at the expected T_c of the samples, based on the temperatures which were seen to affect the monomer decays in Figure 3.6. As with the monomer decays, $<\tau_N>_E$ increases with decreasing oxygen quenching and a less efficient process of excimer formation. The general trend for a_{E-}/a_{E+} agrees with the trends obtained with the other parameters, becoming less negative as T_c is reached due to an increase in the molar fraction of aggregated pyrenes. The large error bars observed for Py$_2$-PNIPAM(25K) below T_c reflect large variations in a_{E-}/a_{E+} for decays obtained in this temperature range.

At this stage, the light scattering intensity, the $(I_E/I_M)^{SS}$ ratios, the average monomer $<\tau_N>_M$ and excimer $<\tau_N>_E$ decay times, the polydispersity index of the monomer decays (PDI), and the ratio a_{E-}/a_{E+} have all been shown to undergo significant changes around T_c for each

sample studied. Thus it stands to reason that these parameters may also be used to determine T_c. The T_c value retrieved from these trends have been reported in Table 3.3. As the T_c values show a fairly narrow distribution, they are best reported as an aggregate value, all of which are shown in Table 3.3.
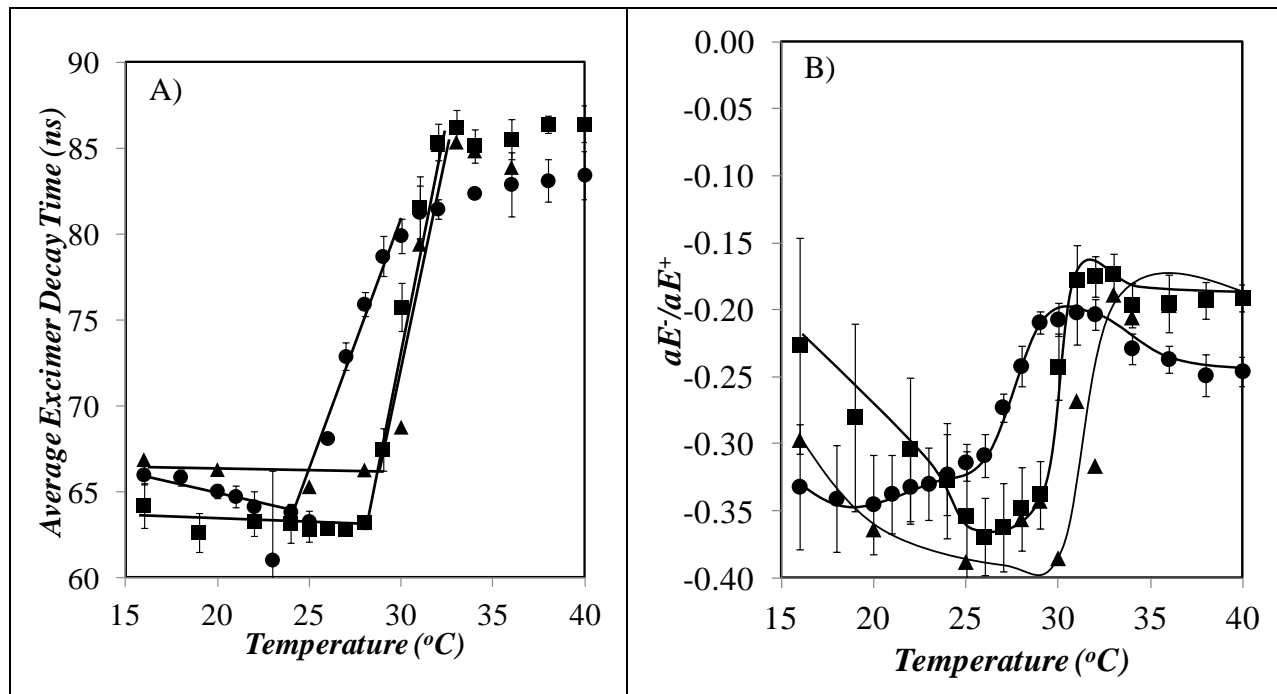
Figure 3.7: A) $<\tau_N>_E$ obtained with decay times having positive pre-exponential factors and B) a_{E^-}/a_{E^+} ratio as a function of solution temperature. both: (●) Py$_2$-PNIPAM(14K), (■) Py$_2$-PNIPAM(25K), and (▲) Py$_2$-PNIPAM(45K)

Table 3.3: T_c values obtained from the study of aqueous solutions of the Py$_2$-PNIPAM samples with different techniques.

Sample	T_c (^{o}C) as determined by:							
	L.S.	$(I_E/I_M)^{SS}$	$<\tau_N>_M$	PDI	$<\tau_N>_E$	a_{E-}/a_{E+}	$<k>$ (MFA)	Average
Py$_2$-PNIPAM(14K)	24	24	25	26	24	27	25	25.0 ± 1.2
Py$_2$-PNIPAM(25K)	28	29	28	30	28	30	29	28.9 ± 0.9
Py$_2$-PNIPAM(45K)	28	29	29	31	29	31	N/A	29.5 ± 1.2

The cloud point transition temperature of each solution was determined by the average of the T_c values measured by the techniques listed in Table 3.3. As shown in Table 3.3, a maximum spread of approximately 1 ^{o}C is obtained for all three Py$_2$-PNIPAM samples, likely due to the fact that certain techniques probe the transition at either the high or low end of the temperature distribution. Light scattering and $(I_E/I_M)^{SS}$ give the lowest transition temperatures, while the PDI and a_{E-}/a_{E+} ratio retrieved from the fluorescence decay analysis give the highest transition temperatures, implying that lifetime-derived parameters may not be as sensitive to the cloud point transition.

The characterization of the thermal response of solutions of Py$_2$-PNIPAM was followed by the study of the semi-telechelic Py$_1$-PNIPAM samples. To this end, the light scattering intensity, the $(I_E/I_M)^{SS}$ ratio, the decay times $<\tau_N>_M$, and PDI were obtained from the analysis of the steady-state fluorescence spectra and time-resolved fluorescence decays of aqueous solutions of Py$_1$-PNIPAM(7K), Py$_1$-PNIPAM(12K), and Py$_1$-PNIPAM(25K). The trends obtained by plotting these parameters as a function of temperature are shown in Figure 3.8.

The light scattering intensity, presented in Figure 3.8A, shows a sharp increase at 30 $^{\circ}$C for all three samples. Based on the trends obtained by light scattering, the transition at 30 $^{\circ}$C was assigned to T_c. After a sharp rise, the light scattering intensity reached a plateau whose value increased with increasing M_n. The $(I_E/I_M)^{SS}$ ratio in Figure 3.8B underwent significant changes for the Py$_1$-PNIPAM(7K) and Py$_1$-PNIPAM(12K) samples as the temperature increased past T_c, while $(I_E/I_M)^{SS}$ remained small and relatively constant for Py$_1$-PNIPAM(25K). The $\langle\tau_N\rangle$ behavior of the Py$_1$-PNIPAM samples shown in Figure 3.8C closely resembles that of the Py$_2$-PNIPAM samples, increasing at T_c and plateauing above T_m while the PDI values in Figure 3.8D were all smaller than 1.15 and did not show much of a change at T_c.

The trends observed with the Py$_1$-PNIPAM samples exhibit some features that are similar to those obtained with the Py$_2$-PNIPAM samples. The light scattering intensity, $(I_E/I_M)^{SS}$, and $\langle\tau_N\rangle$ show a pronounced change at T_c. There are however significant differences between the two families of Py-PNIPAM samples. The Py$_1$-PNIPAM samples do not show any M_n dependence with regard to T_c as determined by light scattering, $(I_E/I_M)^{SS}$, or $\langle\tau_N\rangle$. $\langle\tau_N\rangle$ remains constant with temperature in Regime I, and $(I_E/I_M)^{SS}$ does not pass through a maximum at T_c but instead, begins to increase with increasing temperature once T_c is reached for the Py$_1$-PNIPAM(7K) and Py$_1$-PNIPAM(7K) samples.

Figure 3.8: Light scattering and fluorescence results for aqueous solutions of the Py$_1$-PNIPAM samples. (●) Py$_1$-PNIPAM(7K), (■) Py$_1$-PNIPAM(12K), and (▲) Py$_1$-PNIPAM(25K). A) Light scattering intensity.; B) $(I_E/I_M)^{SS}$; C) $<\tau_N>_M$; D) PDI.

The differences in behaviour for $<\tau_N>$ and $(I_E/I_M)^{SS}$ between the Py$_1$-PNIPAM samples and their corresponding Py$_2$-PNIPAM samples are best explained by the fact that Py$_1$-PNIPAM forms significantly less excimer than Py$_2$-PNIPAM. As the temperature increases in Regime I, $<\tau_N>$ and $(I_E/I_M)^{SS}$ for Py$_1$-PNIPAM remain constant because each chain contains only one pyrene. Thus a decrease in the radius of gyration of the chains has no effect on pyrene excimer formation for these singly labelled chains. When mesoglobules form in Regime II, the significant reduction in the mobility of pyrene does not result in a decrease in $(I_E/I_M)^{SS}$ as was observed for the Py$_2$-PNIPAM polymers in Figure 3.5 since very little diffusional excimer was present before the transition which could be affected by this change. Instead, the aggregation of chains into larger particles actually increases the local pyrene concentration and allows more excimer to form. While interesting in its own right, the characterization of the Py$_1$-PNIPAM samples also provides the value of the monomer lifetime in Regimes I, II, and III, which is necessary for a more complete analysis of the fluorescence decays according to the Model Free Analysis (MFA) conducted hereafter on the Py$_2$-PNIPAM samples.

The trends observed for $(I_E/I_M)^{SS}$, PDI, and a_{E-}/a_{E+} for the Py$_2$-PNIPAMs suggest that the molar fractions of pyrenes that do not form excimer, form excimer by diffusion, or are involved in pyrene aggregates, respectively, undergo significant changes as T_c is reached, with the additional strong likelihood that the rate constant for excimer formation $<k>$ is also affected. Quantitative information about the molar fractions of the different pyrene species and the average rate constant of excimer formation was obtained through MFA of the monomer and excimer fluorescence decays. To improve the accuracy of the parameters retrieved from the MFA, the lifetimes τ_M, τ_{E0}, τ_{EL}, and τ_{ES} were all fixed in the final analysis of the fluorescence decays. The only parameters that were optimized were the coupled lifetimes (τ_i) and the pre-

exponential factors (a_i) in Eqs. 3.4 and 3.5. Since any variation of the lifetimes was found to have a significant impact on the values obtained for the fluorescence fractions, great care was taken to ensure their accuracy.

The value of τ_M was obtained using the Py$_1$-PNIPAM samples as model compounds for the Py$_2$-PNIPAM samples with equivalent M_n. The longest lifetime of the tri-exponential fits of the monomer fluorescence decays of Py$_1$-PNIPAM(12K) were used as the value of τ_M for Py$_2$-PNIPAM(14K) across the entire temperature range in this study. The long decay times below T_c for Py$_1$-PNIPAM(12K) were averaged, as were the decay times above T_c. The value of these decay times are reported in Table 3.4. The same procedure was applied to the monomer decays of Py$_1$-PNIPAM(25K) to determine the values of τ_M above and below T_c for Py$_2$-PNIPAM(25K). The value of τ_M for both Py$_1$-PNIPAM samples at T_c was between the two averaged values below and above T_c. Consequently the specific value of the long lifetime for Py$_1$-PNIPAM(25K) was used for τ_M for the Py$_2$-PNIPAM samples at T_c. The average T_c listed in Table 3.2 was used to select the τ_M values below and above T_c for the Py$_2$-PNIPAM samples.

Table 3.4: Free pyrene monomer lifetimes (τ_M) used in the MFA of the Py$_2$-PNIPAM samples determined from the fluorescence decays acquired with Py$_1$-PNIPAM.

Sample	Average T_c (^{o}C)	τ_M below T_c (^{o}C) (ns)	τ_M at T_c (^{o}C) (ns)	τ_M above T_c (^{o}C) (ns)
Py$_2$-PNIPAM(14K)	25	113	126	140
Py$_2$-PNIPAM(25K)	29	123	150	169

The value of τ_{E0} was obtained by first fitting the Py$_2$-PNIPAM(12K) decays globally with Eqs. 3.4 and 3.5 and allowing τ_{E0} and τ_{EL} to be optimized in the analysis. The values of τ_{E0} for all temperatures not within 2 ^{o}C of T_c were averaged. The resulting value of 51 ns was used as

88

the value of τ_{E0} to be fixed in the analysis. The values obtained for τ_{EL} were found to be relatively contant across each thermodynamic regime and were averaged. The values obtained for τ_{EL} for Regimes I, II, and III were 88.5, 112, and 118 ns, respectively. The MFA was then repeated for all the fluorescence decays with τ_M, τ_{E0}, and τ_{EL} fixed in the analysis.

The analysis of the Py$_2$-PNIPAM(25K) decays was performed using the same procedure, with an initial round of fitting performed with τ_M fixed while τ_{E0} and τ_{EL} were optimized. The value of τ_{EL} was averaged above T_c, which yielded 135 ns, while below T_c τ_{EL} was found to be unnecessary to achieve a good fit of the data and therefore was not used. The value of τ_{E0} was found to be both highly variable and unusually low. Thus the lifetime of 51 ns obtained from the fits of the Py$_2$-PNIPAM(12K) decays was used as τ_{E0} and fixed in the analysis. The short decay time τ_{ES} was necessary to fit the Py$_2$-PNIPAM(26K) decays, and was fixed at 3.5 ns as done in a previous publication.[43] With the lifetimes τ_M, τ_{E0}, τ_{ES}, and τ_{EL} fixed to their appropriate values, a second round of fitting was performed on the Py$_2$-PNIPAM(26K) fluorescence decays. The results of the application of MFA for both Py$_2$-PNIPAM samples are reported in Figure 3.9.

The value of $<k>$ for Py$_2$-PNIPAM(14K), shown in Figure 3.9A, was relatively high and close to 2×10^7 s^{-1} in Region I, dropping significantly at T_c and staying at a consistently lower value near 0.5×10^7 s^{-1} throughout regions II and III. This drop in $<k>$ reflects a significant reduction in either the mobility of pyrene, and by extension the PNIPAM chains to which they are attached, or significant dilution of the pyrene labels once mesoglobule formation occurs. The standard deviation error bars attaced to $<k>$, obtained by acquiring the fluorescence decays in triplicate, are significantly smaller above T_c, implying that the fits of the decays below T_c are more prone to variance. As a further demonstration that the transition at T_c observed for $<k>$ in Figure 3.9A for Py$_2$-PNIPAM(14K) was due to a CGT, the fluorescence decays of Py$_2$-

PNIPAM(14K) were acquired in ethanol as a function of temperature, and they were analyzed according to the MFA and Birks' scheme to yield k_{cy} and $\langle k \rangle$, which are plotted in Figure SI3.3 as a function of temperature. PNIPAM remains soluble in ethanol and both k_{cy} and $\langle k \rangle$ increased continuously with temperature and showed no transition at $T_c = 25\ ^\circ C$, contrary to what was observed in water for $\langle k \rangle$. Furthermore, $\langle k \rangle$ for Py_2-PNIPAM in water was about one order of magnitude larger than either k_{cy} or $\langle k \rangle$ for Py_2-PNIPAM in ethanol at temperatures smaller than T_c. This result further confirms that the pyrenyl pendants are much closer to each other in water than they are in ethanol, a consequence of their hydrophobicity.

The values for f_{diff} and f_{agg} increased with increasing temperature in Region I while f_{free} decreased, indicating a decrease in coil size as T_c is approached. Increasing the temperature above T_c caused a massive drop in f_{free} and an increase in f_{diff} which is consistent with solvated PNIPAM coils dehydrating, collapsing, and forming mesoglobules that bring the pyrene labels close to each other. Above T_c, the values for f_{agg} and f_{diff} show some small variations, while f_{free} increases from its minimum at T_c until it reaches a new, stable maximum at T_m (34 $^\circ C$).

At temperatures greater than T_m, f_{free}, f_{agg}, and f_{diff} remained essentially constant in Region III. These changes are consistent with the full melting of micellar structures within the mesoglobule once T_m is reached, followed by a stabilization of the resulting polymeric assembly in Region III. These trends are best explained using the Model developed by Winnik et al. for lip_2-PNIPAM in aqueous solution,[9,14-16] a schematic representation of which may be found in Scheme 3.1. An application of the model to describe the behaviour of the Py_2-PNIPAM samples would read as follows.
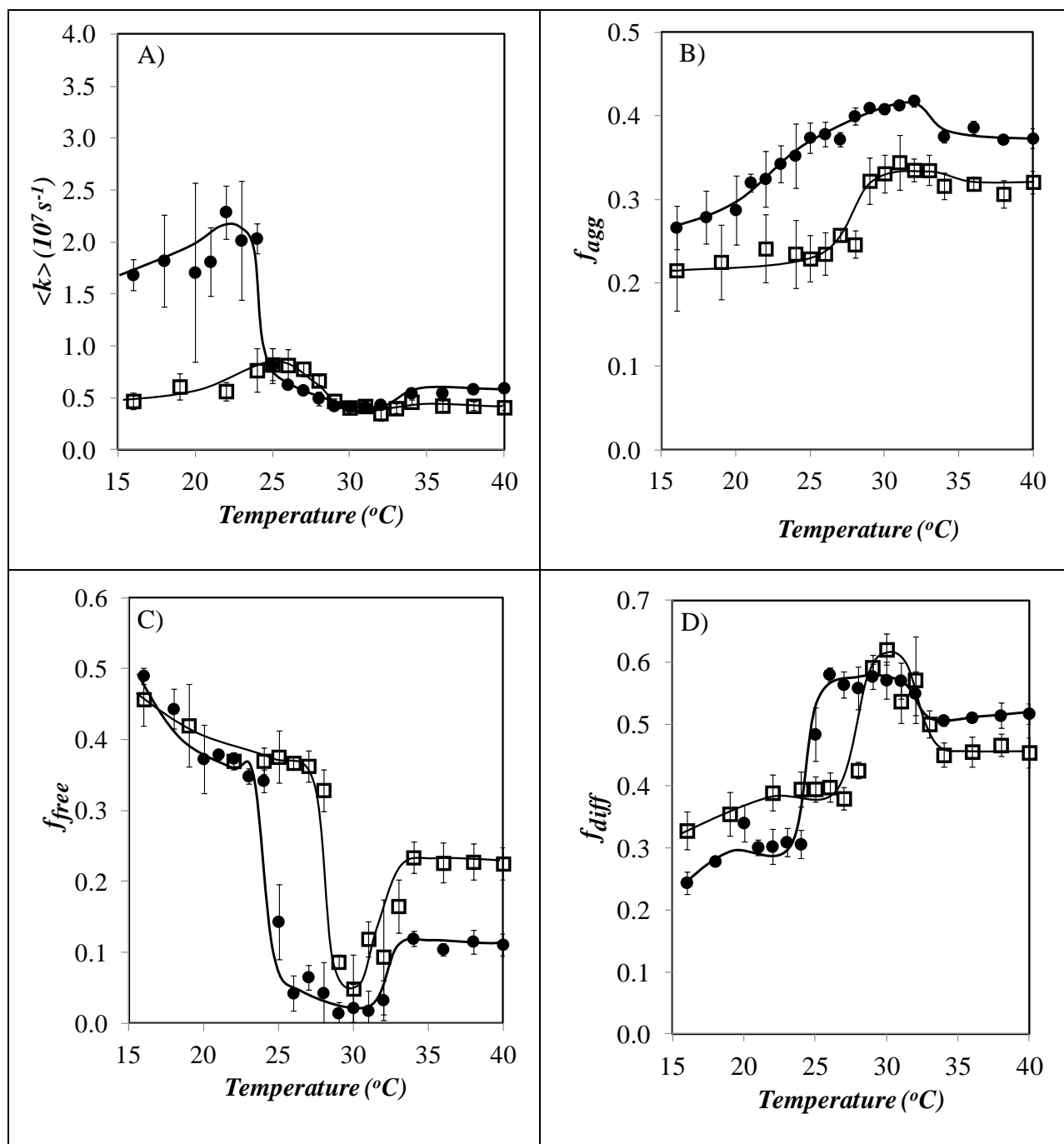
Figure 3.9: MFA results for the Py$_2$-PNIPAM samples. ($\bullet$) Py$_2$-PNIPAM(14K), ($\square$)Py$_2$-PNIPAM(25K). A) Average rate constant for diffusional excimer formation. B) Fraction of aggregated pyrenes. C) Fraction of pyrenes incapable of forming excimer. D) Fraction of pyrenes forming excimer by diffusion.

In Region I, Py$_2$-PNIPAM forms micelles containing a hydrophobic pyrene core, a hydrated PNIPAM shell and a middle region composed of dehydrated PNIPAM segments. The kinetics of pyrene excimer formation are determined by two populations of pyrenes, those in the shell and those in the core or middle region. Pyrene groups in the core and middle region are close enough to one another to form excimer, either by aggregating in the ground-state or via a diffusive process with a small $<k>$. The shell contains pyrenes that are either able to form excimer via a diffusive process with a large $<k>$, or are isolated and therefore unable to form excimer. The parameter $<k>$ depends on both the mobility and local concentration of pyrene. As such, the higher value for $<k>$ found for pyrenes in the shell of the micelle reflects either greater local mobility or greater local concentration. Pyrene may be found in the shell because of the pearl necklace conformation that hydrated PNIPAM adopts in solution, and the dehydrated PNIPAM in the pearls is sufficiently hydrophobic to solubilize pyrene. As the temperature approaches T_c, the coils contract and increase the local pyrene concentration. As this phenomenon unfolds, it leads to a reduction in the fraction of pyrenes that are too isolated to form excimer (f_{free} decreases gently with increasing temperature in Figure 3.9C), an increase in the fraction of aggregated pyrenes (f_{agg} increases gently in Figure 3.9B), while not significantly altering the rate of excimer formation and the fraction of pyrenes forming excimer by diffusion ($<k>$ and f_{diff} remain constant within experimental error in Figure 3.9A and D, respectively).
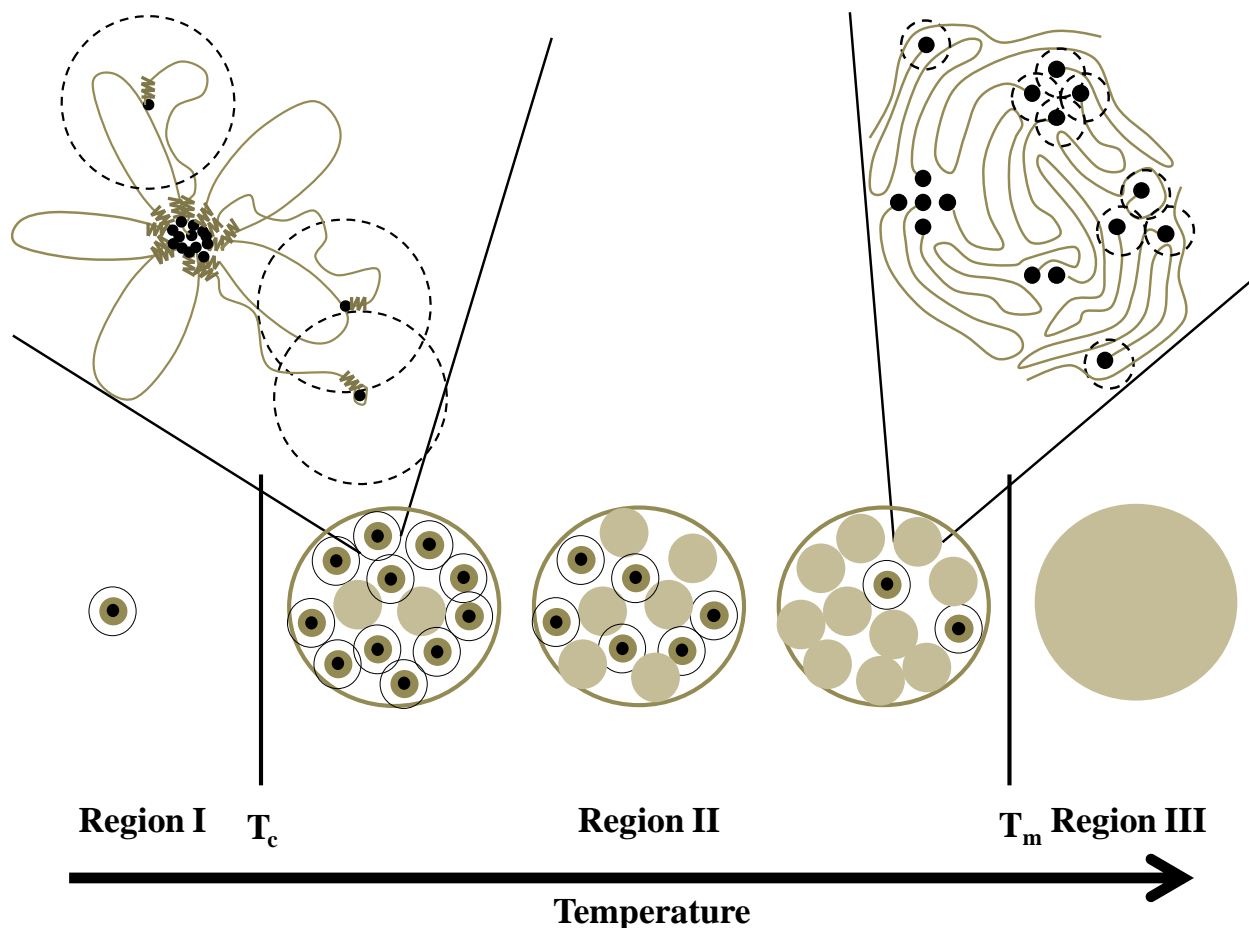
Scheme 3.1: Effect of temperature on the distribution of the pyrene species and the morphology of the lip$_2$-PNIPAM chains.

As the temperature increases past T_c, the solution enters Region II and the Py$_2$-PNIPAM micelles associate to form mesoglobules, which are initially composed of collapsed micelles. One significant consequence of mesoglobule formation is that intermicellar associations should occur initially between the shells of each micelle. Since the shell is the primary location of isolated pyrenes, and intermicellar associations would bring these peripheral pyrenes into close proximity with one another, they could begin to form excimer either by diffusion or direct

excitation of aggregated pyrenes. The main result of this process is a reduction of the amount of free pyrene present, as was observed for f_{free} in Figure 3.9C and an increase in f_{diff} in Figure 3.9D.

Pyrenes inside a mesoglobule in Region II are surrounded by dehydrated PNIPAM chains and are either aggregated, isolated in the dehydrated PNIPAM matrix, or close enough to one another to form excimer by a slow diffusive process. The slow kinetics of excimer formation are due to the higher viscosity of the aggregated PNIPAM chains. However, the existence of diffusional excimer formation shows that the system is not kinetically frozen. As the temperature increases in Region II, the hydrophobes in the collapsed micelles dissolve in the dehydrated PNIPAM matrix, while the apparent molecular weight of the mesoglobules increases due to the agglomeration of smaller mesoglobules to form larger particles.[9] Dissolution of the hydrophobes leads to an increase in the molar fraction of isolated pyrenes (f_{free}) in Figure 3.9C at T_{m}. Once the solution temperature passes through T_{m} at 34 $^{\text{o}}$C to enter Region III, the fully dehydrated mesoglobules have reached a stable state, and the distribution of the three pyrene species stabilizes. This is reflected in the constant values observed for $<k>$, f_{agg}, f_{free}, and f_{diff} for temperatures greater than T_{m}.

The MFA parameters retrieved for Py$_2$-PNIPAM(25K), particularly f_{free}, f_{diff}, and f_{agg}, show trends above T_{c} which agree very well with those obtained for Py$_2$-PNIPAM(14K). The relative values of the fractions depend on the pyrene content of the polymer, with the Py$_2$-PNIPAM(25K) sample showing higher f_{free}, but lower f_{diff} and f_{agg} values in Regions II and III where the MFA is able to provide meaningful fits of the decays obtained from the sample thanks to the greater PDI (see Figure 3.6B). Below T_{c} in Region I, the fluorescence fractions are retrieved with larger error bars due to a combination of factors that affect the monomer decays, namely a low PDI, indicating quasi mono-exponential behaviour (see Figure 3.6B), high f_{free}

which suggests little excimer formation, and a τ_M value which is close to one of the coupled decay times in Eqs. 4 and 5. The combination of these factors makes it difficult to differentiate free pyrene from pyrenes able to form excimer by diffusion in these specific circumstances, making accurate recovery of the fluorescence fractions challenging. Thus, the conclusions drawn from results below T_c are mainly based on Py$_2$-PNIPAM(14K) while being generally supported by those obtained with the Py$_2$-PNIPAM(25K) sample.

The trends obtained with the parameters retrieved via MFA for both Py$_2$-PNIPAM samples studied agree with most of the predictions of the model proposed by Winnik et al., with the possible exception of the fluidity of the mesoglobules above T_c. If the mesoglobules were vitreous, then it would be impossible for excimer to form over time, and the only pyrene emission that should be observed would be from aggregated or free pyrenes. Since approximately 50% of the emission is diffusional (see f_{diff} in Figure 3.9D), this is clearly not the case. It is, however, possible that the pyrene aggregates themselves are not vitreous, in which case re-arrangement of pyrenes to form excimer could occur on a time scale similar to that which is normally observed for long range excimer formation below T_c. While $<k>$ for Py$_2$-PNIPAM(14K) in Regions II and III is reduced by a factor of 4, it is not reduced to zero confirming that some mobility is experienced by the pyrene pendants.

One last point to be made about this study is to address the concern always present when dealing with fluorescently labelled polymers, namely that the probe may distort the behaviour of the polymer being studied. For this particular study this is not an issue, as the probe is a pyrene molecule with a 4 carbon alkyl linker, which replaces an 18 carbon alkyl chain used in other studies of lip$_2$-PNIPAM.[9,14-16] The size difference between the two groups is small, and one

would expect pyrene to exhibit lower mobility than an octadecyl group due to the ability of the former to bind to itself via π-π stacking.

3.5 Conclusions

The use of fluorescence to probe the behaviour of aqueous solutions of pyrene end-labelled PNIPAMs has provided detailed information on the behaviour of the hydrophobes present in the samples. Turbidimetry and light scattering have shown that the value of T_c depends on the hydrophobe content of the telechelic polymers, which is consistent with earlier work.[7] Steady-state fluorescence spectra have shown that the excimer intensity for the Py_2-PNIPAM samples reaches a maximum at T_c, due to excimer formation being most efficient at this temperature. Multi-exponential fits of the monomer decays show that the PDI of the decays goes through a maximum at T_c, while $<\tau_N>_M$ increases sharply above T_c. Fits of the excimer decays showed similar trends for $<\tau_N>_E$ and a_{E-}/a_{E+}, both increasing at T_c. All these methods yielded values of T_c that were fairly tight. The Py_1-PNIPAM samples showed significant behavioral changes at T_c even though the change in behaviour was different from that observed with the Py_2-PNIPAM samples. These differences could be traced back to the differences in the ability of telechelic and semi-telechelic PNIPAM to form pyrene excimer. Application of the MFA equations to the time-resolved fluorescence decays allowed the calculation of the rate constant for excimer formation $<k>$, as well as the fluorescence fractions f_{agg}, f_{free}, and f_{diff}. The values of $<k>$, f_{free}, and f_{diff} showed changes at both T_c and T_m which are largely consistent with the model developed by Winnik et al. for lip_2-PNIPAM in aqueous solution.[9,14-16] Specifically, the movement of the chain segments from the shell into the middle region in Regime I, the formation of mesoglobules in Regime II, and the stabilization of the mesoglobules in Regime III have all been confirmed via

96

steady-state and time-resolved fluorescence measurements. While the mesoglobules in Regime III do not appear to be vitreous and therefore kinetically frozen, these results otherwise conform to the predictions made by F.M. Winnik et al. with regard to the behaviour of lip_2-PNIPAM in water.[15]

Chapter 4:

Temperature Response of Aqueous Mixtures of Pyrene End-Labeled and Unmodified Poly(*N*-isopropylacrylamide)s Probed by Fluorescence

4.1 Overview

The temperature-dependent behaviour of aqueous solutions composed of an excess of non-fluorescent poly(N-isopropylacrylamide) (PNIPAM) and a small amount of a pyrene-labelled telechelic or semi-telechelic PNIPAM were characterized using light scattering (LS) and steady-state and time-resolved fluorescence. LS intensity showed a transition at T_c, the coil-to-globule transition (CGT) temperature for the pyrene-labelled polymer, and at T_m, the CGT temperature for the unlabelled polymer. These two transitions were also observed as a decrease in the $(I_E/I_M)^{SS}$ ratio obtained from steady-state fluorescence spectra. The emission maximum of the excimer spectra was only affected by increasing the temperature above T_c. The observed blue-shift was attributed to a change in the aggregation behaviour of the excimer. Time-resolved fluorescence decays of the monomer were acquired and fitted with a sum of exponentials. The parameters retrieved from the analysis all showed trends that reflected the polymer transitions at T_c and T_m. The Model-Free Analysis (MFA) was applied to the time-resolved fluorescence decays to determine the molar fractions of the pyrene species that were aggregated (f_{agg}), did not form excimer (f_{free}), and formed excimer by diffusion (f_{diff}), respectively, as well as the average rate constant for excimer formation ($<k>$). Increasing the temperature above T_m caused an increase in f_{free} and a decrease in f_{diff}, while having no significant effect on $<k>$. The changes in behaviour at T_c were consistent with what was observed for solutions composed solely of pyrene end-labelled PNIPAMs. The effects observed at T_m were best explained by the mixing of labelled and unlabelled chains as the latter became insoluble at T_m, which is only possible if the mesoglobules composed of labelled chains above T_c are not vitreous.

4.2 Introduction

Poly(*N*-isopropylacrylamide) (PNIPAM) in aqueous solution possesses a lower critical solution temperature (LCST) or cloud temperature (T_c) that was first observed in the late 1960s.[1] Consequently, the polymer is soluble at low temperatures but becomes insoluble once the temperature is raised above T_c. The ability to use temperature to control the solubility of PNIPAM in water has triggered major interest in the scientific community to characterize the interactions that take place between the hydrophobic groups of amphiphilic molecules and PNIPAM, as the strength of these interactions naturally changes with the water solubility of the polymer. The types of molecules whose interactions with PNIPAM have been investigated includes hydrophobically modified polymers,[2,3] small molecule surfactants,[4,5] or hydrophobic groups covalently attached to the PNIPAM chain itself.[6-13] The decrease in T_c due to the covalent attachment of hydrophobic groups onto PNIPAM[6,11-13] or the disruption of hydrophobic aggregates due to the presence of PNIPAM as it undergoes a coil-to-globule transition (CGT) at T_c[2] are among the phenomena which have been previously reported to occur in the literature. The techniques that have been successfully employed to characterize these interactions include viscometry,[2,4] turbidimetry,[3,4,9,11] light scattering,[13] fluorescence,[3,8,10,13] and small angle neutron scattering.[6,7,12]

Fluorescence is a particularly useful tool for studying the manner in which hydrophobes interact both with each other and the PNIPAM chain. Hydrophobic fluorophores such as pyrene have been used to target the hydrophobic pockets which form in aqueous solutions of PNIPAM both below and above T_c and report on their properties.[3,13] The widespread use of pyrene as a fluorophore is a result of its high quantum yield (0.32 in cyclohexane), its ability to report on the polarity of its local environment, its long lifetime, and its ability to form an excited dimer called

an excimer.[14]   When pyrene absorbs a photon of UV light, the excited pyrene might either fluoresce as a monomer in the blue region of the visible spectrum with a lifetime τ_M, or diffusionally encounter another pyrene molecule in the ground-state and form an excimer. Once formed, the excimer fluoresces in the green region of the visible spectrum with a lifetime τ_{E0}. Pyrene excimer may also form pseudo-instantaneously from pyrenes which are associated in the ground-state.

The properties of pyrene-labelled polymers can be successfully characterized from the analysis of their steady-state fluorescence spectra and time-resolved fluorescence decays of the pyrene monomer and excimer. Steady-state fluorescence spectra yield the ratio of the excimer to monomer fluorescence intensity, or the $(I_E/I_M)^{SS}$ ratio, which is a measure of the relative amount of excimer being formed. Time-resolved fluorescence decays may be fitted with a sum of exponentials to gain information on the time scale over which pyrene excimer formation occurs. Since the time scale of pyrene excimer formation relates to the chain dynamics undergone by the polymer to which it is attached, steady-state and time-resolved fluorescence have been used to study the long-range polymer chain dynamics of pyrene-labelled polymers in solution.[15-18]

A series of hydrophobically modified telechelic PNIPAM samples were recently synthesized with the hydrophobic chromophore pyrene acting as the hydrophobic group (Py$_2$-PNIPAM), as pyrene is a useful probe for studying hydrophobically modified polymers.[17,19-21] The previous chapter demonstrated that these Py$_2$-PNIPAM samples reported faithfully on the hydrophobic interactions which take place around T_c, specifically the aggregation level of the hydrophobes as well as the rate at which they formed excimer. The solution behaviour of telechelic PNIPAM hydrophobically modified with lipophilic alkyl groups (lip$_2$-PNIPAM), has been extensively studied by F. M. Winnik and colleagues.[6,7,12,13] The results of these studies

were applied to the development of a model which describes the changes in the behaviour exhibited by the lip$_2$-PNIPAM chains as the solution temperature increases. This model postulates that aqueous solutions of lip$_2$-PNIPAM exist in different states that correspond to three temperature regimes, with Regime I being below T_c which is the temperature signaling the onset of phase separation, Regime II being between T_c and T_m which is the temperature where dehydration of PNIPAM occurs, and Regime III being above T_m. In the case of the Py$_2$-PNIPAM samples, which should follow similar behaviour to lip$_2$-PNIPAM, the following observations were made as the solution temperature was increased past T_c and T_m.

In Regime I, Py$_2$-PNIPAM chains aggregated via hydrophobic forces induced by the pyrene hydrophobes to form three layered flower-like spherical micelles, with the innermost core composed primarily of the hydrophobic pyrenes, the outermost layer composed of solvated PNIPAM loops, and the middle layer between them composed of a mixture of aggregated dehydrated PNIPAM loops and a small amount of water. A significant amount of isolated pyrene was found for the Py$_2$-PNIPAM solutions, and it was concluded that the isolated pyrene labels were present in the "pearls" of dehydrated PNIPAM found in the otherwise solvated loops constituting the shell.[12,22] Pyrenes in the shell were also able to form excimer by diffusion as the rate of pyrene excimer formation was found to be quite high, specifically in Regime I. As the temperature increased in Regime I, a fraction of the loops in the shell layer dehydrated and entered the middle layer, decreasing the total volume of the micelle.[7] A decrease in overall volume increased the local pyrene concentration which caused the value of $(I_E/I_M)^{SS}$ to increase with increasing temperature throughout Regime I.

Once the solution temperature reached T_c, catastrophic dehydration of the shell led to micellar aggregation and the formation of larger particles called mesoglobules,[23-26] resulting in a

sharp increase in the ability of the solution to scatter light associated with the CGT that occurs at the LCST. The shell regions of the micelles, which had become part of a mesoglobule, overlapped and the amount of isolated pyrene decreased sharply due to the now much higher local pyrene concentration found in the overlapping shells. The rate of pyrene excimer formation also decreased sharply due to the more hindered kinetics within a mesoglobule as opposed to the hydrated shell of a dispersed micelle. As the temperature increased in Regime II, the Py_2-PNIPAM chains within the mesoglobules were no longer solely localized in individual micelles and began to disperse throughout the bulk of the mesoglobule, causing the hydrophobic pyrene groups to leave the micellar cores and disperse as well. This resulted in a decrease in $(I_E/I_M)^{SS}$ and an increase in the molar fraction of isolated pyrenes. This process was accompanied by the removal of some water from the mesoglobules.[7] These trends continued throughout Regime II until the solution reached T_m, which was found to be 34 ^{o}C for the samples studied thus far.[13]

The behaviour of the solutions of aqueous Py_2-PNIPAM did not change above T_m in Regime III, where the mesoglobule size is expected to remain essentially constant and no additional water should be expelled from the mesoglobules.[13] The local environment of pyrene was also found not to change throughout Regime III, with relatively small changes occurring at T_m for the molar fractions of aggregated or isolated pyrenes. This lack of change in behaviour is due to the system having reached either stable equilibrium or a kinetically frozen state due to the absence of chain motion within the mesoglobule at temperatures above T_m.

The determination of whether the Py_2-PNIPAM solution above T_m has reached stable equilibrium or is in a kinetically frozen state has proven difficult thus far, as illustrated by the study presented in the previous chapter of this thesis. Studies performed on aqueous solutions of

unmodified PNIPAM have found that the mesoglobules were gel like, i.e. not glassy, for all temperatures above T_c.[27] It is the purpose of the present study to investigate whether this holds true for aqueous solutions of pyrene end-labelled PNIPAM samples (Py-PNIPAM). To accomplish this, solutions were prepared which contained both Py-PNIPAM and unmodified PNIPAM, as the former and latter samples show a transition at a variable T_c and a fixed T_m of 34 °C, respectively. Interactions above T_m between the two polymers may be monitored by pyrene excimer formation, and these interactions should only be possible if the Py-PNIPAM mesoglobules are not vitreous and therefore kinetically mobile.

4.3 Experimental

The PNIPAM samples labelled at one or two ends with pyrene (Py-PNIPAM) were synthesized according to protocols described in earlier publications.[28] The samples used in this study, as well as their number-average molecular weight (M_n), may be found in Table 4.1. The Py$_1$-PNIPAM nomenclature refers to pyrene-labelled semi-telechelic samples, while Py$_2$-PNIPAM refers to the telechelic chains. The M_n of the PNIPAM backbone is denoted by the number in brackets. Unmodified PNIPAM with a molecular weight of 22 kg/mol was purchased from Sigma-Aldrich and used as received. Milli-Q water with a resistivity of over 18 MΩ·cm was used to prepare all aqueous solutions, and ethanol (HPLC grade reagent alcohol) was supplied by Fischer Scientific.

Aqueous mixtures of PNIPAM(22K) and the Py-PNIPAM samples were prepared by dissolving the Py-PNIPAM sample in ethanol, determining the concentration of this solution by applying the Beer-Lambert law to the absorbance of pyrene at 342 nm and using the molar absorbance coefficient of 1-pyrenebutanol in ethanol ($\varepsilon_{Py} = 42{,}500$ M^{-1}.L.cm^{-1}), then transferring a sufficient quantity into a vial to yield the desired concentration in water. The ethanol was

evaporated under a stream of nitrogen before adding 0.2 mL of water to the vial. The solution was vortexed before adding 0.8 mL of water and the solution was vortexed again. A known mass of PNIPAM(22K) was dissolved in water to yield a stock solution which was diluted to the desired concentration. This PNIPAM(22K) solution (3 mL) was added to the 1 mL Py-PNIPAM aqueous solution to yield a mixture with a known concentration of Py-PNIPAM, and a PNIPAM(22K) concentration in g/L equal to 10× that of Py-PNIPAM in g/L. The mixture was allowed to stand for a minimum of 30 minutes at 4 °C. Solutions composed solely of unlabelled PNIPAM were prepared by diluting the PNIPAM(22K) stock solution. Polymer solutions were prepared with a constant pyrene concentration of 2.5 μM, resulting in Py-PNIPAM and PNIPAM(22K) solutions whose concentrations are listed in Table 4.1.

Table 4.1: Polydispersity index (PDI) and number-average molecular weight (M_n) of the PNIPAM samples and their concentrations.

Sample	M_n (kg/mol)	Polydispersity Index	[Py-PNIPAM] (g/L)	[PNIPAM(22K)] (g/L)
Py$_2$-PNIPAM(14K)	13.7	1.10	0.017	0.17
Py$_2$-PNIPAM(25K)	25.4	1.07	0.032	0.32
Py$_2$-PNIPAM(45K)	44.5	1.10	0.056	0.56
Py$_1$-PNIPAM(7K)	7.68	1.02	0.018	0.18
Py$_1$-PNIPAM(12K)	12.3	1.02	0.030	0.30
Py$_1$-PNIPAM(25K)	23.5	1.09	0.059	0.59
PNIPAM(22K)	20-25			

Acquisition of the light scattering intensity profile as a function of wavelength, steady-state fluorescence, and time-resolved fluorescence decays have been described in the previous chapter. Excimer emission was isolated from the Py-PNIPAM fluorescence spectra and the $(I_E/I_M)^{SS}$ ratio was calculated from the corrected fluorescence spectra. The pyrene monomer and excimer decays were fitted with a sum of exponentials using Eq. 3.1 (page 70). Eqs. 3.2 and 3.3

(page 71) were used to calculate the number-average ($<\tau_N>_M$) and weight-average ($<\tau_W>_M$) lifetimes of the pyrene monomer fluorescence decays according to the procedure outlined in Chapter 3. The ratio $<\tau_W>_M/<\tau_N>_M$, was taken as the polydispersity index (PDI) of the monomer decays.

All decays were fitted using the MFA which has been described in detail in a number of publications[29-32] using Eqs. 3.4 and 3.5 (page 73). The decay times and pre-exponential factors retrieved from the MFA were used to calculate the fluorescence fractions of each species, namely f_{free}, f_{diff}, and f_{agg}, the latter fraction being equal to the sum of f_{E0}, and f_{EL}. The fractions refer to the pyrene labels that form excimer by diffusion (f_{diff}), do not form excimer (f_{free}), and form excimer instantaneously from pyrenes which were aggregated in the ground state (f_{agg}). The contribution of f_{ES} was found to only become significant when $(I_E/I_M)^{SS}$ was below 0.1, which led to the conclusion that it is likely due to the presence of a minute amount of a contaminating fluorescent species and not pyrene excimer, since it became noticeable only when little to no excimer was being formed. As such, it was excluded from the f_{agg} calculation. The equations used to calculate these fractions can be found in a previous publication.[29]

4.4 Results and Discussion

An investigation into the effect of T_m on the behaviour of the Py-PNIPAM samples was initiated by monitoring the right-angle light scattering (LS) intensity of solutions of Py$_2$-PNIPAM with a 10× massic excess of unlabelled PNIPAM(22K) as a function of temperature. The resulting LS intensity profiles are presented in Figure 4.1. The samples were prepared by first solvating the Py$_2$-PNIPAM chains, which are capable of forming micelles, before adding a solution of unlabelled PNIPAM(22K). The experimental results presented hereafter were performed on

solutions whose temperature was initially set at 20 ^{o}C, where both labelled and unlabelled polymers are soluble. The temperature was then increased in small increments, typically 1 ^{o}C, with a minimum equilibration time of 10 minutes before performing fluorescence measurements until a temperature of 40 ^{o}C was reached, where the two polymers are no longer water-soluble and undergo some mixing. The solutions were then cooled to 20 ^{o}C at a maximum cooling rate of 0.5 ^{o}C per minute to redissolve the polymers, and the experiments were repeated to determine if the thermal history of the samples affected the aggregation behaviour of the labelled chains below T_c.

The ascending and re-ascending LS intensity of Py$_2$-PNIPAM(14K) and Py$_2$-PNIPAM(25K) mixed with PNIPAM(22K) are shown in Figure 4.1A and B, respectively. Although they do not overlap perfectly, they are similar in both intensity and shape. In particular, they share the same temperatures at which their LS intensity profile shows a sharp break point, regardless of whether the polymers have been freshly prepared or previously heated to 40 ^{o}C. The first of the transitions observed for all three Py$_2$-PNIPAM mixtures occurs at T_c, which indicates that the labelled chains have formed mesoglobules and entered Regime II. This was also observed in Figure 3.3 (page 76) for Py$_2$-PNIPAM solutions. The Py$_2$-PNIPAM mixtures show a second increase in LS intensity at 34 ^{o}C, which represents both T_m for the Py$_2$-PNIPAM chains and the temperature at which the PNIPAM(22K) chains dehydrate and form aggregates. The increase in LS intensity due to the dehydration of the PNIPAM(22K) in a solution where Py$_2$-PNIPAM chains are already aggregated due to the formation of mesoglobules might lead to mixing of these two polymers once the solution temperature reaches 34 ^{o}C.

Finally, the LS intensity profile of the Py$_2$-PNIPAM(45K) and PNIPAM(22K) mixture shown in Figure 4.1C shared similar features to those obtained with the two other Py$_2$-PNIPAM samples. Two break points were observed as a function of temperature reflecting the transitions taking place at T_c and T_m. The LS intensity profile of PNIPAM(22K) also shown in Figure 4.1C indicated a single transition at T_m corresponding to the CGT of the homopolymer.
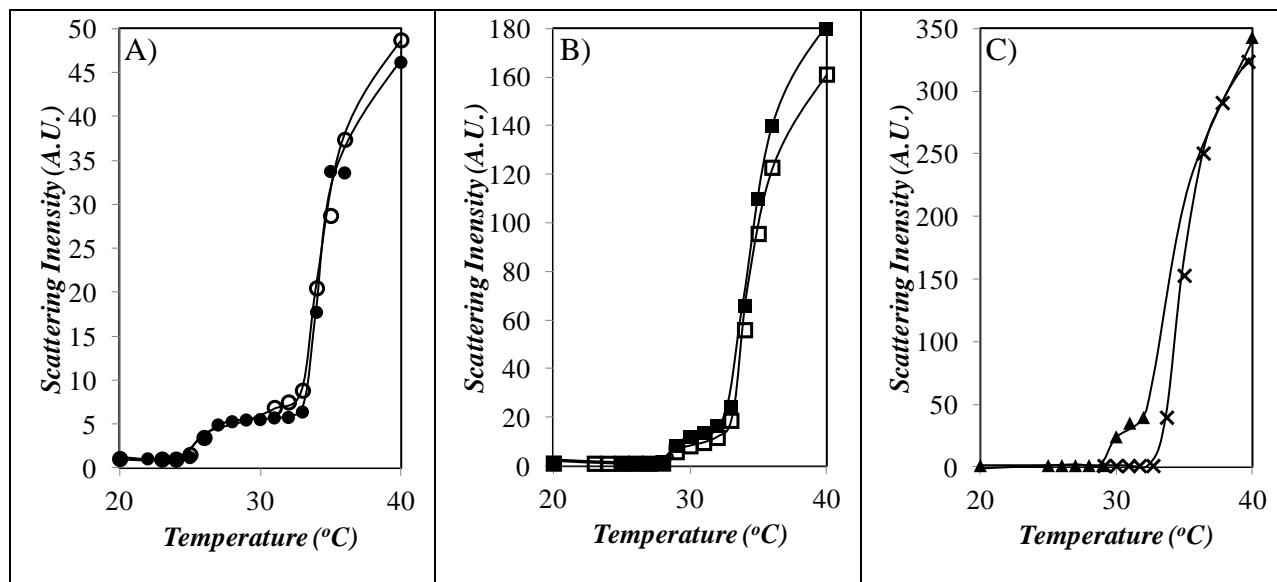
Figure 4.1: Plots of light scattering intensity of aqueous mixtures of Py$_2$-PNIPAM and PNIPAM(22K) as a function of temperature. ($\bullet$,$\circ$) Py$_2$-PNIPAM(14K), ($\blacksquare$,$\square$) Py$_2$-PNIPAM(25K), ($\blacktriangle$) Py$_2$-PNIPAM(45K), and ($\times$) PNIPAM(22K). Hollow symbols: re-ascending temperature.

In order to ascertain whether the Py$_2$-PNIPAM and PNIPAM(22K) polymers would undergo some mixing above T_m, the steady-state fluorescence spectra of each sample were acquired. The spectra for Py$_2$-PNIPAM(14K) are shown in Figure 4.2. The relative excimer fluorescence intensity increases with increasing temperature in Regime I as the solution approaches T_c, and then decreases with increasing temperature thereafter. What is of particular

108

interest is the significant drop in excimer fluorescence intensity as the solution passes through T_m, the temperature at which PNIPAM(22K) goes through its CGT. Since this drop in excimer fluorescence intensity was not observed in solutions prepared without PNIPAM(22K) (see Figure 3.4, page 78), it is reasonable to conclude that it is caused by interactions with the dehydrated PNIPAM(22K).
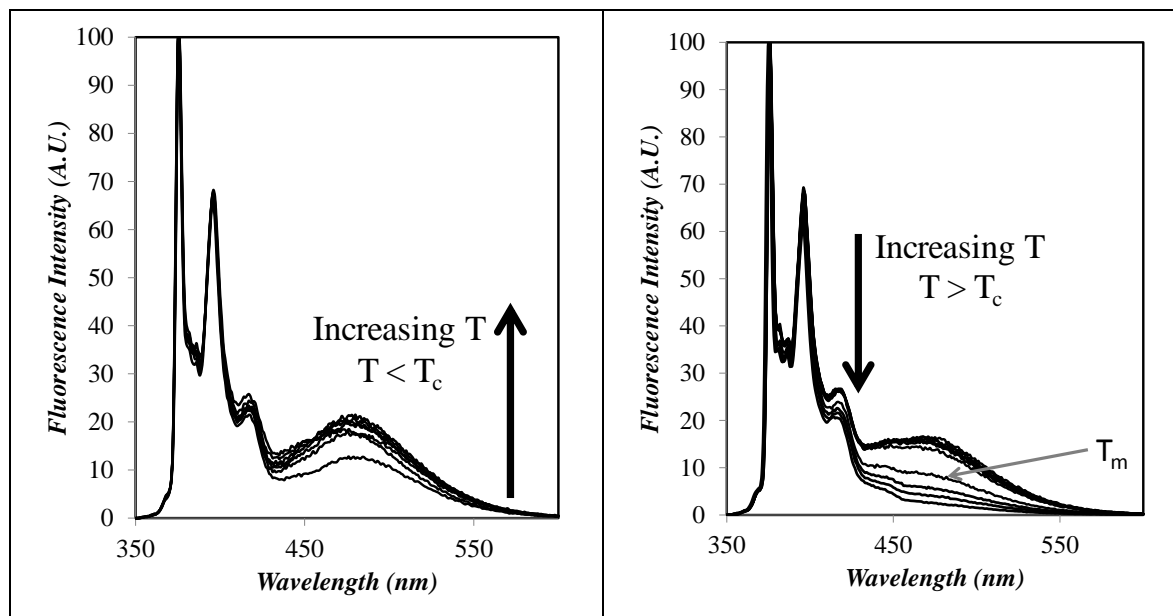
Figure 4.2: Steady-state fluorescence spectra of aqueous mixtures of Py$_2$-PNIPAM(14K) and PNIPAM(22K) at different temperatures. A) T increases from 15 to 25 ^{o}C. B) T increases from 26 to 40 ^{o}C.

The pyrene fluorescence spectra of the Py$_2$-PNIPAM samples provide a qualitative representation of the temperature dependence of the excimer fluorescence intensity on temperature. The ratio $(I_E/I_M)^{SS}$ was calculated from these spectra in order to describe more quantitatively the effect that aggregation of the PNIPAM(22K) chains has on excimer fluorescence. The $(I_E/I_M)^{SS}$ ratios for the three Py$_2$-PNIPAM mixtures were plotted as a function

of temperature in Figure 4.3. All three samples show an increase in $(I_E/I_M)^{SS}$ with increasing temperature throughout Regime I before showing a steep decrease at T_c, followed by an additional decrease at T_m for both Py$_2$-PNIPAM(14K) and Py$_2$-PNIPAM(25K). The $(I_E/I_M)^{SS}$ ratio of Py$_2$-PNIPAM(45K) shows only a single transition at T_c, possibly because the drop in $(I_E/I_M)^{SS}$ is so massive due to the long PNIPAM chain that the few excimer forming pyrenes which remain at temperatures above T_c are not noticeably affected by the CGT of PNIPAM(22K) at T_m. The temperatures at which the T_c and T_m transitions of Py$_2$-PNIPAM(14K) and PNIPAM(22K) occurred did not change after the solution had been previously heated to 40 ^{o}C. A reduction in $(I_E/I_M)^{SS}$ as observed at T_c and T_m in Figure 4.3 may be caused by a reduction in either the mobility of pyrene or the local pyrene concentration, which together hinder diffusional excimer formation. The dilution of pyrene also reduces the formation of ground-state pyrene aggregates, which upon direct excitation would otherwise generate excimer instantaneously. The decrease in $(I_E/I_M)^{SS}$ at T_c might be caused by all three effects, as they are all expected to occur upon mesoglobule formation. However, the work conducted in Chapter 3 has shown that the kinetics of pyrene excimer formation do not change significantly at T_m if no unlabelled PNIPAM is present in the solution. This result suggests that the dehydrated PNIPAM matrix does not affect the diffusive motions of the excimer forming pyrene labels at T_m. Consequently, the decrease in $(I_E/I_M)^{SS}$ at T_m is most certainly due to interactions taking place between PNIPAM(22K) and Py$_2$-PNIPAM that lead to the dissolution of the pyrene aggregates into the dehydrated PNIPAM matrix. Further evidence for this phenomenon is presented at a later point in the discussion.
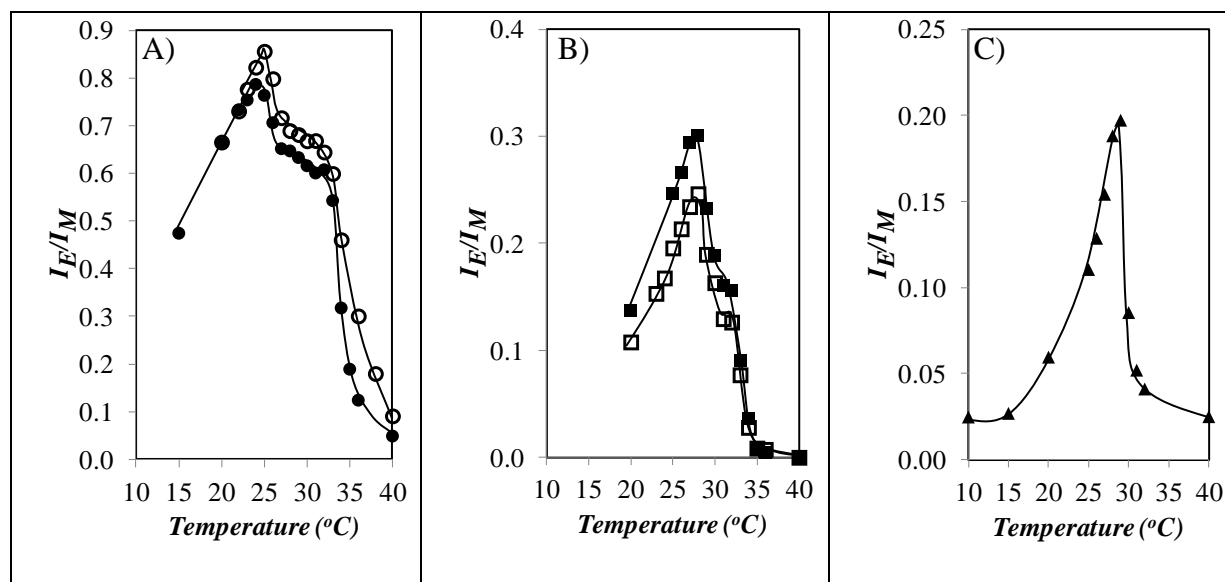
Figure 4.3: Plots of the $(I_E/I_M)^{SS}$ ratio for aqueous mixtures of Py$_2$-PNIPAM and PNIPAM(22K) as a function of solution temperature. ($\bullet$,$\circ$) Py$_2$-PNIPAM(14K), ($\blacksquare$,$\square$) Py$_2$-PNIPAM(25K), and ($\blacktriangle$) Py$_2$-PNIPAM(45K). Hollow symbols: re-ascending temperature.

An alternate cause for a decrease in pyrene excimer fluorescence intensity would be the formation of pyrene aggregates that are known to absorb and emit light more weakly than excimer formed through the diffusive encounter of two isolated pyrenes.[30,33,34] However, any such changes in excimer stacking can also be inferred from a shift in the wavelength at the emission maximum (λ_{max}), with a blue-shift in emission corresponding to overall higher levels of poorly stacked pyrene aggregates. Accordingly, λ_{max} was calculated by fitting the excimer fluorescence spectra with a polynomial and finding mathematically the wavelength corresponding to its maximum. This analysis and several others relying on pyrene excimer formation were not attempted with the Py$_2$-PNIPAM(45K) sample. The absence of sufficiently strong excimer fluorescence intensity across the entire temperature range studied for the Py$_2$-PNIPAM(45K) sample led to its dismissal from further analysis, as only three data points

111

possessed a value of $(I_E/I_M)^{SS}$ greater than 0.15 in Figure 4.3C. The trends obtained with λ_{max} for

Py$_2$-PNIPAM(14K) and Py$_2$-PNIPAM(25K) are shown in Figure 4.4.
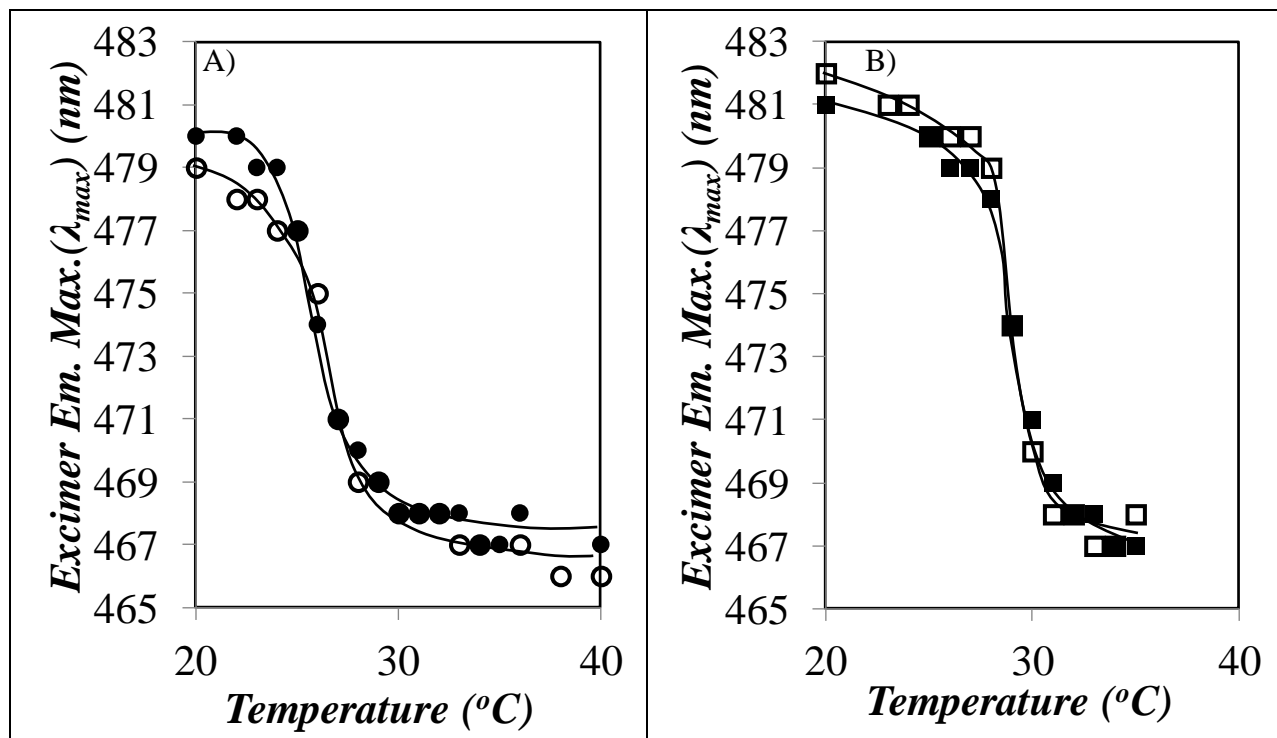
Figure 4.4: Plots of the maximum wavelength of excimer fluorescence for aqueous mixtures of Py$_2$-PNIPAM and PNIPAM(22K) as a function of solution temperature. (●,○) Py$_2$-PNIPAM(14K) and (■,□) Py$_2$-PNIPAM(25K). Hollow symbols: re-ascending temperature.

The value of λ_{max} presented in Figure 4.4 for the Py$_2$-PNIPAM(14K) and Py$_2$-PNIPAM(25K) samples both showed blue-shifts in their excimer emission when each sample temperature reached its respective T_c, indicating that a significant change occurred with regard to the types of pyrene aggregates being formed when Py$_2$-PNIPAM undergoes its cloud point transition. The Py$_2$-PNIPAM(14K) sample did not show any significant change in λ_{max} at or above T_m, up to and including a temperature of 40 ^{o}C. The spectra of Py$_2$-PNIPAM(25K) could

not be accurately fitted above 35 $^{\circ}$C due to the low intensity of pyrene excimer fluorescence yielding values of $(I_E/I_M)^{SS}$ in Figure 4.3B of 0.05 or less. Based on the trend obtained with Py$_2$-PNIPAM(14K), which shows sufficient excimer formation at temperatures greater than T_c, the absence of any shift in λ_{max} at T_m demonstrates that the decrease in $(I_E/I_M)^{SS}$ at T_m is not due to a change in the type of pyrene aggregates formed, and must be due to a change in either the rate of pyrene excimer formation by diffusion or the overall level of pyrene aggregation in the sample.

Information about the rate of pyrene excimer formation by diffusion of the Py$_2$-PNIPAM samples can be obtained from the analysis of the time-resolved fluorescence decays of pyrene. To this end, the time-resolved fluorescence decays of the pyrene monomer were acquired and fitted with Eq. 3.1. The parameters retrieved from the fits were used to calculate $<\tau_N>_M$ and $<\tau_W>_M$ via Eqs. 3.2 and 3.3, respectively. The values obtained for $<\tau_N>_M$ as well as the polydispersity index (PDI), which equals $<\tau_W>_M/<\tau_N>_M$, were plotted as a function of temperature in Figure 4.5.

Most clearly observeable in the $<\tau_N>_M$ trend for Py$_2$-PNIPAM(14K) in Figure 4.5A are the two transitions at T_c and T_m where $<\tau_N>_M$ increases significantly with increasing temperature. An increase in $<\tau_N>_M$ must correspond to a decrease in the rate of diffusional excimer formation, an increase in the amount of isolated pyrenes unable to form excimer, or a decrease in the efficiency of oxygen quenching, alone or in combination. All of these effects might be induced by the hydrophobic collapse of PNIPAM at T_c and T_m. While the transition for $<\tau_N>_M$ at T_c may reasonably be influenced by a change in the rate of excimer formation, as seen in the previous chapter, there is less evidence to support such an explanation for the change in $<\tau_N>_M$ that occurs at T_m. An increase in the amount of isolated pyrene monomers and a decrease in the efficiency of oxygen quenching is consistent with interactions between PNIPAM(22K) and

113
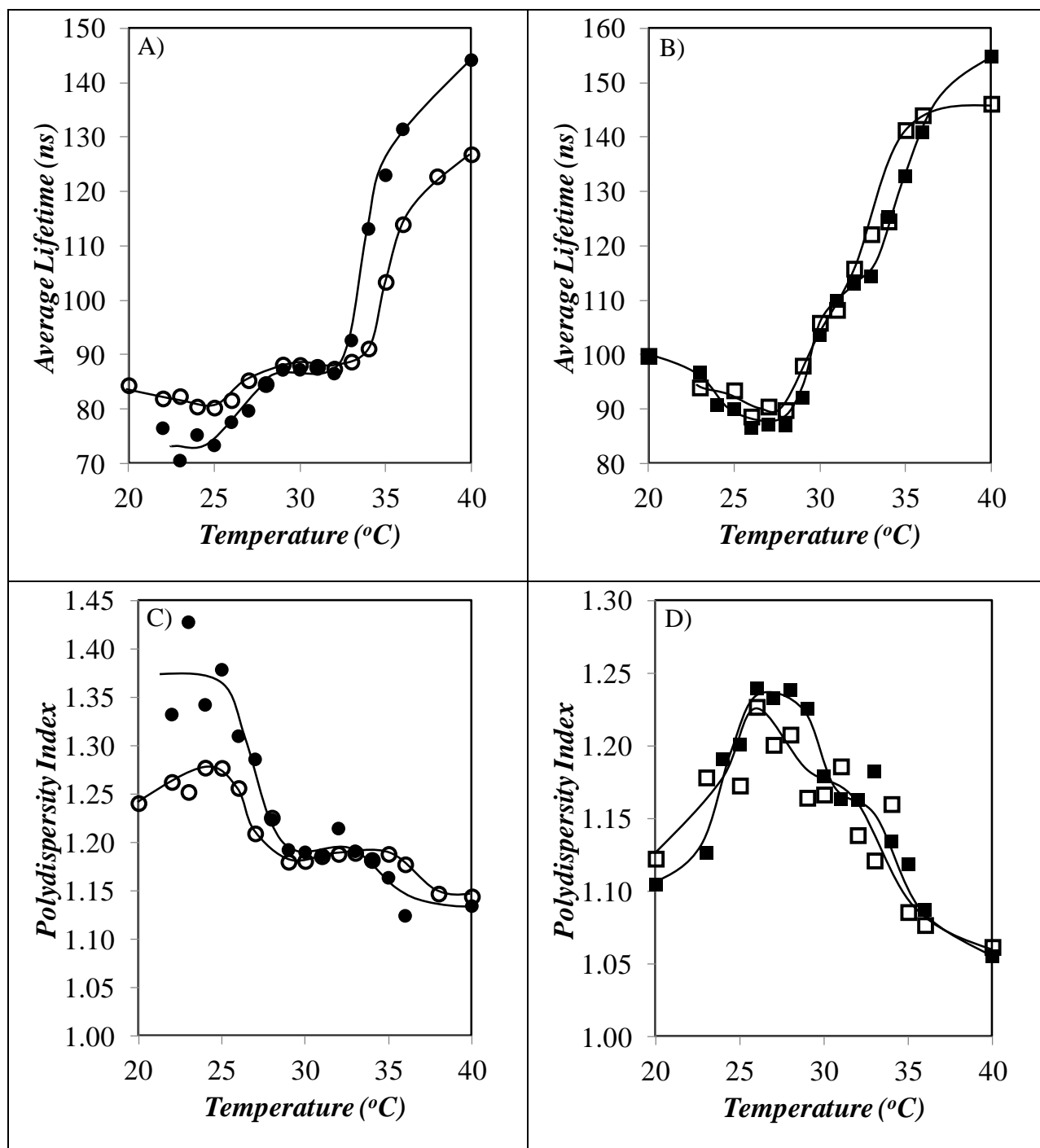
Figure 4.5: Plots of $\langle\tau_N\rangle_M$ and PDI of pyrene monomer decays for aqueous mixtures of Py$_2$-PNIPAM and PNIPAM(22K) as a function of solution temperature. ($\bullet$,$\circ$) Py$_2$-PNIPAM(14K) and ($\blacksquare$,$\square$) Py$_2$-PNIPAM(25K). Hollow symbols: re-ascending temperature.

Py$_2$-PNIPAM(14K) above T_m causing more pyrenes to be surrounded by PNIPAM chain segments which hinder diffusion. The values of $<\tau_N>_M$ for Py$_2$-PNIPAM(25K) shown in Figure 4.5B show transitions that are consistent with those observed for Py$_2$-PNIPAM(14K), also increasing with increasing temperature at T_c and T_m. The two transitions are not as well resolved from one another as for Py$_2$-PNIPAM(14K) however, as the T_c value of Py$_2$-PNIPAM(25K) is much closer to that of T_m.

The PDI values for Py$_2$-PNIPAM(14K) and Py$_2$-PNIPAM(25K), observed in Figure 4.5C and Figure 4.5D, respectively, both show a step decrease at T_c and T_m. A decrease in PDI results from a decrease in the curvature of the decay, which reflects a decrease in diffusional excimer formation. The decrease in PDI at T_c was observed and discussed in the previous chapter. The transition at T_m implies that there is a change in either the rate of excimer formation by diffusion or an increase in the molar fraction of isolated pyrenes. Unfortunately, the two phenomena cannot be differentiated based on this analysis alone. This result however does indicate that the manner in which hydrophobes present in the Py$_2$-PNIPAM samples diffusionally encounter one another is influenced by the interactions that take place between PNIPAM(22K) and Py$_2$-PNIPAM at temperatures greater than T_m.

The formation of pyrene excimer by diffusion results in both a decay time in the monomer decays and a rise time and excimer fluorescence decays. As a result, any factor which influences the formation of pyrene excimer by diffusion, as observed in the pyrene monomer fluorescence decays, must also influence the pyrene excimer decays. Therefore the pyrene excimer fluorescence decays were also acquired and fitted with Eq. 3.1, and the parameters obtained from these fits have been listed in Table SI.3-SI.4 in supporting information. These parameters were used to calculate the ratio a_{E-}/a_{E+}, equal to the sum of the negative pre-

exponential factors over the sum of the positive pre-exponential factors in the excimer decay. The decay times with positive pre-exponential factors were used to calculate $<\tau_N>_E$ for the excimer decays using Eq. 2. The values for $<\tau_N>_E$ and a_{E-}/a_{E+} are plotted as a function of temperature in Figure 4.6.

At temperatures corresponding to Regime I for both Py$_2$-PNIPAM(14K) and Py$_2$-PNIPAM(25K), the value of $<\tau_N>_E$ shown in Figure 4.6A and Figure 4.6B stays relatively constant then increases significantly at T_c, a phenomenon which is best explained by a significant reduction in the efficiency of oxygen quenching due to the dehydration and collapse of PNIPAM. Above T_c, variations in $<\tau_N>_E$ as a function of temperature are too scattered for meaningful interpretation. The value of a_{E-}/a_{E+} also shows a sharp increase at T_c for the initial temperature ascent of Py$_2$-PNIPAM(14K), although this value stays constant within experimental error for the second ascent. The Py$_2$-PNIPAM(25K) sample yields more consistent trends between temperature ramps, with both trends showing a decrease in a_{E-}/a_{E+} with increasing temperature in Regime I, a sharp increase at T_c, then a minor decrease with increasing temperature throughout Regime II. Compared with the lifetimes which provide information about the magnitude of a rate, the ratio a_{E-}/a_{E+} reflects the relative contributions to excimer formation of diffusive encounters of pyrene labels or direct excitation of aggregated ground-state pyrenes, respectively. A more negative a_{E-}/a_{E+} ratio indicates a stronger contribution from the former process. The behaviour of a_{E-}/a_{E+} for Py$_2$-PNIPAM(25K) is consistent with a decrease in the amount of excimer formed by diffusion that occurs once the sample reaches T_c, followed by a slight increase once the sample reaches T_m. Unfortunately, values of a_{E-}/a_{E+} for the
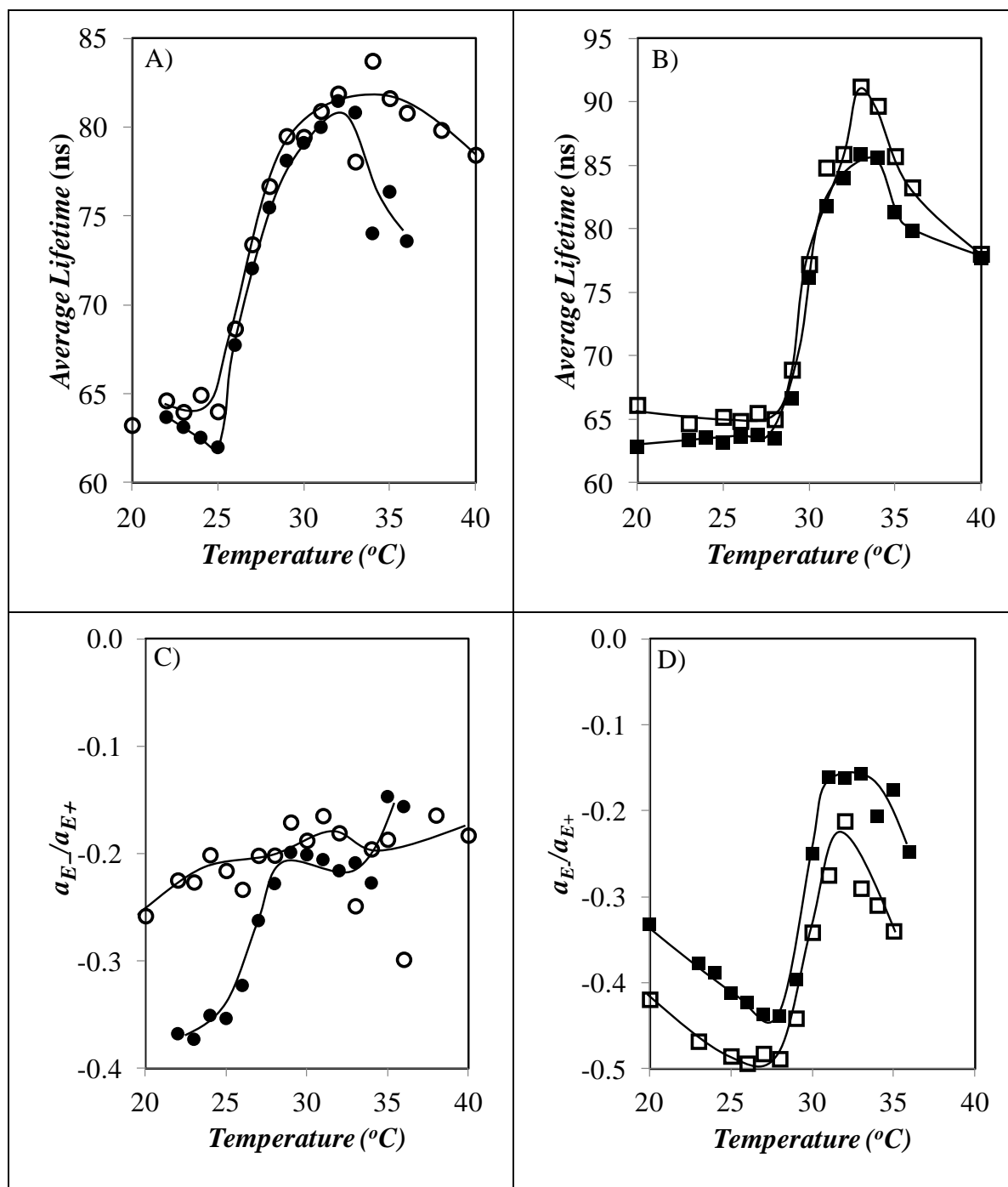
Figure 4.6: Plot of A) and B) $\langle \tau_N \rangle_E$ value of the excimer and C) and D) a_{E-}/a_{E+} ratio for aqueous mixtures of Py_2-PNIPAM and PNIPAM(22K) as a function of temperature. ($\bullet$,$\circ$) Py_2-PNIPAM(14K) and ($\blacksquare$,$\square$) Py_2-PNIPAM(25K). Hollow symbols: re-ascending temperature.

Py$_2$-PNIPAM(14K) sample do not lend themselves to clear-cut interpretation, with only the initial ascent showing a clear increase at T_c.

The techniques which have been discussed thus far show that distinct changes occur for the solution behavior of mixtures of Py$_2$-PNIPAM and PNIPAM(22K) at T_c and T_m, whose values have been reported in Table 4.2. The values for T_c closely matched those obtained for solutions composed of only Py$_2$-PNIPAM and reported in Chapter 3, which indicates that the presence of PNIPAM(22K) has a minimal influence on the CGT of the Py$_2$-PNIPAM samples. The values obtained for T_m are closely distributed around 33 $^{\circ}$C, which is within a single degree of the commonly reported value of 34 $^{\circ}$C for the CGT temperature of PNIPAM. Not all trends obtained with different techniques yielded clear transitions at T_c and T_m for the Py$_2$-PNIPAM samples. When this was the case, the transition temperatures were not reported.

The observations reported thus far show that increasing the solution temperature above T_m causes major changes in the trends observed for LS intensity, $(I_E/I_M)^{SS}$, and $<\tau_N>_M$ for aqueous Py$_2$-PNIPAM mixtures. These samples showed a significant amount of pyrene excimer formation which allowed their characterization by fluorescence. However, there remains the possibility that pyrene excimer formation is causing, rather than reporting on, the behavioural changes which occur above T_m. In order to address this concern, semi-telechelic Py$_1$-PNIPAM mixtures were prepared and characterized as they show significantly less excimer formation. The study of these samples was initiated by monitoring the changes in light scattering intensity which take place as a function of temperature, the results of which are reported in Figure 4.7.

Table 4.2: T_c and T_m values resulting from a transition in the trends obtained by different techniques for aqueous mixtures of Py$_2$-PNIPAM and PNIPAM(22K)

Sample	T_c (°C) as determined by:								
	L.S.	(I_E/I_M)	$<\tau_N>_M$	PDI	$<\tau_N>_E$	a_{E-}/a_{E+}	λ_{max}	$<k>$ (MFA)	Average
Py$_2$-PNIPAM(14K)	25	25	25	26	25	25	25	26	25.1 ± 0.4
Py$_2$-PNIPAM(25K)	28	28	28	30	28	28	28	29	28.3 ± 0.8
Py$_2$-PNIPAM(45K)	29	29							29
Sample	T_m (°C) as determined by:								
	L.S.	(I_E/I_M)	$<\tau_N>_M$	PDI	$<\tau_N>_E$	a_{E-}/a_{E+}	λ_{max}	$<k>$ (MFA)	Average
Py$_2$-PNIPAM(14K)	33	32	33	34					32.7 ± 0.6
Py$_2$-PNIPAM(25K)	33	32	33	33					32.8 ± 0.6
Py$_2$-PNIPAM(45K)	33								33

The three Py$_1$-PNIPAM samples all show an increase in light scattering intensity with increasing temperature, with the onset of this increase occurring at a temperature of about 30 °C, which is below T_m and was attributed to T_c. A T_c value of 30 °C is similar to that obtained for pure Py$_1$-PNIPAM solutions in the previous chapter, indicating that PNIPAM(22K) has little effect on the CGT of the Py$_1$-PNIPAM samples. The magnitude of the increase in light scattering intensity at T_c for Py$_1$-PNIPAM(7K) and Py$_1$-PNIPAM(12K) is quite small relative to the changes that occur at T_m. In an effort to ensure the visibility of both transitions, a logarithmic scale was used in Figure 4.7 for the scattering intensity. The two transitions in light scattering intensity at T_c and T_m, seen in Figures 4.7A and 4.7B, are similar to those seen in Figure 4.1
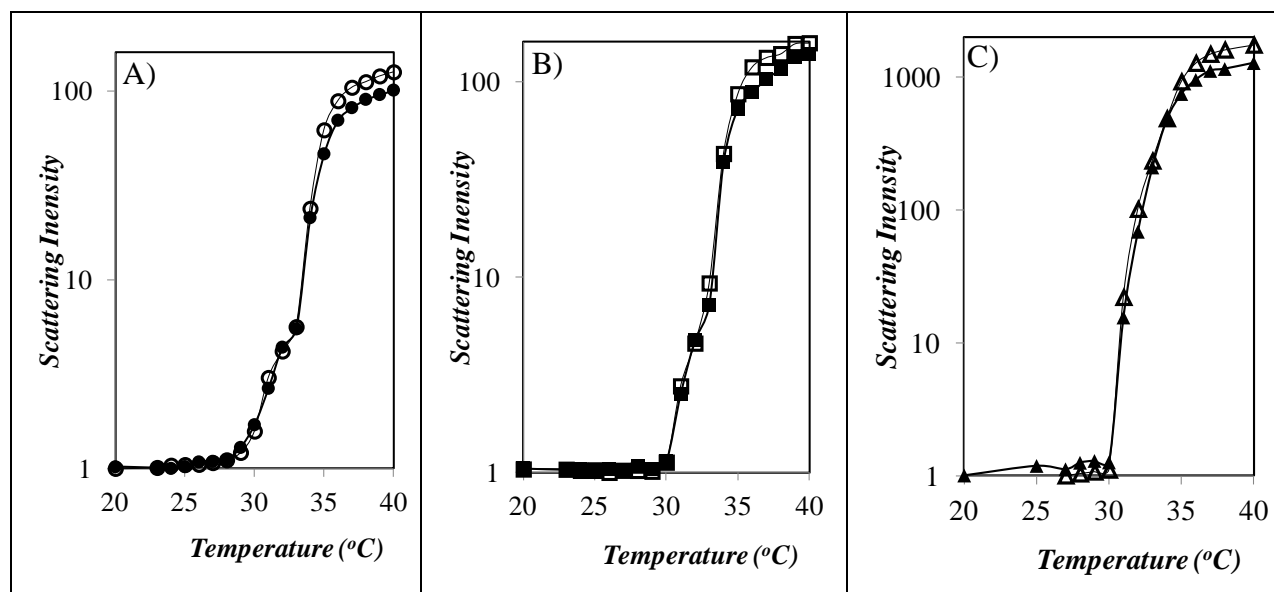
Figure 4.7: Light scattering intensity of aqueous mixtures of Py_1-PNIPAM and PNIPAM(22K) as a function of solution temperature. ($\bullet$,$\circ$) Py_1-PNIPAM(7K), ($\blacksquare$,$\square$) Py_1-PNIPAM(12K), and ($\blacktriangle$,$\triangle$) Py_1-PNIPAM(25K). Hollow symbols: re-ascending temperature.

for the Py_2-PNIPAM samples. Accordingly, the Py_1-PNIPAM samples should also display differences in pyrene fluorescence behaviour, as each sample undergoes transitions first at the cloud point, and then at T_m. In the case of the Py_1-PNIPAM(25K) sample, the light scattering intensity only shows a single observable transition. This is due to the Py_1-PNIPAM(25K) sample possessing a T_m transition which causes a significantly higher light scattering signal relative to the other samples, making it impossible to distinguish the T_c and T_m transitions. In order to determine if the transitions probed by light scattering in Figure 4.7 affect the behaviour of the hydrophobic pyrenes of Py_1-PNIPAM, the steady-state fluorescence spectra of the Py_1-PNIPAM samples were acquired and used to calculate the ratio $(I_E/I_M)^{SS}$ which is presented as a function of temperature in Figure 4.8.

120

The value of $(I_E/I_M)^{SS}$ for each sample shown in Figure 4.8A-C reached a maximum value at a temperature immediately below T_m. $(I_E/I_M)^{SS}$ increased gently with increasing temperature, before showing a sharp increase at $T_c = 30$ °C due to the increase in local pyrene concentration as the Py$_1$-PNIPAM chains aggregated to form mesoglobules. The fact that $(I_E/I_M)^{SS}$ decreased with increasing temperature once the solution reached T_m led to the conclusion that interactions between PNIPAM(22K) and Py$_1$-PNIPAM are the cause of this phenomenon.
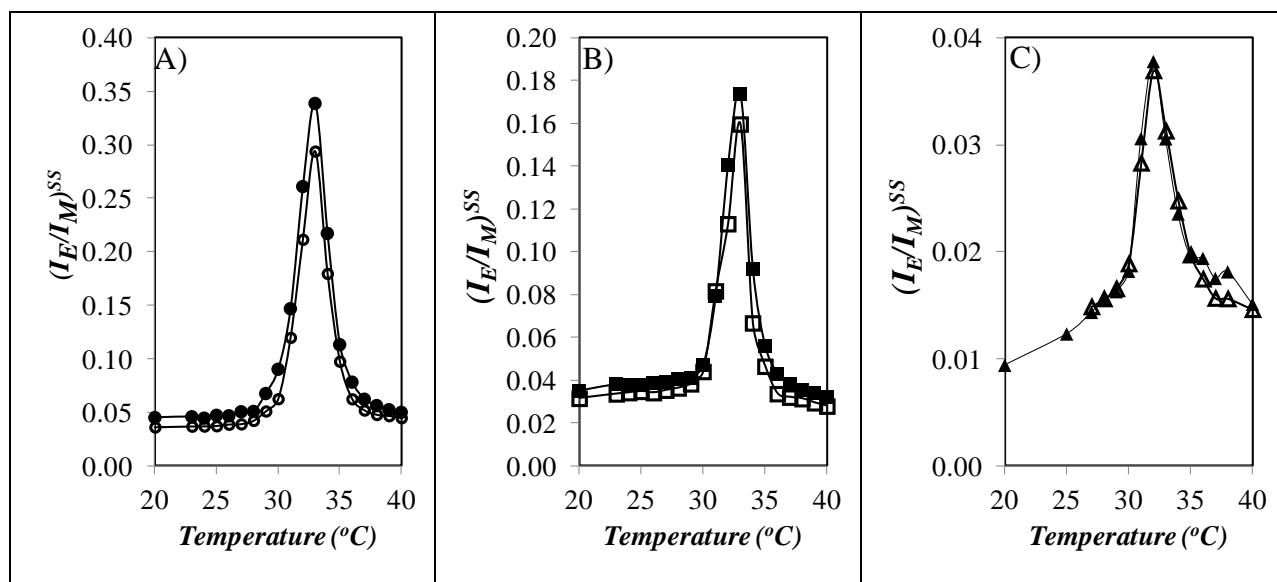
Figure 4.8: Plots of $(I_E/I_M)^{SS}$ for aqueous mixtures of Py$_1$-PNIPAM and PNIPAM(22K) as a function of solution temperature. A) ($\bullet$,$\circ$) Py$_1$-PNIPAM(7K), B) ($\blacksquare$,$\square$) Py$_1$-PNIPAM(12K), and C) ($\blacktriangle$,$\triangle$) Py$_1$-PNIPAM(25K). Hollow symbols: re-ascending temperature.

Time-resolved fluorescence decays of the pyrene monomer were also acquired to determine the effect of T_m on singly labelled chains. The number-average lifetime $<\tau_N>_M$ for the monomer decays was calculated using Eq. 2, and is presented as a function of temperature in Figure 4.9.
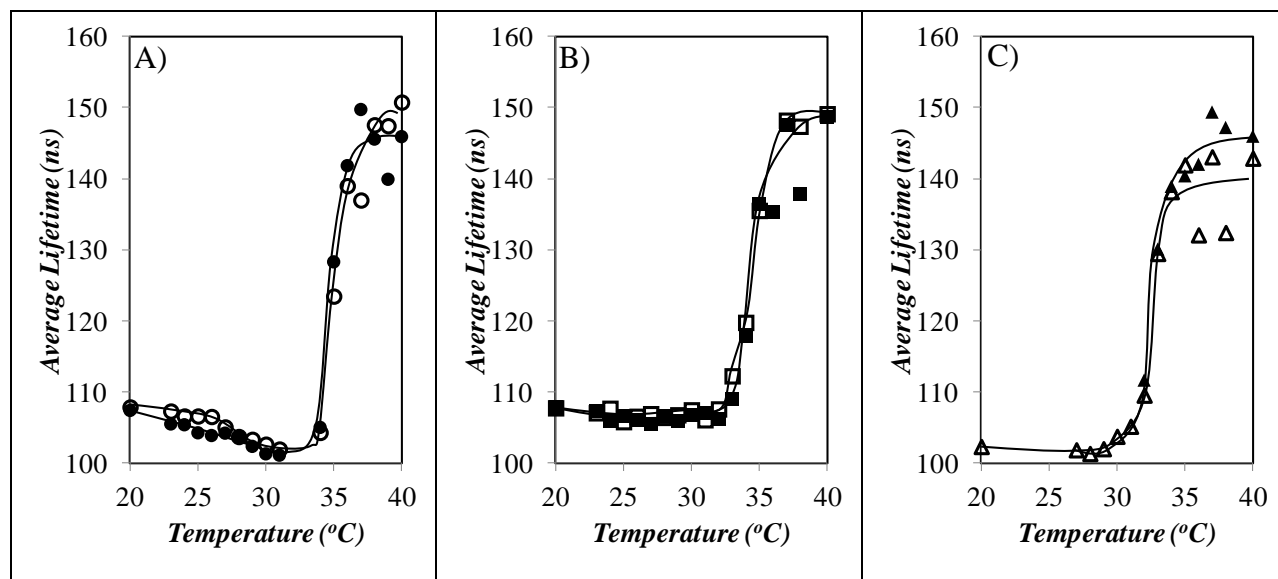
Figure 4.9: Plots of the number average lifetime of pyrene monomer decays for aqueous mixtures of Py$_1$-PNIPAM and PNIPAM(22K) as a function of solution temperature. A) (●,○) Py$_1$-PNIPAM(7K), B) (■,□) Py$_1$-PNIPAM(12K), and C) (▲,Δ) Py$_1$-PNIPAM(25K). Hollow symbols: re-ascending temperature.

The three semi-telechelic Py$_1$-PNIPAM samples showed remarkably consistent trends for the value of $<\tau_N>_M$ as it stayed relatively constant in Regime I and II, before increasing sharply at T_m, above which it remained relatively constant throughout Regime III. The average lifetime $<\tau_N>_M$ of Py$_1$-PNIPAM(7K) in Figure 4.9A showed a small decrease in $<\tau_N>_M$ in Regime I but the trend is otherwise consistent with the other Py$_1$-PNIPAM samples. The slight decrease in $<\tau_N>_M$ below T_c is likely due to the fact that Py$_1$-PNIPAM(7K) is the Py$_1$-PNIPAM sample with the highest pyrene content and therefore is most likely to form aggregates in solution such as micelles. These intermolecular interactions allow diffusional excimer formation to occur within the pyrene-rich micellar core which will affect $<\tau_N>_M$. However, while the $(I_E/I_M)^{SS}$ ratio for Py$_1$-PNIPAM(7K) is the highest of the three Py$_1$-PNIPAM samples, it is too low to acquire the

122

excimer decay within a reasonable experimental time. Consequently, the extent of diffusional excimer formation could not be determined by time-resolved fluorescence. As the Py_1-PNIPAM mixtures pass through $T_c = 30\ ^oC$ there is no significant change in $<\tau_N>_M$, which leads to the conclusion that mesoglobule formation does not significantly affect the efficiency of oxygen quenching. However, as the mixtures pass through T_m $<\tau_N>_M$ increases sharply, implying that interactions between Py_1-PNIPAM and PNIPAM(22K) do increase oxygen quenching efficiency. Therefore it is reasonable to conclude that the similar changes in decay times observed at T_m for the Py_2-PNIPAM samples in Figure 4.5 and Figure 4.6 are the result of changes in how pyrene groups interact with PNIPAM(22K) above T_m.

In order to understand how the interactions between PNIPAM(22K) and Py_2-PNIPAM that occur at T_m affect the association of the hydrophobic pyrene end-groups of Py_2-PNIPAM, and consequently the changes in the fluorescence behaviour observed thus far, the behaviour of the pyrene labels needed to be described in a more quantitative manner. To obtain this information, the time-resolved fluorescence decays of the pyrene monomer and excimer were fitted globally according to the MFA using Eqs. 3.4 and 3.5. The manner in which the MFA was applied, specifically whether certain lifetimes were optimized or fixed in the analysis, was found to significantly impact the parameters retrieved from the MFA of the decays. The exact procedure applied to conduct the MFA of the time resolved fluorescence decays with Eqs. 4.4 and 4.5 is presented hereafter.

Regardless of temperature, the value of the excimer lifetime τ_{E0} was fixed at 51 ns for all analyses, as it was determined in the previous chapter. The value of the monomer lifetime τ_M for each decay was fixed to the value of the long decay time retrieved from the multiexponential fits of the Py_1-PNIPAM monomer decays. The longest decay times obtained from the tri-

exponential fits of the Py_1-PNIPAM(12K) decays were averaged for Regime I, II, and III and found to equal 114 ± 1, 140 ± 7, and 167 ± 2 ns, respectively. They were used as the fixed value of τ_M for the Py_2-PNIPAM(14K) sample in its corresponding Regime I, II, and III. The longest decay time obtained from the multiexponential fits of the Py_1-PNIPAM(25K) monomer decays were also averaged across Regime I (120 ns ± 1), II (167 ns ± 3), and III (167 ns ± 3) and used to fix τ_M for the Py_2-PNIPAM(25K) sample in each corresponding Regime. When the need for the decay time τ_{ES} was identified to account for the presence of a short-lived species in the excimer decays, it was fixed at a value of 3.5 ns as done in previous work.[35]

The appropriate τ_{EL} value that needed to be fixed in the MFA was determined by globally fitting the time-resolved monomer and excimer fluorescence decays with the MFA equations, optimizing the coupled decay times, the pre-exponential factors, and τ_{EL}, and keeping the other lifetimes τ_{E0} and τ_M fixed. The τ_{EL} values obtained from this analysis were averaged across Regime I, II, and III and found to equal 89 ± 4, 110 ± 3, and 131 ± 15 ns, respectively for Py_2-PNIPAM(14K). These values were similar to the τ_{EL} values of 88.5, 112, and 135 ns previously obtained from triplicate repeat analysis of solutions composed solely of Py_2-PNIPAM(14K). Thus, the triplicate values were used instead. In addition to the triplicate values being less prone to random error, this also made the analysis of the mixtures of Py_2-PNIPAM and PNIPAM(22K) directly comparable to the previous analysis of solutions composed solely of Py_2-PNIPAM. The value of τ_{EL} for the Py_2-PNIPAM(25K) sample was averaged for temperatures at or above T_c and found to equal 142 ns. This value of τ_{EL} was also deemed sufficiently close to the triplicate repeat value of 135 ± 4 ns, thus the value of 135 ns was used instead, to afford a direct comparison with the results obtained in the previous chapter. Having established a set of τ_{ES}, τ_{E0}, τ_{EL}, and τ_M values to be fixed in the MFA of the decays for each temperature regime and each

Py$_2$-PNIPAM sample, the decays were re-analyzed with the MFA equations with all non-coupled lifetimes now fixed. The results retrieved from the analysis were used to calculate the parameters $<k>$, f_{agg}, f_{free}, and f_{diff}, which are presented as a function of temperature in Figures 4.10 and 4.11.

In Regime I, the value of $<k>$ for the Py$_2$-PNIPAM(14K) sample shown in Figure 4.10A remained constant and equal to $2.1 \pm 0.1 \times 10^7$ s^{-1} for the initial temperature ascent, and $1.5 \pm 0.1 \times 10^7$ s^{-1} for the reascending temperature ramp. This is consistent with the trends obtained with $<\tau_N>_M$, PDI (Figure 4.5A and C), $<\tau_N>_E$, and the ratio a_{E-}/a_{E+} (Figure 4.6A and C) which also showed differences in the behaviour between mixtures of Py-PNIPAM and PNIPAM(22K) depending on whether they had or had not gone through a heating ramp beforehand. The small variance between temperature points in Regime I, coupled with the distinct difference between ascending and re-ascending temperature ramps, provides conclusive evidence that the process of heating the solutions to 40 ^{o}C results in a clear change in the behaviour of the structures formed in solution, even after they have been brought back to T = 20 ^{o}C where both Py$_2$-PNIPAM and PNIPAM(22K) are supposed to be soluble. In this case, the difference resides in a decrease in the rate at which pyrene groups encounter one another via diffusion below T_c, which results from either a decrease in the mobility of the pyrene groups or a reduction in the local concentration of pyrene after the polymers have been mixed. Above T_c, the value of $<k>$ remained relatively constant and equal to $0.55 \pm 0.07 \times 10^7$ s^{-1} across the temperature range studied, with no significant change occurring at T_m.
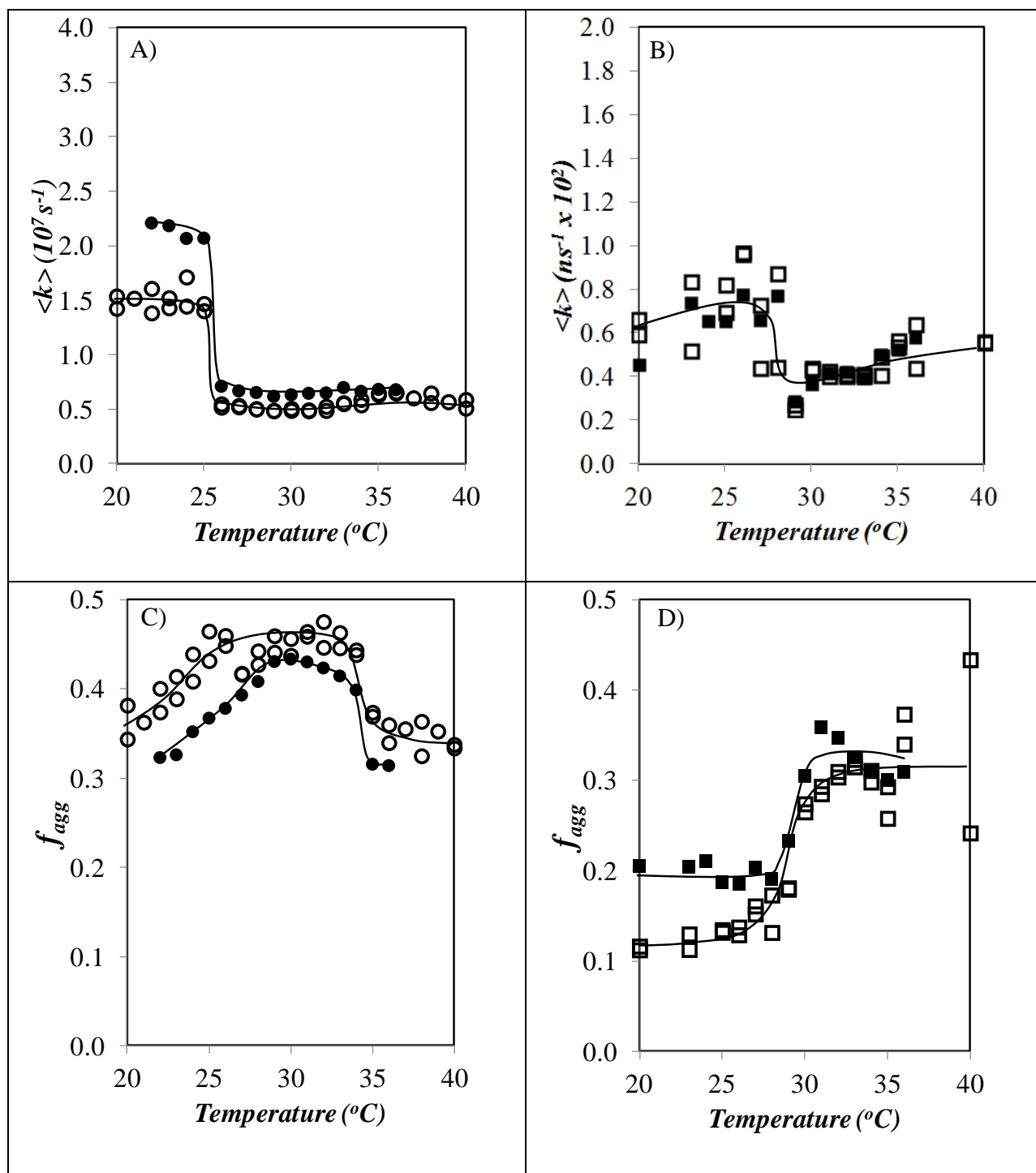
Figure 4.10: MFA parameters $<k>$ and f_{agg} for aqueous mixtures of Py$_2$-PNIPAM and PNIPAM(22K) plotted as a function of solution temperature. ($\bullet$,$\circ$) Py$_2$-PNIPAM(14K), and ($\blacksquare$,$\square$) Py$_2$-PNIPAM(25K). Hollow symbols: re-ascending temperature.

The trend observed for the value of $<k>$ for Py$_2$-PNIPAM(25K) shown in Figure 4.10B agrees with those observed for Py$_2$-PNIPAM(14K), decreasing at T_c and remaining at a constant value of $0.46 \pm 0.07 \times 10^7$ s^{-1}, again showing no significant transition at T_m. The values obtained below T_c show significant scatter which was also observed for Py$_2$-PNIPAM(25K) solutions with no PNIPAM(22K) in the previous chapter. This behaviour can be attributed to a combination of low PDI, high f_{free}, and coupled decay times being too close to τ_M, which complicated the analysis of the fluorescence decays.

The value of f_{agg} for Py$_2$-PNIPAM(14K) in Regime I shown in Figure 4.10C increased with increasing temperature until T_c was reached. In Regime II, f_{agg} stayed relatively constant, and decreased significantly as it passed through T_m. Re-ascending temperature ramps of the solution did not yield overlapping values of f_{agg}, though the trends remained similar. The value of f_{agg} for Py$_2$-PNIPAM(25K) remained constant in Regime I, increasing significantly at T_c before reaching a plateau in Regime II, and showing wider variations above T_m. The mixtures of PNIPAM with both Py$_2$-PNIPAM samples yield MFA parameters whose trends are consistent with previous work conducted with Py$_2$-PNIPAM-only solutions for temperatures below T_m. In particular, the behaviour of f_{agg} above T_m is similar to what was observed from the previous study carried out without PNIPAM(22K). However, the decrease in f_{agg} at T_m as the solution enters Regime III is more pronounced in the presence of PNIPAM(22K), and is consistent with PNIPAM(22K) interacting with the Py$_2$-PNIPAM mesoglobules and reducing the local pyrene concentration, hindering pyrene aggregation, and favoring the existence of isolated pyrenes, as illustrated in Figure 4.11.
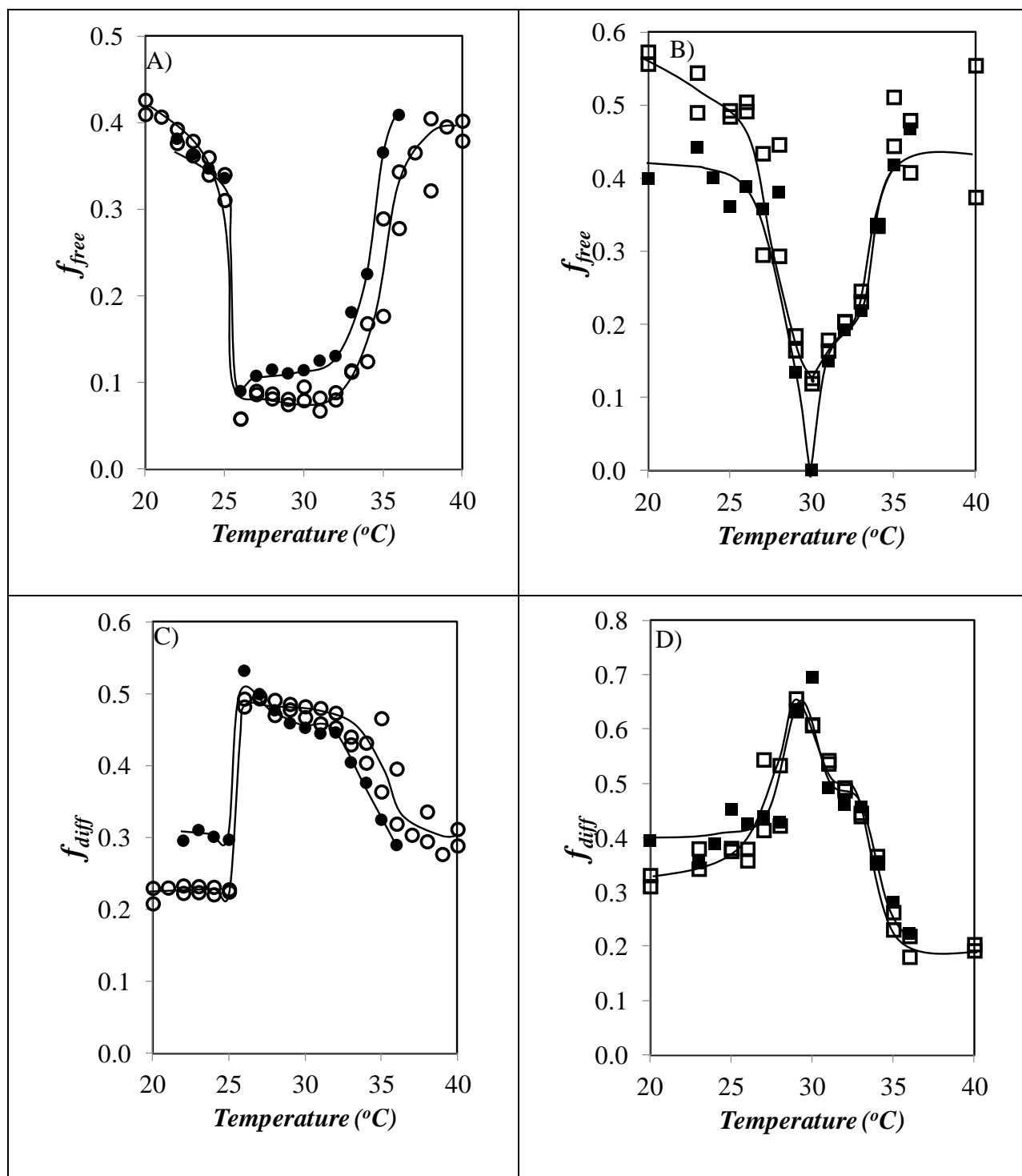
Figure 4.11: MFA parameters f_{free} and f_{diff} for aqueous mixtures of Py$_2$-PNIPAM and PNIPAM(22K) plotted as a function of solution temperature. (●,○) Py$_2$-PNIPAM(14K) and (■,□) Py$_2$-PNIPAM(25K). Hollow symbols: re-ascending temperature.

The trends observed for the f_{free} values of Py$_2$-PNIPAM(14K) in Figure 4.11A show essentially a mirror image of the behaviour of f_{agg}. Throughout Regime I, f_{free} decreases with increasing temperature and decreases sharply at T_c, before increasing slightly with increasing temperature through most of Regime II and increasing sharply as T_m is approached, then reaching a plateau in Regime III. The value of f_{free} for Py$_2$-PNIPAM(25K) in Figure 4.11B results in similar transitions and behaviour with regard to temperature. The value of f_{diff} for Py$_2$-PNIPAM(14K) and Py$_2$-PNIPAM(25K) shown in Figure 4.11C and D, respectively, are both effectively constant in Regime I, increase sharply at T_c, and decrease with increasing temperature thereafter before undergoing a sharp drop at T_m. The increase in the value of f_{free} and the decrease in the value of f_{diff} in Regime III are also consistent with a decrease in local pyrene concentration caused by interactions taking place between PNIPAM(22K) and Py$_2$-PNIPAM mesoglobules that reduce the local pyrene concentration.

The initial temperature ascent for Py$_2$-PNIPAM(14K) shows a number of changes in behaviour when compared to its re-ascending temperature ramp, namely that the re-ascending temperature ramp shows a lower value for $<k>$, a higher value for f_{agg}, and a lower value for f_{diff} below T_c. These effects may be explained by the presence of PNIPAM(22K) mixed with Py$_2$-PNIPAM(14K) within the polymer micelles where it sterically hinders diffusion, lowering the rate of excimer formation by diffusion $<k>$, reducing the molar fraction f_{diff} of pyrenes forming excimer by diffusion, and increasing the molar fraction f_{agg} of aggregated pyrenes. The MFA parameters for the Py$_2$-PNIPAM(25K) sample only show differences between ascending and re-ascending temperature ramps for the values of f_{free} and f_{agg} below T_c, leading to the conclusion that the mixing of polymers which occurs at high temperature causes an increase in the mole

fraction of free pyrene, in contrast to the Py_2-PNIPAM(14K) sample which showed an increase in the mole fraction of aggregated pyrene.

The MFA parameters f_{agg}, f_{free}, and f_{diff} all show significant changes as the solution temperature approaches and surpasses T_m at 34 ^{o}C, with the value of f_{agg} and especially f_{diff} decreasing while f_{free} increases. These trends are consistent with a decrease in local pyrene concentration. Furthermore, the changes in f_{free} and f_{diff} above T_m do not occur in solutions composed solely of Py_2-PNIPAM. Therefore, the decrease in local pyrene concentration must be caused by interactions between aggregated Py_2-PNIPAM and PNIPAM(22K). The only possible cause for a decrease in the pyrene concentration within a Py_2-PNIPAM mesoglobule is if the PNIPAM(22K) is able to interact and mix with the already aggregated Py_2-PNIPAM as PNIPAM(22K) undergoes its CGT. This mixing continues to occur well above T_m, particularly for the Py_2-PNIPAM(14K) sample, and this process is only possible if the Py_2-PNIPAM mesoglobules are still capable of undergoing chain rearrangements in Regime III. This observation implies that the Py_2-PNIPAM mesoglobules cannot be vitreous above T_m, a conclusion that is consistent with work performed on dilute aqueous solutions using Brillouin spectroscopy.[27]

It is remarkable that while the mixing which takes place between the Py_2-PNIPAM samples and PNIPAM(22K) above T_m has such a strong effect on the fractions f_{diff}, f_{free}, and f_{agg} due to the dilution of the pyrene pendants, the rate constant of pyrene excimer formation by diffusion $<k>$ remains constant as the solution temperature increases past T_m. Since $<k>$ is the product of a bimolecular rate constant k_{diff} and the local pyrene concentration $[Py]_{loc}$ in the volume probed by an excited pyrene, the fact that $<k>$ does not change at T_m represents a clear indication that as the overall pyrene concentration inside a mesoglobule decreases, $[Py]_{loc}$

remains constant. For this to happen, $<k>$ must represent the rate constant of excimer formation in pyrene aggregates as it insures a constant $[Py]_{loc}$ and thus a constant $<k>$, as was observed experimentally. In turn, this observation leads to the conclusion that above T_c, where $<k>$ retains the same value throughout Regime II and III, pyrene aggregates represent the loci for excimer formation, whether the excimer is formed pseudo-instantaneously or via short-range diffusion.

4.5 Conclusions

Aqueous mixtures of Py-PNIPAM and PNIPAM(22K) have been studied using light scattering, steady-state fluorescence, and time-resolved fluorescence. Light scattering measurements demonstrated that the Py_2-PNIPAM and PNIPAM(22K) samples undergo their CGT at separate temperatures. The Py_2-PNIPAM chains became insoluble at T_c, whose value depended on the chain length of the Py_2-PNIPAM sample while the PNIPAM(22K) chains became insoluble at T_m. Acquisition of the steady-state fluorescence spectra of the Py_2-PNIPAM and PNIPAM(22K) mixtures allowed the calculation of $(I_E/I_M)^{SS}$, which was found to decrease significantly at both T_c and T_m. The emission maximum of the excimer, λ_{max}, underwent a blue-shift of over 10 nm at T_c indicating an increase in the formation of pyrene aggregates.

Exponential fits of the time-resolved fluorescence decays of the pyrene monomer and excimer yielded the average decay time of the pyrene monomer and excimer which increased with increasing temperature at T_c, and with $<\tau_N>_M$ showing a marked increase at T_m. The increase in decay times for the pyrene monomer and excimer at T_m indicated that PNIPAM(22K) chains were able to interact with Py_2-PNIPAM mesoglobules as the PNIPAM(22K) chains underwent their CGT. Fits of both the pyrene time-resolved fluorescence decays yielded the polydispersity index and the ratio a_{E-}/a_{E+} for the monomer and excimer decays, respectively,

131

and these parameters were found to undergo transitions at T_c that were consistent with what was observed for solutions of pure Py$_2$-PNIPAM. Accounting for their different T_c values, semi-telechelic Py$_1$-PNIPAM mixtures showed similar trends for light scattering, $(I_E/I_M)^{SS}$, and $<\tau_N>_M$ when compared to the telechelic Py$_2$-PNIPAM samples.

MFA of the time-resolved fluorescence decays of the Py$_2$-PNIPAM mixtures yielded $<k>$, as well as the fluorescence fractions f_{agg}, f_{free}, and f_{diff}. The fluorescence fractions f_{agg}, f_{free}, and f_{diff} were all found to show significant changes in the trends observed at both T_c and T_m. While the changes in the MFA parameters at T_c were consistent with observations made for solutions composed of only Py$_2$-PNIPAM in the previous chapter, the changes which occurred at T_m were unique to the mixtures containing PNIPAM(22K). These behavioural changes, namely a decrease in the molar fraction of diffusional and ground-state excimer formation and an increase in the molar fraction of isolated pyrenes, are consistent with a decrease in the local pyrene concentration due the mixing of the Py$_2$-PNIPAM samples and PNIPAM(22K) as PNIPAM(22K) becomes insoluble in water at T_m. The CGT that occurred at T_c caused a significant drop in $<k>$ which is consistent with mesoglobule formation reducing the mobility of pyrene, while its value was unaffected by the mixing of Py$_2$-PNIPAM and PNIPAM(22K) which occurred at T_m.

Since $<k>$ depends on both the mobility and concentration of pyrene, it decreases as either factor decreases. Therefore one would expect to observe a decrease in $<k>$ at T_m as the incoming PNIPAM(22K) chains reduce the pyrene concentration in the Py$_2$-PNIPAM mesoglobules. The best explanation for this behaviour is that the limited mobility of pyrene within a mesoglobule results in diffusional excimer formation occurring over very short distances. Consequently, an excited pyrene will form an excimer by diffusion if it is located

132

within a pyrene aggregate. A reduction in pyrene concentration inside a mesoglobule due to dilution by PNIPAM(22K) results in a decrease in the amount of pyrene forming excimer by diffusion, since it reduces the amount of pyrene that is located within an aggregate. However, since the pyrene concentration is constant within a pyrene aggregate, the rate of excimer formation by diffusion will not change. Consequently the kinetic parameter $<k>$ reports on the rate of excimer formation inside a pyrene aggregate, while the fluorescence fractions f_{agg}, f_{free}, and f_{diff} report on the changes which occur throughout the mesoglobule. Finally, the changes probed by steady-state and time-resolved fluorescence of pyrene observed at T_m for mixtures of Py$_2$-PNIPAM and PNIPAM(22K) are only possible if the already precipitated Py$_2$-PNIPAM mesoglobules are not frozen in a glassy state to allow interactions between the two polymers.

Chapter 5:

Studying Pyrene-Labelled Macromolecules with the Model Free Analysis

5.1 Overview

The Model Free (MF) analysis was applied to the fluorescence decays of 33 pyrene-labelled macromolecules to probe their internal dynamics. Depending on whether pyrene moieties were attached to the chain ends of a linear chain, randomly along a polymer backbone, or at the chain terminals of dendrimers, the results were interpreted in terms of the dynamics of polymer ring closure, backbone flexibility, or chain terminal mobility, respectively. For those polymeric constructs whose decays could be fitted according to Birks' scheme or the Fluorescence Blob Model (FBM), good agreement was obtained between the rate constant for excimer formation retrieved from the MF analysis, $<k^{MF}>$, and those obtained according to the Birks' scheme or FBM analyses. The MF analysis was also applied to conduct the first successful direct comparison of the chain terminal dynamics of two types of pyrene end-labelled dendrons. Finally, the MF analysis was employed to build a calibration curve against which the internal dynamics of any pyrene-labelled macromolecule can now be benchmarked. This study further confirms the versatility and robustness of the MF analysis to study any type of pyrene-labelled macromolecule.

5.2 Introduction

Excimer formation between pyrenyl groups covalently attached onto macromolecules yields information about the extent of translational diffusion undergone by the units of the macromolecule bearing the pyrenyl pendants, which in turn reflects the internal dynamics of the macromolecule which undergoes a conformational rearrangement to enable the diffusive encounter of the pyrenyl pendants.[1-5] Careful design of the synthetic protocol applied to

covalently attach a pyrenyl derivative onto a macromolecule enables one to probe the effects that molecular parameters such as chain length or chain flexibility for a linear polymer[1-4] or internal crowding of a dendrimer[5] have on the macromolecule considered. For instance, the attachment of pyrene to the chain ends of a series of linear monodispersed polymers[1,6-11] or alkyl chains[12-14] of different chain lengths provides information about the effect of chain length on the rate constant of ring closure.   Linear chains randomly labelled with pyrene can be used to assess how the chemical structure of a monomer affects the internal dynamics of the resulting polymer.[3,15-20] Labelling the chain ends of dendrimers of different generations enables one to probe the chain end dynamics as crowding of the dendrimer interior increases with increasing generation number.[21-36] These examples represent the most advanced uses of pyrene excimer formation to characterize a specific aspect of the internal dynamics of different macromolecules and they have been summarized in a number of reviews.[1-5]

In each study, the process of excimer formation is characterized by a rate constant which is obtained by fitting the pyrene monomer and excimer fluorescence decays acquired with a pyrene-labelled macromolecule with an appropriate model.   The DMD model,[27] Birks' scheme,[1,28] Fluorescence Blob Model (FBM),[3,15] and Model Free (MF) analysis[5,26] are typically applied to determine the rate constant of pyrene excimer formation for pyrene end-labelled alkyl chains, pyrene end-labelled linear chains, linear chains randomly labelled with pyrene, and pyrene end-labelled dendrimers, respectively. Out of these four analyses, the MF analysis has been touted as being capable of handling any type of macromolecular architecture labelled with pyrene.[4] This report investigates the validity of this claim by applying the MF analysis to two series of pyrene end-labelled linear chains, three series of polystyrenes randomly labelled with pyrene, and two series of pyrene end-labelled dendrons, and comparing the rate constant of

136
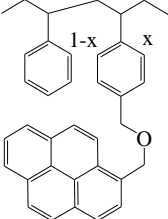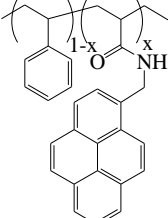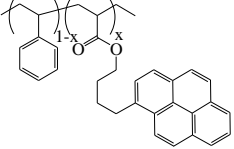
pyrene excimer formation $<k^{MF}>$ obtained by the MF analysis to k_{cy} obtained with the Birks scheme for the end-labelled linear chains and the product $k_{blob} \times N_{blob}$ obtained with the FBM for the randomly labelled linear chains. Considering that the MF analysis does not make any assumption on the modeling details used to describe excimer formation, the good agreement reported herein between $<k^{MF}>$, k_{cy}, and $k_{blob} \times N_{blob}$ is remarkable. This agreement consolidates the claim that the MF analysis can be applied to any type of pyrene-labelled macromolecule. In particular, it validates the use of the MF analysis to conduct the first comparison of the chain end dynamics of two different types of pyrene end-labelled dendrons. Possibly more importantly, the MF analysis was used to generate a universal scale for the ratio of the fluorescence intensity of the excimer I_E over that of the monomer I_M obtained from the MF analysis of the fluorescence decays acquired by the single photon counting (SPC) method, namely the $(I_E/I_M)^{SPC}$ ratio, against which the $(I_E/I_M)^{SPC}$ ratio of any other pyrene-labelled macromolecule can now be compared.
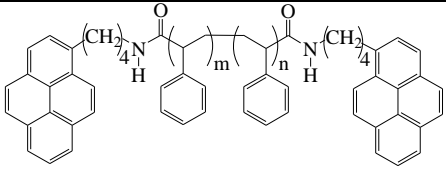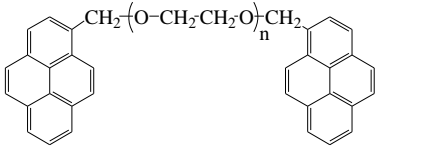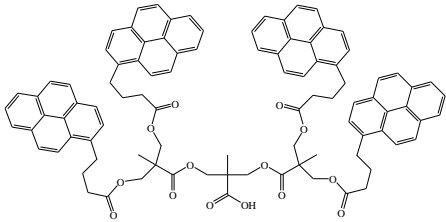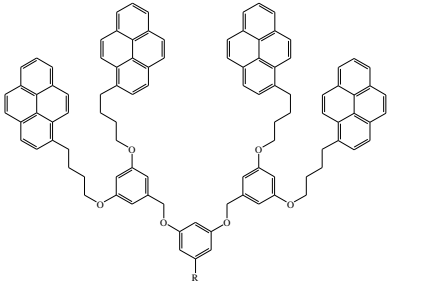
5.3 Experimental

The chemical structure of all pyrene-labelled macromolecules considered is shown in Table 5.1. These macromolecules include three series of polydispersed polystyrene constructs randomly labelled with pyrene (CoEt-PS-MPy and CoAm-PS-MPy labelled with a 1-pyrenemethyl derivative[29] and CoEt-PS-BuPy labelled with a 1-pyrenebutyl derivative[30]), a series of monodispersed polystyrenes end-labelled with 1-pyrenebutylamine (PS-BuPy$_2$),[18] a series of monodispersed poly(ethylene oxide) end-labelled with 1-pyrenemethanol (PEO-MPy$_2$),[11] a series of generation 1 – 4 dendrons made of a bis(hydroxymethyl)propionic acid backbone end-labelled with 1-pyrenebutyric acid (PP-G1-BuPy$_2$, PP-G2-BuPy$_4$, PP-G3-BuPy$_8$, PP-G4-BuPy$_{16}$)[30] and two polyaryl Fréchet-type dendrons labelled with 1-pyrenebutanol (PA-G1-BuPy$_2$ and PA-G2-

BuPy$_4$).[31]   Together, these pyrene-labelled macromolecules offer a variety of molecular architectures between linear chains (CoEt-PS-MPy, CoAm-PS-MPy, CoEs-PS-BuPy, PS-BuPy$_2$, PEO-MPy$_2$) and branched dendrons (PP-G1-BuPy$_2$, PP-G2-BuPy$_4$, PP-G3-BuPy$_8$, PP-G4-BuPy$_{16}$, PA-G1-BuPy$_2$, and PA-G2-BuPy$_4$), modes of labelling between labelling at the ends (PS-BuPy$_2$, PEO-MPy$_2$, PP-G1-BuPy$_2$, PP-G2-BuPy$_4$, PP-G3-Py$_8$, PP-G4-Py$_{16}$, PA-G1-BuPy$_2$, and PA-G2-BuPy$_4$) and randomly along the chain (CoEt-PS-MPy, CoAm-PS-MPy, CoEs-PS-BuPy), and types of pyrene labels between derivatives of 1-pyrenemethyl (CoEt-PS-MPy, CoAm-PS-MPy, PEO-MPy$_2$) and 1-pyrenebutyl (CoEs-PS-BuPy, PS-BuPy$_2$, PP-G1-BuPy$_2$, PP-G2-BuPy$_4$, PP-G3-BuPy$_8$, PP-G4-BuPy$_{16}$, PA-G1-BuPy$_2$, and PA-G2-BuPy$_4$). The acquisition of the steady-state fluorescence spectra and time-resolved fluorescence decays of these macromolecules have been described in earlier publications for CoEt-PS-MPy,[18] CoAm-PS-MPy,[18] CoEs-PS-BuPy,[32] PS-BuPy$_2$,[18] PEO-MPy$_2$,[11] and the pyrene-labelled PP-[26] and PA-[31] dendrimers. A brief summary of the procedures used for the photophysical studies is provided hereafter. Absorption spectra of the polymer solutions were recorded on a CARY 100 Bio UV-Vis spectrophotometer or HP 8452A diode-array spectrophotometer. All of the solutions used for fluorescence measurements had an absorption of less than than 0.1 at 344 nm in tetrahydrofuran, equivalent to a pyrene concentration of 2.5×10^{-6} mol.L^{-1}, low enough to ensure that the process of excimer formation occurs intramolecularly.

Table 5.1: Pyrene contents expressed as the molar fraction x in mol% of pyrene-labelled monomer and λ_{Py} in $\mu mol.g^{-1}$, number-average molecular weights, and PDIs.

Sample structure	Sample name	x mol% Py	λ_{Py} $\mu mol.g^{-1}$	M_n kg.mol^{-1}	PDI
	CoEt-PS-MPy	1.5	141	35	1.81
		1.8	169	45	1.87
		3.2	284	32	1.99
		4.8	412	16	1.85
		5.1	436	34	1.80
		6.4	533	46	1.65
	CoAm-PS-MPy	1.1	105	43	1.88
		2.5	230	39	2.04
		3.7	331	55	1.90
		5.0	437	28	1.88
		5.2	459	34	1.96
		6.4	550	39	1.91
	CoEs-PS-BuPy	2.1	190	46	1.65
		3.1	280	43	1.67
		4.5	390	49	1.62
		5.4	467	53	1.69
		6.0	510	46	1.68
		1.6 [a]	157 [a]	12.7 [a]	1.20 [a]
		2.6	250	8.0	1.09

	PS-BuPy$_2$	4.6	444	4.5	1.12
		6.9	667	3.0	1.10
	PEO-MPy$_2$	0.5	113	16.5	1.05
		0.9	184	10.0	1.05
		1.8	350	5.0	1.08
		4.4	800	2.0	1.10
	PP-G1-BuPy$_2$	n.a.	2,967	0.67	1.0
	PP-G2-BuPy$_4$	n.a.	2,766	1.45	1.0
	PP-G3-BuPy$_8$	n.a.	2,676	2.99	1.0
	PP-G4-BuPy$_{16}$	n.a.	2,632	6.08	1.0
	PP-G4-BuPy$_{16}$ (purified by GPC[15])	n.a.	2,632	6.08	1.0
	PA-G1-BuPy$_2$	n.a.	3,221	0.62	1.0
	PA-G2-BuPy$_4$	n.a.	2,905	1.38	1.0

[a] These samples yielded too little excimer to determine the $(I_E/I_M)^{SS}$ ratio with sufficient accuracy.

Steady-state fluorescence measurements were performed on a Photon Technology International (PTI) LS-100 steady-state fluorometer with an Ushio UXL-75Xe Xenon lamp and a PTI 814 photomultiplier detection system. To determine the ratio of the fluorescence intensity of the pyrene excimer over that of the pyrene monomer from the steady-state (SS) fluorescence spectra, namely the $(I_E/I_M)^{SS}$ ratio, I_M and I_E were determined by taking the integral under the fluorescence spectra over the wavelength range $372 - 378$ nm and $500 - 530$ nm, respectively. Fluorescence decays were acquired using an IBH Ltd. time-resolved fluorometer equipped with an IBH 340 nm NanoLED. The samples were excited at 344 nm and the monomer and excimer fluorescence decays were acquired at 375 and 510 nm, respectively. Residual light scattering was blocked off from reaching the detector with cutoff filters at 370 nm and 480 nm, respectively. All decays were fitted using the MF analysis which has been described in a number of articles.[26,33-35] The decays acquired with the end-labelled linear chains (PS-BuPy$_2$ and PEO-MPy$_2$) were fitted according to the Birks scheme[1,11,18] whereas those acquired with the randomly labelled linear polystyrene (CoEt-PS-MPy, CoAm-PS-MPy, CoEs-PS-BuPy) were fitted with the FBM.[3,15,18,30] The equations used for the analysis of the fluorescence decays are provided in Supporting Information (SI5). Optimization of the pre-exponential factors and decay times was accomplished with the Marquardt-Levenberg algorithm.[36] The quality of the fits was determined from the χ^2 parameter ($\chi^2 < 1.30$) and the random distribution of the residuals and the autocorrelation of the residuals. The parameters retrieved from the analysis of the fluorescence decays with the different models are listed in Tables SI5.1-10 in SI5.

5.4 Results

The fluorescence decays of the pyrene monomer and excimer of all the pyrene-labelled macromolecules presented in this study have been acquired in earlier publications.[18,26,30,31] All decays were fitted according to the MF analysis. In the case of the end-labelled samples and the randomly labelled polystyrenes, their decays were also fitted according to, respectively, Birks' scheme and the FBM for comparison purposes. The equations used to fit the fluorescence decays have been derived earlier[18,26,30,31] and are provided in SI5. The three types of analyses fitted the fluorescence decays of the pyrene monomer and excimer globally and optimized the actual photophysical parameters used to derive the pre-exponential factors and decay times of the equations employed by each model.

The analysis of fluorescence decays acquired with pyrene-labelled macromolecules assumes that excimer formation occurs via either diffusion between an excited pyrene Py^*_{diff} and a ground-state pyrene, or direct excitation of a pyrene dimer $E0$ or D. The difference between the $E0$ and D dimers is whether they are constituted of two properly or improperly stacked pyrene monomers, respectively. After absorption of a photon, $E0^*$ emits as an excimer with a natural lifetime τ_{E0}, whereas D^* emits with a different lifetime τ_D. Beside Py^*_{diff}, $E0^*$, and D^*, a fourth pyrene species often encountered when dealing with pyrene-labelled macromolecules is the species Py^*_{free} which represents those pyrene monomers that do not form excimer and emit with the natural lifetime of pyrene τ_M, either because they are located in a pyrene-poor subdomain of the macromolecule[3,15,16,18-20] or they are not covalently bound to the macromolecule.[5,26,32] Whereas excimer formation is described by a single rate constant in Birks' scheme[1,6-11,28] or a distribution of rate constants in the FBM resulting from the Poisson

distribution of the pyrene labels among the *blobs*,[3,15-20] no assumption is being made in the MF analysis regarding physical processes that determine the diffusive encounters between the pyrene labels.[4,5,26,31-33] Equations 3.4 and 3.5 (page 73) were used to fit the monomer and excimer decays, respectively. The decay of the excimer-forming monomers is represented by a sum of exponentials ($\Sigma a_i \exp(-t/\tau_i)$) whose pre-exponential factors (a_i) and decay times (τ_i where $\tau_i < \tau_M$) are used to describe the excimers which form via diffusion. MF analysis of the pyrene monomer and excimer decays is conducted globally and yields the molar fractions of the four pyrene species present in solution, namely f_{diff}, f_{free}, f_{E0}, and f_D for the Py^*_{diff}, Py^*_{free}, $E0^*$, and D^* species, respectively, the excimer lifetimes τ_{E0} and τ_D, and the pre-exponential factors (a_i) and decay times (τ_i). In turn, the set of a_i and τ_i parameters is used to calculate the average rate constant of pyrene excimer formation, $<k^{MF}>$, whose expression is given in Equation 5.1.

$$< k^{MF} >= \frac{1}{<\tau>} - \frac{1}{\tau_M} \tag{5.1}$$

In Equation 5.1, $<\tau>$ is the number average lifetime of the pyrene monomer ($\Sigma a_i \tau_i / \Sigma a_i$) which excludes the contribution of Py^*_{free}.

Comparison of MF and Birks' scheme analysis: Birks' scheme was applied solely to the PEO-MPy$_2$ and PS-BuPy$_2$ samples. The main difference between an analysis based on Birks' scheme or the MF is the use of an excimer dissociation rate constant (k_{-cy}) in the former analysis.[1,28] In the latter analysis, k_{-cy} is neglected.[4,5] The analysis of the fluorescence decays acquired with pyrene end-labelled linear chains is difficult because these samples are notorious for forming

very little excimer as the chain holds the pyrene labels away from each other.[18] The weak

excimer formation results in the pyrene monomer decaying in a quasi-monoexponential fashion,

which complicates the recovery of the various parameters involved in the kinetic scheme. To

constrain the MF and Birks' scheme analysis, the excimer lifetime (τ_{E0}) in the analysis of the

fluorescence decays was fixed to the value recovered with the shortest PS-BuPy$_2$ (τ_{E0} = 48 ns)

and PEO-MPy$_2$ (τ_{E0} = 55 ns) samples which formed the most excimer. The results of these

analyses are listed in Tables SI5.1-3 for the MF analysis and Tables SI5.5-7 for the Birks'

scheme analysis. As typically observed for pyrene end-labelled polymers,[1,7-11] the k_{-cy} values

recovered from the Birks' scheme analysis were small and equal to 3.7 ($\pm$ 0.6) $\times$ 10^6 s^{-1} and 2.9

($\pm$ 0.7) $\times$ 10^6 s^{-1} for the PS-BuPy$_2$ and PEO-MPy$_2$ series, respectively. The small k_{-cy} values

support the assumption made in the MF and FBM analysis that k_{-cy} can be neglected.

The rate constants of excimer formation k_{cy} and $<k^{MF}>$ were determined and plotted in

Figure 5.1 as a function of polymer chain length in terms of the number of atoms constituting the

chains using 2 and 3 atoms for a styrene and ethylene oxide monomer, respectively. In all cases,

k_{cy} was between 10 – 40% larger than $<k^{MF}>$. As has been observed in numerous examples with

k_{cy}, both data series showed a strong decrease in the rate constant of excimer formation with

increasing polymer chain length.

The flexible PEO backbone made of ether bonds enables easier excimer formation than

polystyrene with its bulky phenyl side-group. This is clearly reflected by both k_{cy} and $<k^{MF}>$

which, for a given chain length, take much larger values for the PEO-MPy$_2$ series than for the

PS-BuPy$_2$ series. The scaling exponent (α) for k_{cy} ($\sim N^{-\alpha}$) was found to equal 0.87 ($\pm$0.13) and

1.38 ($\pm$0.23) for PS-BuPy$_2$ and PEO-MPy$_2$, respectively. Within experimental error, the same α

exponents were obtained for $<k^{MF}>$ taking values of 0.95 ($\pm$0.09) and 1.52 ($\pm$0.24) for PS-BuPy$_2$

and PEO-MPy$_2$, respectively. These exponents fall within the 0.9 – 1.9 range typically obtained for a Birks' scheme analysis of fluorescence decays acquired with pyrene end-labelled linear chains.[1,9,11,37]

While an excellent agreement was obtained between $<k^{MF}>$ from the MF analysis and k_{cy} from the Birks' scheme analysis in Figure 5.1, it is worthwhile to point out that the α–values obtained for k_{cy} of 0.87 ± 0.13 for PS-BuPy$_2$ and 1.38 ± 0.23 for PEO-MPy$_2$ in THF are somewhat different from those of 1.62 and 0.91 ± 0.12 reported by Winnik et al.[7] and Ghiggino et al.[9] for PS in toluene and PEO in THF, respectively. In the case of PEO, the k_{cy} values obtained by Ghiggino et al. agree very well with ours as can be seen in Figure SI5.1. We suspect that the difference in the α–value of the exponent is a consequence of the small number of data points used in both studies, three in the study by Ghiggino and four in our study. Averaging these seven data points in Figure SI5.1 results in an α–value of 1.18 ± 0.12, intermediate between the two α–values of 0.91 and 1.38. In the case of polystyrene, the solvents are different. However, toluene and THF are both good solvents for polystyrene and both have similar viscosity. Consequently, pyrene excimer formation should proceed in a similar manner in both solvents. This is indeed observed in Figure SI5.2 where the k_{cy} values obtained by Winnik et al. are similar to our values, except for the longer chains. It must be pointed that we did not include in our report a longer PS-BuPy$_2$ sample with an M_n of 15 K, for which the monomer decay could hardly be distinguished from that of the model compound. For these longer chains, we find that the polymer is so long that some excited pyrenes can no longer probe the entire polymer coil. This is evidenced by the large f_{Mfree} value of 0.49 in Table SI5.5 found for the PS-BuPy$_2$ sample with an M_n value of 13 K. A recent study has found that, under such conditions, an excited pyrene probes a subvolume of the polymer coil referred to as a *blob* and

k_{cy} plateaus as it represents excimer formation inside V_{blob}, and thus no longer depends on chain length.
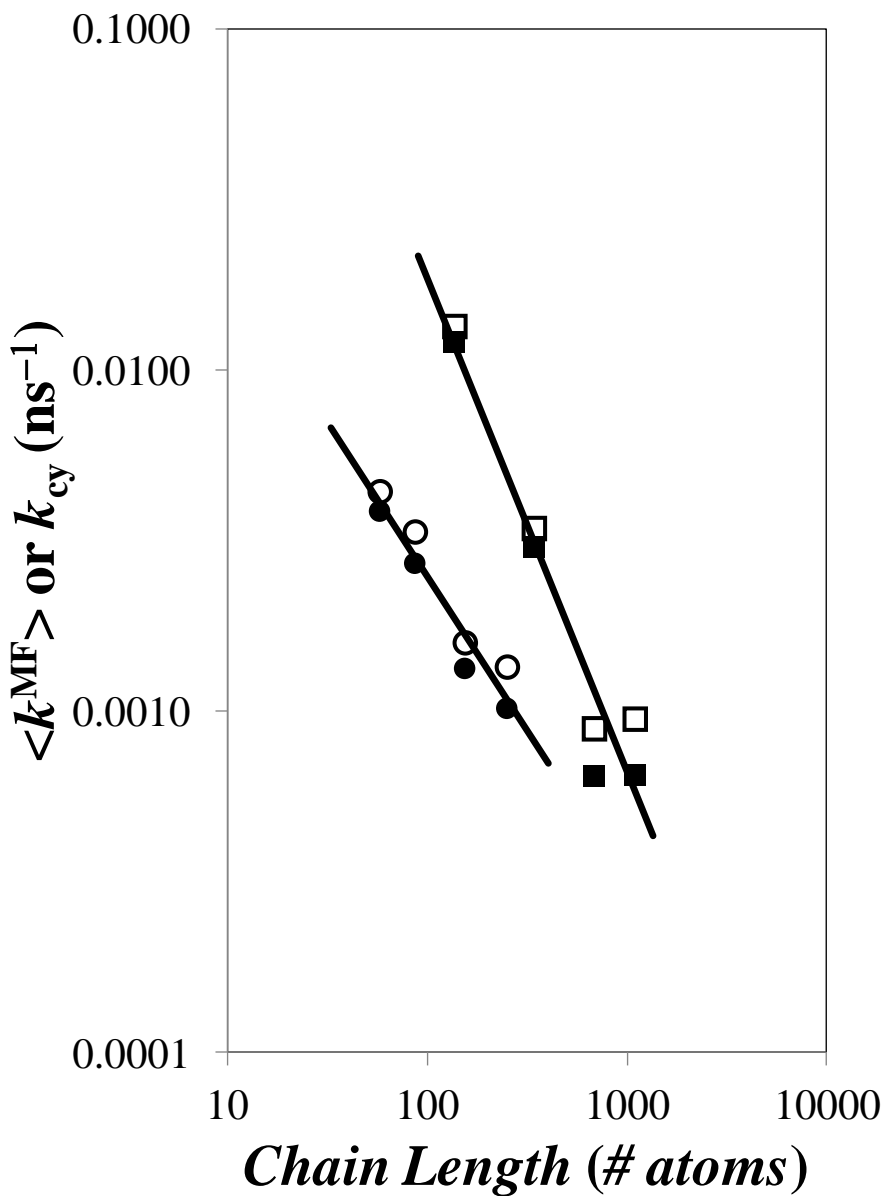
Figure 5.1: Plot of $<k^{MF}>$ (filled symbols) and k_{cy} (open symbols) versus chain length for PS-BuPy$_2$ (circles) and PEO-MPy$_2$ (squares) in tetrahydrofuran. [Py] = 2.5×10^{-6} mol.L^{-1}.

In the Winnik et al. study,[7] the fluorescence decays of the pyrene monomer were fitted with two exponentials without accounting for those pyrenes that did not form excimer, namely the Py^*_{free} species. It is possible that the presence of the Py^*_{free} species resulted in longer decay times which, in turn, led to smaller k_{cy} values in the study by Winnik et al. and an apparently steeper drop in k_{cy} as a function of M_n. However, these discrepancies could also be due to the small number of samples used in our study.

In any case, the purpose of the present study was not to determine the scaling law between k_{cy} and M_n, in which case a much larger number of samples would have been needed, but rather, to demonstrate that the MF and Birks' scheme analysis provided similar information about the kinetics of excimer formation for end-labelled linear chains. The good agreement found in Figure 5.1 indicates that this is indeed the case. Considering that the MF analysis makes no assumption about the process of excimer formation, the similarity between the trends shown in Figure 5.1 for $<k^{MF}>$ and k_{cy} and the ability of $<k^{MF}>$ to report on the known flexibility of the PEO chain versus that of polystyrene is quite remarkable.

Comparison of MF and FBM analysis: The results obtained from the MF and FBM analyses of the fluorescence decays acquired with the randomly labelled polystyrenes are listed in Tables SI5.1-3 and SI5.8-10, respectively. Within the FBM framework,[3,15-20] an excited pyrene probes a finite volume within the polymer coil while it remains excited. This volume is referred to as a *blob* or V_{blob}. V_{blob} represents a unit volume that is used to divide the polymer coil into a cluster of *blobs* among which the randomly attached pyrene labels distribute themselves randomly according to a Poisson distribution. Excimer formation occurs sequentially with slow diffusive encounter inside the *blobs* of the monomers bearing the pyrene labels characterized by a rate constant k_{blob}, followed by a rapid rearrangement of these pyrene labels to form an excimer with

a rate constant k_2. FBM analysis of the fluorescence decays yields k_{blob} and $<n>$, the average pyrene content inside one *blob*. The parameter $<n>$ is used to determine N_{blob}, the number of monomers constituting the polymer stretch encompassed inside a *blob*. The expression of N_{blob} is given in Equation 5.2.

$$N_{blob} = \frac{1 - f_{Mfree}}{\lambda_{Py}} \times \frac{<n>}{x \times M_{Py} + (1 - x) \times M} \qquad (5.2)$$

In Equation 5.2, f_{Mfree} represents the fraction of pyrenes that do not form excimer in the pyrene monomer decay, λ_{Py} is the pyrene content listed in Table 5.1 and expressed in moles of pyrene per gram of polymer, and M_{Py} and M are the molar masses of the pyrene labelled monomer and the styrene monomer, respectively. In several instances, the product $k_{blob} \times N_{blob}$ has been shown to provide a good representation of the polymer chain dynamics and remains constant with varying pyrene content.[20,30,38] This trend is observed in Figure 5.2 where the products $k_{blob} \times N_{blob}$ takes values of 0.60 (± 0.05), 0.47 (± 0.01), and 0.37 (± 0.02)$\times 10^9$ s^{-1} for the CoEt-MPy, CoEs-PS-BuPy, and CoAm-PS-MPy, respectively. This trend is consistent with those published earlier[30] where the decays acquired for CoEt-MPy and CoAm-PS-MPy were fitted with a simpler version of the FBM.

According to the FBM, k_{blob} is a pseudo-unimolecular rate constant equal to the product of the bimolecular rate constant k_{diff} describing the diffusive encounters between two pyrene labels and the local pyrene concentration equivalent to one pyrene inside a blob, namely $1/V_{blob}$. By comparison, $<k^{MF}>$ obtained with the MF analysis equals the product of k_{diff} and the local

pyrene concentration inside the polymer coil which can be estimated as $<n>/V_{blob}$. These considerations lead to Equation 5.3 that relates the product $k_{blob} \times N_{blob}$ to the rate constant $<k^{MF}>$.

$$k_{blob} \times N_{blob} = \frac{<k^{MF}>}{<n>} \times N_{blob} = \frac{1 - f_{Mfree}}{\lambda_{Py}} \times \frac{<k^{MF}>}{x \times M_{Py} + (1-x) \times M} = <k^{MF}>^{blob} \qquad (5.3)$$

$<k^{MF}>^{blob}$ was plotted in Figure 5.2 as a function of pyrene content for the three polystyrene series in THF. Here again the agreement between $k_{blob} \times N_{blob}$ and $<k^{MF}>^{blob}$ is rather good, considering that no assumption is being made to obtain $<k^{MF}>$. $<k^{MF}>^{blob}$ equals 0.56 ($\pm$0.02), 0.43 ($\pm$0.04), and 0.33 ($\pm$0.02)$\times 10^9$ s^{-1} for CoEt-MPy, CoEs-PS-BuPy, and CoAm-PS-MPy, respectively. Within experimental error, $<k^{MF}>^{blob}$ and $k_{blob} \times N_{blob}$ were found to be equivalent.

As for the product $k_{blob} \times N_{blob}$, the differences in $<k^{MF}>^{blob}$ reflect the mode of attachment of the pyrene derivative.[30] In the case of CoEt-PS-MPy, pyrene is bound to polystyrene via a flexible ether bridge linked to the phenyl ring. Pyrene being further away from the backbone probes a larger V_{blob} which results in larger $<k^{MF}>^{blob}$ and $k_{blob} \times N_{blob}$ values in Figure 5.2. The amide linker connecting pyrene to the polystyrene backbone of CoAm-PS-MPy is short and rigid. Consequently, small N_{blob} values were retrieved and $<k^{MF}>^{blob}$ and $k_{blob} \times N_{blob}$ took the smallest values. CoEs-PS-BuPy with its butyl linker holds the pyrene labels at an intermediate distance between CoAm-PS-Mpy and CoEt-PS-MPy and intermediate values of $<k^{MF}>^{blob}$ and $k_{blob} \times N_{blob}$ were obtained in Figure 5.2.

The trends shown in Figures 5.1 and 5.2 indicate that $<k^{MF}>$ provides a reasonable representation of the internal dynamics of end-labelled and randomly labelled polymers when compared with the results obtained with well-established models. It is now used to probe the internal dynamics of two end-labelled types of dendrons.
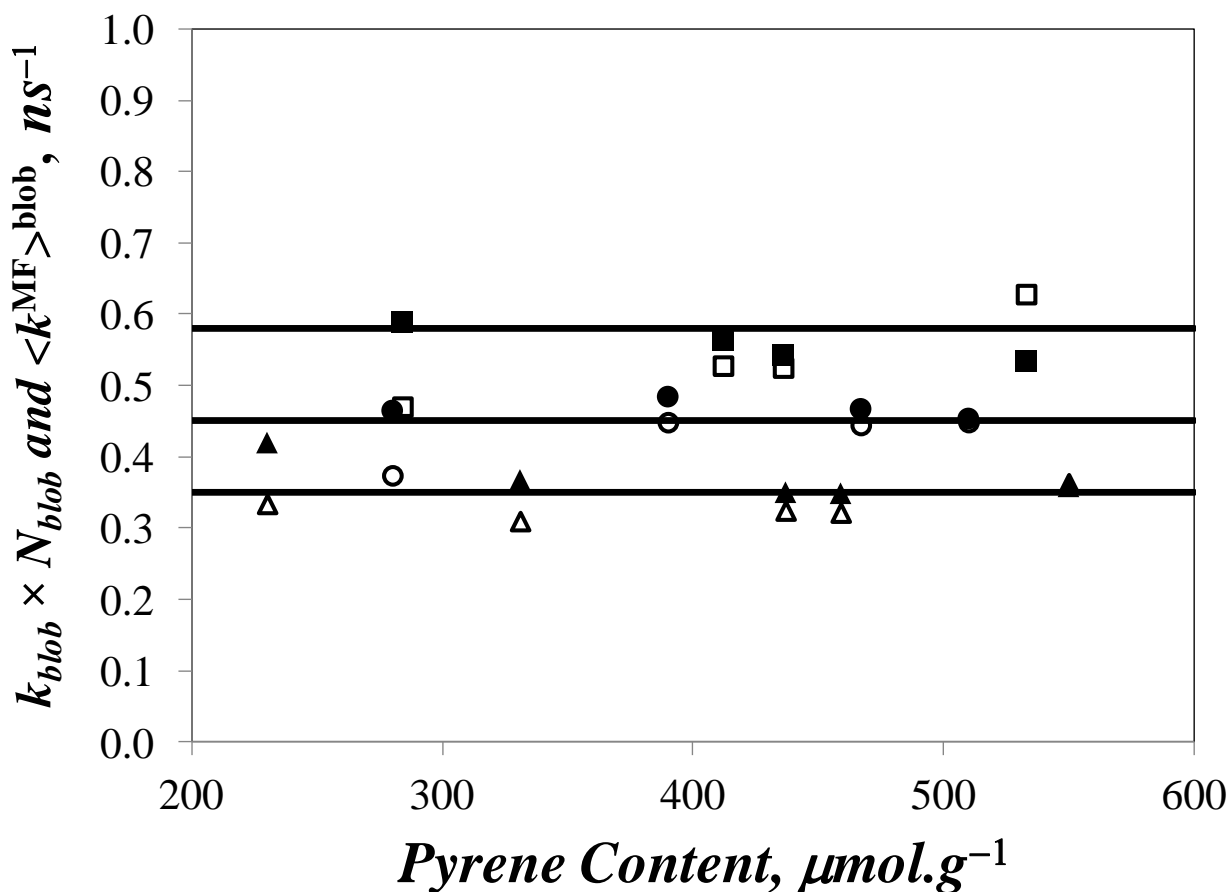
Figure 5.2. Plot of $k_{blob} \times N_{blob}$ (filled) and $<k^{MF}>^{blob}$ (empty) versus pyrene content for CoEt-MPy (squares), CoEs-PS-BuPy (circles), and CoAm-PS-MPy (triangles) in tetrahydrofuran. [Py] = 2.5×10^{-6} mol.L^{-1}.

MF analysis of the fluorescence decays acquired with the pyrene end-labelled dendrons: The fluorescence decays acquired for the pyrene monomer and excimer of the PP- and PA-based dendrons were fitted according to the MF analysis. The results of these analyses are listed in Tables SI5.1-3. To date, the MF analysis represents the only procedure available in the literature that can be employed to draw quantitative information about the internal dynamics of dendrons end-labelled with pyrene.[5,26] A plot of $<k^{MF}>$ versus generation number is shown in Figure 5.3.

150
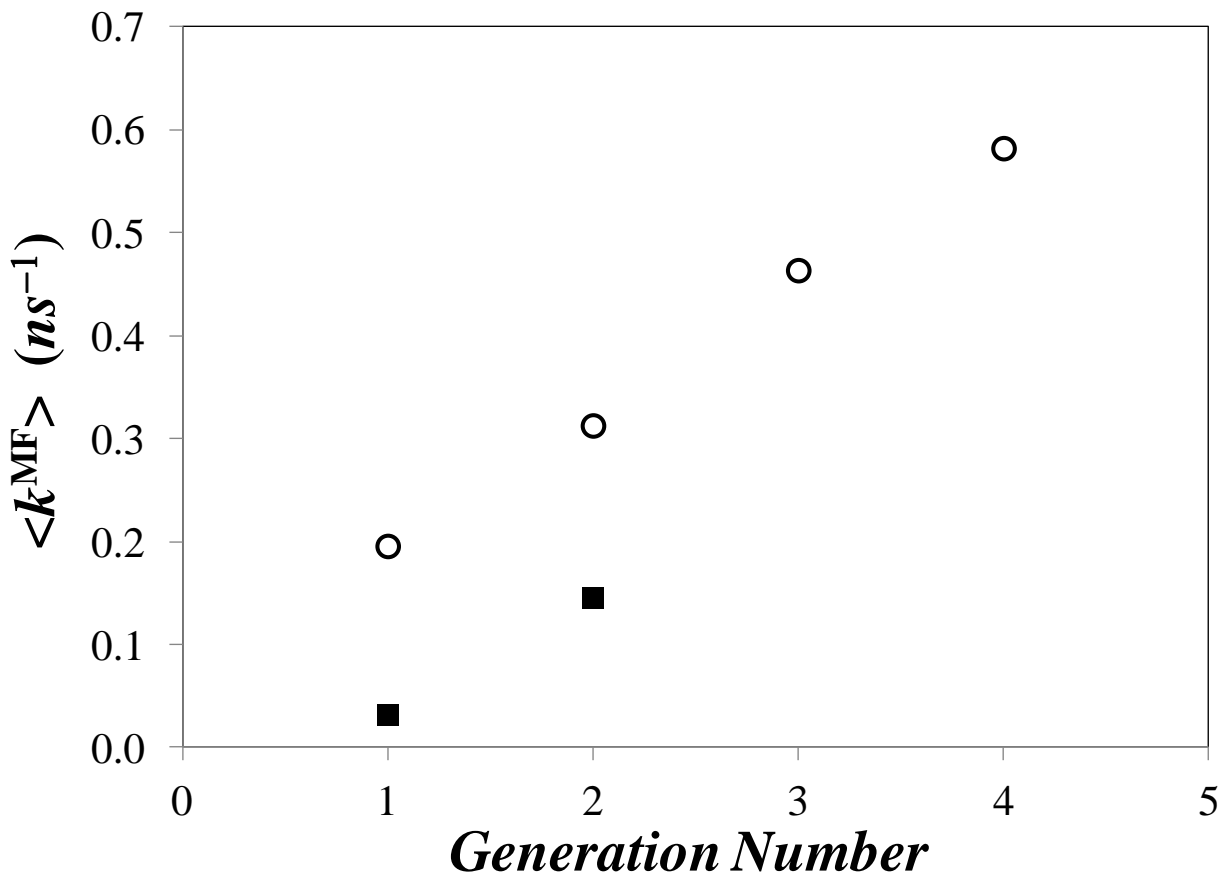
Figure 5.3. Plot of $<k^{MF}>$ versus generation number for (○) PP- and (■) PA-based dendrons in tetrahydrofuran. [Py] = 2.5×10^{-6} mol.L^{-1}.

Although the trend of $<k^{MF}>$ versus generation number for the PP-dendrons has been reported earlier,[26] it is the first time that this trend is being compared to that obtained with another type of dendron. The rigid phenyl building blocks constituting PA-G1-BuPy$_2$ and PA-G2-BuPy$_4$ hinder substantially excimer formation, resulting in a much smaller $<k^{MF}>$ value for a given generation. The crowded and rigid environment of the PA-dendrons prevented the successful labelling of the higher generation dendrons with 1-pyrenebutanol. Literature on the preparation of PA-dendrons labelled with pyrene indicates that this problem is not uncommon.[39,40] $<k^{MF}>$ for PA-G1-BuPy$_2$ and PA-G2-BuPy$_4$ was found to be 1.7×10^8 s^{-1} smaller

151

than the PP-based dendrons for the same generation number. It would be interesting to investigate whether this difference in $<k^{MF}>$ remains the same for higher generation dendrons and whether it reflects the difference in chemical structure between the PP- and PA-based dendrons end-labelled with pyrene.

5.5 Discussion

On the one hand, excimer formation of any pyrene-labelled macromolecule (PLM) can be characterized qualitatively from the ratio of the steady-state (SS) fluorescence of its excimer (I_E) over that of its monomer (I_M) by using the $(I_E/I_M)^{SS}$ ratio. On the other hand, the time scale over which pyrene excimer formation takes place is characterized by time-resolved fluorescence, but the quantitative analysis of the fluorescence decays requires a model. The models which have been developed to fit the decays of PLMs are conceptually different and can only be applied to the precise macromolecular architecture for which they were designed. As mentioned earlier, Birks' scheme is only applicable to monodispersed short end-labelled linear polymers[1,7-11] whereas the FBM is used with linear chains randomly labelled with pyrene.[3,15-20] The DMD model was derived to describe excimer formation for short alkyl chains end-labelled with pyrene.[12-14,27] In contrast to these models, which apply to specific PLMs, the MF analysis can be employed to fit the decays of any PLM, and as Figures 5.1–3 suggest, it provides relevant information about the internal dynamics of a given PLM which compares very well with that provided by the more specific models. In effect, the versatility of the MF analysis implies that it could be used to probe the dynamics of pyrene excimer formation in the same comprehensive manner as the $(I_E/I_M)^{SS}$ ratio obtained by steady-state fluorescence is being used to characterize the efficiency of pyrene excimer formation for any PLM. The following argument demonstrates

152

that this is indeed the case, and that contrary to the $(I_E/I_M)^{SS}$ ratio whose experimental determination is subject to a number of complications,[43] information obtained from the MF analysis is impervious to the nature of the pyrene derivative used to label the macromolecule and yields an absolute value of the I_E/I_M ratio.

The MF analysis of the pyrene monomer and excimer decays yields the molar fractions f_{diff}, f_{free}, f_{E0}, and f_D of the pyrene species Py^*_{diff}, Py^*_{free}, $E0^*$, and D^*, respectively. In turn, these fractions can be combined with the rate constant $<k^{MF}>$ and the lifetimes $<\tau>$, τ_M, τ_{E0}, and τ_D to yield the $(I_E/I_M)^{SPC}$ ratio whose expression is shown in Equation 5.4.

$$\left(\frac{I_E}{I_M}\right)^{SPC} = \frac{f_{diff}\times <k^{MF}>\times\tau_{E0}\times<\tau>+f_{E0}\times\tau_{E0}+f_D\times\tau_D}{f_{diff}\times<\tau>+f_{free}\times\tau_M} \qquad (5.4)$$

Under the condition that all excited pyrenes form excimer by diffusion exclusively, then f_{diff} equals unity, the fractions f_{free}, f_{E0}, and f_D equal zero, and Equation 5.4 predicts that $(I_E/I_M)^{SPC}_{ffree=0}$ equals the product $<k>\times\tau_{E0}$. This result is reassuring as similar relationships have been proposed for excimer formation in solution through the diffusive encounters of molecular pyrene free in solution[28] or covalently bound onto a linear polymer.[1,6,41,42] Equation 5.4 was used for all constructs listed in Table 5.1 except for the CoAm-PS-MPy series and the PA-dendrons for which a slightly modified version of Equation 5.4 was used (see Equation SI5.6 in SI5 for more details).

The fluorescence spectra and decays of the samples listed in Table 5.1 were analyzed to yield their $(I_E/I_M)^{SS}$ and $(I_E/I_M)^{SPC}$ ratios which were compared in Figure 5.4. The $(I_E/I_M)^{SS}$ and $(I_E/I_M)^{SPC}$ ratios cluster along straight lines having a slope of unity but are shifted up and down

by a set value depending on the pyrene derivative used to prepare the macromolecular construct. The discrepancy between the trends is due to differences in fluorescence intensity at 375 nm used to determine I_M in the $(I_E/I_M)^{SS}$ ratio since the $S_{1,0} \rightarrow S_{0,0}$ transition is partially and fully allowed for the 1-pyrenemethyl bearing a heteroatom in the β–position and 1-pyrenebutyl derivatives, respectively.[11] This is illustrated in Figure SI5.3 in Supporting Information where the fluorescence spectra of a CoEs-PS-BuPy and CoEt-PS-MPy sample labelled with, respectively, 3.1 and 2.7 mol% of pyrene are shown side-by-side. Although the samples are chemically identical, CoEt-PS-MPy seems to form much more excimer relative to the monomer than CoEs-PS-BuPy. Consequently, the $(I_E/I_M)^{SS}$ ratio is inherently larger for the PEO-MPy$_2$, CoEt-PS-MPy, and CoAm-PS-MPy samples which were labelled with a 1-pyrenemethyl moiety, as found experimentally in Figure 5.4. The long butyl linker insulates pyrene more efficiently so that the trends obtained in Figure 5.4 with the 1-pyrenebutyl derivative are much better aligned with one another than those obtained with the 1-pyrenemethyl derivative.

The linear relationship obtained between the $(I_E/I_M)^{SS}$ and $(I_E/I_M)^{SPC}$ ratios indicates that both quantities are equivalent. Even though all fluorescence spectra were acquired in a same laboratory, thereby avoiding many of the pitfalls associated with the analysis of steady-state fluorescence spectra acquired in different laboratories,[43] little can be done to account for the inherent differences in I_M values obtained with different pyrene derivatives (see Figure SI5.3). Interestingly, the $(I_E/I_M)^{SPC}$ ratio is not affected by the many complications that plague the determination of the $(I_E/I_M)^{SS}$ ratio as it deals with absolute quantities (see Equation 5.4). It takes thus an absolute value that can be reproduced in any other laboratory.
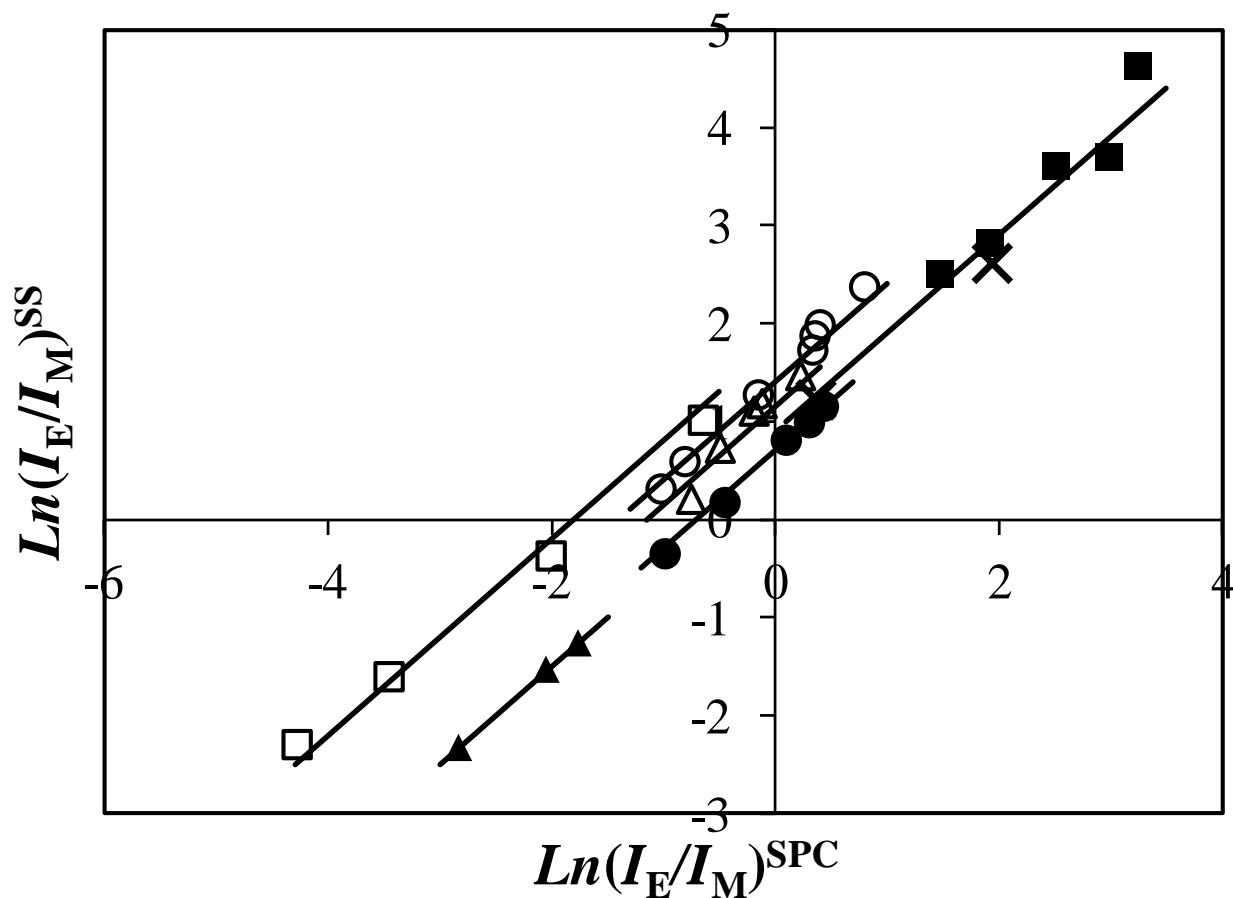
Figure 5.4. Comparison of the $(I_E/I_M)^{SS}$ and $(I_E/I_M)^{SPC}$ ratios obtained for the (■) PP- and (×) PA-dendrons, and the samples CoEs-PS-BuPy (●), PS-BuPy$_2$ (▲), CoEt-PS-MPy (○), CoAm-PS-MPy (Δ), and PEO-MPy$_2$ (□) in tetrahydrofuran. [Py] = 2.5×10^{-6} mol.L^{-1}. Lines with slopes equal to unity have been drawn through the data points to guide the eye.

The efficiency of pyrene excimer formation for PLMs in solution depends on the local pyrene concentration $[Py]_{loc}$ inside the solution volume occupied by the macromolecule and the polymer flexibility.[1,3-5,40,41] In this respect, Figure 5.4 highlights how the molecular architecture affects the efficiency of excimer formation. Considering the trend obtained with the 1-pyrenebutyl derivative, the PS-BuPy$_2$ samples where the pyrene pendants are held apart by the chain yield the smallest I_E/I_M ratios although their pyrene content λ_{Py} in Table 5.1 is similar to

that of the randomly labelled polymers CoEs-PS-BuPy. For both the PS-BuPy$_2$ and CoEs-PS-BuPy series, the $(I_E/I_M)^{SS}$ and $(I_E/I_M)^{SPC}$ ratios increase with λ_{Py} as expected since a larger λ_{Py} value results in a larger $[Py]_{loc}$. Yet the dendrons having a similar λ_{Py} value for all generations see their $(I_E/I_M)^{SS}$ and $(I_E/I_M)^{SPC}$ ratios increase linearly with increasing generation number, a consequence of the increased branching.[26] The CoEt-PS-MPy and CoAm-PS-MPy series having a similar architecture and being both labelled with a 1-pyrenemethyl derivative yield similar $(I_E/I_M)^{SS}$ and $(I_E/I_M)^{SPC}$ ratios which are offset from those obtained with the constructs labelled with a 1-pyrenebutyl linker due to the different spectral features shown in Figure SI5.3.

Both the $(I_E/I_M)^{SS}$ and $(I_E/I_M)^{SPC}$ ratios and the average rate constant of excimer formation $<k^{MF}>$ are measures of the efficiency of excimer formation. Consequently, the $(I_E/I_M)^{SPC}$ ratio was plotted as a function of $<k^{MF}>$ in Figure 5.5. Except for the pyrene-labelled dendrimers and the end-labelled linear chains whose $(I_E/I_M)^{SPC}$ ratios showed substantial scatter, $(I_E/I_M)^{SPC}$ was found to increase linearly with increasing $<k^{MF}>$ as Equation 5.4 predicts if f_{diff} equals unity and all other molar fractions f_{free}, f_{E0}, and f_D equal 0. Indeed, f_{diff} is always larger than 0.80 in Table SI5.3 except for the longest PS-BuPy$_2$ and PEO-MPy$_2$ samples which indicates that pyrene excimer is formed essentially by diffusion as would be expected in tetrahydrofuran which is a good solvent for pyrene. However, earlier studies have pointed out that the $(I_E/I_M)^{SPC}$ ratio obtained with pyrene-labelled dendrimers is highly sensitive to unattached pyrene labels even though f_{free} for these samples is smaller than 0.03.[5,26,32]
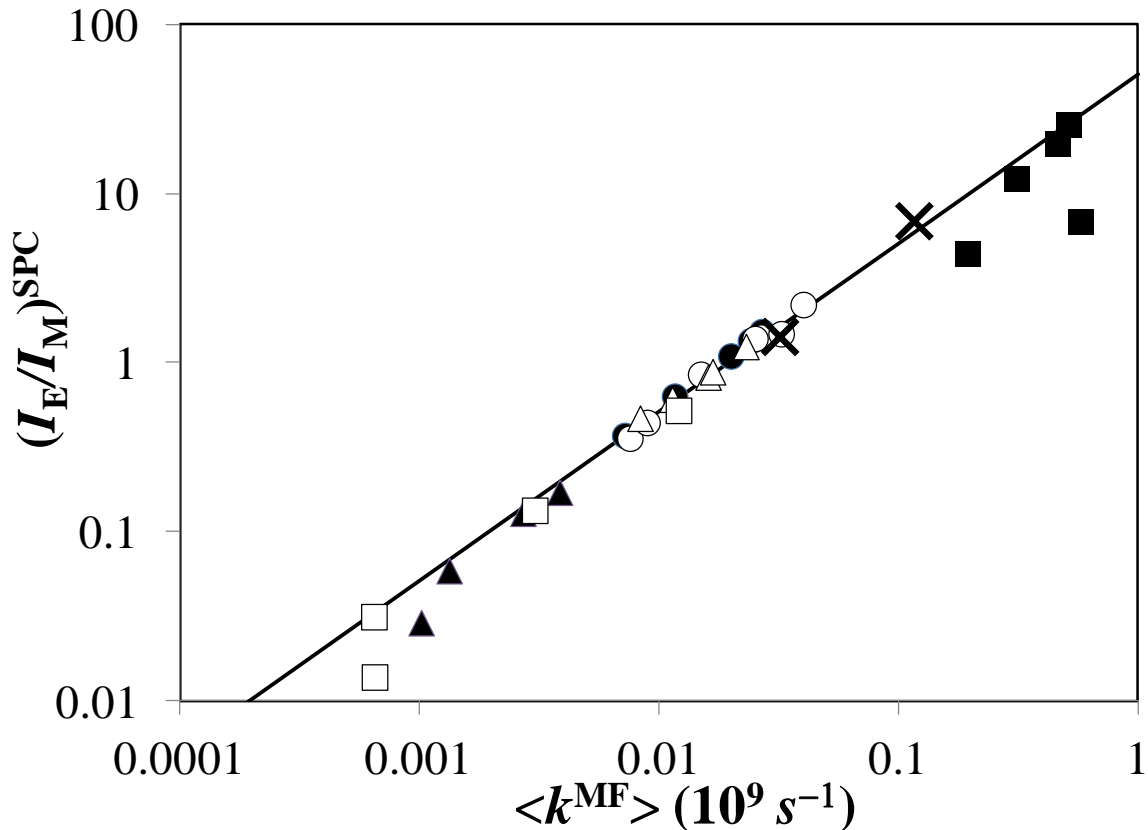
Figure 5.5. Comparison of the $(I_E/I_M)^{SPC}$ ratios with the $<k^{MF}>$ values obtained for the (■) PP- and (×) PA-dendrons, and the samples CoEs-PS-BuPy (●), PS-BuPy$_2$ (▲), CoEt-PS-MPy (○), CoAm-PS-MPy (Δ), and PEO-MPy$_2$ (□) in tetrahydrofuran. [Py] = 2.5×10^{-6} mol.L^{-1}.

Also, a recent study has indicated that as the chain length of an end-labelled polymer increases, the excited pyrene located at one end of the polymer can no longer probe the entire polymer coil and emits with the natural lifetime of the monomer.[11] This phenomenon leads to an increase in f_{free} which results in a decrease of the $(I_E/I_M)^{SPC}$ ratio while $<k^{MF}>$ tends to a constant value, as observed in Figure 5.5 for PS-BuPy$_2$ and PEO-MPy$_2$. As can be seen in Figure 5.6, setting f_{free} equal to 0.0 in Equation 5.4 yields a perfect trend where the $(I_E/I_M)^{SPC}_{ffree=0}$ ratio of all pyrene-

labelled constructs listed in Table 5.1 increases linearly with increasing $<k^{MF}>$ with a slope τ_{E0} of

51 ns, a reasonable value for the pyrene excimer lifetime in tetrahydrofuran.[28]
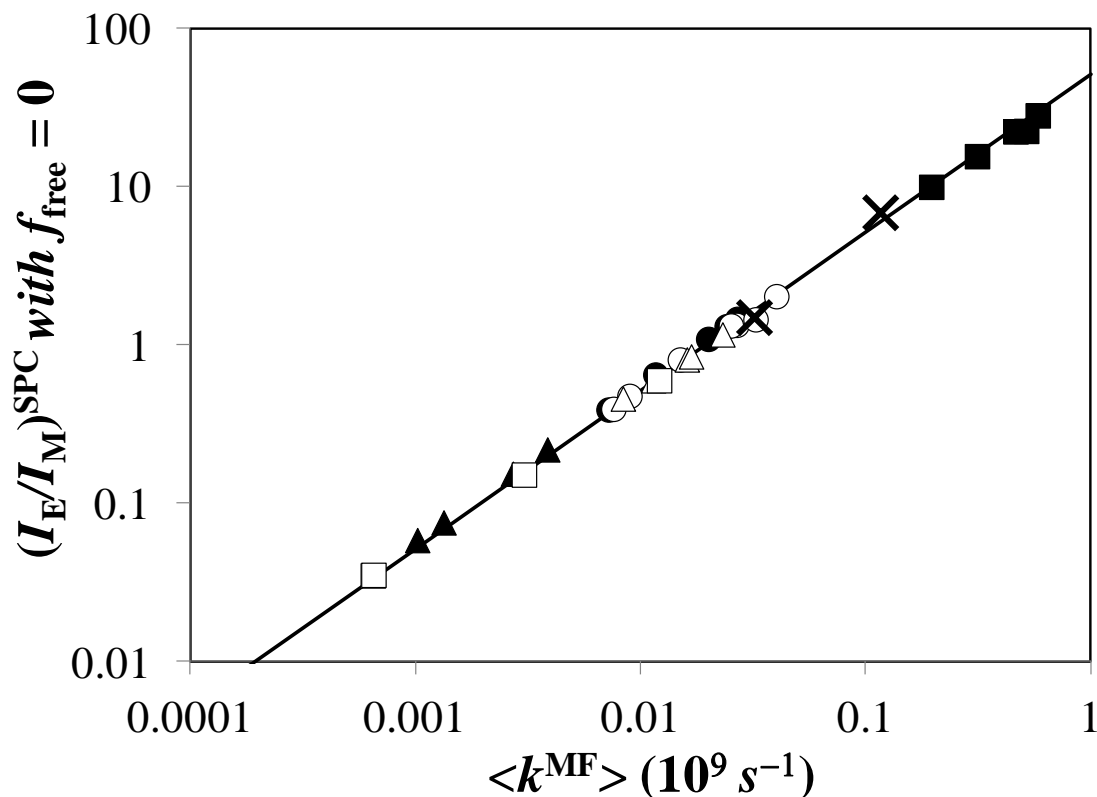
Figure 5.6. Comparison of the $(I_E / I_M)^{SPC}_{ffree=0}$ ratios with the $<k^{MF}>$ values obtained for the (■)

PP- and (×) PA-dendrons, and the samples CoEs-PS-BuPy (●), PS-BuPy$_2$ (▲), CoEt-PS-MPy

(○), CoAm-PS-MPy (Δ), and PEO-MPy$_2$ (□) in tetrahydrofuran. $[Py] = 2.5 \times 10^{-6}$ mol.L^{-1}.

It might first seem inconsistent that the $(I_E/I_M)^{SS}$ and $(I_E/I_M)^{SPC}$ ratios which show such

good correlations with one another in Figure 5.4 would yield a more scattered $(I_E/I_M)^{SPC}$-versus-

$<k^{MF}>$ trend in Figure 5.5, as observed for the dendrimers and the end-labelled linear chains. Yet

this result is expected. As a matter of fact, the $(I_E/I_M)^{SS}$ and $(I_E/I_M)^{SPC}$ ratios both take into

account the contributions of all pyrene species found in solution including that of Py^*_{free}, whereas $<k^{MF}>$ is the average rate constant of excimer formation for those pyrenes that form excimer by diffusion, namely the Py^*_{diff} species. Thus $(I_E/I_M)^{SS}$ and $(I_E/I_M)^{SPC}$ are expected to behave differently from $<k^{MF}>$ if pyrene species other than Py^*_{diff} can be found in solution as is the case for the pyrene-labelled dendrimers where the presence of minute amounts of Py^*_{free} has a dramatic effect on the $(I_E/I_M)^{SS}$ and $(I_E/I_M)^{SPC}$ ratios.[5,26,32] The trend shown in Figure 5.6 indicates that excimer formation is the most and the least efficient for the highly branched dendritic and the end-labelled polystyrene samples, respectively. All linear polystyrenes randomly labelled with pyrene yield similar $(I_E/I_M)^{SPC}$ ratios and $<k^{MF}>$ values which are intermediate between those obtained for the end-labelled polystyrenes and the highly branched dendrons.

Most importantly, Figure 5.6 demonstrates that the internal dynamics of any PLM can be compared to those of the macromolecules listed in Table 5.1, as long as the pyrene monomer and excimer fluorescence decays acquired with PLMs are analyzed globally in a manner that accounts for all pyrene species in solution quantitatively as the MF analysis does. For instance, the $(I_E/I_M)^{SPC}$ ratios determined with the MF and FBM have been shown to yield equivalent results in cases where the FBM applies (see Figure 5.2 and reference 30). The plot shown in Figure 5.6 spans more than 3 orders of magnitude in terms of the dynamic range of $(I_E/I_M)^{SPC}_{ffree=0}$ ratios and $<k^{MF}>$ values. This represents the widest range of $(I_E/I_M)^{SPC}_{ffree=0}$ ratios and $<k^{MF}>$ values over which the dynamics of PLMs have ever been compared. Finally, the trend shown in Figure 5.6 represents the only example in the literature where the I_E/I_M ratios of different PLMs are directly compared.

Critical appraisal of the different models currently used to study pyrene excimer formation in pyrene-labelled macromolecules: The trend shown in Figure 5.6 conveys the impression that it represents an absolute rule obeyed by any PLM. In turn, this impression unavoidably leads to question why such a seemingly general trend would have never been reported earlier after close to 40 years of investigations devoted to probing pyrene excimer formation in PLMs. This legitimate concern can be addressed by reviewing the various developments that contributed to the field as is being done hereafter.

Following the demonstration by Zachariasse and Kühnle (ZK) in 1976 that the process of pyrene excimer formation probed by steady-state fluorescence (SSF) provided valuable information about the conformation of a series of pyrene end-labelled alkyl chains,[12] the molecular architecture adopted in the ZK study was quickly applied in 1977 by Perico and Cuniberti to study a series of pyrene end-labelled poly(ethylene oxide)s by SSF.[6] This study reported the first example where $(I_E/I_M)^{SS}$ was found to decrease as a function of polymer chain length (N). In 1980, M. A. Winnik et al. used time-resolved fluorescence (TRF) to acquire the pyrene monomer and excimer fluorescence decays of a series of pyrene end-labelled polystyrenes.[7] Applying Birks' scheme to analyze the decays, they obtained for the first time a direct measure of the rate constant of pyrene excimer formation or end-to-end cyclization (k_{cy}) which decreased strongly with polymer chain length as $N^{-1.6}$ and showed that k_{cy} was proportional to $(I_E/I_M)^{SS}$. This study led to the rapid development of the use of TRF to obtain k_{cy} for pyrene end-labelled polymers.[1,6-11,18,40-60] As the study of PLMs was extended to polymeric architectures more representative of those encountered in polymer science that differ from pyrene end-labelled monodispersed polymers, it became ever clearer that handling the kinetics of pyrene excimer formation with a single pyrene excimer formation rate constant as done in Birks'

scheme was unsatisfactory.[61,62] Macromolecules bearing more than two pyrene pendants generated a distribution of rate constants corresponding to the distribution of chain lengths separating every two pyrene labels, and the fluorescence decays needed to be fitted with more than the two exponentials required by Birks' scheme.[1,28] Considering the well known uncertainties associated with the analysis of fluorescence decays with sums of exponentials,[63,64] the scientific community held the view that only qualitative information could be retrieved about the internal dynamics of a macromolecule labelled with more than one pyrene. Although not explicitly stated, this point of view was reflected in the 1993 review by F. M. Winnik[2] which described a large number of qualitative results obtained with a wide variety of pyrene-labelled macromolecules. Since no model could handle these complex fluorescence decays, no equations existed to fit the monomer and excimer decays acquired with these pyrene-labelled macromolecules, and both $(I_E / I_M)^{SPC}$ and $(I_E / I_M)^{SPC}_{ffree=0}$ could not be determined and a plot such as the one shown in Figure 5.6 could not be obtained.

To the best of our knowledge, the first successful attempt made at fitting sets of pyrene monomer and excimer fluorescence decays that did not obey Birks' scheme was achieved by applying the DMD model to the decays of 1,3-di(1-pyrenyl)propane where excimer formation occurred in a non-ideal manner within a highly constrained geometry.[65] According to the DMD model, an excited monomer can form two distinct excimer species with two rate constants, and these two excimers can dissociate or fluoresce with two dissociation rate constants and lifetimes, respectively. These conditions lead to a set of three differential equations which can be handled by using a matrix-based formalism. The mathematical derivation leads to the conclusion that the monomer and excimer decays are a sum of three exponentials that share the same decay times but have different pre-exponential factors. Interestingly, this derivation does not yield a

mathematical expression that would describe the monomer and excimer fluorescence decays as done in Birks' scheme, and thus, cannot yield an expression of $(I_E/I_M)^{SPC}$ and $(I_E/I_M)^{SPC}_{ffree=0}$. Within the framework of the DMD model, the decay times and pre-exponential factors retrieved from the triexponential global analysis of the fluorescence decays are linear functions of the kinetic parameters that describe the process of pyrene excimer formation. Since the exponentials are the same in the monomer and excimer fluorescence decays, three decay times, and six pre-exponential factors (3 for the monomer decay and three for the excimer decay) are required, resulting in nine ($3 \times n = 9$ where n is the number of exponentials) floating parameters which are optimized with no constraint other than that the fit of the decay be good. The nine floating parameters retrieved from the fit are then optimized to yield the kinetic parameters. While the procedure associated with the DMD model has proved its worth for pyrene-labelled macromolecular constructs forming excimer with a finite number (= 2) of excimer formation rate constants,[48,65-68] its application to polymeric systems forming pyrene excimer with a distribution of rate constants seemed more problematic.[69] This is illustrated in the following example.

The DMD model was applied to analyze the monomer and excimer fluorescence decays acquired with an aqueous solution of poly(acrylic acid) randomly labelled with pyrene (sample = PAAMePy(2)52).[69] Since the polymers had a low labelling level, the species Py^*_{free} needed to be accounted for and the monomer and excimer fluorescence decays were fitted with 4 coupled exponentials, resulting in $3 \times 4 = 12$ floating parameters. The results of this analysis are presented in Table 5.2. The long decay time τ_4 was attributed to the natural lifetime τ_M of the pyrenes that do not form excimer (Py^*_{free}). In turn, the other decays times and associated pre-exponential factors describe excimer formation. However, close analysis of Table 5.2 indicates a number of problems. First, the pre-exponential factors of the pyrene monomer should all be positive. This

is not the case as a_{M3} equals -0.080. The authors quickly point out that its contribution is negligible, which is true when compared to a_{M4}, the contribution of Py^*_{free}. However, the ratio $|a_{M3}|/(a_{M1}+a_{M2}+|a_{M3}|)$ equals 0.26 which is far from negligible with respect to the other pre-exponential factors a_{M1} and a_{M2} that describe pyrene excimer formation. Thus not only a_{M3} is negative instead of being positive, but it also represents a major contribution in the monomer decay with respect to pyrene excimer formation.

Table 5.2. Pre-exponential factors and decay times retrieved from the tetraexponential global analysis of the pyrene monomer and excimer decays of PAAMePy(2)52 conducted in ref. #69

Decay times (ns)	$\tau_1 = 7.0$	$\tau_2 = 53.5$	$\tau_3 = 104$	$\tau_4 = 220$
Monomer	$a_{M1} = 0.066$	$a_{M2} = 0.164$	$a_{M3} = -0.080$	$a_{M4} = 0.771$
Excimer	$a_{E1} = -0.149$	$a_{E2} = 0.719$	$a_{E3} = 0.281$	$a_{E4} = -0.024$

Another negative pre-exponential factor is a_{E4} which, again, is not physically possible, as it implies that the excimer fluorescence intensity is negative at long times. Since a_{M3} and a_{E4} are off, the other parameters used to fit the decays are necessarily off as well, which in turn affects the determination of the kinetic parameters. Interestingly, these kinetic parameters were not determined in ref. #69, probably due to the faulty set of parameters a_{Mi}, a_{Ei}, and τ_i with $i = 1 - 3$ retrieved from the analysis and listed in Table 5.2. The problems highlighted in Table 5.2 are caused in part by the absence of equations describing the monomer and excimer decay that could be used to introduce additional constraints in the analysis program used to retrieve the pre-exponential factors and decay times from the fit of the fluorescence decays. All analyses carried out by the Duhamel laboratory take full advantage of the mathematical expressions derived to

represent the monomer and excimer decays. The pre-exponential factors and decay times of the sums of exponentials used to fit globally the monomer and excimer decays are optimized as a function of the kinetic parameters used to describe pyrene excimer formation. This procedure adds more constraints to the optimization package and ensures that anomalies such as those described in Table 5.2 are never a concern. These improvements have been described in detail in two recent reviews.[4,5]

Another procedure which has been introduced in the literature to deal with the multiexponential decays associated with macromolecules labelled with more than two pyrenes has been to lower the pyrene content of the macromolecule.[69,70] Since increasing the number of pyrene labels increases the number of chain lengths between every two pyrene pairs, thus the number of pyrene excimer formation rate constants, and consequently the number of exponentials that needs to be applied to fit the fluorescence decays,[15] the pyrene content can be lowered to such a level that a minimal number of exponentials need to be used. When this is the case, two coupled exponentials with a third exponential for Py^{*}_{free} fit the monomer and excimer decays well and the pre-exponential factors and decay times retrieved from the two coupled exponentials can be interpreted according to Birks' Scheme. Unfortunately, the results retrieved from this analysis conducted in a few number of examples[69,70] consistently yield large pyrene excimer dissociation rate constant k_{-1} that are $2-6$ times larger than 5×10^{6} s^{-1}, which is the upper value typically obtained for short monodispersed polymers end-labelled with pyrene. Longer chains yield larger k_{-1} values due to a breakdown of Birks' scheme under these conditions, as demonstrated in a recent study.[11]

To summarize the procedures described up to this point, none of the analyzes presented earlier aimed to address the inherent distribution of rate constants resulting from the distribution

of chain lengths separating the pyrene pendants covalently attached to a macromolecule. This is unfortunate, since the vast majority of pyrene-labelled macromolecules contain more than two pyrene labels which are not separated by a set chain length. Furthermore, these analyses have been found to yield kinetic parameters which are inconsistent with commonly accepted facts about the process of pyrene excimer formation, most importantly that k_{-1} takes values smaller than 5×10^6 s^{-1}.

In contrast with these earlier studies, the FBM was the first model specifically designed to handle the distribution of rate constants encountered in polymers randomly labelled with pyrene. After demonstrating in 1999 that the FBM could satisfyingly handle the monomer decays acquired with a series of polystyrenes randomly labelled with pyrene,[15] the analysis program was improved to enable the global analysis of the monomer and excimer fluorescence decays.[71] Since the FBM provided explicit expressions for the time-dependent behavior of the pyrene monomer and excimer given in Equations SI5.11 and SI5.12, an expression of $(I_E/I_M)^{SPC}$ and $(I_E/I_M)^{SPC}_{ffree=0}$ could be derived for polymers randomly labelled with pyrene.[72] However, the FBM could not handle all pyrene-labelled macromolecules as the labelling of macromolecules is not always conducted in a random manner, a pre-requisite for application of the FBM. After noting that any fluorescence decay could be fitted with a sum of exponentials, the MF analysis was introduced, in which the pyrene monomer decay is fitted with a sum of exponentials, and an expression for the excimer decay is obtained using the same procedure as was applied for the FBM.[31] Here again, mathematical expressions could be derived for the pyrene monomer and excimer decay as shown in Equations SI5.1 and SI5.2 which could be integrated to yield $(I_E/I_M)^{SPC}$ and $(I_E/I_M)^{SPC}_{ffree=0}$ as described in Equation 5.4.[26,32,33] The main limitation of the MF analysis is that it yields an average $<k>$ value which loses some of the

molecular details of pyrene excimer formation that would be provided otherwise by an analysis based on Birks' scheme, the DMD model, or the FBM. However, this limitation is compensated by the demonstrated applicability of the MF analysis to describe the internal dynamics of a presently unmatched variety of pyrene-labelled macromolecular constructs,[26,31,33-35,73] as further illustrated in this report. The MF achieves this result by capturing the main features of the decays and summarizing them into a small set of parameters which are the average rate constant of pyrene excimer formation $<k>$, the excimer lifetime τ_{E0}, and the molar fractions of the different species that fluoresce in solution.

Whereas the studies conducted with PLMs using models other than the FBM or MF have been applied to a limited number of PLMs and yield sets of kinetic parameters that are questionable and somewhat inconsistent with what is generally accepted about pyrene excimer formation, the FBM and MF analyses have been applied successfully to a wide variety of pyrene-labelled macromolecular constructs as demonstrated by this report and yield sets of kinetic parameters consistent with the established consensus about pyrene excimer formation and expectations about the PLM invetigated. Furthermore, FBM and MF analyses are currently the only procedures that provide mathematical expressions for the pyrene monomer and excimer that can be applied directly to fit the complex fluorescence decays acquired with a wide range of PLMs and to derive the only expressions of $(I_E/I_M)^{SPC}$ and $(I_E/I_M)^{SPC}_{ffree=0}$ currently available in the literature for PLMs that contain more than two pyrenes attached at two specific positions of a macromolecule.

5.6 Conclusions

This study demonstrates that the MF analysis of the fluorescence decays of PLMs is a powerful and versatile procedure to gain information about the internal dynamics of any type of PLM. Comparison of k_{cy} and $<k^{MF}>$ obtained from, respectively, the Birks' scheme and MF analysis yielded trends for the end-labelled polymers that were similar, and at the very least, provided identical information about the macromolecules studied, namely that $<k^{MF}>$ decreases as a power law with increasing chain length and that $<k^{MF}>$ for relatively stiff polystyrene is much smaller than for comparatively flexible PEO. It was also shown that $<k^{MF}>^{blob}$ derived from $<k^{MF}>$ yielded identical trends for the randomly labelled polystyrenes with respect to the $k_{blob} \times N_{blob}$ values retrieved from the more traditional FBM analysis. In particular, $<k^{MF}>^{blob}$ reflected satisfyingly the nature of the spacer connecting the pyrene derivative to the polymer backbone. Finally, the MF analysis was shown to probe the end-group dynamics of pyrene end-labelled dendrons in a manner that reflected the molecular flexibility expected from the chemical composition of the dendrons.

The overall agreement between the trends obtained with the MF analysis and the more traditional models is quite remarkable, considering that the MF analysis is conceptually different from the other models. In particular, the MFA makes no assumption about the mathematical details used to model pyrene excimer formation. The MF analysis also accounts quantitatively for all pyrene species present in solution, most importantly the Py^{*}_{free} species. This represents an advantage over other analytical procedures in cases where elimination of all unattached dyes from PLMs is challenging and the fluorescence signal is sensitive to their contribution, as was found with the pyrene-labelled dendrons. The MF analysis takes also advantage of the design of our analysis programs where the monomer and excimer fluorescence decays are fitted globally

and the decay times and pre-exponential factors in the sum of exponentials are optimized as a function of the kinetic parameters involved in the kinetic schemes representing pyrene excimer formation. This ensures that erroneous results without physical meaning such as those reported in Table 5.2 are avoided. Last but not least, the quantities $(I_E / I_M)_{ffree=0}^{SPC}$ and $<k^{MF}>$ determined by the MF analysis are absolute and can be reproduced in any laboratory.

The versatility and generality of the MF analysis were further illustrated by demonstrating that a plot of $(I_E / I_M)_{ffree=0}^{SPC}$ versus $<k^{MF}>$ generates a master curve in Figure 5.6 along which all PLMs studied converge without a single exception. Thus, the master curve in Figure 5.6 constitutes a calibration curve against which the internal dynamics of any other PLM can now be gauged. It should prove highly valuable to the many scientists who use pyrene excimer formation to probe the internal dynamics of macromolecules.

Finally, it must be pointed out that although this report has demonstrated the general applicability of the MF analysis to study the internal dynamics of PLMs, its realm of application is actually much broader. The MF analysis also yields the fractions weighed by the molar absorption coefficient and radiative rate constant of the different pyrene species contributing to the monomer and excimer fluorescence decays.[31] In turn, these fractions can be used to determine the actual molar fractions of the pyrene species. This feature allowed some of us to assess the extreme sensitivity of the $(I_E/I_M)^{SS}$ and $(I_E/I_M)^{SPC}$ ratios obtained for pyrene end-labelled dendrimers to the presence of free pyrene labels.[26] It led to the determination of the molar absorbance coefficient of pyrene aggregates generated by a poly(ethylene oxide) labelled at one end with pyrene.[73] It was applied to determine the concentration of unmicellized surfactant for a pyrene-labelled gemini surfactant which demonstrated that above the CMC of the surfactant, the concentration of unassociated surfactant remains constant and equals the CMC.[33]

168

More recent experiments have shown that the MF analysis can be employed not only to study pyrene excimer formation, but for any fluorescence experiment dealing with two communicating fluorescence channels, such as in a FRET experiment. In particular, the MF analysis was successfully applied to probe the kinetics of FRET between an excited pyrene donor to a ground-state porphyrin acceptor in two pyrene dendronized porphyrin constructs.[31] These earlier results together with those presented in this report further demonstrate that the MF analysis is a powerful and versatile analytical procedure to investigate the behavior of PLMs in solution.

Chapter 6

Concluding Remarks and Future Work

6.1. Summary of Accomplished Work

Polymers which are able to change their conformation in solution in response to changing solution conditions have been the subject of a number of studies, whether they are *pH* sensitive polyelectrolytes[1-4] or temperature sensitive PNIPAM chains.[5-9] The inter- and intramolecular interactions which drive these solution responses are reliably characterized by a number of techniques that include steady-state and time-resolved fluorescence. Time-resolved fluorescence decays of solutions of solvated pyrene-labelled polymers, or mixtures of unlabelled polymers and dissolved pyrene, have been acquired and analyzed since the mid 1970s[10-13] and have yielded information about the rate at which the pyrene labels interact and by extension the rate of interaction for the polymer chain segments to which the pyrene labels are attached. The analysis of the time-resolved fluorescece decays of pyrene labelled polymers typically requires the use of a model which describes the nature of the physical processes which give rise to pyrene excimer formation, and historically these models have only been capable of dealing with decays acquired from fully solvated chains. Consequently, the quantitative characterization of the solution behaviour of inhomogeneous mixtures of pyrene-labelled polymers using time-resolved fluorescence has not been possible until recently. The Model Free Analysis (MFA) has been proposed as a technique which is able to analyze the decays resulting from complex systems, including aggregated polymer chains.[14-16] The ability of the MFA to analyze inhomogeneous mixtures makes it an ideal tool for determining the solution response of pyrene labelled polymers.

The application of time-resolved fluorescence combined with the use of MFA provides information on the changes which occur in the local environment of pyrene-labelled polymers as the chain conformation responds to changes in the solution environment. Polymers that have not

been labelled with pyrene may still be characterized by fluorescence if a fluorophore such as pyrene is added to the solution as a free probe. The hydrophobic microdomains which form as the ionization level of sequential amphiphilic polypeptide solutions decreases constitute an ideal target for pyrene whose fluorescence can be employed to probe these hydrophobic regions of the solution. In particular, pyrene fluorescence reports on the changes in chain aggregation behaviour which occur as the ionization level of the polymer decreases, and the chain conformation evolves from that of an extended coil to that of a collapsed globule as determined by the balance between the ionization level and the hydrophobicity of the polypeptide.[17] Pyrene fluorescence is also particularly well suited to the characterization of hydrophobically end-labelled PNIPAM, a system that has been well characterized by other techniques,[6,7,18] where the hydrophobic pyrene group was used to replace a similarly hydrophobic octadecyl group.

The first investigation undertaken in this thesis was the determination of the effect of changes in *pH* on the collapse and aggregation (C&A) behaviour of a series of aqueous sequential polypeptides. These polypeptides were previously synthesized using a tri- or tetra-peptide monomer with a well-defined sequence of aspartic acid (Asp) and phenylalanine (Phe), resulting in polymers where both the content and order of the amino acids were tightly controlled.[19] Five polypeptide samples were used in this study, namely $(Asp_3Phe_1)_n$, $(Asp_2Phe_1)_n$, $(Asp_1Phe_1)_n$, $(Asp_1Phe_2)_n$, and $(Asp_1Phe_3)_n$, which provided a broad range for the hydrophilic/lipophilic balance (HLB) of the samples. Changes in solution *pH* were then used to control the ionization of the Asp residues, while the amino acid sequence of the polymer was used to control the hydrophobicity of the chains.

Titration of polypeptide solutions allowed the calculation of the degree of ionization (α) of the polymer samples, which was used to calculate the apparent pK_a (pK_a^{app}) of each polymer.

The pK_a^{app} of the polymer reflects the relative acidity of the Asp residues. The more hydrophobic Phe-rich polymers $(Asp_1Phe_2)_n$ and $(Asp_1Phe_3)_n$ bearing isolated Asp residues showed ionization behaviour reminiscent of monomeric organic acids, with the pK_a^{app} of $(Asp_1Phe_2)_n$ and $(Asp_1Phe_3)_n$ remaining essentially constant with α. The pK_a^{app} for these samples was found to be higher than for $(Asp)_n$, which was due to the hydrophobic environment experienced by the Asp residues being flanked by Phe residues on each side. These flanking Phe groups increased the pK_a of Asp since the Phe groups stabilized the neutral form of Asp, requiring a higher pH to cause them to ionize. The lack of α dependence for pK_a^{app} was due to the Phe groups insulating each Asp residue from adjacent Asp residues. The more hydrophilic Asp-rich samples $(Asp_3Phe_1)_n$, $(Asp_2Phe_1)_n$, and $(Asp_1Phe_1)_n$ showed polyelectrolyte ionization behaviour, with the pK_a^{app} decreasing linearly with decreasing α. For these three samples, the pK_a^{app} behaviour was due to the Asp residues being separated by at most a single Phe residue, allowing the ionization of one Asp to affect the ionization of its neighbours. The pK_a^{app} for these samples was also significantly lower than those of the more hydrophobic polypeptides. The significant difference in pK_a^{app} behaviour between the hydrophilic and hydrophobic polypeptides clearly demonstrates the differences in solution behaviour which is dependent on the amino acid sequence of the samples.

The C&A behaviour of the solutions was further investigated by measuring the light scattering intensity of the solutions as the pH was decreased. All solutions but the most hydrophilic $(Asp_3Phe_1)_n$ became turbid and showed a sharp increase in light scattering at a pH where α was equal to 0.2. The steady-state fluorescence spectra of pyrene-loaded aqueous polymer solutions of the samples were also acquired, as pyrene has been previously shown to target the hydrophobic Phe residues responsible for forming hydrophobic microdomains, either

173

inter- or intramolecularly, in solution.[19]   The I_1/I_3 ratio of pyrene was determined for each sample

as the *pH* decreased. The solutions of the hydrophilic samples showed I_1/I_3 values which closely

matched those of pyrene in water, while the hydrophobic samples showed much lower I_1/I_3

values corresponding to a much more hydrophobic environment for pyrene, indicating that

hydrophobic microdomains only exist to any significant degree in the hydrophobic samples. The

time-resolved fluorescence decays of the pyrene monomer were then acquired and fitted with a

sum of exponentials. All samples showed a short lifetime close to that of pyrene in water, while

the three most hydrophobic samples also showed a long lifetime above 300 ns. The ability of

pyrene in oxygenated aqueous solution to show such a long lifetime in water is only possible if it

is located in a hydrophobic microdomain where oxygen quenching is inhibited.[20]   The

contribution of this lifetime to the overall decay was also found to increase with decreasing α,

indicating that more hydrophobic domains were present to solubilize and protect the pyrene at

low *α*. This process was found to be reversible.

From these two investigative techniques, one can reasonably conclude that the

hydrophobicity and ionization level of the polymers are the major factors determining the C&A

behaviour of the polypeptides in solution. Based on the results of this study, it may be possible

to predict the behaviour of a random copolymer of these two amino acids based on the

knowledge gained by studying how short stretches of amino acids behave in these sequential

copolymers.

The goal of the next study undertaken in this thesis was to determine the solution

response of aqueous pyrene end-labelled poly(*N*-isopropylacrylamide)s (Py$_2$-PNIPAM)s using

turbidimetry, light scattering (LS), and steady-state and time-resolved fluorescence. PNIPAM is

a thermoresponsive polymer which is soluble in cold water but undergoes a coil-to-globule

transition (CGT) at approximately 34 °C. The critical temperature (T_c) where a PNIPAM sample becomes insoluble in water varies depending on the end-groups of the polymer, shifting to lower temperatures if the end-groups are hydrophobic.[18] Py$_2$-PNIPAM in aqueous solution was expected to behave in a manner which is consistent with a model proposed by F. M. Winnik et al. for hydrophobically end-labelled PNIPAM (lip$_2$-PNIPAM),[7,9,21,22] forming micelles below T_c, aggregating to form mesoglobules above T_c, and reaching stable behaviour above 34 °C (T_m) where PNIPAM homopolymers undergo their CGT.

Turbidimetry and LS both showed that T_c increased with increasing molecular weight (M_n) for Py$_2$-PNIPAM, confirming that T_c depends on the hydrophobe content of the sample. Steady-state fluorescence spectra were acquired and the ratio I_E/I_M was calculated to estimate the relative amount of pyrene excimer formed in the sample. All samples showed an increase in I_E/I_M as the temperature increased approaching T_c, then decreased above T_c, showing that the amount of excimer formed reaches a maximum at T_c. The wavelength corresponding to the maximum of excimer fluorescence underwent a blue-shift at T_c, reflecting an increase in the aggregation of ground-state pyrenes leading to the formation of the excimer. Time-resolved fluorescence decays of the monomer and excimer were acquired and fitted with a sum of exponentials. The decay times and pre-exponential factors which resulted from the fits were used to calculate the number-average decay time of the monomer and excimer ($<\tau_N>_M$ and $<\tau_N>_E$, respectively), the polydispersity index (PDI) of the monomer decays, and the ratio a_{E-}/a_{E+} which reflects the amount of excimer formed by diffusion. $<\tau_N>_M$ and $<\tau_N>_E$ both increased at T_c, indicating that mesoglobule formation inhibits the quenching of pyrene by oxygen present in solution. The value of PDI went through a maximum and the ratio a_{E-}/a_{E+} became more positive at T_c, both trends indicating that mesoglobule formation at T_c leads to a reduction in the amount

of excimer formed by diffusion. The parameters listed previously were also found to undergo transitions at T_c for pyrene mono-labelled chains in aqueous solution, though the transitions were not necessarily identical.

Model-Free Analysis (MFA) was applied to the fluorescence decays in order determine the behaviour of the hydrophobes in solution. The rate of excimer formation $<k>$, as well as the molar fractions f_{agg}, f_{free}, and f_{diff} which are respectively the fractions of pyrenes which are aggregated, isolated, and forming excimer by diffusion, were obtained. Increasing the temperature above T_c caused a decrease in $<k>$ and f_{free} and an increase in f_{diff}, while all of the parameters retrieved from the MFA were found to be constant above T_m. The results obtained from the MFA of the decays are consistent with the behaviour predicted by F. M. Winnik et al. for lip$_2$-PNIPAM.[7,21-23] Below T_c in Region I, lip$_2$-PNIPAM chains form micelles with a hydrophobic core, a dehydrated PNIPAM middle region, and a hydrated PNIPAM shell. As the temperature is increased, the hydrated PNIPAM in the shell dehydrates and reduces the size of the micelle, increasing f_{agg} and decreasing f_{free} due to the increased local pyrene concentration. Mesoglobule formation at T_c causes the shell region of the micelles to overlap, essentially eliminating f_{free} and sharply increasing f_{diff} while leaving f_{agg} relatively unchanged. Increasing the temperature in Region II to T_m causes the micellar structures in the mesoglobules to break apart, with the hydrophobes becoming dispersed. This phenomenon results in an increase in f_{free} and a decrease in f_{diff} and f_{agg}, the values of which remained constant above T_m.

The results obtained by turbidimetry, LS, and fluorescence are all consistent with the expected behaviour of lip$_2$-PNIPAM in aqueous solution, with these techniques also serving as viable tools to determine T_c for the solutions with little variation in the temperatures reported by each method. The MFA results conform in detail to the predictions of the model proposed by F.

M. Winnik et al, with one exception. It had been proposed that the mesoglobules above T_m are kinetically frozen and vitreous. Excimer formation by diffusion still occurred above T_m which indicates that the mesoglobules cannot be totally vitreous. Consequently the pyrene aggregates must provide some residual mobility allowing excimer formation to proceed by diffusion. However the extent of this mobility cannot be determined from this study.

The third investigation undertaken in this thesis focused on aqueous mixtures of Py$_2$-PNIPAM and unlabelled PNIPAM(22K), as the latter undergoes a CGT at T_m while the former undergoes a CGT at its T_c. These mixtures were studied using some of the same procedures as for the previous chapter, namely LS, steady-state fluorescence, time-resolved fluorescence, and MFA. All solutions showed the same transitions at T_c as was observed in the previous chapter and the mixtures typically showed a second change in behaviour at T_m.

The mixtures studied showed an increase in LS intensity at both T_c and T_m, demonstrating that each polymer underwent its CGT at a distinct temperature. Steady-state fluorescence spectra yielded the I_E/I_M ratio, which showed a decrease at both T_c and T_m, indicating that the CGT transition of PNIPAM(22K) at T_m is able to affect the fluorescence of the pyrene labels attached to the Py$_2$-PNIPAM chains already aggregated in mesoglobules at this temperature. The value of λ_{max}, which represents the wavelength at which the excimer fluorescence intensity was at its maximum, was unaffected by passing through T_m and only showed the same blue-shift at T_c as was observed in Chapter 3. This blue-shift has been attributed to an increase in pyrene aggregation. Time-resolved fluorescence decays of the monomer and excimer were acquired and fitted with a sum of exponentials, yielding $<\tau_N>_M$, $<\tau_N>_E$, PDI, and the ratio a_{E-}/a_{E+}. The PDI of the monomer decays showed a decrease at both T_c and T_m, while $<\tau_N>_M$ showed an increase at these temperatures. These trends show that the CGT of PNIPAM(22K) at T_m causes similar

changes in the time-resolved fluorescence of the monomer as mesoglobule formation causes at T_c. The values of $<\tau_N>_E$ and a_{E-}/a_{E+} showed only small changes at T_m, possibly due to the already small amounts of excimer formation occurring immediately below T_m. The trends observed for the mono-labelled chains by LS, I_E/I_M and $<\tau_N>_M$ also showed transitions at both T_c and T_m.

The time-resolved fluorescence decays were fitted with the MFA equations, yielding $<k>$, f_{agg}, f_{free}, and f_{diff}. These parameters showed the same transitions at T_c as was observed in the previous chapter, differing only at T_m. While $<k>$ remained constant through the T_m transition, f_{free} increased while f_{agg} and f_{diff} decreased at and above T_m. The constant value observed as $<k>$ passed through the T_m transition was unusual, as $<k>$ depends not only on the bimolecular rate constant of pyrene excimer formation by diffusion but also on the local pyrene concentration. The fluorescence fractions showed that the overall pyrene concentration decreased as PNIPAM(22K) chains entered the mesoglobules at T_m. Yet $<k>$ did not reflect this. The best explanation for this is that diffusional pyrene excimer formation only occurs within pyrene aggregates, where the high local pyrene concentration remains constant regardless of the influx of PNIPAM(22K). Thus it is possible for f_{diff}, representing the amount of diffusional excimer formation, to decrease while the rate constant of excimer formation does not. The changes in fluorescence fractions were found to be reversible.

The results of the MFA of the fluorescence decays are consistent with the mixing of PNIPAM(22K) chains and Py$_2$-PNIPAM mesoglobules as the former undergoes its CGT at T_m, causing dilution of the pyrene groups. Since this mixing occurs above 34 ^{o}C, the Py$_2$-PNIPAM mesoglobules must still be relatively fluid to allow entry of the PNIPAM(22K) chains. It is therefore unreasonable to suppose that Py$_2$-PNIPAM is vitreous and kinetically frozen at or

above T_m. This work has shown that time-resolved fluorescence is able to detect both the presence and the extent of intermolecular interactions which occur in mixtures of labelled and unlabelled polymer chains. The rate of pyrene excimer formation and the distribution of pyrenes within the sample also support the model proposed by F. M. Winnik et al. [7,21-23]

While the previous three chapters focused on monitoring pyrene fluorescence in solutions which become heterogeneous upon changing either pH or temperature, the final investigation focuses on pyrene-labelled polymers which remain soluble in organic solvent to evaluate the ability of time-resolved fluorescence to reproduce the results of steady-state fluorescence in order to validate the MFA, which has been used thus far. In order to do this, steady-state fluorescence spectra and time-resolved fluorescence decays were acquired for linear polymers and dendrons, including end-labelled poly(ethylene oxide) (PEO), end-labelled polystyrene (PS), three families of randomly labelled PS with varying pyrene labels, four generations of bis(hydroxymethyl)propionic acid (PP) dendrons and two generations of polyaryl Fréchet-type (PA) dendrons.

The $(I_E/I_M)^{SS}$ ratio was calculated from the steady-state fluorescence spectra, while the time-resolved fluorescence decays were fitted globally with varying mathematical models. The end-labelled polymers were fitted with the Birks scheme, the randomly labelled polymers were fitted with the Fluorescence Blob Model (FBM), and all samples were fitted with the MFA equations. Birks' scheme analysis yielded the rate constant of cyclization k_{cy}, the FBM analysis yielded the product $k_{blob} \times N_{blob}$, and MFA yielded $<k^{MF}>$, all of which represented a measure of the rate constant for excimer formation by diffusion. The parameters derived from the MFA were also used to calculate $(I_E/I_M)^{SPC}$, which reflects the ratio of fluorescence intensities of the excimer and monomer as determined from the time-resolved fluorescence decays.

Comparison of k_{cy} and $<k^{MF}>$ for the end-labelled polymers indicated that both parameters took values that were highly similar, and showed not only the same power law dependence on molecular weight but also the same dependence on polymer backbone structure. Comparison of $k_{blob} \times N_{blob}$ and $<k^{MF}>$ values obtained for the randomly labelled polymers showed values which were also similar, and that both reflected differences in pyrene mobility related to the nature of the linker between the label and the polymer. The ability of the MFA to faithfully reproduce trends and values obtained by fitting a given polymer architecture with established models such as Birks' scheme or the FBM lends a great deal of credibility to the MFA as a viable alternative for fitting fluorescence decays. This was further demonstrated by fitting the fluorescence decays of the dendrons with the MFA, which was at the time the only model capable of fitting the decays of these pyrene-labelled macromolecules. The value of $<k^{MF}>$ was found to increase linearly with generation number for both sets of dendrons, one consisting of a rigid Fréchet-type polyaryl backbone while the other had a bis-hydroxypropionic acid polymer backbone. The less flexible PA dendrons showed lower $<k^{MF}>$ values compared to the more flexible PP dendrons.

Further validation of the MFA was pursued by comparing the $(I_E/I_M)^{SS}$ and $(I_E/I_M)^{SPC}$ values, which showed a linear relationship for each type of pyrene label used. These families of pyrene labels showed the same slope, with only the y-intercept varying with the pyrene label. This difference in y-intercept is due to changes in the shape of the pyrene fluorescence spectrum which occur when the nature of the label is changed, thus affecting the value of $(I_E/I_M)^{SS}$ but not that of $(I_E/I_M)^{SPC}$. The $(I_E/I_M)^{SPC}$ and $(I_E/I_M)^{SS}$ ratios as well as $<k^{MF}>$ all report on the efficiency of excimer formation. Consequently, $(I_E/I_M)^{SPC}$ was plotted as a function of $<k^{MF}>$ and was

180

found to scale almost linearly, with the dendrimer samples showing the greatest deviation. The origin of the deviation was attributed to the presence of free pyrene in the dendrimer solution. Since free pyrenes which are not attached to the polymer should not affect the kinetics of pyrene excimer formation, their exclusion from the calculation of $(I_E/I_M)^{SPC}$ was expected to better reflect the inherent relationship that exists between $(I_E/I_M)^{SPC}$ and $<k^{MF}>$. Fortunately the MFA yields f_{free}, so that its exclusion from the calculation of $(I_E/I_M)^{SPC}$ turned into a straightforward exercise. Plotting $(I_E/I_M)^{SPC}$ with no contribution from f_{free} as a function of $<k^{MF}>$ yielded a straight line with a slope τ_{E0} equal to 51 ns, which is a reasonable value for the lifetime of the pyrene excimer in THF.

These combined results obtained with 30 pyrene-labelled macromolecules of varied architectural complexity demonstrated that the MFA is a powerful tool for fitting time-resolved fluorescence decays of pyrene labelled polymers, regardless of their architecture. This result was significant because the MFA is conceptually distinct from both the Birks scheme and FBM as it makes no mathematical assumptions about the process of pyrene excimer formation. MFA allows the fluorescence fraction f_{free} to be calculated, which is especially useful when the physical elimination of traces of free pyrene is both experimentally difficult but necessary to obtain reliable fluorescence data, as was the case with the dendrons studied here. Additionally, MFA allows the calculation of $(I_E/I_M)^{SPC}$ which is an absolute quantity representative of the ratio of the fluorescence intensity of the pyrene excimer over that of the pyrene monomer that is reproducible in any laboratory. The value obtained for $(I_E/I_M)^{SPC}$ may then be compared to its corresponding $<k^{MF}>$ value as shown in the master curve in Chapter 5, allowing a comparison of the rate of excimer formation between different polymer backbones and architectures. The fluorescence fractions, in combination with the molar absorbance coefficients, allow the molar

fractions of the various pyrene species to be calculated. This has led to a number of applications, including a determination of the molar absorbance coefficient of pyrene aggregates for mono-and randomly labelled polymers[24,25] and the concentration of free pyrene-labelled gemini surfactant for solutions above the CMC,[26] amongst others.[16,27,28]

This thesis has demonstrated the ability of steady-state and especially time-resolved fluorescence to characterize the behaviour of polymers in solution. This was particularly evident in aqueous solution, where pyrene is able to target hydrophobic microdomains within polymer aggregates. In the case of amphiphilic polypeptides, this thesis has demonstrated that the formation of polypeptide aggregates depends on both the sequence and ionization level of the polymer. Pyrene fluorescence was able to demonstrate that the behaviour of aqueous solutions of Py_2-PNIPAM as a function of temperature follows the predictions made my F. M. Winnik et al. for lip_2-PNIPAM, and that aggregated Py_2-PNIPAM is able to mix with unlabelled PNIPAM as the latter undergoes its CGT. Finally, the MFA applied heavily in the third and fourth chapters of this thesis has been demonstrated to be a robust tool for characterizing pyrene labelled polymers in solution, based on its ability to faithfully reproduce the steady-state fluorescence intensities of a wide variety of polymer architectures labelled with pyrene.

6.2. Future Work

The techniques used to characterize the *pH* dependent behaviour of $(Asp_xPhe_y)_n$ polypeptides should be extended to other amino acid pairs such as $(Lys_xPhe_y)_n$, as the basic Lys residue should show a decrease in pK_a^{app} when flanked by Phe similar to what was observed for Asp in $(Asp_xPhe_y)_n$. Furthermore, these Lys containing polypeptides would be able to complex effectively with DNA. It would be interesting to apply the various fluorescence tools used in this

thesis to the characterization of the $(Lys_xPhe_y)_n$-DNA aggregates. To better characterize the ability of $(Asp_xPhe_y)_n$ to solubilize hydrophobic compounds, it would be of interest to prepare pyrene-loaded solutions at a starting *pH* lower than 9.5. A preparative *pH* that targets a value of α equal to 0.5, ranging from *pH* 4 to *pH* 6 depending on the sample, would allow pyrene loading to take place in chains and aggregates which are significantly more hydrophobic than equivalent solutions at *pH* 9.5. This investigation would provide information on the effect of preparative *pH* on both loading capacity, as well as the manner in which the protective ability of polypeptide aggregates changes as *pH* is either decreased or increased.

The study of aqueous Py_2-PNIPAM, and whether it fully adheres to the model proposed by F. M. Winnik et al., would benefit from the performance of non-radiative energy transfer (NRET) experiments. The synthesis of naphthalene end-labelled PNIPAM samples, when combined with the already available pyrene-labelled samples, would allow mixtures of these two polymers to be created which could then be used to characterize the CGT of these polymers by monitoring the NRET between the naphthalene and pyrene labels. If the samples were prepared as separate solutions, they could then be mixed at different temperatures to determine the rate of exchange of the PNIPAM chains trapped in different structures such as micelles or mesoglobules. Mixing solutions at temperatures below T_c, above T_c but below T_m, and above T_m would allow the monitoring of the rate of exchange of chains between micelles, mesoglobules, and stable mesoglobules, respectively, using NRET. The temperatures for these exchange experiments would have to be chosen carefully as the pyrene and naphthalene labels differ in both size and hydrophobicity, implying that the labelled polymers are unlikely to possess matching values for T_c. If the rate of mixing in any or all of these temperature regimes occurs on a time scale which can be determined using a steady-state fluorometer the experiment could be

repeated with mixtures of chains labelled with either phenanthrene (Phen) or anthracene (An). These fluorophores constitute a known NRET donor-acceptor pair and are much closer in size and hydrophobicity. Thus a full series of temperature experiments with these Phen- and An-labelled PNIPAMS could be performed to determine the rate of mixing. Additionally, the ability of Py_2-PNIPAM to act as a thermoresponsive surfactant could be investigated using oil-in-water emulsions. The kinetics and distribution of pyrene labels could then be monitored to determine the effect of T_c on these parameters. In both the NRET and emulsion experiments, the effect of adding a 10× massic excess of unlabelled PNIPAM would allow the effect of PNIPAM mixing to be determined, as well as further confirm the non-vitreous nature of the mesoglobules. Varying the ratio of unlabelled PNIPAM, from 2× to 20×, would also be worth investigating to determine the dependence of the magnitude of the T_m transition on the amount of unlabelled PNIPAM present in solution.

The validation of the MFA by comparing its results to that of the Birks Scheme or FBM would be further advanced by acquiring fluorescence spectra and decays of the pyrene-labelled macromolecules investigated in Chapter 5 in solvents such as dimethylformamide or toluene. This would vary the solvent quality towards both the polymer backbone and the pyrene label, while toluene would also disrupt π-π stacking between pyrene labels. If samples became synthetically available, it would be of interest to apply the MFA to additional polymer architectures such as pyrene labelled hyperbranched, dendritic, or sequential polymers, and even swollen gels as MFA should be able to determine both the fluorescence fractions and rate of excimer formation for all of these samples.

Letters of Copyright Permission

ACS Publications
High quality. High impact.

Title: Effect of Sequence on the Ionization Behavior of a Series of Amphiphilic Polypeptides

Author: Michael Fowler, Bushra Siddique, and Jean Duhamel

Publication: Langmuir

Publisher: American Chemical Society

Date: Apr 1, 2013

Copyright © 2013, American Chemical Society

PERMISSION/LICENSE IS GRANTED FOR YOUR ORDER AT NO CHARGE

187

RightsLink®

ACS Publications
High quality. High impact.

Title: Studying Pyrene-Labeled Macromolecules with the Model-Free Analysis

Author: Michael A. Fowler, Jean Duhamel, Greg J. Bahun, Alex Adronov, Gerardo Zaragoza-Galán, and Ernesto Rivera

Publication: The Journal of Physical Chemistry B

Publisher: American Chemical Society

Date: Dec 1, 2012

Copyright © 2012, American Chemical Society

Logged in as:
Michael Fowler
Account #:

LOGOUT

Quick Price Estimate

Permission for this particular request is granted for print and electronic formats, and translations, at no charge. Figures and tables may be modified. Appropriate credit should be given. Please print this page for your records and provide a copy to your publisher. Requests for up to 4 figures require only this record. Five or more figures will generate a printout of additional terms and conditions. Appropriate credit should read: "Reprinted with permission from {COMPLETE REFERENCE CITATION}. Copyright {YEAR} American Chemical Society." Insert appropriate information in place of the capitalized words.

I would like to... reuse in a Thesis/Dissertation

Requestor Type Author (original work)

Portion Full article

Format Print and Electronic

Will you be translating? No

Select your currency USD - $

Quick Price Click Quick Price

QUICK PRICE | CONTINUE

This service provides permission for reuse only. If you do not have a copy of the article you are using, you may copy and paste the content and reuse according to the terms of your agreement. Please be advised that obtaining the content you license is a separate transaction not involving Rightslink.

188

References

Chapter 1

1.   Liu, S.; Ames, S. P. Recent Advances in the Synthesis of Polymeric Surfactants. *Curr. Opin. Colloid Interface Sci.* **2001**, *6*, 249-256.

2.   Winnik, M.; Yekta, A. Associative Polymers in Aqueous Solution. *Curr. Opin. Colloid Interface Sci.* **1997**, *2*, 424-436.

3.   Rodriguez-Hernandez, J.; Checot, F.: Gnanou, Y.: Lecommandoux, S. Toward 'Smart' Nano-Objects by Self-Assembly of Block Copolymers in Solution. *Prog. Polym. Sci.* **2005**, *30*, 691-724.

4.   Torchilin, V. P. Structure and Design of Polymeric Surfactant-Based Drug Delivery Systems. *J. Control. Release* **2001**, *73*, 137-172.

5.   Discher, D.; Eisenberg, A. Polymer Vesicles. *Science* **2002**, *297*, 967-973.

6.   Laschewsky, A. Polymerized Micelles with Compartments. *Curr. Opin. Colloid Interface Sci.* **2003**, *8*, 274-281.

7.   Lutz, J.-F. Solution Self-Assembly of Tailor-Made Macromolecular Building Blocks Prepared by Controlled Radical Polymerization Techniques. *Polym. Int.* **2006**, *55*, 979-993.

8.   Mai, Y.; Eisenberg, A. Self-Assembly of Block Copolymers. *Chem. Soc. Rev.* **2012**, *41*, 5969-5985.

9.   Olea, A. F. Hydrophobic Polyelectrolytes. In *Ionic Interactions in Natural and Synthetic Macromolecules*, Ciferri, A. P., A., Ed. Wiley & Sons: Hoboken, NJ, 2012; pp 211-233.

10.   Glass, J. E. *Associative Polymers in Aqueous Media*. ACS Advances in Chemistry; American Chemical Society: Washington, D. C., 2000.

11.   Rapoport, N. Physical Stimuli-Responsive Polymeric Micelles for Anti-Cancer Drug Delivery. *Prog. Polym. Sci.* **2007**, *32*, 962-990.

12.   Wever, D. A. Z.; Picchioni, F.; Broekhuis, A. A. Polymers for Enhanced Oil Recovery: A Paradigm for Structure-Property Relationship in Aqueous Solution. *Prog. Polym. Sci.* **2011**, *36*, 1558-1628.

13.   Trivedi, B. C.; Culbertson, B. M. In *Maleic Anhydride*, Plenum Press: New York, 1982; pp 307-458.

14.   Siddique, B.; Duhamel, J. Effect of Polypeptide Sequence on Polypeptide Self-Assembly. *Langmuir* **2011**, *27*, 6639-6650.

15.   Murnen, H. K.; Khokhlov, A. R.; Khalatur, P. G.; Segalman, R. A.; Zuckermann, R. N. Impact of Hydrophobic Sequence Patterning on the Coil-to-Globule Transition of Protein-like Polymers. *Macromolecules* **2012**, *45*, 5229-5236.

16.   Kokhlov, A. R.; Khalatur, P. G. Conformation-Dependent Sequence Design Engineering of AB Copolymers. *Phys. Rev. Lett.* **1999**, *82*, 3456-3459.

17.   Ashbaugh, H. S. Tuning the Globular Assembly of Hydrophobic/Hydrophilic Heteropolymer Sequences. *J. Phys. Chem. B* **2009**, *113*, 14043-14046.

18.   Yamamoto, H.; Mizusaki, M.; Yoda, K.; Morishima, Y. Fluorescence Studies of Hydrophobic Association of Random Copolymers of Sodium 2-(Acrylamido)-2-methylpropanesulfonate and N-Dodecylmethacrylamide in Water. *Macromolecules* **1998**, *31*, 3588-3594.

19.   Yusa, S.; Kamachi, M.; Morishima, Y. Hydrophobic Self-Association of Cholesterol Moieties Covalently Linked to Polyelectrolytes: Effect of Spacer Bond. *Langmuir* **1998**, *14*, 6059-6067.

20.   Ulrich, S.; Laguecir, A.; Stol, S. Titration of Hydrophobic Polyelectrolytes Using Monte Carlo Simulations. *J. Chem. Phys.* **2005**, *122*, 094911.

21.   Berger, A.; Katchalski, E. Poly-L-Aspartic Acid. *J. Am. Chem. Soc.* **1951**, *70*, 4084-4088.

22.   McDiarmid, R.; Doty, O. The Spectrophotometric Titration of Polyacrylic, Poly-L-Aspartic, and Poly-L-Glutamic Acids. *J. Phys. Chem. B* **1966**, *116*, 7560-7565.

23.   Colombani, O.; Lejeune, E.; Charbonneau, C.; Chassenieux, C.; Nicolai, T. Ionization of Amphiphilic Acidic Block Copolymers. *J. Phys. Chem. B* **2012**, *116*, 7560-7565.

24.   Bennett, E. L.; Niemann, C. The Apparent Ionization Constants and Ultraviolet Spectra of o- m- and p-Fluoro-D,L-Phenylalanine. *J. Am. Chem. Soc.* **1950**, *72*, 1804-1805.

25.   Urry, D. W.; Gowda, D. C.; Peng, S.; Parker, T. M.; Jing, N.; Harris, R. D. Nanometric Design of Extraordinary Hydrophobic-Induced pKa Shifts for Aspartic Acid: Relevance to Protein Mechanisms. *Biopolymers* **1994**, *34*, 889-896.

26.   Song, J.; Laskowski, M.; Qasum, M. A.; Markley, J. L. NMR Determination of pKa Values for Asp, Glu, His, and Lys Mutants at Each Variable Contiguous Enzyme-Inhibitor Contact Position of the Turkey Ovomucoid Third Domain. *Biochemistry* **2003**, *42*, 2847-2856.

27.   Thurlkill, R. L.; Grimsley, G. R.; Scholtz, J. M.; Pace, C. N. Hydrogen Bonding Markedly Reduces the pK of Buried Carboxyl Groups in Proteins. *J. Mol. Biol.* **2006**, *362*, 594-604.

28.   Urry, D. W.; Gowda, D. C.; Peng, S.; Parker, T. M.; Jing, N.; Harris, R. D. Design at Nanometric Dimensions to Enhance Hydrophobicity-Induced pK Shifts. *J. Am. Chem. Soc.* **1992**, *114*, 8716-8717.

29.   Langsetmo, K.; Fuchs, J. A.; Woodward, C. The Conserved, Buried Aspartic Acid in Oxidized Escherichia Coli Thioredoxin Has a pKa of 7.5. Its Titration Produces a Related Shift in Global Stability. *Biochemistry* **1991**, *30*, 7603-7609.

30.   Keyes-Baig, C.; Mathew, M.; Duhamel, J. Lateral Distribution of Charged Species Along a Polyelectrolyte Probed with a Fluorescence Blob Model. *J. Am. Chem. Soc.* **2012**, *134*, 16791-16797.

31.   Heskins, M.; Guillet, J. E. Solution Properties of Poly(N-isopropylacrylamide). *J. Macromol. Sci.: A - Chem.* **1968**, *2*, (8), 1441-1445.

32.   Okada, Y.; Tanaka, F. Cooperative Hydration, Chain Collapse, and Flat LCST Behavior in Aqueous Poly(N-isopropylacrylamide) Solutions. *Macromolecules* **2005**, *38*, 4465-4471.

33.   Kujawa, P.; Aseyev, V.; Tenhu, H.; Winnik, F. M. Temperature-Sensitive Properties of Poly(N-isopropylacrylamide) Mesoglobules Formed in Dilute Aqueous Solutions Heated above Their Demixing Point. *Macromolecules* **2006**, *39*, 7686-7693.

34.   Tanaka, F.; Koga, T.; Kojima, H.; Winnik, F. M. Hydration and Phase Separation of Temperature-Sensitive Water-Soluble Polymers. *Chin. J. Polym. Sci.* **2011**, *29*, 13-21.

35.   Tanaka, F.; Koga, T.; Winnik, F. M. Competitive Hydrogen Bonds and Cononsolvency of Poly(N-isopropylacrylamide)s in Mixed Solvents of Water/Methanol. *Progr. Colloid Polym. Sci.* **2009**, *136*, 1-8.

36.   Tanaka, F.; Koga, T.; Kaneda, I.; Winnik, F. M. Hydration, Phase Separation and Nonlinear Rheology of Temperature-Sensitive Water-Soluble Polymers. *J. Phys. Condens. Matter* **2011**, *23*, 284105-284112.

37.   Duan, M.; Fang, S.; Guo, H.; Zhang, L. Viscometric Studies of Interactions between Hydrophobically Modified Acrylamide Copolymer and Poly(N-isopropylacrylamide) in Dilute Solutions. *J. Macromol. Sci. B* **2009**, *48*, 834-843.

38.   Yang, H.; Cheng, R.; Wang, Z. A Quantitative Analyses of the Viscometric Data of the Coil-To-Globule and Globule-To-Coil Transition of Poly(N-isopropylacrylamide) in Water. *Polymer* **2003**, *44*, 7175-7180.

39.   Fang, Z.; Zhen, T. Molecular Chain Properties of Poly(N-isopropylacrylamide). *Sci. in China Ser. B* **1998**, *42*, (3), 290-297.

40.   Ishii, N.; Mamiya, J.; Ikeda, T.; Winnik, F. M. Solvent Induced Amplification of the Photoresponsive Properties of α,ω-Di-[4-Cyanophenyl-4′-(6-Hexyloxy)-Azobenzene]-Poly(N-isopropylacrylamide) in Aqueous Media. *Chem. Commun.* **2011**, *47*, 1267-1269.

41.   Mylonas, Y.; Bokias, G.; Iliopoulos, I.; Staikos, G. Interpolymer Association between Hydrophobically Modified Poly(Sodium Acrylate) and Poly(N-isopropylacrylamide) in Water: the Role of Hydrophobic Interactions and Polymer Structure. *Eur. Polym. J.* **2006**, *42*, 849-857.

42.   Qiu, X.; Koga, T.; Tanaka, F.; Winnik, F. M. New Insights Into the Effects of Molecular Weight and End Group on the Temperature-Induced Phase Transition of Poly(N-isopropylacrylamide) in Water. *Sci. China. Chem.* **2013**, *56*, 56-64.

43.   Pamies, R.; Zhu, K.; Kjoniksen, A.; Nystrom, B. Thermal Response of Low Molecular Weight Poly-(N-isopropylacrylamide) Polymers in Aqueous Solution. *Polym. Bull.* **2009**, *62*, 487-502.

44.   Kujawa, P.; Tanaka, F.; Winnik, F. M. Temperature-Dependent Properties of Telechelic Hydrophobically Modified Poly(N-isopropylacrylamides) in Water: Evidence from Light Scattering and Fluorescence Spectroscopy for the Formation of Stable Mesoglobules at Elevated Temperatures. *Macromolecules* **2006**, *39*, 3048-3055.

45.   Yip, .J.; Duhamel. J.; Qiu, X. P.; Winnik, F. M. Fluorescence Studies of a Series of Monodispersed Telechelic α,ω-Dipyrenyl Poly(N-isopropylacrylamide)s in Ethanol and Water. *Can. J. Chem.* **2011**, *89*, 163-172.

46.   Yip, J.; Duhamel, J.; Qiu, X. P.: Winnik, F. M. Long-Range Polymer Chain Dynamics of Pyrene-Labelled Poly(N-isopropylacrylamide)s Studied by Fluorescence. *Macromolecules* **2011**, *44*, 5363-5372.

47.   Chee, C. K.; Rimmer, S.; Soutar, I.; Swanson, L. Time-Resolved Fluorescence Anisotropy Studies of the Temperature-Induced Intramolecular Conformational Transition of Poly(N-isopropylacrylamide) in Dilute Aqueous Solution. *Polymer* **1997**, *38*, 483-486.

48.   Iliopoulos, I.; Halary, J. L.; Audebert, R. Polymer Complexes Stabilized through Hydrogen Bonds. Influence of "Structure Defects" on Complex Formation: Viscometry and Fluorescence Polarization Measurements. *J. Polym. Sci. A* **1988**, *26*, 275-284.

49.   Koga, T.; Tanaka, F.; Motokawa, R.; Koizumi, S.; Winnik F. M. Theoretical Modelling of Hierarchically Associated Structures in Hydrophobically Modified PNIPAM Aqueous Solutions on the Basis of a Neutron Scattering Study. *Macromol. Symp.* **2010**, *291-292*, 177-185.

50.   Schild, H. G. Poly(N-isopropylacrylamide): Experiment, Theory and Application. *Prog. Polym. Sci.* **1992**, *17*, 163-249.

51.	Fujishige, S.; Kubota, K.; Ando, I. Phase Transition of Aqueous Solutions of Poly(N-isopropylacrylamide) and Poly(N-isopropylmethacrylamide). *J. Phys. Chem.* **1989**, *93*, 3311-3313.

52.	Ringsdorf, H.; Venzmer, J.; Winnik, F. M. Interaction of Hydrophobically-Modified Poly-N-isopropylacrylamides with Model Membranes-or Playing a Molecular Accordion. *Angew. Chem. Int. Ed. Engl.* **1991**, *30*, 315-318.

53.	Lakowicz, J. R. *Principles of Fluorescence Spectroscopy*. Plenum Press: New York, 1983.

54.	Berlman, I. B. Handbook of Fluorescence Spectra of Aromatic Molecules. Academic Press: New York, 1971.

55.	Birks, J. B. Photophysics of Aromatic Molecules. In Wiley: New York, 1970; p p. 301.

56.	Kalyanasundraran, K.; Tomas, J. K. Environmental Effects on Vibronic Band Intensities in Pyrene Monomer Fluorescence and their Application in Studies of Micellar Systems. *J. Am. Chem. Soc.* **1977**, *99*, 2039-2044.

57.	Dong, D. C.; Winnik, M. A. The Py Scale of Solvent Polarities. *Can. J. Chem.* **1984**, *62*, 2560-2565.

58.	Claracq, J.; Santos, S. F. C. R.; Duhamel, J.; Dumousseaux, C.; Corpart, J.-M. Rigid Interior of Styrene−Maleic Anhydride Copolymer Aggregates Probed by Fluorescence Spectroscopy. *Langmuir* **2002**, *18*, 3829-3835.

59.	Duhamel, J. In *Molecular Interfacial Phenomena of Polymers and Biopolymers*, Chen, P., Ed. Woodhead: New York, 2005; pp 214-248.

60.	Winnik, F. M. Photophysics of Preassociated Pyrenes in Aqueous Polymer Solutions and in Other Organized Media. *Chem. Rev.* **1993**, *93*, 587-614.

61.   Duhamel, J. Internal Dynamics of Dendritic Molecules Probed by Pyrene Excimer Formation. *Polymers* **2012**, *4*, 211-239.

62.   Winnik, F. M.; Regismond, S. T. A. Fluorescence Methods in the Study of the Interactions of Surfactants with Polymers. *Colloids Surf., A* **1996**, *118*, 1-39.

63.   Pina, J.; Costa, T.; Seixas de Melo, J. S. In *Photochemistry*, Albini, A., Ed. 2011; Vol. *38*, pp 67-109.

64.   Zachariasse, K.; Kuhnle, W. Intramolecular Excimers with α, ω-Diarylalkanes. *Z. Phys. Chem.* **1976**, *101*, 267-276.

65.   Cuniberti, C.; Perico, A. Intramolecular Excimers and Microbrownian Motion of Flexible Polymer Molecules in Solution. *Eur. Polym. J.* **1977**, *13*, 369-374.

66.   Winnik, M. A.; Redpath, T.; Richards, D. H. The Dynamics of End-to-End Cyclization in Polystyrene Probed by Pyrene Excimer Formation. *Macromolecules* **1980**, *13*, 328-335.

67.   Winnik, M. A. End-To-End Cyclization of Polymer Chains. *Acc. Chem. Res.* **1985**, *18*, 73-79.

68.   Svirskaya, P.; Danhelka, J.; Redpath, A. E. C.; Winnik, M. A. Cyclization Dynamics of Polymers: 7. Applications of the Pyrene Excimer Technique to the Internal Dynamics of Poly(dimethylsiloxane) Chains. *Polymer* **1983**, *24*, 319-322.

69.   Ghiggino, K. P.; Snare, M. J.; Thistlethwaite, P. J. Cyclization Dynamics in Poly(ethylene oxide). Chain Length and Temperature Dependence. *Eur. Polym. J.* **1985**, *21*, 265-272.

70.   Boileau, S.; Mechin, F.; Martinho, J. M. G.; Winnik, M. A. End-to-end Cyclization of a Pyrene End-Capped Poly(bisphenol A-diethylene glycol carbonate). *Macromolecules* **1989**, *22*, 215-220.

71.   Chen, S.; Duhamel, J. Probing End-to-End Cyclization beyond Willemski and Fixman. *J. Phys. Chem. B* **2011**, *115*, 3289-3302.

72.   Ingratta, M.; Hollinger, J.; Duhamel, J. A Case for Using Randomly Labelled Polymers to Study Long-Range Polymer Chain Dynamics by Fluorescence. *J. Am. Chem. Soc.* **2008**, *130*, 9420-9428.

73.   Kanaya, T.; Goshiki, K.; Yamamoto, M.; Nishijima, Y. Intramolecular End-to-End Excimer Formation of Bis((1-pyrenylmethoxy)carbonyl)alkanes. A Study of End-to-End Collisional Frequency on a Chain Molecule. *J. Am. Chem. Soc.* **1982**, *104*, 3580-3587.

74.   Seixas de Melo, J.; Costa, T.; Francisco, A.; Maçanita, A. L.; Gago, S.; Goncalves, I. Dynamics of Short as Compared with Long Poly(Acrylic Acid) Chains Hydrophobically Modified with Pyrene, as Followed by Fluorescence Techniques. *Phys. Chem. Chem. Phys.* **2007**, *9*, 1370-1385.

75.   Seixas de Melo, J.; Costa, T.; Miguel, M. d. G.; Lindman, B.; Schillen, K. Time-Resolved and Steady-State Fluorescence Studies of Hydrophobically Modified Water-Soluble Polymers. *J. Phys. Chem. B* **2003**, *107*, 12605-12621.

76.   Winnik, M. A.; Li, X..-B.; Guillet, J. E. Cyclization Dynamics of Polymers. 13. Effects of Added Polymer on the Conformation and Dynamics of Polystyrene Containing Evenly Spaced Pyrene Groups. *Macromolecules* **1984**, *17*, 699-702.

77.   Winnik, M. A.; Egan, L. S.; Tencer, M.; Croucher, M. D. Luminescence Studies on Sterically Stabilized Polymer Colloid Particles: Pyrene Excimer Formation. *Polymer* **1987**, *28*, 1553-1560.

78.   James, D. R.; Ware, W. R. A Fallacy in the Interpretation of Fluorescence Decay Parameters. *Chem. Phys. Lett.* **1985**, *120*, 455-459.

79.   Zachariasse, K. A.; Busse, R.; Duveneck, G.; Kuhnle, W. J. Intramolecular monomer and excimer fluorescence with dipyrenylpropanes: double-exponential versus triple-exponential decays. *J. Photochem.* **1985**, *28*, 237-253.

80.   Slomkowski, S.; Winnik, M. A. Fluorescence Quenching in Pyrene/Benzyl End-Labelled Poly(tetramethylene oxide). Cyclization Dynamics in Polymers. *Macromolecules* **1986**, *19*, 500-501.

81.   Zachariasse, K. A.; Duveneck, G. Linear Free Energy Relationships for Excimers. *J. Am. Chem. Soc.* **1987**, *109*, 3790-3792.

82.   Zachariasse, K. A.; Kuhnle, W.; Leinhos, U.; Reynders, P.; Strikers, G. Time-Resolved Monomer and Excimer Fluorescence of 1,3-di(1-pyrenyl)propane at Different Temperatures: No Evidence for Distributions from Picosecond Laser Experiments with Nanosecond Time Resolution. *J. Phys. Chem.* **1991**, *95*, 5476-5488.

83.   Mathew, A. K.; Siu, H.; Duhamel, J. A Blob Model To Study Chain Folding by Fluorescence. *Macromolecules* **1999**, *32*, 7100-7108.

84.   Tachiya, M. Application of a Generating Function to Reaction Kinetics in Micelles. Kinetics of Quenching of Luminescent Probes in Micelles. *Chem. Phys. Lett.* **1975**, *33*, 289-292.

85.   Siu, H.; Duhamel, J. Global Analysis of the Fluorescence Decays of a Pyrene-Labelled Polymer Using a Blob Model. *Macromolecules* **2004**, *37*, 9287-9289.

86.   Siu, H; Duhamel, J. The Importance of Considering Nonfluorescent Pyrene Aggregates for the Study of Pyrene-Labelled Associative Thickeners by Fluorescence. *Macromolecules* **2005**, *38*, 7184-7186.

87.   Siu, H.; Duhamel, J. Comparison of the Association Level of a Pyrene-Labelled Associative Polymer Obtained from an Analysis Based on Two Different Models. *J. Phys. Chem. B* **2005**, *109*, 1770-1780.

88.   Yip, J.; Duhamel, J.; Bahun, G. J.; Adronov, A. A Study of the Dynamics of the Branch Ends of a Series of Pyrene-Labelled Dendrimers Based on Pyrene Excimer Formation. *J. Phys. Chem. B* **2010**, *114*, 10254-10265.

89.   Chen, S.; Duhamel, J.; Bahun, G.; Adronov, A. Quantifying the Presence of Unwanted Fluorescent Species in the Study of Pyrene-Labelled Macromolecules. *J. Phys. Chem. B* **2011**, *115*, 9921-9929.

90.   Keyes-Baig, C.; Duhamel, J.; Wettig, S. Characterization of the Behavior of a Pyrene Substituted Gemini Surfactant in Water by Fluorescence. *Langmuir* **2011**, *27*, 3361-3371.

91.   Duhamel, J. New Insights in the Study of Pyrene Excimer Fluorescence to Characterize Macromolecules and their Supramolecular Assemblies in Solution. *Langmuir* **2012**, *28*, 6527-6538.

92.   Zaragoza-Galan, G.; Fowler, M.; Duhamel, J.; Rein, R., Solladie, N.; Rivera, E. Synthesis and Characterization of Novel Pyrene-Dendronized Porphyrins Exhibiting Efficient Fluorescence Resonance Energy Transfer: Optical and Photophysical Properties. *Langmuir* **2012**, *28*, 11195-11205.

93.   Siu, H; Duhamel, J. Molar Absorbance Coefficient of Pyrene Aggregates in Water Generated by a Poly(ethylene oxide) Capped at a Single End with Pyrene. *J. Phys. Chem. B* **2012**, *116*, 1226-1233.

94.   Duhamel, J. Polymer Chain Dynamics in Solution Probed with a Fluorescence Blob Model. *Acc. Chem. Res.* **2006**, *39*, 953-960.

95.   Kanagalingam, S.; Spartalis, J.; Cau, T.; Duhamel, J. Scaling Relations Related to the Kinetics of Excimer Formation between Pyrene Groups Attached onto Poly(N,N-dimethylacrylamide)s. *Macromolecules* **2002**, *35*, 8571-8577.

96.   Picarra, S.; Relogio, P.; Afonso, C. A. M.; Marinho, J. M. G.; Farinha, J. P. S. Coil−Globule Transition of Poly(Dimethylacrylamide): Fluorescence and Light Scattering Study. *Macromolecules* **2003**, *36*, 8119-8129.

97.   Teertstra, S. J.; Lin, W. Y.; Gauthier, M.; Ingratta, M.; Duhamel, J. Comparison of the Long Range Polymer Chain Dynamics of Polystyrene and Cis-Polyisoprene Using Polymers Randomly labelled with Pyrene. *Polymer* **2009**, *50*, 5456-5466.

98.   Wilken, R.; Adams, J. End-group dynamics of fluorescently labelled dendrimers. *Macromol. Rapid Commun.* **1997**, *18*, 659-665.

99.   Baker, L. A.; Crooks, R. M. Photophysical Properties of Pyrene-Functionalized Poly(propylene imine) Dendrimers. *Macromolecules* **2000**, *33*, 9034-9039.

100.   Brauge, L.; Caminade, A.-M.; Majoral, J.-P.; Slomkowski, S.; Wolszczak, M. Segmental Mobility in Phosphorus-Containing Dendrimers. Studies by Fluorescent Spectroscopy. *Macromolecules* **2001**, *33*, 9034-9039.

101.   Wang, B.-B.; Zhang, X.; Jia, X.-R.; Li, Z.-C.; Ji, Y.; Yang, L.; Wei, Y. Fluorescence and Aggregation Behavior of Poly(amidoamine) Dendrimers Peripherally Modified with Aromatic Chromophores: the Effect of Dendritic Architectures. *J. Am. Chem. Soc.* **2004**, *126*, 15180-15194.

102.   Cicchi, S.; Fabbrizzi, P.; Ghini, G.; Brandi, A.; Foggi, P.; Marcelli, A.; Righini, R.; Botta, C. Pyrene-Excimers-Based Antenna Systems. *Chem. Eur. J.* **2009**, *26*, 754-764.

103.   Duhamel, J. Global Analysis of Fluorescence Decays to Probe the Internal Dynamics of Fluorescently Labeled Macromolecules. *Langmuir* **2013**, *Article ASAP*, (DOI: 10.1021/la403714u).

Chapter 2

1.   Winnik, M. A.; Yekta, A. Associative Polymers in Aqueous Solution. *Curr. Opin. Colloid Interface Sci.* **1997**, *2*, 424-436.

2.   Liu, S.; Armes, S. P. Recent Advances in the Synthesis of Polymeric Surfactants. Curr. Opin. Colloid Interface Sci. 2001, 6, 249-256.Rodriquez-Hernandez, J., Checot, F., Gnanou, Y., Lecommandoux, S. *Prog. Polym. Sci*. **2005**, *30*, 691-724.

3.   Torchilin, V. P. Structure and Design of Polymeric Surfactant-Based Drug Delivery Systems. *J. Control Release* **2001**, *73*, 137-172.

4.   Discher, D.; Eisenberg, A. Polymer Vesicles. *Science* **2002**, *297*, 967-973.

5.   Laschewsky, A. Polymerized Micelles with Compartments. Curr. Opin. *Colloid Interface Sci.* **2003**, *8*, 274-281.

6.   Rodriquez-Hernandez, J., Checot, F., Gnanou, Y., Lecommandoux, S. Toward Smart Nano-Objects by Self-Assembly of Block Copolymers in Solution. *Prog. Polym. Sci*. **2005**, *30*, 691-724.

7.   Lutz, J.-F. Solution Self-Assembly of Tailor-Made Macromolecular Building Blocks Prepared by Controlled Radical Polymerization Techniques. *Polym. Int*. **2006**, *55*, 979-993.

8.   Olea, A. F. Hydrophobic Polyelectrolytes. In *Ionic Interactions in Natural and Synthetic Macromolecules* Eds. Ciferri A. and Perico, A. Wiley & Sons, NJ, 2012, pp211-233.

9.   Mai, Y.; Eisenberg, A. Self-Assembmly of Block Copolymers. *Chem. Soc. Rev.***2012**, *41*, 5969-5985.

10.   *Associative Polymers in Aqueous Media*; Glass, J. E., Ed.; ACS Advances in Chemistry, 2000.

11.   Rapoport N. Physical Stimuli-Responsive Polymeric Micelles for Anti-Cancer Drug Delivery. *Prog. Polym. Sci.* **2007**, *32*, 962-990.

12.   Wever, D. A. Z.; Picchioni, F.; Broekhuis, A. A. Polymers for Enhanced Oil Recovery: A Paradigm for Structure-Property Relationship in Aqueous Solution. *Prog. Polym. Sci.* **2011**, *36*, 1558-1628.

13.   Trivedi, B. C.; Culbertson, B. M. *Maleic Anhydride* Plenum Press NY, **1982**, pp 307-458.

14.   Khokhlov, A. R.; Khalatur, P. G. Conformation-Dependent Sequence Design (Engineering) of AB Copolymers. *Phys. Rev. Lett.* **1999**, *82*, 3456-3459.

15.   Ashbaugh, H. S. Tuning the Globular Assembly of Hydrophobic/Hydrophilic Heteropolymer Sequences. *J. Phys. Chem. B* **2009**, *113*, 14043-14046.

16.   Murnen, H. K.; Khokhlov, A. R.; Khalatur, P. G.; Segalman, R. A.; Zuckermann, R. N. Impact of Hydrophobic Sequence Patterning on the Coil-to-Globule Transition of Protein-Like Polymers. *Macromolecules* **2012**, *45*, 5229-5236.

17.   Siddique, B.; Duhamel, J. Effect of Polypeptide Sequence on Polypeptide Self-Assembly. *Langmuir* **2011**, *27*, 6639-6650.

18.   Ulrich, S.; Laguecir, A.; Stoll, S. Titration of Hydrophobic Polyelectrolytes Using Monte Carlo Simulations. *J. Chem. Phys.* **2005**, *122*, 094911.

19.   Press, W. H.; Flannery, B. P.; Teukolsky, S. A.; Vetterling, W. T. *Numerical Recipes. The Art of Scientific Computing (Fortran Version);* Cambridge University Press: Cambridge, 1992.

20.   Bennett, E. L.; Niemann, C. The Apparent Ionization Constants and Ultraviolet Spectra of o-, m-, and p-Fluoro-DL-Phenylalanine. *J. Am. Chem. Soc.* **1950**, *72*, 1804-1805.

21.   Siu, H.; Duhamel, J. Molar Extinction Coefficient of Pyrene Aggregates in Water. *J. Phys. Chem. B* **2008**, *112*, 15301-15312.

22.   Siu, H. ; Duhamel, J. Molar Absorption Coefficient of Pyrene Aggregates in Water Generated by a Poly(ethylene oxide) Capped at a Single End with Pyrene. *J. Phys. Chem. B* **2012**, *116*, 1226-1233.

23.   Berger, A.; Katchalski, E. Poly-L-Aspartic Acid. *J. Am. Chem. Soc.***1951**, *73*, 4084-4088.

24.   McDiarmid, R.; Doty, P. The Spectrophotometric Titration of Polyacrylic, Poly-L-aspartic, and Poly-L-glutamic Acids. *J. Phys. Chem.* **1966**, *70*, 2620-2627.

25.   Colombani, O.; Lejeune, E.; Charbonneau, C. ; Chassenieux, C. ; Nicolai, T. Ionization of Amphiphilic Acidic Block Copolymers. *J. Phys. Chem. B* **2012**, *116*, 7560-7565.

26.   Urry, D. W.; Gowda, D. C.; Peng, S.; Parker, T. M.; Jing, N.; Harris, R. D. Nanometric Design of Extraordinary Hydrophobic-Induced pKa Shifts for Aspartic Acid: Relevance to Protein Mechanisms. *Biopolymers* **1994**, *34*, 889-896.

27.   Song, J.; Laskowski, M.; Qasim, M. A.; Markley, J. L. NMR Determination of pKa Values for Asp, Glu, His, and Lys Mutants at Each Variable Contiguous Enzyme-Inhibitor Contact Position of the Turkey Ovomucoid Third Domain. *Biochemistry* **2003**, *42*, 2847-2856.

28. Thurlkill, R. L.; Grimsley, G. R.; Scholtz, J. M.; Pace, C. N. Hydrogen Bonding Markedly Reduces the pK of Buried Carboxyl Groups in Proteins. *J. Mol. Biol*. **2006**, *362*, 594-604.

29. Urry, D. W.; Gowda, D. C.; Peng, S. Q.; Parker, T. M.; Harris, R. D. Design at Nanometric Dimensions to Enhance Hydrophobicity-Induced pKa Shifts. *J. Am. Chem. Soc*. **1992**, *114*, 8716-8717.

30. Langsetmo, K.; Fuchs, J. A.; Woodwrd, C. The Conserved, Buried Aspartic Acid in Oxidized Escherichia coli Thioredoxin Has a pKa of 7.5. Its Titration Produces a Related Shift in Global Stability. *Biochemistry*, **1991**, *30*, 7603-7609.

31. Keyes-Baig, C.; Mathew, M.; Duhamel,J. Lateral Distribution of Charged Species along a Polyelectrolyte Probed with a Fluorescence Blob Model. *J. Am. Chem. Soc.* **2012**, *134*, 16791-16797.

32. Kalyanasundaram, K.; Thomas, J. K. Environmental Effects on Vibronic Band Intensities in Pyrene Monomer Fluorescence and Their Application in Studies of Micellar Systems. *J. Am. Chem. Soc.* **1977**, *99*, 2039-2044.

33. Dong, D. C.; Winnik, M. A. The Py Scale of Solvent Polarities. Solvent Effects on the Vibronic Fine Structure of Pyrene Fluorescence and Empirical Correlations with ET and Y Values. *Photochem. Photobiol*. **1982**, *35*, 17-21.

34. Dong, D. C.; Winnik, M. A. The Py Scale of Solvent Polarities. *Can. J. Chem.* **1984**, *62*, 2560-2565.

35. Claracq, J. ; Santos, S. F. C. R. ; Duhamel, J.; Dumousseaux, C. ; Corpart, J.-M. Probing the Viscous Interior of Styrene/Maleic Anhydride Copolymer Aggregates in Water by Fluorescence Spectroscopy. *Langmuir* **2002**, *18*, 3829-3835.

36.   Chu, D.-Y.; Thomas, J. K. Photophysical and Photochemical Studies on a Polymeric Intramolecular Micellar System, PA-18K2. *Macromolecules* **1987**, *20*, 2133-2138.

Chapter 3

1.   Heskins, M.; Guillet, J. E. Solution Properties of Poly(N-isopropylacrylamide). *J. Macromol. Sci.: A - Chem.* **1968**, *2*, (8), 1441-1445.

2.   Duan, M.; Fang, S.; Guo, H.; Zhang, L. Viscometric Studies of Interactions between Hydrophobically Modified Acrylamide Copolymer and Poly(N-isopropylacrylamide) in Dilute Solutions. *J. Macromol. Sci. B Phys.* **2009**, *48*, 834-843.

3.   Yang, H.; Cheng, R.; Wang, Z. A Quantitative Analyses of the Viscometric Data of the Coil-to-Globule and Globule-to-Coil Transition of Poly(N-isopropylacrylamide) in Water. *Polymer* **2003**, *44*, 7175-7180.

4.   Fang, Z.; Zhen, T. Molecular Chain Properties Of Poly(N-Isopropyl Acrylamide). *Sci. in China Ser. B* **1998**, *42*, (3), 290-297.

5.   Ishii, N.; Mamiya, J.; Ikeda, T.; Winnik, F. M. Solvent Induced Amplification of the Photoresponsive Properties of α,ω-di-[4-cyanophenyl-4′-(6-hexyloxy)-azobenzene]-Poly(N-isopropylacrylamide) in Aqueous Media. *Chem. Commun.* **2011**, *47*, 1267-1269.

6.   Mylonas, Y.; Bokias, G.; Iliopoulos, I.; Staikos, G. Interpolymer Association Between Hydrophobically Modified Poly(sodium acrylate) and Poly(N-isopropylacrylamide) in Water: the Role of Hydrophobic Interactions and Polymer Structure. *Eur. Polym. J.* **2006**, *42*, 849-857.

7.   Qiu, X.; Koga, T.; Tanaka, F.; Winnik, F. M. New Insights into the Effects of Molecular Weight and End Group on the Temperature-Induced Phase Transition of Poly(N-isopropylacrylamide) in Water. *Sci. China Chem.* **2013**, *56*, 56-64.

8.   Pamies, R.; Zhu, K.; Kjoniksen, A.; Nystrom, B. Thermal Response of Low Molecular Weight Poly(N-isopropylacrylamide) Polymers in Aqueous Solution. *Polym. Bull.* **2009**, *62*, 487-502.

9.   Kujawa, P.; Tanaka, F.; Winnik, F. M. Temperature-Dependent Properties of Telechelic Hydrophobically Modified Poly(N-isopropylacrylamides) in Water: Evidence from Light Scattering and Fluorescence Spectroscopy for the Formation of Stable Mesoglobules at Elevated Temperatures. *Macromolecules* **2006**, *39*, 3048-3055.

10.   Yip, .J.; Duhamel. J.; Qiu, X. P.; Winnik, F. M. Fluorescence Studies of a Series of Monodispersed Telechelic α,ω-dipyrenyl Poly(N-isopropylacrylamide)s in Ethanol and Water. *Can. J. Chem.* **2011**, *89*, 163-172.

11.   Yip, J.; Duhamel, J. Long-Rage Polymer Chain Dynamics of Pyrene-Labeled Poly(N-isopropylacrylamide)s Studied by Fluorescence. *Macromolecules* **2011**, *44*, 5363-5372.

12.   Chee, C. K.; Rimmer, S.; Soutar, I.; Swanson, L. Time-Resolved Fluorescence Anisotropy Studies of the Temperature-Induced Intramolecular Conformational Transition of Poly(N-isopropylacrylamide) in Dilute Aqueous Solution. *Polymer* **1997**, *38*, (2), 483-486.

13.   Iliopoulos, I.; Halary, J. L.; Audebert, R. Polymer Complexes Stabilized through Hydrogen Bonds. Influence of "Structure Defects" on Complex Formation: Viscometry and Fluorescence Polarization Measurements. *J. Polym. Sci. A* **1988**, *26*, 275-284.

14.   Tanaka, F.; Koga, T.; Kojima, H.; Winnik, F. M. Hydration and Phase Separation of Temperature-Sensitive Water-Soluble Polymers. *Chin. J. Polym. Sci.* **2011**, *29*, 13-21.

15.   Koga, T.; Tanaka, F.; Motokawa, R.; Koizumi, S.; Winnik F. M. Theoretical Modelling of Hierarchically Associated Structures in Hydrophobically Modified PNIPAM Aqueous Solutions on the Basis of a Neutron Scattering Study. *Macromol. Symp.* **2010**, *291-292*, 177-185.

16.   Tanaka, F.; Koga, T.; Kaneda, I.; Winnik, F. M. Hydration, Phase Separation and Nonlinear Rheology of Temperature-Sensitive Water-Soluble Polymers. *J. Phys.: Condens. Matter* **2011**, *23*, 284105-284112.

17.   Schild, H. G. Poly(N-isopropylacrylamide): Experiment, Theory, and Application. *Prog. Polym. Sci.* **1992**, *17*, (2), 163-249.

18.   Afroze, F.; Nies, E; Berghmans, H. Phase Transitions in the System Poly(N-isopropylacrylamide)/Water and Swelling Behaviour of the Corresponding Networks. *J. Mol. Structure* **2000**, *554*, (1), 55-68.

19.   de Azevedo, R. G.; Rebelo, L. P. N.; Ramos, A. M.; Szydlowski,J.; de Sousa, H. C.; Klein, J. Phase Behavior of (Polyacrylamides + Water) Solutions: Concentration, Pressure and Isotope Effects. *Fluid Phase Eq.* **2001**, *185*, 189-198.

20.   Rebelo, L. P. N.; Visak, Z. P.; de Sousa, H. C.; Szydlowski, J.; de Azevedo, R. G.; Ramos, A. M.; Najdanovic-Cisak, V.; da Ponte, M. N.; Klein, J. Double Critical Phenomena in (Water + Polyacrylamides) Solutions. *Macromolecules* **2002**, *35*, 1887-1895.

21.   Milewska, A.; Szydlowski, J.; Rebelo, L. P. N. Viscosity and Ultrasonic Studies of Poly(N-isopropylacrylamide)–Water Solutions. *J. Polym. Sci. Polym. Phys. Ed.* **2003**, *41*, 1219-1233.

22.   Okada, Y.; Tanaka, F. Cooperative Hydration, Chain Collapse, and Flat LCST Behavior in Aqueous Poly(N-isopropylacrylamide) Solutions. *Macromolecules* **2005**, *38*, 4465-4471.

23.   Kujawa, P.; Aseyev, V.; Tenhu, H.; Winnik, F. M. Temperature-Sensitive Properties of Poly(N-isopropylacrylamide) Mesoglobules Formed in Dilute Aqueous Solutions Heated Above their Demixing Point. *Macromolecules* **2006**, *39*, 7686-7693.

24.   Fujishige, S.; Kubota, K.; Ando, I. Phase Transition of Aqueous Solutions Of Poly(N-isopropylacrylamide) and Poly(N-isopropylmethacrylamide). *J. Phys. Chem.* **1989**, *93*, 3311-3313.

25.   Tanaka, F.; Koga, T.; Winnik, F. M. Competitive Hydrogen Bonds and Cononsolvency of Poly(N-isopropylacrylamide)s in Mixed Solvents of Water/Methanol. *Progr. Colloid Polym. Sci.* **2009**, *136*, 1-8.

26.   Rinsdorf, H.; Venzmer, J.; Winnik, F.M. Interaction of Hydrophobically-Modified Poly-N-isoprop ylacrylamides with Model Membranes-or Playing a Molecular Accordion. *Angew.Chem. Int. Ed.Engl.* **1991**, *30*, 315-318.

27.   Cuniberti, C.; Perico, A. Intramolecular Diffusion-Controlled Reactions and Polymer Dynamics. *Prog. Polym. Sci.* **1984**, *10*, 271-316.

28.   Winnik, M. A. End-to-End Cyclization of Polymer Chains. *Acc. Chem. Res.* **1985**, *18*, 73-79.

29.   Duhamel, J., Molecular Interfacial Phenomena of Polymers and Biopolymers. Woodhead: New York, 2005.

30.   Duhamel, J. Polymer Chain Dynamics in Solution Probed with a Fluorescence Blob Model. *Acc. Chem. Res.* **2006**, *39*, 953-960.

31.   Kujawa, P.; Segui, F.; Shaban, S.; Diab, C.; Okada, Y.; Tanaka, F.; Winnik, F. M. Impact of End-Group Association and Main-Chain Hydration on the Thermosensitive Properties of

Hydrophobically Modified Telechelic Poly(N-isopropylacrylamides) in Water. *Macromolecules* **2006**, *39*, 341-348.

32.   Winnik, F. M. Photophysics of Preassociated Pyrenes in Aqueous Polymer Solutions and in Other Organized Media. *Chem. Rev.* **1993**, *93*, 587-614.

33.   Winnik, F. M.; Regismond, S. T. A. Fluorescence Methods in the Study of the Interactions of Surfactants with Polymers. *Colloids Surf., A* **1996**, *118*, 1-39.

34.   Pina, J.; Costa, T.; Seixas de Melo, J. S. In *Photochemistry*, Albini, A., Ed. 2011; Vol. *38*, pp 67-109.

35.   Duhamel, J. Internal Dynamics of Dendritic Molecules Probed by Pyrene Excimer Formation. *Polymers* **2012**, *4*, 211-239.

36.   Demas, J. N. *Excited State Lifetime Measurements*. Academic Press: New York, 1983.

37.   Yip, J.; Duhamel, J.; Bahun, G. J.; Adronov, A. A Study of the Dynamics of the Branch Ends of a Series of Pyrene-Labeled Dendrimers Based on Pyrene Excimer Formation. *J. Phys. Chem. B* **2010**, *114*, 10254-10265.

38.   Siu, H.; Duhamel, J. Comparison of the Association Level of a Pyrene-Labeled Associative Polymer Obtained from an Analysis Based on Two Different Models. *J. Phys. Chem. B* **2005**, *109*, 1770-1780.

39.   Chen, S.; Duhamel, J.; Bahun, G.; Adronov, A. Quantifying the Presence of Unwanted Fluorescent Species in the Study of Pyrene-Labeled Macromolecules. *J. Phys. Chem. B* **2011**, *115*, 9921-9929.

40.   Keyes-Baig, C.; Duhamel, J.; Wettig, S. Characterization of the Behavior of a Pyrene Substituted Gemini Surfactant in Water by Fluorescence. *Langmuir* **2011**, *27*, 3361-3371.

41.   Khakhel, O. A. Absorption Spectra of Pyrene Aggregates in Saturated Solutions. *J. Appl. Spec.* **2001**, *68*, (2), 280-286.

42.   Dutta, A. K.; Misra, T. N. A Spectroscopic Study of Nonamphiphilic Pyrene Assembled in Langmuir-Blodgett Films: Formation of Aggregates. *Langmuir* **1996**, *12*, 459-465.

43.   Siu, H; Duhamel, J. Molar Absorbance Coefficient of Pyrene Aggregates in Water Generated by a Poly(ethylene oxide) Capped at a Single End with Pyrene. *J. Phys. Chem. B* **2012**, *116*, 1226-1233.

Chapter 4

1.   Heskins, M.; Guillet, J. E. Solution Properties of Poly(N-isopropylacrylamide). *J. Macromol. Sci.: A - Chem.* **1968**, *2*, (8), 1441-1445.

2.   Duan, M.; Fang, S.; Guo, H.; Zhang, L. Viscometric Studies of Interactions between Hydrophobically Modified Acrylamide Copolymer and Poly(N-isopropylacrylamide) in Dilute Solutions. *J. Macromol. Sci. B Phys.* **2009**, *48*, 834-843.

3.   Mylonas, Y.; Bokias, G.; Iliopoulos, I.; Staikos, G. Interpolymer Association Between Hydrophobically Modified Poly(sodium acrylate) and Poly(N-isopropylacrylamide) in Water: the Role of Hydrophobic Interactions and Polymer Structure. *Eur. Polym. J.* **2006**, *42*, 849-857.

4.   Yang, H.; Cheng, R.; Wang, Z. A Quantitative Analyses of the Viscometric Data of the Coil-to-Globule and Globule-to-Coil Transition of Poly(N-isopropylacrylamide) in Water. *Polymer* **2003**, *44*, 7175-7180.

5.   Rinsdorf, H.; Venzmer, J.; Winnik, F.M. Interaction of Hydrophobically-Modified Poly-N-isoprop ylacrylamides with Model Membranes-or Playing a Molecular Accordion. *Angew.Chem. Int. Ed.Engl.* **1991**, *30*, 315-318.

6.   Tanaka, F.; Koga, T.; Kaneda, I.; Winnik, F. M. Hydration, Phase Separation and Nonlinear Rheology of Temperature-Sensitive Water-Soluble Polymers. *J. Phys.: Condens. Matter* **2011**, *23*, 284105-284112.

7.   Koga, T.; Tanaka, F.; Motokawa, R.; Koizumi, S.; Winnik F. M. Theoretical Modelling of Hierarchically Associated Structures in Hydrophobically Modified PNIPAM Aqueous Solutions on the Basis of a Neutron Scattering Study. *Macromol. Symp.* **2010**, *291-292*, 177-185.

8.   Yip, .J.; Duhamel. J.; Qiu, X. P.; Winnik, F. M. Fluorescence Studies of a Series of Monodispersed Telechelic α,ω-dipyrenyl Poly(N-isopropylacrylamide)s in Ethanol and Water. *Can. J. Chem.* **2011**, *89*, 163-172.

9.   Ishii, N.; Mamiya, J.; Ikeda, T.; Winnik, F. M. Solvent Induced Amplification of the Photoresponsive Properties of α,ω-di-[4-cyanophenyl-4′-(6-hexyloxy)-azobenzene]-Poly(N-isopropylacrylamide) in Aqueous Media. *Chem. Commun.* **2011**, *47*, 1267-1269.

10.   Chee, C. K.; Rimmer, S.; Soutar, I.; Swanson, L. Time-Resolved Fluorescence Anisotropy Studies of the Temperature-Induced Intramolecular Conformational Transition of Poly(N-isopropylacrylamide) in Dilute Aqueous Solution. *Polymer* **1997**, *38*, (2), 483-486.

11.   Qiu, X.; Koga, T.; Tanaka, F.; Winnik, F. M. New Insights into the Effects of Molecular Weight and End Group on the Temperature-Induced Phase Transition of Poly(N-isopropylacrylamide) in Water. *Sci. China Chem.* **2013**, *56*, 56-64.

12.   Tanaka, F.; Koga, T.; Kojima, H.; Winnik, F. M. Hydration and Phase Separation of Temperature-Sensitive Water-Soluble Polymers. *Chin. J. Polym. Sci.* **2011**, *29*, 13-21.

13. Kujawa, P.; Tanaka, F.; Winnik, F. M. Temperature-Dependent Properties of Telechelic Hydrophobically Modified Poly(N-isopropylacrylamides) in Water: Evidence from Light Scattering and Fluorescence Spectroscopy for the Formation of Stable Mesoglobules at Elevated Temperatures. *Macromolecules* **2006**, *39*, 3048-3055.

14. Birks, J. B. Photophysics of Aromatic Molecules. In Wiley: New York, 1970; p p. 301.

15. Cuniberti, C.; Perico, A. Intramolecular Diffusion-Controlled Reactions and Polymer Dynamics. *Prog. Polym. Sci.* **1984**, *10*, 271-316.

16. Winnik, M. A. End-to-End Cyclization of Polymer Chains. *Acc. Chem. Res.* **1985**, *18*, 73-79.

17. Duhamel, J., Molecular Interfacial Phenomena of Polymers and Biopolymers. Woodhead: New York, 2005.

18. Duhamel, J. Polymer Chain Dynamics in Solution Probed with a Fluorescence Blob Model. *Acc. Chem. Res.* **2006**, *39*, 953-960.

19. Winnik, F. M. Photophysics of Preassociated Pyrenes in Aqueous Polymer Solutions and in Other Organized Media. *Chem. Rev.* **1993**, *93*, 587-614.

20. Winnik, F. M.; Regismond, S. T. A. Fluorescence Methods in the Study of the Interactions of Surfactants with Polymers. *Colloids Surf., A* **1996**, *118*, 1-39.

21. Pina, J.; Costa, T.; Seixas de Melo, J. S. In *Photochemistry*, Albini, A., Ed. 2011; Vol. *38*, pp 67-109.

22. Tanaka, F.; Koga, T.; Winnik, F. M. Competitive Hydrogen Bonds and Cononsolvency of Poly(N-isopropylacrylamide)s in Mixed Solvents of Water/Methanol. *Progr. Colloid Polym. Sci.* **2009**, *136*, 1-8.

23.   Schild, H. G. Poly(N-isopropylacrylamide): Experiment, Theory, and Application. *Prog. Polym. Sci.* **1992**, *17*, (2), 163-249.

24.   Okada, Y.; Tanaka, F. Cooperative Hydration, Chain Collapse, and Flat LCST Behavior in Aqueous Poly(N-isopropylacrylamide) Solutions. *Macromolecules* **2005**, *38*, 4465-4471.

25.   Kujawa, P.; Aseyev, V.; Tenhu, H.; Winnik, F. M. Temperature-Sensitive Properties of Poly(N-isopropylacrylamide) Mesoglobules Formed in Dilute Aqueous Solutions Heated Above their Demixing Point. *Macromolecules* **2006**, *39*, 7686-7693.

26.   Fujishige, S.; Kubota, K.; Ando, I. Phase Transition of Aqueous Solutions Of Poly(N-isopropylacrylamide) and Poly(N-isopropylmethacrylamide). *J. Phys. Chem.* **1989**, *93*, 3311-3313.

27.   Philipp, M; Muller, U.; Aleksandrova, R.; Sanctuary, R.; Muller-Bushbaum, P.; Kruger, J. K. On the Elastic Nature of the Demixing Transition of Aqueous PNIPAM Solutions. *Soft Matter* **2012**, *8*, 111387-111395.

28.   Yip, J.; Duhamel, J. Long-Rage Polymer Chain Dynamics of Pyrene-Labeled Poly(N-isopropylacrylamide)s Studied by Fluorescence. *Macromolecules* **2011**, *44*, 5363-5372.

29.   Yip, J.; Duhamel, J.; Bahun, G. J.; Adronov, A. A Study of the Dynamics of the Branch Ends of a Series of Pyrene-Labeled Dendrimers Based on Pyrene Excimer Formation. *J. Phys. Chem. B* **2010**, *114*, 10254-10265.

30.   Siu, H.; Duhamel, J. Comparison of the Association Level of a Pyrene-Labeled Associative Polymer Obtained from an Analysis Based on Two Different Models. *J. Phys. Chem. B* **2005**, *109*, 1770-1780.

31.   Chen, S.; Duhamel, J.; Bahun, G.; Adronov, A. Quantifying the Presence of Unwanted Fluorescent Species in the Study of Pyrene-Labeled Macromolecules. *J. Phys. Chem. B* **2011**, *115*, 9921-9929.

32.   Keyes-Baig, C.; Duhamel, J.; Wettig, S. Characterization of the Behavior of a Pyrene Substituted Gemini Surfactant in Water by Fluorescence. *Langmuir* **2011**, *27*, 3361-3371.

33.   Siu, H; Duhamel, J. Molar Absorption Coefficient of Pyrene Aggregates in Water. *J. Phys. Chem. B* **2008**, *112*, 15301-15312.

34.   Siu, H.; Duhamel, J. The Importance of Considering Nonfluorescent Pyrene Aggregates for the Study of Pyrene-Labeled Associative Thickeners by Fluorescence. *Macromolecules* **2005**, *38*, 7184-7186.

35.   Siu, H; Duhamel, J. Molar Absorbance Coefficient of Pyrene Aggregates in Water Generated by a Poly(ethylene oxide) Capped at a Single End with Pyrene. *J. Phys. Chem. B* **2012**, *116*, 1226-1233.

Chapter 5

1.   Winnik, M. A. *Acc. Chem. Res.* **1985**, *18*, 73-79.

2.   Winnik, F. M. *Chem. Rev.* **1993**, *93*, 587 – 614.

3.   Duhamel, J. *Acc. Chem. Res.* **2006**, *39*, 953-960.

4.   Duhamel, J. *Langmuir* **2012**, *28*, 6527-6538.

5.   Duhamel, J. *Polymers* **2012**, *4*, 211-239.

6. Cuniberti, C.; Perico, A. *Eur. Polym. J.* **1977**, *13*, 369-374.

7. Winnik, M. A.; Redpath, T.; Richards, D. H. *Macromolecules* **1980**, *13*, 328-335.

8. Svirskaya, P.; Danhelka, J.; Redpath, A. E. C.; Winnik, M. A. *Polymer* **1983**, *24*, 319-322.

9. Ghiggino, K. P.; Snare, M. J.; Thistlethwaite, P. J. *Eur. Polym. J.* **1985**, *21*, 265– 272.

10. Boileau, S.; Méchin, F.; Martinho, J. M. G.; Winnik, M. A. *Macromolecules* **1989**, *22*, 215– 220.

11. Chen, S.; Duhamel, J.; Winnik, M. A. *J. Phys. Chem. B* **2011**, *115*, 3289-3302.

12. Zachariasse, K.; Kühnle, W. *Z. Phys. Chem. Neue Fol.* **1976**, *101*, 267-276.

13. Kanaya, T.; Goshiki, K.; Yamamoto, M.; Nishijima, Y. *J. Am. Chem. Soc.* **1982**, *104*, 3580-3587.

14. Zachariasse, K. A.; Maçanita, A. L.; Kühnle, W. *J. Phys. Chem. B* **1990**, *103*, 9356-9365.

15. Mathew, A.; Siu, H.; Duhamel, J. *Macromolecules* **1999**, *32*, 7100– 7108.

16. Kanagalingam, S.; Spartalis, J.; Cao, T.-C.; Duhamel, J. *Macromolecules* **2002**, *35*, 8571–8577.

17. Picarra, S.; Relogio, P.; Afonso, C. A. M.; Martinho, J. M. G.; Farinha, J. P. S. *Macromolecules* **2003**, *36*, 8119-8129.

18. Ingratta, M.; Hollinger, J.; Duhamel, J. *J. Am. Chem. Soc.* **2008**, *130*, 9420– 9428.

19. Teertstra, S. J.; Lin, W. Y.; Gauthier, M.; Ingratta, M.; Duhamel, J. *Polymer* **2009**, *50*, 5456–5466.

20. Yip, J.; Duhamel, J.; Qiu, X. P.; Winnik, F. M. *Macromolecules* **2011**, *44*, 5363-5372.

21. Wilken, R.; Adams, J. *Macromol. Rapid. Commun.* **1997**, *18*, 659-665.

22. Baker, L. A.; Crooks, R. M. *Macromolecules* **2000**, *33*, 9034-9039.

23.   Brauge, L.; Caminade, A.-M.; Majoral, J.-P.; Slomkowski, S.; Wolszczak, M. *Macromolecules* **2001**, *34*, 5599-5606.

24.   Wang, B.-B.; Zhang, X.; Jia, X.-R.; Li, Z.-C.; Ji, Y.; Yang, L.; Wei, Y. *J. Am. Chem. Soc.* **2004**, *126*, 15180-15194.

25.   Cicchi, S.; Fabbrizzi, P.; Ghini, G.; Brandi, A.; Foggi, P.; Marcelli, A.; Righini, R.; Botta, C. *Chem. Eur. J.* **2009**, *15*, 754-564.

26.   Yip, J.; Duhamel, J.; Bahun, G. J.; Adronov, A. *J. Phys. Chem. B* **2010**, *114*, 10254-10265.

27.   Zachariasse, K. A.; Busse, R.; Duveneck, G.; Kühnle, W. *J. Photochem.* **1985**, *28*, 237-253.

28.   Birks, J. B. *Photophysics of Aromatic Molecules*. Wiley: New York, 1970; p 301.

29.   Ingratta, M.; Duhamel, J. *Macromolecules* **2007**, *40*, 6647-6657.

30.   Bahun, G. J.; Adronov, A. *J. Polym. Sci. A*: *Polym. Chem.* **2010**, *48*, 1016-1028.

31.   Zaragoza-Galán, G.; Fowler, M.; Duhamel, J.; Rein, R.; Solladié, N.; Rivera, E. *Langmuir* **2012**, *28*, 11195-11205.

32.   Ingratta, M.; Mathew, M.; Duhamel, J. *Can. J. Chem.* **2010**, *88*, 217-227.

33.   Siu, H.; Duhamel, J. *J. Phys. Chem. B* **2005**, *109*, 1770-1780.

34.   Chen, S.; Duhamel, J.; Bahun, G.; Adronov, A. *J. Phys. Chem. B* **2011**, *115*, 9921-9929.

35.   Keyes-Baig, C.; Duhamel, J.; Wettig, S. *Langmuir* **2011**, *27*, 3361–3371.

36.   Press, W. H.; Flannery, B. P.; Teukolsky, S. A.; Vetterling, W. T. *Numerical Recipes. The Art of Scientific Computing (Fortran Version)*; Cambridge University Press: Cambridge, 1992.

37.   Svirskaya, P.; Danhelka, J.; Redpath, A. E. C.; Winnik, M. A. *Polymer* **1983**, *24*, 319-322.

38.   Ingratta, M.; Duhamel, J. *J. Phys. Chem. B* **2009**, *113*, 2284-2292.

39.   Stewart, G. M.; Fox, M. A. *J. Am. Chem. Soc.* **1996**, *118*, 4354-4360.

40.   Vanjinathan, M.; Lin, H.-C.; Nasar, A. S. *Macromol. Chem. Phys.* **2011**, *212*, 849-859.

41.   Cuniberti, C.; Perico, A. *Eur. Polym. J.* **1980**, *16*, 887-893.

42.   Cuniberti, C.; Perico, A. *Prog. Polym. Sci.* **1984**, *10*, 271-316.

43.   Steady-state fluorescence spectra depend on the slit width used for the excitation and emission monochromators, the geometry (front-face or right angle) used for the acquisition, and the sensitivity of the phtomultiplier tube with wavelength and the procedure used to determine the $(I_E/I_M)_{SS}$ ratios.

44.   Cheung, S.-T.; Winnik, M. A.; Redpath, A. E. C. *Macromol. Chem. Phys.* **1982**, *183*, 1815-1824.

45.   Redpath, A. E. C.; Winnik, M. A. *J. Am. Chem. Soc.* **1982**, *104*, 5604-5607.

46.   Winnik, M. A.; Redpath, A. E. C.; Paton, K.; Danhelka, J. *Polymer* **1984**, *25*, 91-99.

47.   Boileau, S.; Méchin, F.; Martinho, J. M. G.; Winnik, M. A. *Macromolecules* **1989**, *22*, 215– 220.

48.   Slomkowski, S.; Winnik, M. A. *Macromolecules* **1986**, *19*, 500– 501.

49.   Xu, H.; Martinho, J. M. G.; Winnik, M. A.; Beinert, G. *Makromol. Chem.* **1989**, *190*, 1333-1343.

50.   Farinha, J. P. S.; Martinho, J. M. G.; Xu, H.; Winnik, M. A.; Quirk, R. P. *J. Polym. Sci., Part B: Polym. Phys.* **1994**, *32*, 1635-1642.

51.   Martinho, J. M. G.; Reis e Sousa, A. T.; Winnik, M. A. *Macromolecules* **1993**, *26*, 4484-4488.

52.   Duhamel, J.; Khayakin, Y.; Hu, Y. Z.; Winnik, M. A.; Boileau, S.; Méchin, F. *Eur. Polym. J.* **1994**, *30*, 129– 134.

53.   Lee, S.; Winnik, M. A. *Macromolecules* **1997**, *30*, 2633– 2641.

54.   Lee, S.; Duhamel, J. *Macromolecules* **1998**, *31*, 9193– 9200.

55.   Reis e Sousa, A. T.; Castanheira, E. M. S.; Fedorov, A.; Martinho, J. M. G. *J. Phys. Chem. A* **1998**, *102*, 6406-6411.

56.   Piçarra, S.; Gomes, P. T.; Martinho, J. M. G. *Macromolecules* **2000**, *33*, 3947– 3950.

57.   Farinha, J. P. S.; Piçarra, S.; Miesel, K.; Martinho, J. M. G. *J. Phys. Chem. B* **2001**, *105*, 10536-10545.

58.   Kim, S. D.; Torkelson, J. M. *Macromolecules* **2002**, *35*, 5943– 5952.

59.   Gardinier, W. E.; Bright, F. V. *J. Phys. Chem. B* **2005**, *109*, 14824–14829.

60.   Costa, T.; Seixas de Melo, J.; Burrows, H. D. *J. Phys. Chem. B* **2009**, *113*, 618– 626.

61.   Winnik, M. A.; Li, X.-B.; Guillet, J. E. *Macromolecules***1984**, *17*, 699-702.

62.   Winnik, M. A.; Egan, L. S.; Tencer, M.; Croucher, M. D. *Polymer* **1987**, *28*, 1553-1560.

63.   Lakowicz, J. R. *Principles of Fluorescence Spectroscopy*; Plenum Press: New York, 1983.

64.   James, D. R.; Ware, W. R. *Chem. Phys. Lett.* **1985**, *120*, 455-459.

65.   Zachariasse, K. A.; Busse, R.; Duveneck, G.; Kühnle, W. *J. Photochem.* **1985**, *28*, 237-253.

66.   Zachariasse, K. A.; Busse, R.; Duveneck, G. ; Kühnle, W. *J. Photochem.* **1985**, *28*, 237-253.

67.   Zachariasse, K. A.; Duveneck, G. *J. Am. Chem. Soc.* **1987**, *109*, 3790-3792.

68.   Zachariasse, K. A.; Kühnle, W. ; Leinhos, U. ; Reynders, P. ; Strikers, G. *J. Phys. Chem.* **1991**, *95*, 5476-5488.

69.   Seixas, de Melo, J.; Costa, T.; Francisco, A. ; Maçanita, A. L. ; Gago, S. ; Gonçalves, I. S. *Phys. Chem. Chem. Phys.* **2007**, *9*, 1370-1385.

70.   Seixas de Melo, J.; Costa, T.; Miguel, M. d. G. ; Lindman, B. ; Schillén, K. *J. Phys. Chem.* **2003**, *107*, 12605-12621.

71.   Siu, H.; Duhamel, J. *Macromolecules* **2004**, *37*, 9287-9289.

72.   Siu, H.; Duhamel, J. *Macromolecules* **2005**, *38*, 7184-7186.

73.   Siu, H.; Duhamel, J. *J. Phys. Chem. B* **2012**, *116*, 1226-1233.

Chapter 6

1.   Olea, A. F. Hydrophobic Polyelectrolytes. In *Ionic Interactions in Natural and Synthetic Macromolecules*, Ciferri, A. P., A., Ed. Wiley & Sons: Hoboken, NJ, 2012; pp 211-233.

2.   Wang, C.; Ravi, P.; Tam, K. C.; Gan, L. H. Self-Assembly Behavior of Poly(methacrylic acid-block-ethyl acrylate) Polymer in Aqueous Medium: Potentiometric Titration and Laser Light Scattering Studies. *J. Phys. Chem. B* **2004**, *108*, 1621-1627.

3.   Harrisson, S.; Wooley, K. L. Shell-Crosslinked Nanostructures from Amphiphilic AB and ABA Block Copolymers of Styrene-alt-(Maleic Anhydride) and Styrene: Polymerization, Assembly and Stabilization in One Pot. *Chem. Commun.* **2005**, *26*, 3529-3261.

4.   Lutz, J.-F. Solution Self-Assembly of Tailor-Made Macromolecular Building Blocks Prepared by Controlled Radical Polymerization Techniques. *Polym. Int.* **2006**, *55*, 979-993.

5.   Duan, M.; Fang, S.; Guo, H.; Zhang, L. Viscometric Studies of Interactions between Hydrophobically Modified Acrylamide Copolymer and Poly(N-isopropylacrylamide) in Dilute Solutions. *J. Macromol. Sci. B* **2009**, *48*, 834-843.

6.   Pamies, R.; Zhu, K.; Kjoniksen, A.; Nystrom, B. Thermal Response of Low Molecular Weight Poly-(N-isopropylacrylamide) Polymers in Aqueous Solution. *Polym. Bull.* **2009**, *62*, 487-502.

7.   Kujawa, P.; Tanaka, F.; Winnik, F. M. Temperature-Dependent Properties of Telechelic Hydrophobically Modified Poly(N-isopropylacrylamides) in Water: Evidence from Light Scattering and Fluorescence Spectroscopy for the Formation of Stable Mesoglobules at Elevated Temperatures. *Macromolecules* **2006**, *39*, 3048-3055.

8.   Yip, J., Duhamel, J., Qiu, X. P., Winnik, F. M. Long-Range Polymer Chain Dynamics of Pyrene-Labelled Poly(N-isopropylacrylamide)s Studied by Fluorescence. *Macromolecules* **2011**, *44*, 5363-5372.

9.   Tanaka, F.; Koga, T.; Kaneda, I.; Winnik, F. M. Hydration, Phase Separation and Nonlinear Rheology of Temperature-Sensitive Water-Soluble Polymers. *J. Phys. Condens. Matter* **2011**, *23*, 284105-284112.

10.   Zachariasse, K., Kuhnle, W. Intramolecular Excimers with α, ω-Diarylalkanes. *Zeitschrift für Physikalische Chemie* **1976**, *101*, 267-276.

11.   Redpath, A. E. C.; Winnik, M. A. Cyclization Dynamics of Polymers. 2. Dynamics and Thermodynamics of End-to-End Cyclization of Polystyrene in a THETA Solvent. *J. Am. Chem. Soc.* **1980**, *102*, 6869-6871.

12.   Ghiggino, K. P.; Snare, M. J.; Thistlethwaite, P. J. Cyclization Dynamics in Poly(ethylene oxide). Chain Length and Temperature Dependence. *Eur. Polym. J.* **1985**, *21*, 265-272.

13.   Mathew, A. K.; Siu, H.; Duhamel, J. A Blob Model To Study Chain Folding by Fluorescence. *Macromolecules* **1999**, *32*, 7100-7108.

14.   Siu, H.; Duhamel, J. Comparison of the Association Level of a Pyrene-Labelled Associative Polymer Obtained from an Analysis Based on Two Different Models. *J. Phys. Chem. B* **2005**, *109*, 1770-1780.

15.   Duhamel, J. New Insights in the Study of Pyrene Excimer Fluorescence to Characterize Macromolecules and their Supramolecular Assemblies in Solution. *Langmuir* **2012**, *28*, 6527-6538.

16.   Chen, S.; Duhamel, J.; Bahun, G.; Adronov, A. Quantifying the Presence of Unwanted Fluorescent Species in the Study of Pyrene-Labeled Macromolecules. *J. Phys. Chem. B* **2011**, *115*, 9921-9929.

17.   Ulrich, S.; Laguecir, A.; Stol, S. Titration of Hydrophobic Polyelectrolytes Using Monte Carlo Simulations. *J. Chem. Phys.* **2005**, *122*, 094911.

18.   Qiu, X.; Koga, T.; Tanaka, F.; Winnik, F. M. New Insights Into the Effects of Molecular Weight and End Group on the Temperature-Induced Phase Transition of Poly(N-isopropylacrylamide) in Water. *Sci. China. Chem.* **2013**, *56*, 56-64.

19.   Siddique, B.; Duhamel, J. Effect of Polypeptide Sequence on Polypeptide Self-Assembly. *Langmuir* **2011**, *27*, 6639-6650.

20.   Dumas, D.; Muller, S.; Gouin, F.; Baros, F.; Viriot, M.-L.; Stoltz, J.-F. Membrane Fluidity and Oxygen Diffusion in Cholesterol-Enriched Erythrocyte Membrane. *Arch. Biochem. Biophys.* **1997**, *341*, 34-39.

21.   Tanaka, F.; Koga, T.; Kojima, H.; Winnik, F. M. Hydration and Phase Separation of Temperature-Sensitive Water-Soluble Polymers. *Chin. J. Polym. Sci.* **2011**, *29*, 13-21.

22.   Koga, T.; Tanaka, F.; Motokawa, R.; Koizumi, S.; Winnik F. M. Theoretical Modelling of Hierarchically Associated Structures in Hydrophobically Modified PNIPAM Aqueous Solutions on the Basis of a Neutron Scattering Study. *Macromol. Symp.* **2010**, *291-292*, 177-185.

23.   Tanaka, F.; Koga, T.; Kaneda, I.; Winnik, F. M. Hydration, Phase Separation and Nonlinear Rheology of Temperature-Sensitive Water-Soluble Polymers. *J. Phys.: Condens. Matter* **2011**, *23*, 284105-284112.

24.   Siu, H; Duhamel, J. Molar Absorbance Coefficient of Pyrene Aggregates in Water Generated by a Poly(ethylene oxide) Capped at a Single End with Pyrene. *J. Phys. Chem. B* **2012**, *116*, 1226-1233.

25.   Siu, H; Duhamel, J. Molar Absorption Coefficient of Pyrene Aggregates in Water. *J. Phys. Chem. B* **2008**, *112*, 15301-15312.

26.   Keyes-Baig, C.; Duhamel, J.; Wettig, S. Characterization of the Behavior of a Pyrene Substituted Gemini Surfactant in Water by Fluorescence. *Langmuir* **2011**, *27*, 3361-3371.

27.   Siu, H.; Duhamel, J. Comparison of the Association Level of a Pyrene-Labeled Associative Polymer Obtained from an Analysis Based on Two Different Models. *J. Phys. Chem. B* **2005**, *109*, 1770-1780.

28. Yip, J.; Duhamel, J.; Bahun, G. J.; Adronov, A. A Study of the Dynamics of the Branch Ends of a Series of Pyrene-Labeled Dendrimers Based on Pyrene Excimer Formation. *J. Phys. Chem. B* **2010**, *114*, 10254-10265.

Appendices

Appendix SI2 – Supporting Information for Chapter 2: Effect of Sequence on the Ionization

Behaviour of a Series of Amphiphilic Polypeptides
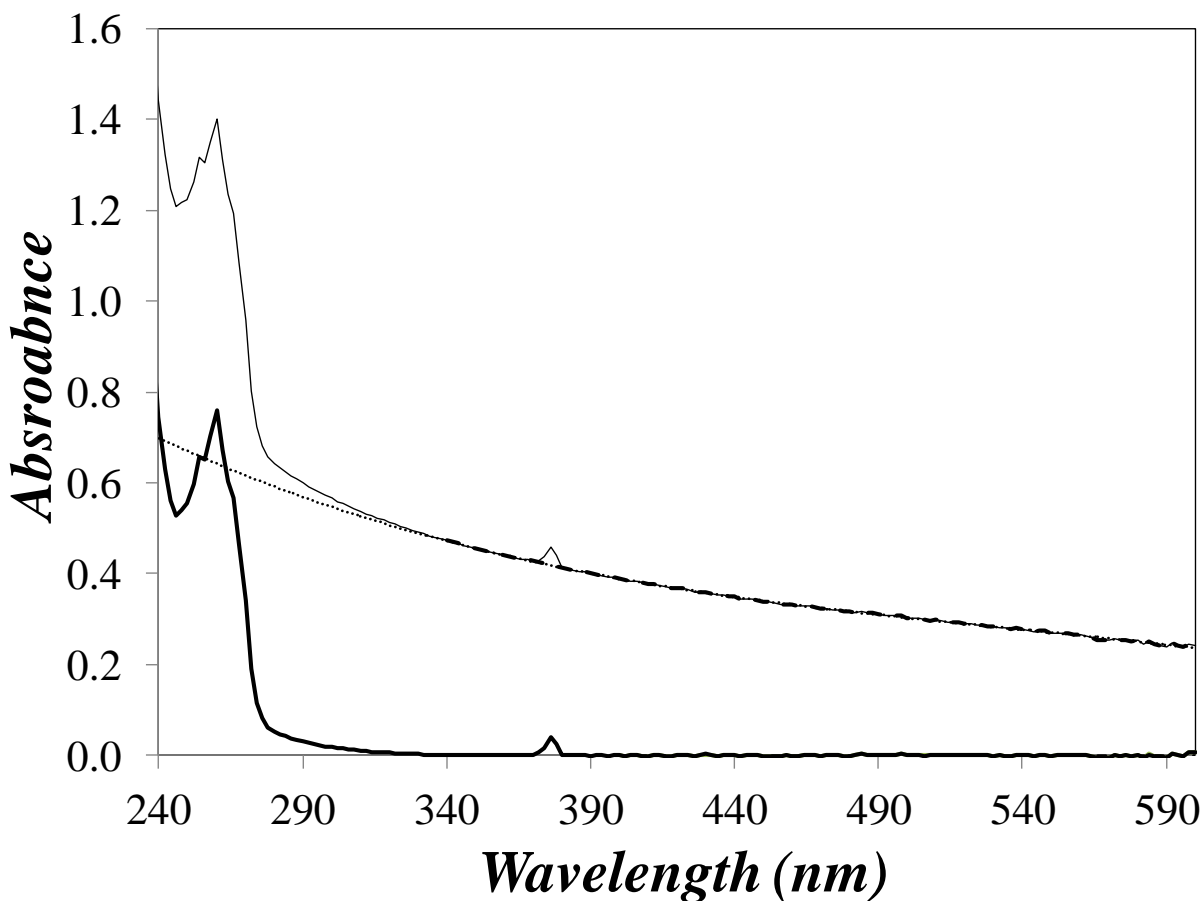
Figure SI2.1. Absorption spectrum of 0.82 g/L $(Asp_1Phe_3)_n$ in 0.01 M NaCl aqueous solution at

pH 9. Uncorrected absorption spectrum (———), polynomial obtained by fitting the part of the

spectrum without absorbance (– – –), extrapolated polynomial (··············), corrected

absorption spectrum (———).
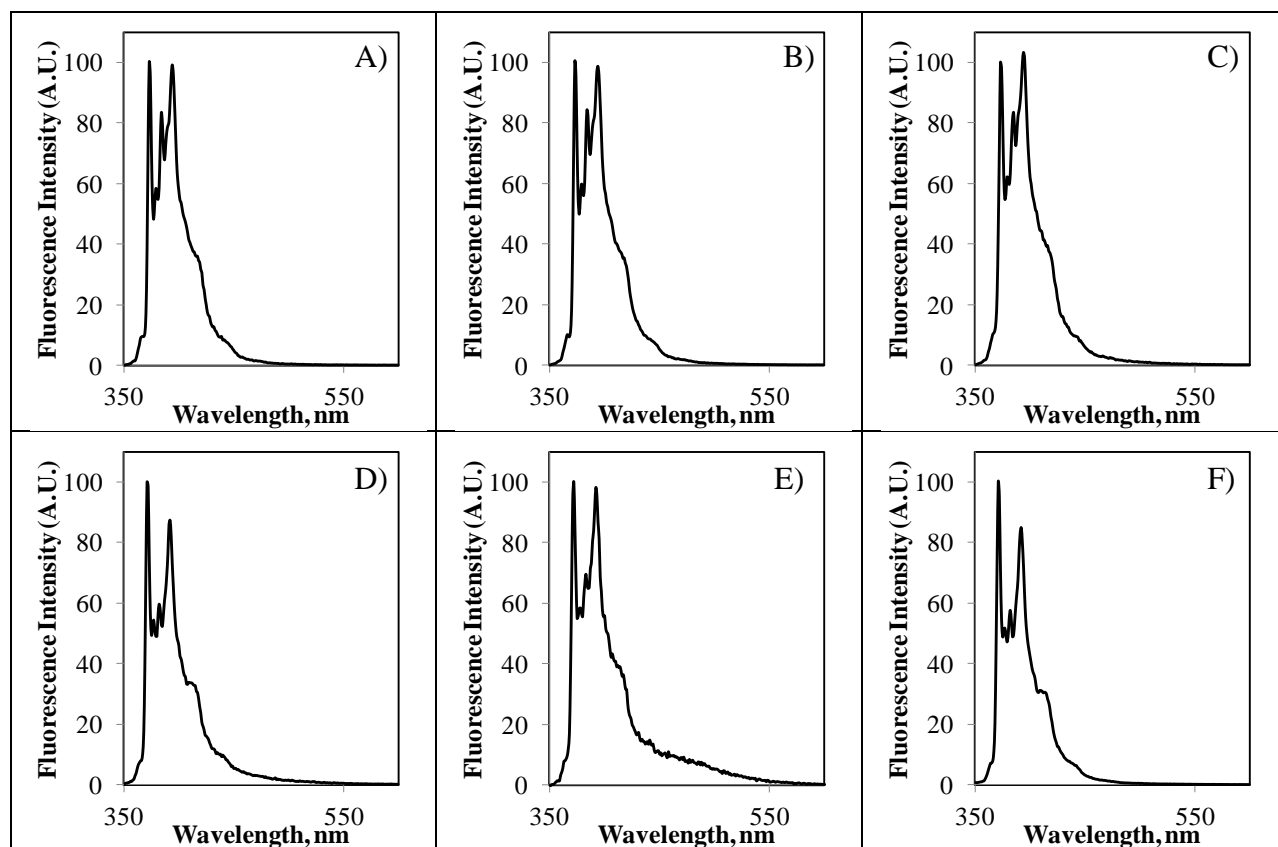
Figure SI2.2. Fluorescence spectra of pyrene in polypeptide solutions for α = 0.5. A) (Asp1Phe3)n with [Py] = 2.7×10−6 M; B) (Asp1Phe2)n with [Py] = 2.5×10−6 M; C) (Asp1Phe1)n with [Py] = 0.7×10−6 M; D) (Asp2Phe1)n with [Py] = 1.3×10−6 M; E) (Asp3Phe1)n with [Py] = 2.0×10−6 M; F) 0.01 M NaCl aqueous solution with [Py] = 0.7×10−6 M.
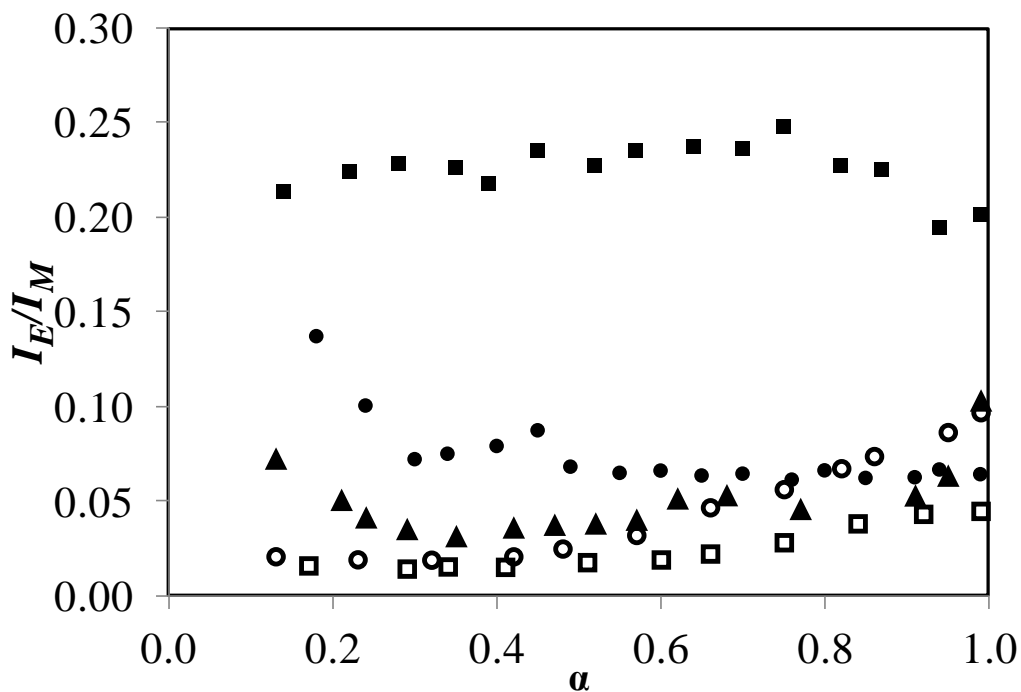
Figure SI2.3. I_E/I_M ratio of pyrene for the $(Asp_xPhe_y)_n$ aqueous solutions. Asp_1Phe_3 (□), Asp_1Phe_2 (○), Asp_1Phe_1 (▲), Asp_2Phe_1 (●), Asp_3Phe_1 (■).

Titrations of each polypeptide sample were performed in triplicate, the resulting pH and titrant volume data was used to calculate the degree of ionization α as well as the apparent pK_a of the polymer using equations 2-4.

Table SI2.1: Raw Titration Data for Asp_3Phe_1.

µL HCl	[HCl] = 0.071 M [Asp₃Phe₁] = 1.00 g/L V solution = 11.6 mL			[HCl] = 0.133 M [Asp₃Phe₁] = 1.06 g/L V solution = 11.2 mL			[HCl] = 0.117 M [Asp₃Phe₁] = 0.550 g/L V solution = 9.24 mL		
	pH	α	pK_a	pH	α	pK_a	pH	α	pK_a
0	9.34	1.000		9.51	1.000		9.27	1.000	
10	8.96	0.991	6.91	8.59	0.985	6.78	8.42	0.964	7.00
20	8.33	0.981	6.61	7.32	0.965	5.88	7.05	0.923	5.97
30	7.60	0.970	6.09	6.85	0.944	5.62	6.56	0.881	5.69
40	7.20	0.959	5.83	6.59	0.924	5.50	6.24	0.839	5.52
50	6.96	0.948	5.70	6.38	0.904	5.41	5.98	0.798	5.38
60	6.78	0.937	5.61	6.22	0.883	5.34	5.76	0.756	5.27

70	6.65	0.925	5.56	6.08	0.863	5.28	5.55	0.715	5.15
80	6.53	0.914	5.50	5.96	0.843	5.23	5.35	0.673	5.04
90	6.43	0.903	5.46	5.85	0.822	5.18	5.16	0.632	4.92
100	6.34	0.892	5.42	5.74	0.802	5.13	4.97	0.592	4.81
110	6.26	0.880	5.39	5.63	0.782	5.08	4.79	0.552	4.70
120	6.18	0.869	5.36	5.53	0.761	5.03	4.62	0.513	4.60
130	6.10	0.858	5.32	5.40	0.741	4.94	4.44	0.475	4.48
140	6.04	0.847	5.30	5.34	0.721	4.93	4.28	0.439	4.39
150	5.97	0.835	5.26	5.26	0.701	4.89	4.11	0.406	4.28
160	5.91	0.824	5.24	5.17	0.680	4.84	3.96	0.375	4.18
170	5.85	0.813	5.21	5.09	0.660	4.80	3.82	0.347	4.09
180	5.79	0.802	5.18	5.00	0.640	4.75	3.70	0.322	4.02
190	5.74	0.791	5.16	4.92	0.620	4.71	3.59	0.300	3.96
200	5.68	0.779	5.13	4.84	0.600	4.66	3.51	0.277	3.93
210	5.63	0.768	5.11	4.77	0.580	4.63	3.42	0.260	3.88
220	5.57	0.757	5.08	4.69	0.561	4.58	3.34	0.244	3.83
230	5.53	0.746	5.06	4.62	0.541	4.55	3.28	0.226	3.81
240	5.47	0.735	5.03	4.54	0.521	4.50	3.22	0.212	3.79
250	5.43	0.723	5.01	4.47	0.502	4.47	3.16	0.201	3.76
260	5.38	0.712	4.99	4.40	0.482	4.43	3.12	0.183	3.77
270	5.33	0.701	4.96	4.33	0.463	4.39	3.07	0.173	3.75
280	5.28	0.690	4.93	4.26	0.444	4.36	3.03	0.160	3.75
290	5.24	0.679	4.92	4.19	0.426	4.32	2.99	0.150	3.74
300	5.19	0.668	4.89	4.12	0.407	4.28	2.95	0.143	3.73
310	5.15	0.657	4.87	4.05	0.389	4.25	2.92	0.130	3.75
320	5.10	0.645	4.84	3.98	0.372	4.21	2.89	0.119	3.76
330	5.05	0.634	4.81	3.91	0.355	4.17			
340	5.02	0.623	4.80	3.84	0.338	4.13			
350	4.99	0.612	4.79	3.78	0.322	4.10			
360	4.94	0.601	4.76	3.71	0.307	4.06			
370	4.89	0.590	4.73	3.64	0.292	4.02			
380	4.85	0.579	4.71	3.58	0.278	3.99			
390	4.81	0.568	4.69	3.52	0.265	3.96			
400	4.77	0.557	4.67	3.46	0.253	3.93			
410	4.72	0.546	4.64	3.41	0.240	3.91			
420	4.69	0.535	4.63	3.35	0.230	3.87			
430	4.65	0.524	4.61	3.30	0.220	3.85			
440	4.61	0.514	4.59	3.26	0.208	3.84			
450	4.57	0.503	4.57	3.21	0.200	3.81			
460	4.53	0.492	4.54	3.17	0.191	3.80			
470	4.49	0.481	4.52	3.13	0.182	3.78			
480	4.45	0.471	4.50	3.09	0.175	3.76			
490	4.42	0.460	4.49	3.06	0.165	3.76			
500	4.38	0.449	4.47	3.02	0.160	3.74			
510	4.34	0.439	4.45	2.99	0.153	3.73			

520	4.30	0.429	4.42	2.96	0.146	3.73		
530	4.26	0.418	4.40	2.93	0.140	3.72		
540	4.23	0.408	4.39	2.91	0.130	3.74		
550	4.19	0.398	4.37	2.88	0.126	3.72		
560	4.15	0.388	4.35	2.86	0.117	3.74		
570	4.11	0.378	4.33	2.83	0.115	3.72		
580	4.08	0.368	4.32	2.80	0.114	3.69		
590	4.04	0.358	4.29					
600	4.00	0.348	4.27					
610	3.96	0.339	4.25					
620	3.93	0.329	4.24					
630	3.89	0.320	4.22					
640	3.86	0.311	4.21					
650	3.82	0.302	4.18					
660	3.79	0.293	4.17					
670	3.75	0.285	4.15					
680	3.72	0.276	4.14					
690	3.68	0.269	4.11					
700	3.65	0.261	4.10					
710	3.62	0.252	4.09					
720	3.58	0.246	4.07					
730	3.55	0.238	4.05					
740	3.52	0.231	4.04					
750	3.49	0.224	4.03					
760	3.46	0.218	4.02					
770	3.44	0.210	4.02					
780	3.40	0.205	3.99					
790	3.38	0.198	3.99					
800	3.35	0.193	3.97					
810	3.32	0.188	3.96					
820	3.30	0.181	3.95					
830	3.28	0.175	3.95					
840	3.25	0.171	3.93					
850	3.23	0.165	3.93					
860	3.21	0.160	3.93					
870	3.19	0.154	3.93					
880	3.16	0.153	3.90					
890	3.14	0.148	3.90					
900	3.12	0.144	3.90					
910	3.10	0.140	3.89					
920	3.09	0.132	3.91					
930	3.07	0.129	3.90					
940	3.05	0.126	3.89					
950	3.04	0.119	3.91					
960	3.01	0.121	3.87					

970	2.99	0.119	3.86						
980	2.97	0.118	3.84						
990	2.96	0.112	3.86						
1000	2.95	0.106	3.88						
1010	2.93	0.106	3.86						

Table SI2.2: Raw Titration Data for Asp_2Phe_1.

	[HCl] = 0.083 M $[Asp_2Phe_1]$ = 0.723 g/L V solution = 10.2 mL			[HCl] = 0.133 M $[Asp_2Phe_1]$ = 0.800 g/L V solution = 11.7 mL			[HCl] = 0.135 M $[Asp_2Phe_1]$ = 1.08 g/L V solution = 8.38 mL		
µL HCl	pH	α	pK_a	pH	α	pK_a	pH	α	pK_a
0	9.24	1.000		9.06	1.000		9.16	1.000	
10	7.86	0.982	6.13	7.76	0.973	6.20	7.90	0.972	6.36
20	7.06	0.959	5.69	6.99	0.944	5.77	6.94	0.941	5.74
30	6.69	0.936	5.52	6.50	0.914	5.47	6.53	0.910	5.53
40	6.45	0.913	5.43	6.24	0.885	5.36	6.25	0.879	5.39
50	6.26	0.890	5.35	6.07	0.855	5.30	6.03	0.848	5.28
60	6.11	0.868	5.29	5.86	0.826	5.18	5.84	0.817	5.19
70	5.97	0.845	5.23	5.70	0.796	5.11	5.66	0.786	5.09
80	5.85	0.822	5.19	5.54	0.767	5.02	5.50	0.756	5.01
90	5.72	0.799	5.12	5.40	0.737	4.95	5.36	0.725	4.94
100	5.62	0.776	5.08	5.28	0.708	4.90	5.21	0.694	4.85
110	5.51	0.754	5.02	5.15	0.679	4.82	5.08	0.664	4.79
120	5.40	0.731	4.97	5.03	0.650	4.76	4.94	0.633	4.70
130	5.31	0.708	4.93	4.91	0.621	4.70	4.81	0.603	4.63
140	5.22	0.686	4.88	4.79	0.592	4.63	4.69	0.573	4.56
150	5.12	0.663	4.83	4.68	0.564	4.57	4.57	0.543	4.49
160	5.03	0.641	4.78	4.57	0.536	4.51	4.44	0.514	4.42
170	4.93	0.618	4.72	4.46	0.509	4.45	4.33	0.485	4.36
180	4.84	0.596	4.67	4.35	0.482	4.38	4.21	0.457	4.28
190	4.75	0.574	4.62	4.25	0.455	4.33	4.09	0.430	4.21
200	4.67	0.552	4.58	4.14	0.430	4.26	3.97	0.404	4.14
210	4.58	0.531	4.53	4.04	0.405	4.21	3.86	0.380	4.07
220	4.49	0.510	4.47	3.94	0.382	4.15	3.75	0.357	4.01
230	4.40	0.489	4.42	3.85	0.359	4.10	3.64	0.336	3.94
240	4.31	0.469	4.36	3.75	0.340	4.04	3.55	0.316	3.89
250	4.23	0.449	4.32	3.67	0.320	4.00	3.46	0.298	3.83
260	4.15	0.430	4.27	3.59	0.302	3.95	3.38	0.281	3.79
270	4.06	0.411	4.22	3.52	0.284	3.92	3.30	0.267	3.74
280	3.98	0.394	4.17	3.44	0.271	3.87	3.24	0.251	3.71
290	3.90	0.377	4.12	3.38	0.256	3.84	3.18	0.238	3.69
300	3.82	0.362	4.07	3.33	0.240	3.83	3.13	0.223	3.67
310	3.74	0.348	4.01	3.27	0.230	3.80	3.08	0.211	3.65

	pH	α	pKa	pH	α	pKa	pH	α	pKa
320	3.67	0.335	3.97	3.23	0.214	3.79	3.04	0.196	3.65
330	3.60	0.323	3.92	3.18	0.204	3.77	3.00	0.183	3.65
340	3.54	0.312	3.88	3.14	0.192	3.76	2.99	0.157	3.72
350	3.48	0.302	3.84	3.11	0.176	3.78	2.95	0.146	3.72
360	3.42	0.293	3.80	3.07	0.167	3.77	2.92	0.132	3.74
370	3.37	0.285	3.77	3.03	0.160	3.75	2.88	0.125	3.73
380	3.32	0.277	3.74	3.00	0.149	3.76	2.85	0.113	3.74
390	3.27	0.272	3.70	2.97	0.139	3.76	2.82	0.103	3.76
400	3.23	0.265	3.67	2.94	0.130	3.76			
410	3.20	0.255	3.67	2.92	0.116	3.80			
420	3.16	0.251	3.64	2.89	0.110	3.80			
430	3.13	0.243	3.62						
440	3.09	0.242	3.59						
450	3.06	0.237	3.57						
460	3.03	0.233	3.55						
470	3.01	0.224	3.55						
480	2.98	0.223	3.52						
490	2.96	0.215	3.52						
500	2.93	0.216	3.49						
510	2.91	0.211	3.48						
520	2.89	0.206	3.48						
530	2.87	0.202	3.47						
540	2.85	0.199	3.46						
550	2.84	0.186	3.48						
560	2.82	0.184	3.47						
570	2.80	0.184	3.45						
580	2.78	0.184	3.43						
590	2.77	0.174	3.45						
600	2.75	0.176	3.42						

Table SI2.3: Raw Titration Data for Asp_1Phe_1.

	[HCl] = 0.071 M [Asp_1Phe_1] = 1.15 g/L V solution = 10.0 mL			[HCl] = 0.071 M [Asp_1Phe_1] = 0.584 g/L V solution = 9.65 mL			[HCl] = 0.127 M [Asp_1Phe_1] = 0.667 g/L V solution = 7.59 mL		
μL HCl	pH	α	pK_a	pH	α	pK_a	pH	α	pK_a
0	9.51	1.000		9.21	1.000		8.33	1.000	
10	9.25	0.986	7.39	8.83	0.969	7.33	7.17	0.952	5.87
20	8.92	0.972	7.39	8.10	0.937	6.93	6.66	0.903	5.69
30	8.37	0.956	7.04	7.14	0.902	6.18	6.34	0.854	5.57
40	7.56	0.939	6.37	6.71	0.867	5.90	6.12	0.805	5.50
50	7.10	0.922	6.03	6.39	0.832	5.70	5.90	0.756	5.41
60	6.82	0.905	5.84	6.18	0.797	5.59	5.71	0.707	5.33

70	6.62	0.888	5.72	5.99	0.762	5.49	5.54	0.659	5.25
80	6.47	0.870	5.64	5.84	0.727	5.42	5.38	0.610	5.19
90	6.34	0.853	5.58	5.70	0.692	5.35	5.24	0.562	5.13
100	6.23	0.836	5.52	5.57	0.657	5.29	5.09	0.514	5.07
110	6.14	0.819	5.48	5.45	0.622	5.23	4.94	0.466	5.00
120	6.05	0.802	5.44	5.33	0.587	5.18	4.76	0.419	4.90
130	5.95	0.784	5.39	5.23	0.553	5.14	4.61	0.373	4.84
140	5.87	0.767	5.35	5.13	0.518	5.10	4.48	0.328	4.79
150	5.80	0.750	5.32	5.02	0.484	5.05	4.35	0.283	4.75
160	5.73	0.733	5.29	4.93	0.450	5.02	4.24	0.239	4.74
170	5.66	0.716	5.26	4.82	0.416	4.97	4.12	0.198	4.73
180	5.60	0.699	5.23	4.71	0.383	4.92	3.96	0.162	4.67
190	5.54	0.682	5.21	4.61	0.351	4.88	3.80	0.133	4.61
200	5.47	0.665	5.17	4.52	0.318	4.85	3.64	0.113	4.54
210	5.41	0.647	5.15	4.44	0.286	4.84			
220	5.35	0.630	5.12	4.38	0.254	4.85			
230	5.30	0.613	5.10	4.32	0.221	4.87			
240	5.24	0.596	5.07	4.25	0.190	4.88			
250	5.19	0.579	5.05	4.14	0.163	4.85			
260	5.14	0.562	5.03	4.04	0.138	4.84			
270	5.09	0.545	5.01	3.93	0.115	4.81			
280	5.04	0.528	4.99						
290	4.99	0.511	4.97						
300	4.95	0.494	4.96						
310	4.90	0.478	4.94						
320	4.84	0.461	4.91						
330	4.79	0.444	4.89						
340	4.74	0.427	4.87						
350	4.69	0.411	4.85						
360	4.64	0.394	4.83						
370	4.60	0.377	4.82						
380	4.56	0.361	4.81						
390	4.52	0.344	4.80						
400	4.49	0.328	4.80						
410	4.46	0.311	4.81						
420	4.43	0.295	4.81						
430	4.40	0.278	4.81						
440	4.37	0.262	4.82						
450	4.34	0.245	4.83						
460	4.30	0.229	4.83						
470	4.25	0.213	4.82						
480	4.19	0.198	4.80						
490	4.13	0.184	4.78						
500	4.07	0.169	4.76						
510	3.99	0.157	4.72						

520	3.93	0.143	4.71					
530	3.85	0.132	4.67					
540	3.77	0.123	4.62					
550	3.69	0.114	4.58					
560	3.62	0.107	4.54					
570	3.55	0.100	4.50					

Table SI2.4: Raw Titration Data for Asp_1Phe_2.

	[HCl] = 0.096 M $[Asp_1Phe_2]$ = 0.937 g/L V solution = 10.4 mL			[HCl] = 0.085 M $[Asp_1Phe_2]$ = 0.742 g/L V solution = 10.2 mL			[HCl] = 0.096 M $[Asp_1Phe_2]$ = 0.937 g/L V solution = 8.92 mL		
µL HCl	pH	α	pK_a	pH	α	pK_a	pH	α	pK_a
0	8.76	1.000		8.84	1.000		8.58	1.000	
10	8.15	0.960	6.77	8.24	0.956	6.90	7.83	0.952	6.53
20	7.36	0.918	6.31	7.46	0.910	6.46	6.91	0.904	5.94
30	6.70	0.876	5.85	6.69	0.863	5.89	6.43	0.855	5.66
40	6.35	0.834	5.65	6.29	0.816	5.64	6.15	0.806	5.53
50	6.12	0.792	5.54	6.03	0.769	5.51	5.95	0.757	5.46
60	5.95	0.750	5.47	5.84	0.723	5.42	5.79	0.708	5.40
70	5.83	0.708	5.45	5.69	0.676	5.37	5.68	0.660	5.39
80	5.73	0.666	5.43	5.58	0.629	5.35	5.57	0.611	5.37
90	5.63	0.624	5.41	5.50	0.582	5.36	5.47	0.562	5.36
100	5.54	0.582	5.40	5.43	0.536	5.37	5.38	0.513	5.36
110	5.46	0.540	5.39	5.37	0.489	5.39	5.28	0.465	5.34
120	5.37	0.499	5.37	5.30	0.442	5.40	5.18	0.416	5.33
130	5.29	0.457	5.37	5.23	0.396	5.41	5.07	0.368	5.30
140	5.20	0.415	5.35	5.15	0.349	5.42	4.95	0.321	5.28
150	5.10	0.374	5.32	5.07	0.303	5.43	4.82	0.273	5.24
160	5.01	0.332	5.31	4.98	0.257	5.44	4.68	0.227	5.21
170	4.90	0.292	5.29	4.87	0.212	5.44	4.53	0.182	5.18
180	4.78	0.251	5.25	4.73	0.168	5.42	4.36	0.140	5.15
190	4.64	0.212	5.21	4.56	0.126	5.40	4.19	0.101	5.14
200	4.52	0.173	5.20						
210	4.36	0.138	5.16						
220	4.22	0.103	5.16						

Table SI2.5: Raw Titration Data for Asp_1Phe_3.

	[HCl] = 0.083 M $[Asp_1Phe_3]$ = 0.822 g/L V solution = 10.3 mL	[HCl] = 0.071 M $[Asp_1Phe_3]$ = 0.638 g/L V solution = 10.0 mL	[HCl] = 0.083 M $[Asp_1Phe_3]$ = 0.671 g/L V solution = 10.1 mL

μL HCl	pH	α	pK$_a$	pH	α	pK$_a$	pH	α	pK$_a$
0	9.06	1.000		8.94	1.000		8.95	1.000	
10	8.60	0.950	7.32	8.44	0.942	7.23	8.03	0.938	6.85
20	7.97	0.897	7.03	7.74	0.881	6.87	7.45	0.869	6.63
30	7.46	0.842	6.73	7.25	0.818	6.60	7.09	0.800	6.49
40	7.15	0.787	6.58	6.98	0.755	6.49	6.85	0.731	6.42
50	6.93	0.732	6.49	6.80	0.692	6.45	6.67	0.662	6.38
60	6.77	0.677	6.45	6.68	0.629	6.45	6.51	0.593	6.35
70	6.62	0.622	6.40	6.51	0.566	6.39	6.37	0.524	6.33
80	6.49	0.567	6.37	6.40	0.503	6.39	6.23	0.455	6.31
90	6.39	0.512	6.37	6.26	0.440	6.36	6.06	0.386	6.26
100	6.28	0.457	6.36	6.12	0.377	6.34	5.84	0.317	6.17
110	6.15	0.402	6.32	5.96	0.314	6.30	5.57	0.249	6.05
120	6.01	0.347	6.28	5.78	0.251	6.25	5.22	0.183	5.87
130	5.86	0.292	6.24	5.56	0.189	6.19	4.78	0.123	5.63
140	5.65	0.237	6.16	5.38	0.127	6.22			
150	5.40	0.184	6.05						
160	5.08	0.132	5.90						

The pH values were plotted as a function of α, and a polynomial fit of each data set was obtained (the polynomial has no physical meaning). These fits were used to interpolate the pH from 0.1 < α < 0.9 for each titration; the values for each α were then averaged and the standard deviation calculated.

The pKa values were plotted, fitted, interpolated and averaged using the same methodology, however a linear fit was sufficient for Asp$_2$Phe$_1$and Asp$_3$Phe$_1$.

Table SI2.6: pH data for the fitted titration curves.

	Asp$_3$Phe$_1$		Asp$_2$Phe$_1$		Asp$_1$Phe$_1$		Asp$_1$Phe$_2$		Asp$_1$Phe$_3$	
α	pH	St. Dev.	pH	St. Dev.	pH	St. Dev.	pH	St. Dev.	pH	St. Dev.
0.20	2.84	0.07	3.20	0.43	4.18	0.08	4.76	0.13	5.48	0.14
0.21	2.88	0.08	3.12	0.39	4.21	0.08	4.79	0.13	5.52	0.13
0.22	2.92	0.08	3.06	0.35	4.25	0.07	4.82	0.12	5.57	0.12
0.23	2.96	0.09	3.01	0.32	4.28	0.07	4.85	0.12	5.61	0.11
0.24	3.00	0.09	2.98	0.29	4.31	0.07	4.87	0.11	5.65	0.10
0.25	3.04	0.10	2.96	0.26	4.34	0.07	4.90	0.11	5.68	0.09
0.26	3.08	0.10	2.96	0.24	4.36	0.06	4.93	0.10	5.72	0.09

0.27	3.12	0.10	2.97	0.22	4.39	0.06	4.95	0.10	5.76	0.08
0.28	3.17	0.11	2.98	0.20	4.42	0.06	4.97	0.09	5.79	0.07
0.29	3.21	0.11	3.00	0.18	4.44	0.05	4.99	0.09	5.82	0.07
0.30	3.26	0.11	3.03	0.16	4.46	0.05	5.02	0.08	5.86	0.07
0.31	3.30	0.12	3.07	0.15	4.49	0.04	5.04	0.08	5.89	0.06
0.32	3.35	0.12	3.11	0.14	4.51	0.04	5.06	0.07	5.92	0.06
0.33	3.39	0.12	3.15	0.12	4.53	0.04	5.08	0.07	5.95	0.06
0.34	3.43	0.12	3.20	0.11	4.56	0.03	5.10	0.06	5.97	0.05
0.35	3.48	0.12	3.24	0.10	4.58	0.03	5.12	0.06	6.00	0.05
0.36	3.52	0.12	3.29	0.09	4.60	0.03	5.14	0.05	6.03	0.05
0.37	3.57	0.12	3.34	0.09	4.63	0.03	5.15	0.05	6.06	0.05
0.38	3.61	0.12	3.40	0.08	4.65	0.04	5.17	0.05	6.08	0.05
0.39	3.66	0.11	3.45	0.07	4.68	0.04	5.19	0.04	6.11	0.05
0.40	3.70	0.11	3.50	0.07	4.70	0.04	5.21	0.04	6.13	0.05
0.41	3.74	0.11	3.55	0.06	4.73	0.05	5.23	0.03	6.16	0.05
0.42	3.78	0.10	3.60	0.06	4.76	0.05	5.24	0.03	6.18	0.05
0.43	3.83	0.10	3.66	0.05	4.78	0.05	5.26	0.03	6.20	0.05
0.44	3.87	0.10	3.71	0.05	4.81	0.05	5.28	0.02	6.23	0.05
0.45	3.91	0.09	3.76	0.05	4.84	0.06	5.30	0.02	6.25	0.05
0.46	3.95	0.09	3.81	0.04	4.87	0.06	5.31	0.02	6.27	0.05
0.47	4.00	0.08	3.85	0.04	4.90	0.06	5.33	0.01	6.29	0.04
0.48	4.04	0.08	3.90	0.04	4.93	0.06	5.35	0.01	6.32	0.04
0.49	4.08	0.07	3.95	0.04	4.97	0.06	5.36	0.01	6.34	0.04
0.50	4.12	0.07	3.99	0.04	5.00	0.06	5.38	0.01	6.36	0.04
0.51	4.16	0.06	4.04	0.04	5.03	0.06	5.40	0.01	6.38	0.04
0.52	4.20	0.06	4.08	0.04	5.07	0.06	5.41	0.01	6.40	0.04
0.53	4.24	0.05	4.12	0.04	5.10	0.06	5.43	0.01	6.42	0.04
0.54	4.29	0.05	4.17	0.03	5.14	0.06	5.45	0.02	6.44	0.04
0.55	4.33	0.05	4.21	0.03	5.17	0.06	5.46	0.02	6.46	0.04
0.56	4.37	0.05	4.25	0.03	5.21	0.06	5.48	0.02	6.48	0.04
0.57	4.41	0.05	4.29	0.03	5.24	0.06	5.50	0.03	6.50	0.04
0.58	4.45	0.05	4.33	0.03	5.28	0.05	5.51	0.03	6.52	0.04
0.59	4.49	0.05	4.37	0.03	5.31	0.05	5.53	0.03	6.54	0.04
0.60	4.53	0.06	4.41	0.03	5.35	0.05	5.55	0.03	6.56	0.04
0.61	4.57	0.06	4.45	0.03	5.38	0.05	5.57	0.04	6.58	0.04
0.62	4.61	0.06	4.49	0.03	5.42	0.04	5.59	0.04	6.61	0.04
0.63	4.65	0.06	4.53	0.03	5.45	0.04	5.61	0.04	6.63	0.04
0.64	4.69	0.07	4.57	0.03	5.49	0.04	5.63	0.04	6.65	0.04
0.65	4.74	0.07	4.61	0.03	5.52	0.04	5.65	0.04	6.67	0.04
0.66	4.78	0.07	4.65	0.03	5.56	0.04	5.67	0.04	6.69	0.04
0.67	4.82	0.08	4.70	0.03	5.59	0.04	5.69	0.04	6.72	0.04
0.68	4.86	0.08	4.74	0.03	5.62	0.03	5.72	0.04	6.74	0.04
0.69	4.90	0.08	4.78	0.03	5.66	0.03	5.74	0.03	6.77	0.04
0.70	4.94	0.09	4.82	0.03	5.69	0.03	5.77	0.03	6.79	0.04
0.71	4.98	0.09	4.86	0.03	5.72	0.03	5.80	0.03	6.82	0.05

0.72	5.02	0.09	4.90	0.03	5.75	0.03	5.83	0.02	6.85	0.05
0.73	5.06	0.09	4.95	0.03	5.79	0.03	5.87	0.02	6.88	0.05
0.74	5.11	0.09	4.99	0.03	5.82	0.03	5.90	0.01	6.91	0.05
0.75	5.15	0.10	5.03	0.03	5.86	0.04	5.94	0.00	6.94	0.06
0.76	5.19	0.10	5.07	0.03	5.89	0.04	5.99	0.01	6.98	0.06
0.77	5.23	0.10	5.12	0.02	5.93	0.04	6.04	0.02	7.02	0.07
0.78	5.27	0.10	5.16	0.02	5.97	0.04	6.09	0.02	7.06	0.07
0.79	5.32	0.10	5.20	0.02	6.01	0.05	6.14	0.04	7.10	0.08
0.80	5.36	0.11	5.25	0.02	6.06	0.05	6.20	0.05	7.15	0.08
0.81	5.40	0.11	5.29	0.02	6.11	0.06	6.27	0.06	7.20	0.09
0.82	5.45	0.11	5.34	0.02	6.16	0.07	6.34	0.07	7.25	0.10
0.83	5.49	0.11	5.38	0.02	6.22	0.07	6.42	0.08	7.31	0.10
0.84	5.54	0.11	5.43	0.03	6.29	0.09	6.51	0.10	7.37	0.11
0.85	5.59	0.12	5.47	0.03	6.36	0.10	6.60	0.11	7.44	0.12
0.86	5.63	0.12	5.52	0.03	6.45	0.12	6.71	0.12	7.51	0.13
0.87	5.68	0.12	5.57	0.03	6.54	0.14	6.82	0.14	7.58	0.14
0.88	5.73	0.13	5.61	0.03	6.64	0.18	6.94	0.15	7.67	0.16
0.89	5.79	0.13	5.66	0.03	6.76	0.22	7.07	0.16	7.75	0.17
0.90	5.84	0.14	5.71	0.04	6.89	0.26	7.22	0.18	7.85	0.18

Table SI2.7: pK_a data for the fitted titration curves.

	Asp_3Phe_1		Asp_2Phe_1		Asp_1Phe_1		Asp_1Phe_2		Asp_1Phe_3	
α	pK_a	St. Dev.	pK_a	St. Dev.	pK_a	St. Dev.	pK_a	St. Dev.	pK_a	St. Dev.
0.20	3.73	0.15	3.63	0.08	4.79	0.07	5.28	0.12	6.07	0.14
0.21	3.75	0.14	3.66	0.08	4.78	0.07	5.29	0.12	6.09	0.13
0.22	3.78	0.14	3.68	0.07	4.78	0.06	5.30	0.12	6.10	0.12
0.23	3.80	0.14	3.71	0.07	4.78	0.05	5.30	0.12	6.12	0.11
0.24	3.82	0.13	3.73	0.07	4.78	0.05	5.31	0.12	6.14	0.10
0.25	3.84	0.13	3.76	0.07	4.78	0.04	5.31	0.12	6.15	0.09
0.26	3.87	0.12	3.79	0.07	4.79	0.04	5.32	0.11	6.17	0.09
0.27	3.89	0.12	3.81	0.07	4.79	0.04	5.32	0.11	6.18	0.08
0.28	3.91	0.12	3.84	0.06	4.80	0.04	5.32	0.11	6.20	0.07
0.29	3.94	0.11	3.86	0.06	4.80	0.04	5.33	0.10	6.21	0.07
0.30	3.96	0.11	3.89	0.06	4.81	0.04	5.33	0.10	6.22	0.07
0.31	3.98	0.11	3.91	0.06	4.81	0.04	5.33	0.09	6.23	0.06
0.32	4.01	0.10	3.94	0.06	4.82	0.04	5.33	0.09	6.25	0.06
0.33	4.03	0.10	3.96	0.06	4.83	0.04	5.33	0.08	6.26	0.06
0.34	4.05	0.09	3.99	0.05	4.84	0.04	5.34	0.08	6.27	0.05
0.35	4.08	0.09	4.01	0.05	4.85	0.04	5.34	0.07	6.28	0.05
0.36	4.10	0.09	4.04	0.05	4.86	0.04	5.34	0.07	6.29	0.05
0.37	4.12	0.08	4.06	0.05	4.87	0.04	5.34	0.06	6.30	0.05
0.38	4.14	0.08	4.09	0.05	4.88	0.04	5.34	0.06	6.30	0.05
0.39	4.17	0.08	4.11	0.05	4.89	0.05	5.34	0.05	6.31	0.04

0.40	4.19	0.07	4.14	0.04	4.90	0.05	5.35	0.05	6.32	0.04
0.41	4.21	0.07	4.16	0.04	4.91	0.05	5.35	0.04	6.33	0.04
0.42	4.24	0.07	4.19	0.04	4.92	0.05	5.35	0.04	6.33	0.04
0.43	4.26	0.07	4.21	0.04	4.93	0.05	5.35	0.03	6.34	0.04
0.44	4.28	0.06	4.24	0.04	4.94	0.05	5.36	0.03	6.34	0.04
0.45	4.31	0.06	4.27	0.04	4.96	0.06	5.36	0.02	6.35	0.04
0.46	4.33	0.06	4.29	0.03	4.97	0.06	5.36	0.02	6.35	0.04
0.47	4.35	0.06	4.32	0.03	4.98	0.06	5.36	0.02	6.36	0.04
0.48	4.38	0.06	4.34	0.03	4.99	0.06	5.37	0.02	6.36	0.04
0.49	4.40	0.05	4.37	0.03	5.00	0.06	5.37	0.02	6.36	0.04
0.50	4.42	0.05	4.39	0.03	5.02	0.06	5.37	0.02	6.36	0.04
0.51	4.44	0.05	4.42	0.03	5.03	0.06	5.37	0.02	6.37	0.04
0.52	4.47	0.05	4.44	0.02	5.04	0.06	5.37	0.02	6.37	0.04
0.53	4.49	0.05	4.47	0.02	5.06	0.06	5.38	0.02	6.37	0.04
0.54	4.51	0.05	4.49	0.02	5.07	0.06	5.38	0.02	6.37	0.04
0.55	4.54	0.05	4.52	0.02	5.08	0.06	5.38	0.02	6.37	0.03
0.56	4.56	0.06	4.54	0.02	5.09	0.06	5.38	0.03	6.38	0.03
0.57	4.58	0.06	4.57	0.02	5.11	0.06	5.38	0.03	6.38	0.03
0.58	4.61	0.06	4.59	0.01	5.12	0.06	5.38	0.03	6.38	0.03
0.59	4.63	0.06	4.62	0.01	5.13	0.06	5.38	0.03	6.38	0.03
0.60	4.65	0.06	4.64	0.01	5.15	0.06	5.39	0.03	6.38	0.03
0.61	4.68	0.06	4.67	0.01	5.16	0.06	5.39	0.03	6.39	0.03
0.62	4.70	0.07	4.70	0.01	5.18	0.06	5.39	0.04	6.39	0.03
0.63	4.72	0.07	4.72	0.01	5.19	0.06	5.39	0.04	6.39	0.03
0.64	4.74	0.07	4.75	0.01	5.20	0.07	5.39	0.04	6.39	0.03
0.65	4.77	0.08	4.77	0.01	5.22	0.07	5.39	0.04	6.40	0.03
0.66	4.79	0.08	4.80	0.01	5.23	0.07	5.39	0.04	6.40	0.03
0.67	4.81	0.08	4.82	0.01	5.25	0.07	5.39	0.04	6.41	0.03
0.68	4.84	0.09	4.85	0.01	5.27	0.07	5.40	0.04	6.41	0.03
0.69	4.86	0.09	4.87	0.01	5.28	0.07	5.40	0.04	6.42	0.03
0.70	4.88	0.09	4.90	0.01	5.30	0.07	5.40	0.04	6.43	0.03
0.71	4.91	0.10	4.92	0.01	5.32	0.07	5.41	0.03	6.44	0.03
0.72	4.93	0.10	4.95	0.01	5.34	0.07	5.42	0.03	6.44	0.03
0.73	4.95	0.10	4.97	0.01	5.35	0.07	5.42	0.03	6.45	0.03
0.74	4.98	0.11	5.00	0.02	5.37	0.07	5.43	0.03	6.47	0.04
0.75	5.00	0.11	5.02	0.02	5.39	0.07	5.44	0.03	6.48	0.04
0.76	5.02	0.11	5.05	0.02	5.42	0.07	5.46	0.03	6.49	0.04
0.77	5.04	0.12	5.07	0.02	5.44	0.07	5.47	0.02	6.51	0.05
0.78	5.07	0.12	5.10	0.02	5.46	0.07	5.49	0.02	6.53	0.05
0.79	5.09	0.13	5.13	0.02	5.49	0.08	5.52	0.03	6.54	0.06
0.80	5.11	0.13	5.15	0.03	5.51	0.09	5.54	0.03	6.57	0.06
0.81	5.14	0.13	5.18	0.03	5.54	0.09	5.57	0.04	6.59	0.07
0.82	5.16	0.14	5.20	0.03	5.57	0.10	5.61	0.04	6.61	0.08
0.83	5.18	0.14	5.23	0.03	5.59	0.11	5.65	0.05	6.64	0.09
0.84	5.21	0.15	5.25	0.03	5.63	0.13	5.69	0.07	6.67	0.09

0.85	5.23	0.15	5.28	0.03	5.66	0.14	5.74	0.08	6.70	0.10
0.86	5.25	0.15	5.30	0.04	5.69	0.16	5.80	0.10	6.73	0.12
0.87	5.27	0.16	5.33	0.04	5.73	0.18	5.86	0.12	6.77	0.13
0.88	5.30	0.16	5.35	0.04	5.76	0.20	5.93	0.14	6.81	0.14
0.89	5.32	0.17	5.38	0.04	5.80	0.23	6.01	0.16	6.85	0.16
0.90	5.34	0.17	5.40	0.04	5.84	0.25	6.10	0.19	6.89	0.17

Table SI2.8. Pre-exponential factors and decay times obtained from the tri-exponential fit of the fluorescence decays acquired with the pyrene-loaded polypeptide solutions. The average lifetime $<\tau>$ was calculated from the weighted average of the two longest lifetimes.

Sample	pH	α	τ_1	a_1	τ_2	a_2	τ_3	a_3	$<\tau>$	χ^2
Asp$_3$Phe$_1$ [polymer] = 0.57 g/L	9.51	0.99	9.60	0.34	70.2	0.17	140	0.49	122	1.15
	6.94	0.94	9.96	0.34	64.4	0.14	137	0.52	122	1.10
	6.32	0.87	11.4	0.35	77.3	0.20	141	0.45	121	1.29
	5.96	0.82	8.60	0.34	47.2	0.15	134	0.51	114	1.05
	5.58	0.75	7.72	0.36	46.0	0.17	135	0.47	111	1.06
	5.36	0.7	8.38	0.38	46.5	0.14	133	0.49	114	0.96
	5.10	0.64	6.13	0.35	37.5	0.17	131	0.48	107	1.13
	4.80	0.57	8.14	0.39	51.4	0.17	136	0.44	113	1.14
	4.63	0.52	8.88	0.38	52.6	0.15	133	0.47	113	1.00
	4.32	0.45	6.52	0.42	36.5	0.19	133	0.39	102	1.19
	4.08	0.39	5.66	0.40	36.4	0.19	132	0.41	102	1.11
	3.91	0.35	7.67	0.46	45.0	0.16	134	0.38	107	7.67
	3.61	0.28	6.72	0.43	39.2	0.18	132	0.39	102	1.14
	3.36	0.22	7.27	0.43	42.0	0.20	135	0.36	102	1.05
	2.99	0.38	18.7	0.25	100	0.22	158	0.15	123	1.24
Asp$_2$Phe$_1$ [polymer] = 0.77 g/L	9.49	0.99	5.30	0.27	27.7	0.06	131	0.67	122	1.11
	6.90	0.94	5.85	0.27	46.8	0.06	129	0.68	123	0.98
	6.51	0.91	4.92	0.24	25.6	0.06	129	0.69	120	0.92
	6.00	0.85	6.23	0.25	51.4	0.04	129	0.71	124	1.02
	5.73	0.80	2.75	0.30	19.9	0.08	128	0.62	115	0.98
	5.53	0.76	5.34	0.24	28.1	0.05	129	0.70	122	0.98
	5.24	0.70	5.53	0.27	48.6	0.05	129	0.68	123	1.01
	5.02	0.65	5.70	0.24	22.8	0.06	128	0.70	120	1.19
	4.80	0.60	2.05	0.43	17.6	0.07	127	0.49	113	0.92
	4.60	0.55	3.98	0.34	22.8	0.08	129	0.58	116	0.98
	4.36	0.49	2.98	0.29	16.6	0.10	128	0.61	112	0.93
	4.20	0.45	3.60	0.31	21.1	0.09	129	0.60	115	1.05
	4.00	0.40	4.41	0.33	30.1	0.08	129	0.59	118	0.99
	3.73	0.34	4.18	0.37	34.3	0.07	131	0.55	119	1.01
	3.52	0.30	5.28	0.34	57.4	0.08	133	0.58	123	1.04

	3.20	0.24	3.89	0.44	34.0	0.10	135	0.46	117	1.13
	2.99	0.18	5.63	0.41	61.1	0.11	140	0.47	125	1.08
Asp$_1$Phe$_1$ [polymer] = 0.69 g/L	10.03	0.99	9.69	0.28	112	0.38	285	0.34	194	1.03
	9.09	0.95	8.31	0.37	112	0.42	281	0.31	184	1.00
	7.08	0.91	9.08	0.28	113	0.40	283	0.32	188	1.09
	5.94	0.77	9.03	0.28	109	0.34	290	0.38	204	0.99
	5.63	0.68	10.03	0.26	108	0.34	290	0.40	205	1.00
	5.43	0.62	11.93	0.27	115	0.35	289	0.38	206	1.16
	5.24	0.57	11.18	0.27	109	0.33	299	0.41	215	1.03
	5.07	0.52	12.29	0.28	111	0.31	304	0.41	221	1.08
	4.91	0.47	13.06	0.28	110	0.30	307	0.42	224	1.09
	4.75	0.42	11.97	0.29	108	0.29	306	0.42	226	1.08
	4.59	0.35	10.19	0.31	100	0.28	307	0.42	225	1.01
	4.44	0.29	17.65	0.27	118	0.30	313	0.43	234	1.23
	4.29	0.24	14.49	0.26	105	0.29	303	0.46	227	1.09
	4.21	0.21	11.06	0.29	105	0.27	302	0.44	227	1.03
	3.89	0.13	10.79	0.28	105	0.24	293	0.48	231	0.97
Asp$_1$Phe$_2$ [polymer] = 0.97 g/L	9.73	0.99	13.5	0.19	122	0.51	300	0.30	188	1.12
	8.06	0.95	11.8	0.21	119	0.49	287	0.30	182	1.14
	6.71	0.86	9.99	0.22	108	0.39	285	0.40	197	1.04
	6.35	0.82	11.3	0.23	108	0.39	279	0.39	194	1.09
	5.94	0.75	10.7	0.21	106	0.38	291	0.41	201	0.99
	5.66	0.66	13.0	0.24	108	0.32	299	0.44	218	1.05
	5.50	0.57	11.2	0.24	110	0.29	310	0.47	234	1.13
	5.35	0.48	12.9	0.20	112	0.27	314	0.52	245	1.13
	5.25	0.42	10.8	0.20	112	0.25	315	0.55	252	1.15
	5.06	0.32	8.54	0.20	115	0.23	318	0.57	261	1.10
	4.85	0.23	8.55	0.21	113	0.20	317	0.57	264	1.05
	4.50	0.13	7.61	0.24	108	0.19	316	0.57	264	1.07
	4.35	0.10	6.76	0.28	110	0.19	316	0.54	263	1.19
	4.04	0.05	8.61	0.26	121	0.20	317	0.55	266	1.09
Asp$_1$Phe$_3$ [polymer] = 0.99 g/L	9.95	0.99	17.0	0.09	141	0.21	311	0.71	273	1.03
	8.02	0.92	10.2	0.09	133	0.20	311	0.70	271	1.09
	7.37	0.84	14.7	0.09	135	0.20	315	0.71	275	1.10
	6.95	0.75	13.8	0.06	134	0.21	321	0.73	279	1.18
	6.70	0.66	14.0	0.11	138	0.20	325	0.69	283	1.07
	6.58	0.60	13.9	0.10	128	0.18	326	0.72	286	1.12
	6.38	0.51	9.1	0.13	115	0.17	323	0.70	283	1.14
	6.16	0.41	15.2	0.09	120	0.18	326	0.73	286	1.12
	5.97	0.34	16.9	0.10	142	0.19	330	0.71	290	1.18
	5.83	0.29	19.4	0.09	149	0.21	330	0.70	288	1.10
	5.35	0.17	12.4	0.09	130	0.18	325	0.73	287	1.05

Pyrene in Water	9.20	0.99	12.2	0.33	128	0.67			90	1.11
	7.07	0.95	12.7	0.26	127	0.74			98	1.00
	5.04	0.62	13.6	0.09	127	0.91			118	0.94
	3.96	0.36	10.8	0.07	126	0.93			118	0.97

Table SI2.9. Pre-exponential factors and decay times obtained from the tri-exponential fit of the fluorescence decays acquired with pyrene-loaded Asp_1Phe_1 solution with descending and ascending pH. The average lifetime $\langle\tau\rangle$ was calculated from the weighted average of the two longest lifetimes.

Sample	pH	α	τ_1	a_1	τ_2	a_2	τ_3	a_3	$\langle\tau\rangle$	χ^2
Asp_1Phe_1 [polymer] = 1.19 g/L	9.02	0.99	16.10	0.18	127	0.37	305	0.45	224	0.99
	6.55	0.86	12.79	0.26	130	0.35	307	0.38	223	1.08
	6.19	0.81	25.65	0.17	133	0.39	303	0.44	223	1.00
	5.91	0.76	16.70	0.19	124	0.36	299	0.44	221	0.88
Descending pH	5.68	0.69	22.34	0.16	122	0.32	296	0.52	229	1.05
	5.49	0.63	12.46	0.22	121	0.31	306	0.47	232	1.11
	5.30	0.57	19.49	0.16	128	0.31	310	0.53	242	1.06
	5.13	0.52	13.78	0.21	123	0.28	310	0.51	244	1.01
	4.98	0.48	15.94	0.16	120	0.29	311	0.55	245	1.06
	4.77	0.41	9.56	0.22	120	0.26	317	0.52	251	0.97
	4.54	0.32	18.25	0.16	125	0.26	320	0.58	260	1.14
	4.41	0.26	17.84	0.17	139	0.28	325	0.55	261	0.97
	4.32	0.22	11.21	0.18	125	0.26	316	0.56	255	1.02
	4.24	0.20	20.41	0.18	153	0.30	319	0.53	259	1.00
Ascending pH	4.35	0.23	12.48	0.23	120	0.25	306	0.52	245	0.97
	4.41	0.26	10.84	0.23	119	0.27	303	0.50	239	1.13
	4.49	0.29	12.69	0.22	113	0.29	300	0.50	232	1.01
	4.56	0.32	17.24	0.21	113	0.30	297	0.49	227	0.99
	4.67	0.37	12.66	0.24	99	0.31	293	0.45	214	1.04
	4.77	0.41	23.43	0.26	121	0.33	303	0.42	224	0.96
	4.90	0.46	19.59	0.26	113	0.34	301	0.40	213	1.09
	5.05	0.50	18.12	0.33	111	0.32	295	0.35	206	1.02
	5.25	0.56	16.28	0.35	98	0.32	280	0.33	190	1.12
	5.45	0.62	21.45	0.39	114	0.34	284	0.27	189	1.05
	5.70	0.69	18.76	0.40	105	0.37	267	0.24	169	1.03
	6.09	0.80	19.64	0.43	106	0.36	258	0.21	162	1.25
	7.30	0.91	16.12	0.47	102	0.35	255	0.19	156	1.05
	9.10	0.99	17.47	0.34	116	0.38	278	0.29	186	0.95

Appendix SI3 – Supporting Information for Chapter 3: Temperature Response of Aqueous Solutions of a Series of Pyrene End-Labeled Poly(N-isopropylacrylamide)s Probed by Fluorescence

Analysis of the Fluorescence Spectra

The analysis of the fluorescence spectra of the doubly labelled PNIPAM samples (Figure SI3.1.A) was performed by first applying a light scattering correction to the spectra to yield the spectrum shown in Figure SI3.1.C, as the intensity did not reach the baseline at 350 nm for the fluorescence spectra acquired above T_c. The monomer fluorescence spectrum obtained from the fluorescence spectrum of Py_1-PNIPAM(25K) at the corresponding temperature (Figure S I3.1.B) was then subtracted to yield the excimer fluorescence spectrum (Figure S I3.1.D).
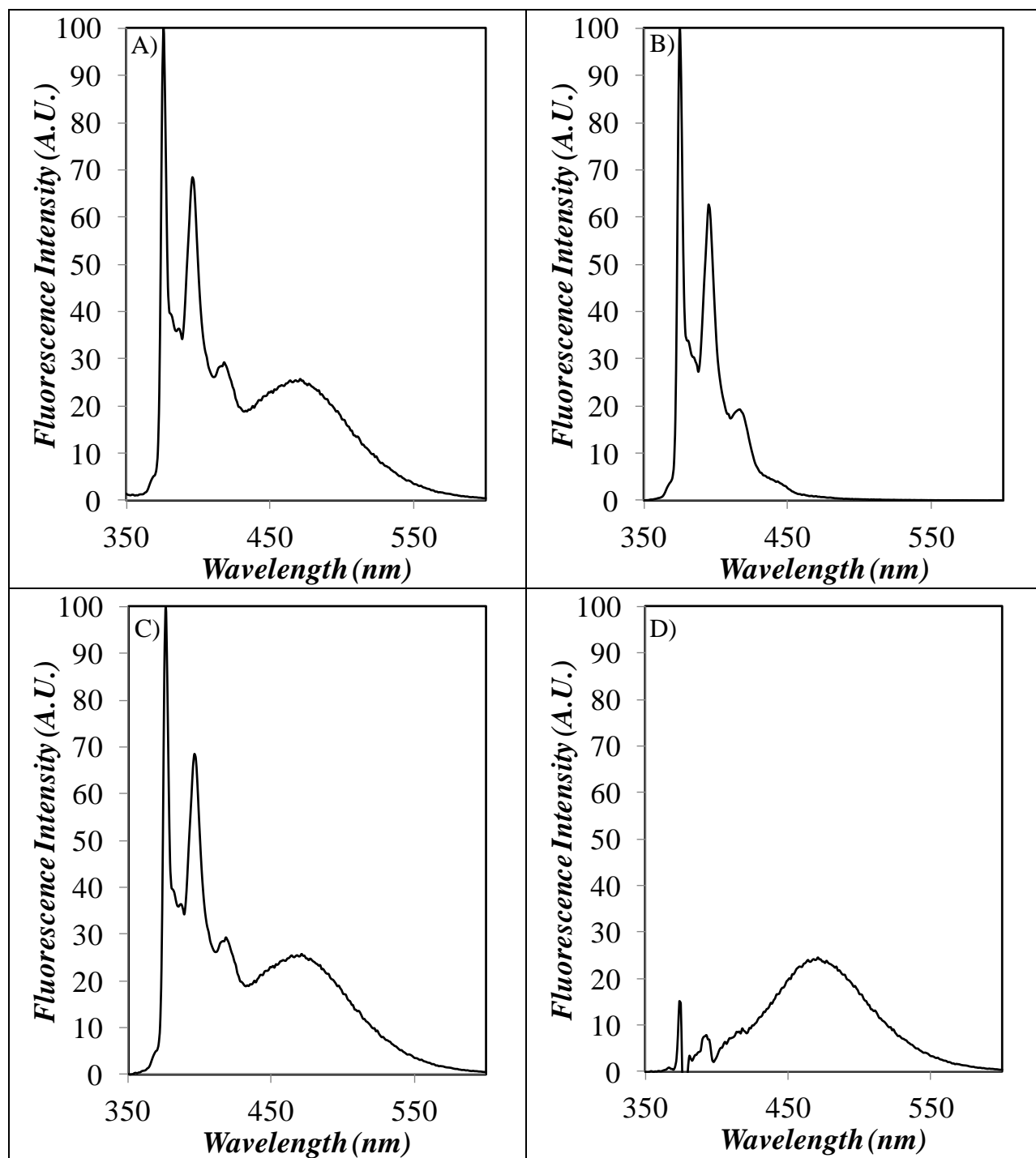
Figure SI3.1: Representative fluorescence spectra of Py$_2$-PNIPAM(14K) at 26 ^{o}C. A) Uncorrected fluorescence spectrum. B) Monomer fluorescence spectrum. C) Spectrum after the application of a light scattering correction. D) Spectrum after subtraction of the monomer fluorescence.

242

Fluorescence Decay Analysis

The fluorescence spectrum of the excimer shown in Figure S1.D fluctuates around the baseline at wavelengths near 375 nm where the monomer fluorescence decays were collected. These fluctuations are likely due to slight differences in the peak widths of the two spectra and they are not expected to reflect any residual emission from the excimer at 375 nm. Consequently, the time-resolved fluorescence decays acquired at 375 nm is expected to represent the behaviour of the pyrene monomer.

Application of the MFA equations was deemed successful if the χ^2 was smaller than 1.3 and if the residuals and the autocorrelation function of the residuals were both distributed randomly around zero. Representative results of a good fit of the fluorescence decays of Py_2-PNIPAM(14K) are shown in Figure S2 using the MFA equations. The χ^2 equals 1.01, and is thus below 1.3, the residuals and the autocorrelation function of the residuals are randomly distributed around zero.
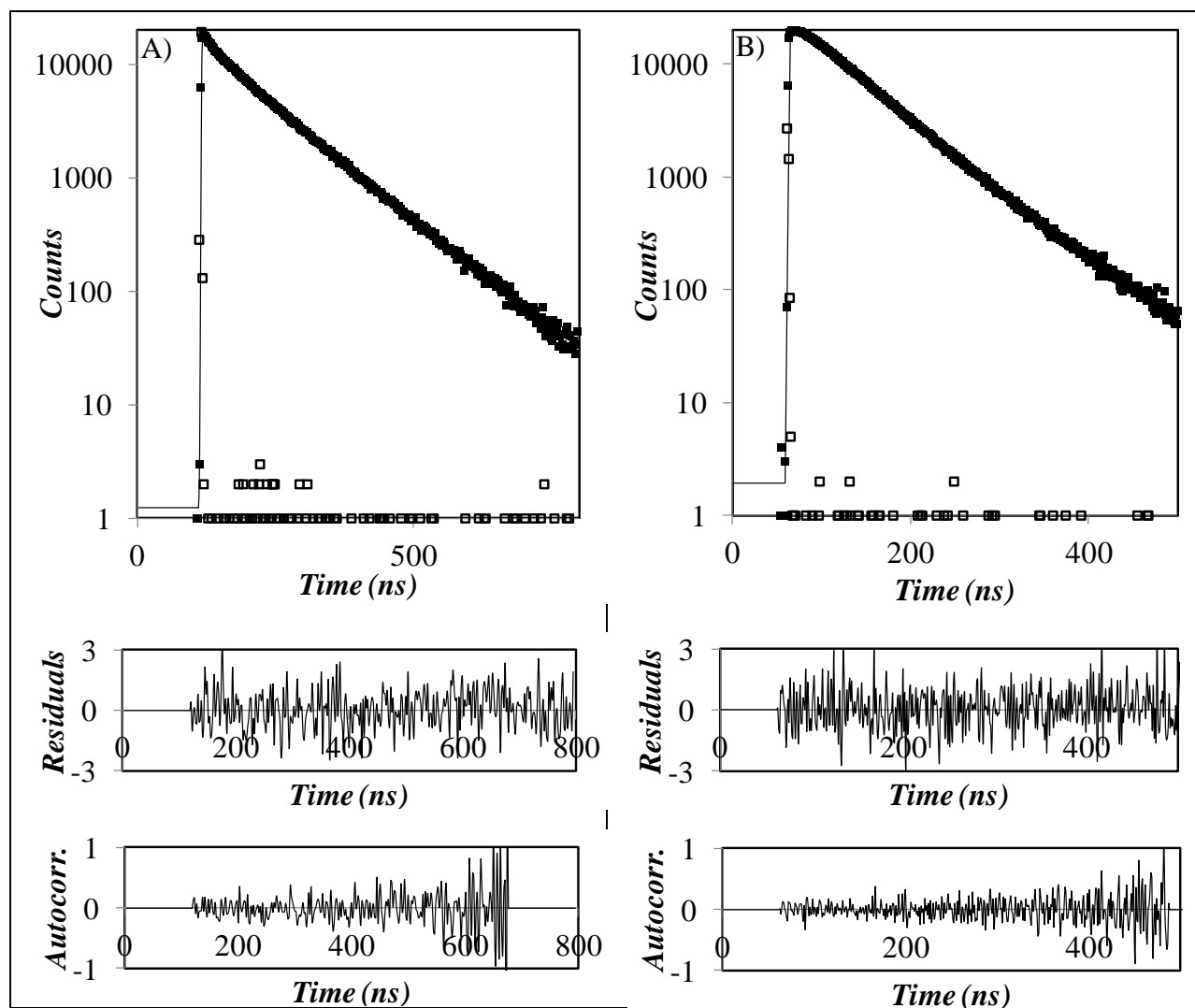
Figure SI3.2: Representative global MFA fits for Py$_2$-PNIPAM(14K) at a temperature of 21 ^{o}C. A) Monomer decay analysis. B) Excimer decay analysis. The value of χ^2 for this analysis was 1.06.

As part of another study Py$_2$-PNIPAM(14K) in ethanol was analyzed using Birks Scheme analysis, the results of which are compared to the results of MFA in Figure SI3.3.
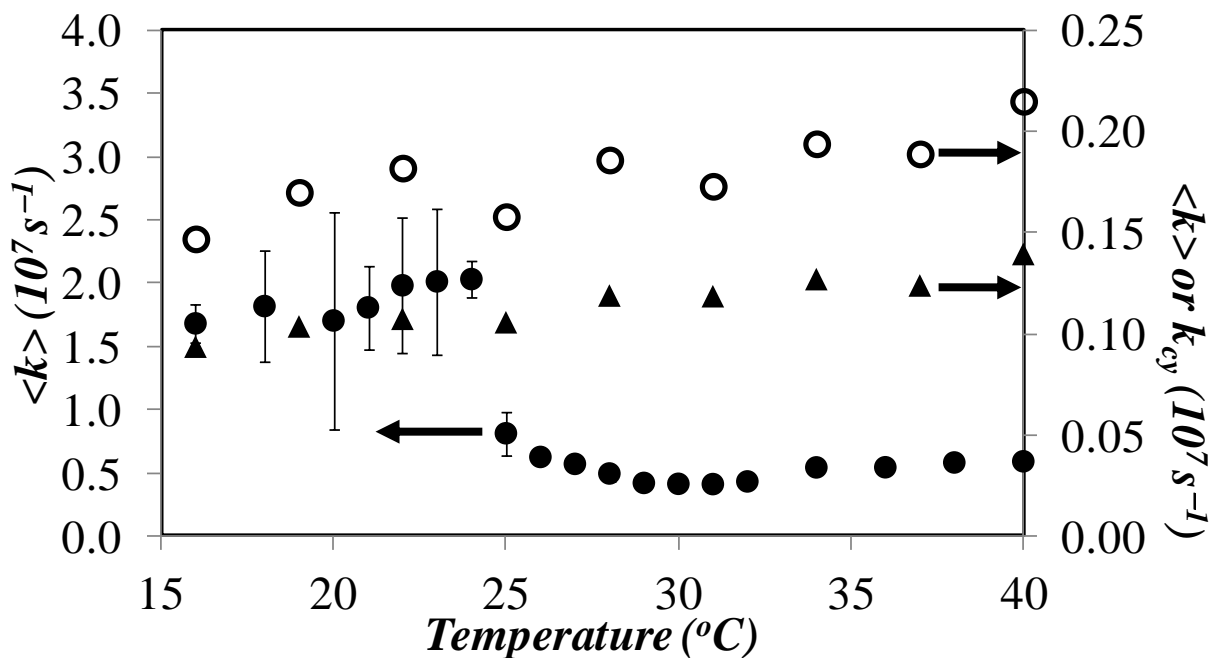
Figure SI3.3: Comparison between the rate constant for excimer formation of 12k Py$_2$-PNIPAM in ethanol and water. (●) MFA, water (▲) MFA, ethanol (○) Birks' Scheme, ethanol

While k_{cy} obtained from Birks' Scheme does not have precisely the same definition as $<k>$ obtained via MFA, they both reflect the time scale over which excimer formation occurs. In a solvent that remains a good solvent for both pyrene and PNIPAM across a given temperature range, k_{cy} increases essentially linearly with increasing temperature. Figure SI3.3 demonstrates that the break point observed for Py$_2$-PNIPAM in water is caused by the cloud point transition, not some other temperature-dependent property of pyrene.

Table SI3.1: Decay times and pre-exponential factors obtained from the triexponential fits of the

monomer decays for Py_2-PNIPAM(14K)

T (°C)	τ_1 (ns)	a_1	τ_2 (ns)	a_2	τ_3 (ns)	a_3	$<\tau_N>$ (ns)	$<\tau_W>$ (ns)	PDI	χ^2
16	8.7	0.11	44.9	0.16	112	0.74	90	106	1.17	1.09
18	8.3	0.16	43.0	0.16	110	0.68	83	103	1.24	1.08
20	11.8	0.15	45.3	0.16	110	0.69	85	102	1.20	1.02
21	9.3	0.17	48.4	0.20	111	0.63	81	102	1.25	0.95
22	7.3	0.19	40.8	0.19	110	0.62	77	101	1.31	1.01
23	8.2	0.18	37.8	0.18	109	0.64	77	100	1.30	1.03
24	10.1	0.23	48.8	0.20	111	0.58	76	100	1.32	1.04
25	10.0	0.21	43.8	0.20	110	0.59	76	100	1.32	1.00
26	11.0	0.18	48.9	0.22	112	0.60	80	101	1.26	0.98
27	8.7	0.15	51.1	0.24	113	0.60	82	102	1.25	1.06
28	9.6	0.14	54.9	0.27	115	0.60	85	103	1.22	0.95
29	8.8	0.11	48.2	0.23	114	0.66	87	104	1.20	1.03
30	9.3	0.10	51.3	0.24	115	0.65	89	105	1.18	1.12
31	11.9	0.11	54.9	0.24	115	0.66	90	105	1.17	0.98
32	11.2	0.10	52.4	0.24	115	0.66	90	105	1.17	0.99
34	14.9	0.11	55.4	0.23	116	0.66	91	106	1.16	1.06
36	9.3	0.10	50.5	0.26	115	0.64	88	105	1.19	1.00
38	12.2	0.09	52.9	0.28	117	0.63	89	105	1.17	1.11
40	11.0	0.12	58.5	0.31	119	0.57	88	105	1.20	1.05
T (°C)	τ_1 (ns)	a_1	τ_2 (ns)	a_2	τ_3 (ns)	a_3	$<\tau_N>$ (ns)	$<\tau_W>$ (ns)	PDI	χ^2
16	6.1	0.14	38.1	0.14	111	0.72	87	106	1.22	1.05
18	8.0	0.14	41.3	0.16	111	0.70	86	104	1.22	1.08
20	6.1	0.16	36.0	0.19	110	0.65	79	102	1.30	1.08
21	8.4	0.17	39.2	0.18	110	0.65	80	102	1.28	1.03
22	10.5	0.19	40.4	0.16	109	0.65	80	101	1.27	1.01
23	12.8	0.19	48.5	0.18	111	0.63	81	101	1.25	1.06
24	6.0	0.19	34.3	0.20	109	0.61	75	100	1.35	1.14
25	5.3	0.17	30.9	0.22	109	0.60	73	100	1.36	1.05
26	11.8	0.17	64.9	0.20	111	0.63	85	102	1.20	0.99
27	10.8	0.16	53.3	0.23	114	0.61	84	103	1.23	1.04
28	7.5	0.12	48.7	0.14	114	0.64	80	107	1.33	0.94
29	9.8	0.11	50.0	0.22	114	0.67	88	105	1.18	1.16
30	18.0	0.14	64.5	0.23	117	0.63	91	105	1.16	0.96

T (°C)	τ_1 (ns)	a_1	τ_2 (ns)	a_2	τ_3 (ns)	a_3	$<\tau_N>$ (ns)	$<\tau_W>$ (ns)	PDI	χ^2
31	15.6	0.10	57.7	0.26	117	0.65	92	106	1.15	1.12
32	18.0	0.12	61.9	0.24	117	0.64	92	106	1.15	0.96
34	9.8	0.11	54.0	0.25	117	0.64	89	106	1.19	1.00
36	10.0	0.10	56.6	0.30	119	0.60	90	106	1.19	1.06
38	6.2	0.12	47.5	0.25	116	0.63	86	105	1.23	1.09
40	8.3	0.11	51.8	0.28	117	0.61	87	105	1.20	0.98

T (°C)	τ_1 (ns)	a_1	τ_2 (ns)	a_2	τ_3 (ns)	a_3	$<\tau_N>$ (ns)	$<\tau_W>$ (ns)	PDI	χ^2
16	10.7	0.15	48.6	0.13	112	0.72	88	106	1.19	0.96
18	6.7	0.16	38.9	0.17	111	0.67	82	104	1.27	1.16
20	9.9	0.18	43.4	0.17	111	0.65	81	102	1.26	1.10
21	6.7	0.17	35.1	0.21	110	0.62	77	102	1.32	1.06
22	8.2	0.21	42.7	0.19	111	0.60	77	101	1.32	0.96
23	8.2	0.22	41.4	0.22	111	0.57	74	100	1.36	1.02
24	10.2	0.19	39.6	0.18	109	0.63	78	100	1.29	0.99
25	8.4	0.18	38.1	0.21	109	0.61	76	100	1.32	0.86
26	10.3	0.20	49.5	0.22	113	0.59	79	101	1.28	1.08
27	9.4	0.13	47.2	0.23	113	0.64	84	103	1.22	1.02
28	8.5	0.14	52.8	0.25	115	0.61	85	104	1.22	1.10
29	9.1	0.10	46.4	0.23	114	0.67	88	104	1.19	1.01
30	16.5	0.10	54.9	0.21	114	0.69	92	105	1.14	1.08
31	12.1	0.10	58.7	0.27	117	0.62	90	105	1.17	1.03
32	6.5	0.12	48.1	0.24	115	0.64	86	105	1.22	0.99
34	8.3	0.12	55.2	0.27	117	0.62	88	105	1.20	1.04
36	13.7	0.17	60.7	0.27	118	0.59	88	105	1.19	0.95
38	11.6	0.09	46.6	0.24	114	0.67	89	105	1.18	1.04
40	10.9	0.10	49.9	0.27	115	0.63	87	104	1.19	1.16

Table SI3.2: Decay times and pre-exponential factors obtained from the triexponential fits of the monomer decays for Py$_2$-PNIPAM(25K)

T (°C)	τ_1 (ns)	a_1	τ_2 (ns)	a_2	τ_3 (ns)	a_3	$<\tau_N>$ (ns)	$<\tau_W>$ (ns)	PDI	χ^2
16			39.8	0.10	115	0.90	107	112	1.04	0.92
19			27.6	0.11	112	0.89	103	110	1.06	1.00
22	12.8	0.10	67.6	0.15	115	0.75	97	109	1.11	1.12
24	14.8	0.12	79.0	0.26	119	0.61	95	108	1.13	0.89
25	6.0	0.08	38.8	0.15	113	0.77	93	107	1.16	0.94
26	12.6	0.10	53.8	0.17	114	0.72	93	107	1.15	0.96
27	11.3	0.11	46.1	0.15	113	0.74	91	106	1.16	0.98
28	14.2	0.14	60.0	0.18	116	0.68	92	107	1.17	1.06

T (^{o}C)	τ_1 (ns)	a_1	τ_2 (ns)	a_2	τ_3 (ns)	a_3	$<\tau_N>$ (ns)	$<\tau_W>$ (ns)	PDI	χ^2
29	15.5	0.13	81.8	0.38	134	0.49	98	115	1.16	0.99
30	15.2	0.08	82.5	0.38	141	0.54	109	123	1.13	0.98
31	25.7	0.10	96.9	0.47	153	0.43	114	128	1.12	1.04
32	8.5	0.08	76.5	0.30	147	0.62	114	132	1.15	1.11
33	8.2	0.09	75.6	0.30	150	0.61	116	135	1.16	1.12
34	22.1	0.09	99.1	0.43	161	0.48	122	137	1.12	0.97
36	9.0	0.08	71.5	0.26	152	0.66	121	139	1.15	1.07
38	5.9	0.09	68.6	0.24	151	0.66	118	138	1.18	0.96
40	18.3	0.06	79.2	0.28	153	0.65	124	139	1.12	1.02
T (^{o}C)	τ_1 (ns)	a_1	τ_2 (ns)	a_2	τ_3 (ns)	a_3	$<\tau_N>$ (ns)	$<\tau_W>$ (ns)	PDI	χ^2
16	4.0	0.12	49.7	0.09	116	0.79	96	112	1.16	1.11
19	6.7	0.08	56.8	0.13	115	0.79	99	110	1.11	1.04
22	7.5	0.09	48.7	0.12	114	0.79	96	109	1.13	1.02
24	11.1	0.12	66.9	0.17	116	0.70	94	108	1.15	0.98
25	8.7	0.11	44.8	0.14	113	0.75	92	108	1.16	0.92
26	4.4	0.18	42.3	0.15	113	0.67	83	107	1.29	1.02
27	5.0	0.12	38.9	0.17	113	0.71	88	107	1.22	1.06
28	10.6	0.15	56.9	0.18	116	0.67	90	107	1.20	1.09
29	8.9	0.13	56.6	0.21	122	0.66	93	113	1.20	0.92
30	14.0	0.10	79.8	0.34	138	0.56	105	121	1.15	1.11
31	9.2	0.06	70.4	0.29	140	0.64	111	126	1.13	1.03
32	22.6	0.08	94.8	0.43	153	0.49	117	131	1.11	0.92
33	4.5	0.12	66.7	0.25	147	0.63	109	134	1.23	1.07
34	12.8	0.09	78.7	0.30	152	0.62	118	137	1.15	0.96
36	6.0	0.09	69.1	0.26	152	0.65	117	138	1.18	1.03
38	8.4	0.09	73.3	0.25	152	0.66	119	139	1.16	1.02
40	31.4	0.09	96.7	0.34	158	0.57	125	139	1.11	1.02
T (^{o}C)	τ_1 (ns)	a_1	τ_2 (ns)	a_2	τ_3 (ns)	a_3	$<\tau_N>$ (ns)	$<\tau_W>$ (ns)	PDI	χ^2
16	8.9	0.06	65.4	0.12	118	0.82	105	113	1.08	0.92
19	9.3	0.09	56.9	0.10	116	0.81	101	112	1.11	0.99
22	10.1	0.09	61.3	0.14	116	0.77	99	111	1.11	1.04
24	13.8	0.09	63.2	0.15	116	0.76	99	110	1.11	1.06
25	8.8	0.10	59.6	0.18	116	0.72	95	109	1.14	0.97
26	8.4	0.10	43.3	0.15	114	0.75	94	109	1.16	1.14
27	12.2	0.12	57.2	0.18	117	0.70	94	109	1.16	0.91
28	12.2	0.11	55.1	0.19	117	0.70	93	108	1.16	0.89
29	11.3	0.12	73.2	0.31	130	0.57	97	115	1.18	1.01
30	14.5	0.09	78.8	0.34	138	0.57	107	122	1.14	1.13
31	11.3	0.10	84.7	0.37	146	0.53	110	127	1.16	0.96

32	20.3	0.06	80.3	0.32	147	0.62	118	131	1.11	0.96
33	6.2	0.09	71.3	0.28	148	0.63	114	134	1.17	1.14
34	12.1	0.08	82.6	0.32	154	0.60	120	137	1.14	0.99
36	14.0	0.06	70.6	0.24	150	0.70	123	138	1.13	1.12
38	13.0	0.07	75.9	0.27	153	0.66	122	139	1.13	1.03
40	17.3	0.07	75.2	0.25	151	0.69	123	139	1.12	0.92

Table SI3.3: Decay times and pre-exponential factors obtained from the triexponential fits of the excimer decays for Py_2-PNIPAM(14K)

T (°C)	τ_1 (ns)	a_1	τ_2 (ns)	a_2	τ_3 (ns)	a_3	$<\tau_N>_E$ (ns)	a_{E-}/a_{E+}	χ^2
16	12.6	-0.39	60.6	1.20	99	0.19	65.9	-0.28	1.20
18	12.2	-0.43	61.9	1.33	110	0.11	65.5	-0.30	1.17
20	12.5	-0.44	60.9	1.33	106	0.12	64.6	-0.31	1.13
21	12.3	-0.45	60.7	1.33	104	0.12	64.3	-0.31	1.05
22	13.6	-0.46	56.8	1.15	87	0.30	63.1	-0.31	1.11
23	12.8	-0.44	59.5	1.31	101	0.13	63.4	-0.31	1.07
24	12.4	-0.43	58.6	1.23	93	0.20	63.3	-0.30	1.04
25	12.8	-0.45	58.0	1.26	97	0.19	63.0	-0.31	1.03
26	12.5	-0.42	61.4	1.24	115	0.18	68.3	-0.30	0.97
27	14.5	-0.36	60.5	1.03	110	0.33	72.4	-0.26	1.07
28	15.8	-0.29	61.5	0.95	114	0.34	75.4	-0.23	1.01
29	17.1	-0.28	59.4	0.83	110	0.45	77.3	-0.22	1.09
30	17.4	-0.25	60.2	0.77	110	0.49	79.5	-0.20	1.04
31	17.1	-0.23	62.0	0.75	111	0.48	81.1	-0.19	1.05
32	17.6	-0.26	61.5	0.76	113	0.49	81.5	-0.20	1.04
34	17.9	-0.28	61.1	0.74	112	0.53	82.3	-0.22	1.07
36	20.5	-0.33	56.6	0.73	110	0.60	80.8	-0.25	1.04
38	16.9	-0.32	60.3	0.73	111	0.59	82.8	-0.24	1.16
40	18.1	-0.34	60.0	0.77	112	0.56	81.9	-0.25	1.10
T (°C)	τ_1 (ns)	a_1	τ_2 (ns)	a_2	τ_3 (ns)	a_3	$<\tau_N>_E$ (ns)	a_{E-}/a_{E+}	χ^2
16	12.9	-0.54	59.5	1.30	98	0.24	65.5	-0.35	1.04
18	12.0	-0.52	62.7	1.43	115	0.09	65.7	-0.34	1.03
20	11.7	-0.53	61.1	1.38	103	0.15	65.2	-0.35	1.18
21	12.5	-0.49	60.5	1.34	100	0.15	64.4	-0.33	1.13
22	12.1	-0.47	60.1	1.31	97	0.17	64.3	-0.32	1.03
23	12.6	-0.48	48.3	1.25	92	0.23	55.0	-0.32	1.16
24	11.9	-0.45	60.4	1.32	102	0.13	64.2	-0.31	1.07
25	13.5	-0.44	55.7	1.11	87	0.33	62.8	-0.30	1.08

T (°C)	τ_1 (ns)	a_1	τ_2 (ns)	a_2	τ_3 (ns)	a_3	$<\tau_N>_E$ (ns)	a_{E-}/a_{E+}	χ^2
26	12.9	-0.43	60.9	1.24	112	0.19	67.8	-0.30	1.01
27	14.8	-0.37	58.8	0.99	107	0.38	72.4	-0.27	1.05
28	16.7	-0.32	57.9	0.85	108	0.47	75.6	-0.24	1.05
29	16.7	-0.25	62.4	0.83	113	0.42	79.3	-0.20	1.01
30	16.7	-0.25	63.1	0.80	113	0.45	81.0	-0.20	1.11
31	15.4	-0.24	67.0	0.85	118	0.38	82.9	-0.19	1.22
32	19.0	-0.27	63.0	0.81	115	0.46	82.0	-0.21	0.97
34	17.5	-0.31	59.6	0.72	110	0.59	82.5	-0.24	0.99
36	15.6	-0.30	64.5	0.81	117	0.49	84.3	-0.23	1.04
38	14.7	-0.31	64.5	0.79	114	0.53	84.5	-0.24	1.03
40	15.2	-0.34	61.4	0.73	110	0.61	83.6	-0.25	1.02

T (°C)	τ_1 (ns)	a_1	τ_2 (ns)	a_2	τ_3 (ns)	a_3	$<\tau_N>_E$ (ns)	a_{E-}/a_{E+}	χ^2
16	11.4	-0.58	62.3	1.43	108	0.15	66.6	-0.37	1.07
18	10.7	-0.62	63.2	1.51	113	0.10	66.4	-0.38	1.15
20	10.8	-0.61	61.8	1.48	104	0.14	65.4	-0.38	1.13
21	10.3	-0.59	63.0	1.52	119	0.07	65.5	-0.37	1.00
22	10.8	-0.57	62.0	1.46	105	0.11	64.9	-0.36	1.10
23	11.1	-0.56	61.1	1.41	98	0.15	64.7	-0.36	1.13
24	11.3	-0.56	59.9	1.38	96	0.17	64.0	-0.36	1.12
25	12.1	-0.49	58.4	1.26	94	0.23	63.9	-0.33	1.10
26	13.8	-0.49	59.0	1.20	106	0.29	68.2	-0.33	0.99
27	14.2	-0.40	60.5	1.03	111	0.37	73.8	-0.28	1.03
28	16.3	-0.35	59.5	0.89	110	0.46	76.7	-0.26	1.00
29	16.9	-0.27	63.4	0.88	115	0.39	79.5	-0.21	1.00
30	18.8	-0.28	58.6	0.77	110	0.52	79.2	-0.22	1.13
31	20.3	-0.30	59.1	0.78	111	0.51	79.8	-0.23	1.03
32	19.2	-0.29	59.5	0.76	112	0.53	80.9	-0.23	1.10
34	18.4	-0.30	60.7	0.76	113	0.54	82.4	-0.23	1.04
36	17.1	-0.30	61.8	0.74	112	0.56	83.6	-0.23	1.07
38	18.6	-0.36	59.8	0.78	112	0.58	82.0	-0.27	1.08
40	14.6	-0.30	67.1	0.84	116	0.47	84.7	-0.23	1.05

Table SI3.4: Decay times and pre-exponential factors obtained from the triexponential fits of the excimer decays for Py$_2$-PNIPAM(25K)

T (°C)	τ_1 (ns)	a_1	τ_2 (ns)	a_2	τ_3 (ns)	a_3	τ_4 (ns)	a_4	$<\tau_N>_E$ (ns)	a_{E-}/a_{E+}	χ^2
16	13.3	-0.16	57.4	0.83	105	0.12	3.5	0.20	63.4	-0.17	1.06
19	15.8	-0.24	55.8	0.96	98	0.17	3.5	0.12	62.3	-0.21	1.04
22	15.4	-0.32	57.7	1.13	102	0.13	3.5	0.06	62.5	-0.25	1.06

T (°C)	τ_1 (ns)	a_1	τ_2 (ns)	a_2	τ_3 (ns)	a_3	τ_4 (ns)	a_4	$<\tau_N>_E$ (ns)	a_{E-}/a_{E+}	χ^2
24	13.9	-0.38	59.1	1.20	107	0.10	3.5	0.07	62.8	-0.29	1.01
25	13.9	-0.47	60.2	1.35	113	0.09	3.5	0.03	63.4	-0.33	1.15
26	15.1	-0.50	58.2	1.34	101	0.16	3.5	0.01	62.6	-0.34	0.97
27	14.6	-0.49	59.7	1.35	112	0.10	3.5	0.04	63.2	-0.34	1.04
28	15.7	-0.47	59.6	1.38	113	0.10	3.5	-0.02	63.3	-0.32	1.07
29	16.1	-0.43	58.9	1.19	120	0.21	3.5	0.04	68.0	-0.31	1.05
30	13.2	-0.24	62.5	0.85	132	0.23	3.5	0.15	77.3	-0.22	1.06
31	15.3	-0.15	62.5	0.69	130	0.29	3.5	0.16	82.5	-0.15	1.09
32	11.7	-0.15	65.5	0.67	136	0.27	3.5	0.22	85.9	-0.16	1.12
33	12.6	-0.15	66.7	0.70	138	0.28	3.5	0.17	87.4	-0.16	1.09
34	18.8	-0.19	59.9	0.68	129	0.38	3.5	0.13	84.7	-0.18	1.06
36	15.1	-0.18	62.7	0.67	131	0.36	3.5	0.14	86.6	-0.17	1.01
38	14.6	-0.18	63.2	0.69	133	0.36	3.5	0.14	86.9	-0.18	1.07
40	13.3	-0.19	63.9	0.69	134	0.34	3.5	0.16	87.1	-0.18	1.06

T (°C)	τ_1 (ns)	a_1	τ_2 (ns)	a_2	τ_3 (ns)	a_3	τ_4 (ns)	a_4	$<\tau_N>_E$ (ns)	a_{E-}/a_{E+}	χ^2
16	13.2	-0.19	56.2	0.80	94	0.19	3.50	0.20	63.5	-0.20	1.08
19	16.3	-0.31	54.8	0.93	95	0.19	3.50	0.18	61.6	-0.27	0.94
22	12.0	-0.35	59.7	1.08	113	0.08	3.50	0.19	63.2	-0.30	0.97
24	14.6	-0.41	58.2	1.16	104	0.11	3.50	0.13	62.2	-0.32	1.13
25	15.0	-0.45	57.3	1.22	99	0.16	3.50	0.08	62.0	-0.33	1.00
26	12.9	-0.48	59.3	1.18	105	0.10	3.50	0.20	62.8	-0.38	1.12
27	14.4	-0.50	59.1	1.31	111	0.09	3.50	0.09	62.6	-0.35	1.23
28	15.0	-0.51	58.9	1.34	109	0.11	3.50	0.06	62.8	-0.35	1.15
29	15.0	-0.45	59.8	1.19	122	0.13	3.50	0.13	66.0	-0.34	1.00
30	15.0	-0.26	61.0	0.86	127	0.22	3.50	0.17	74.7	-0.24	1.18
31	17.2	-0.19	60.5	0.73	130	0.28	3.50	0.18	79.5	-0.19	1.01
32	13.9	-0.16	63.4	0.65	130	0.29	3.50	0.21	84.1	-0.17	0.96
33	13.2	-0.17	65.2	0.68	135	0.28	3.50	0.21	85.8	-0.18	1.03
34	16.9	-0.21	60.9	0.67	130	0.35	3.50	0.19	84.5	-0.21	1.10
36	18.3	-0.23	60.2	0.70	130	0.36	3.50	0.16	84.3	-0.21	1.04
38	15.8	-0.21	62.9	0.70	133	0.34	3.50	0.16	85.9	-0.20	1.08
40	17.9	-0.21	60.9	0.70	131	0.37	3.50	0.13	85.2	-0.19	0.98

T (°C)	τ_1 (ns)	a_1	τ_2 (ns)	a_2	τ_3 (ns)	a_3	τ_4 (ns)	a_4	$<\tau_N>_E$ (ns)	a_{E-}/a_{E+}	χ^2
16	12.7	-0.38	60.7	1.09	115	0.11	3.50	0.18	65.7	-0.32	0.95
19	14.6	-0.49	56.9	1.14	97	0.24	3.50	0.10	63.9	-0.35	1.01
22	14.7	-0.55	60.4	1.44	116	0.10	3.50	0.02	64.1	-0.36	0.98
24	14.6	-0.59	62.0	1.54	135	0.05	3.50	0.00	64.3	-0.37	1.04
25	15.1	-0.67	58.2	1.46	100	0.19	3.50	0.03	63.0	-0.41	1.04
26	15.5	-0.65	59.5	1.53	110	0.12	3.50	0.00	63.1	-0.39	1.12

T											χ^2
27	16.1	-0.66	57.9	1.48	102	0.18	3.50	0.01	62.6	-0.40	1.00
28	15.7	-0.60	58.6	1.39	99	0.19	3.50	0.01	63.5	-0.38	1.04
29	15.4	-0.51	60.7	1.24	123	0.17	3.50	0.10	68.3	-0.36	1.18
30	17.3	-0.32	59.1	0.89	123	0.30	3.50	0.13	75.2	-0.27	1.00
31	15.5	-0.20	64.1	0.74	131	0.28	3.50	0.18	82.6	-0.19	0.99
32	13.4	-0.19	65.5	0.67	133	0.30	3.50	0.22	86.1	-0.19	1.09
33	18.2	-0.20	62.0	0.70	131	0.36	3.50	0.14	85.4	-0.18	1.07
34	15.7	-0.21	62.0	0.66	129	0.37	3.50	0.18	86.2	-0.20	1.07
36	18.4	-0.22	61.6	0.73	133	0.37	3.50	0.12	85.6	-0.20	1.01
38	16.7	-0.21	63.1	0.71	133	0.35	3.50	0.15	86.5	-0.20	1.08
40	15.0	-0.21	63.1	0.69	133	0.36	3.50	0.16	86.9	-0.20	1.02

Table SI3.5: Pre-exponential factors and decay times retrieved from the global analysis of the monomer decays for Py$_2$-PNIPAM(14K) using the MFA.

T (^{o}C)	τ_1 (ns)	a_1	τ_2 (ns)	a_2	τ_3 (ns)	a_3	$<\tau>$ (ns)	τ_M (ns)	f_{Mfree}	χ^2
16	7.8	0.08	24.7	0.10	74	0.13	41.0	113	0.68	1.15
18	7.2	0.11	25.4	0.13	77	0.16	40.8	113	0.60	1.12
20	11.7	0.17	47.0	0.14	102	0.23	59.4	113	0.47	1.09
21	9.9	0.16	33.1	0.11	77	0.17	42.2	113	0.56	1.01
22	4.9	0.07	31.7	0.18	67	0.19	43.0	113	0.56	1.06
23	9.6	0.15	27.8	0.13	77	0.19	41.4	113	0.53	1.04
24	8.2	0.14	20.4	0.14	64	0.19	34.7	113	0.53	1.03
25	12.1	0.22	53.2	0.20	107	0.44	69.6	126	0.14	1.04
26	11.3	0.20	44.4	0.16	108	0.61	77.3	140	0.02	1.01
27	12.5	0.16	50.1	0.18	106	0.58	78.7	140	0.09	1.07
28	14.8	0.15	60.6	0.25	115	0.60	86.4	140	0.00	1.00
29	15.3	0.14	56.2	0.20	111	0.61	85.9	140	0.05	1.08
30	16.0	0.13	63.5	0.26	117	0.61	90.2	140	0.00	1.07
31	15.1	0.11	60.5	0.25	116	0.63	90.7	140	0.00	1.03
32	13.6	0.10	47.2	0.18	108	0.63	85.1	140	0.09	1.03
34	15.4	0.10	42.7	0.12	98	0.59	79.7	140	0.20	1.08
36	17.2	0.12	55.8	0.18	104	0.54	81.3	140	0.16	1.05
38	8.8	0.07	31.8	0.15	94	0.56	74.4	140	0.21	1.16
40	15.3	0.13	47.9	0.14	99	0.55	76.9	140	0.18	1.09
T (^{o}C)	τ_1 (ns)	a_1	τ_2 (ns)	a_2	τ_3 (ns)	a_3	$<\tau>$ (ns)	τ_M (ns)	f_{Mfree}	χ^2
16	8.1	0.09	22.9	0.11	78	0.12	39.6	113	0.67	1.04
18	8.0	0.11	26.8	0.11	78	0.14	40.8	113	0.63	1.04
20	6.2	0.13	23.6	0.15	76	0.16	37.2	113	0.56	1.11

T (°C)	τ_1 (ns)	a_1	τ_2 (ns)	a_2	τ_3 (ns)	a_3	$<\tau>$ (ns)	τ_M (ns)	f_{Mfree}	χ^2
21	8.1	0.13	23.8	0.13	70	0.17	37.4	113	0.57	1.07
22	6.9	0.09	17.4	0.16	64	0.18	34.6	113	0.57	1.03
23	5.8	0.07	16.4	0.19	66	0.20	36.5	113	0.55	1.12
24	7.1	0.15	24.5	0.15	71	0.17	35.8	113	0.53	1.09
25	11.6	0.20	43.3	0.15	96	0.39	62.1	126	0.25	1.17
26	8.6	0.14	31.8	0.17	102	0.59	73.8	140	0.09	0.99
27	11.7	0.14	38.8	0.13	99	0.59	75.8	140	0.14	1.05
28	14.3	0.14	55.2	0.19	110	0.60	84.4	140	0.07	1.04
29	15.3	0.12	57.9	0.23	115	0.65	90.2	140	0.00	1.06
30	16.8	0.13	62.7	0.23	116	0.63	90.6	140	0.01	1.06
31	13.8	0.11	55.0	0.23	116	0.66	90.4	140	0.00	1.19
32	17.4	0.12	55.8	0.20	115	0.68	91.6	140	0.00	0.97
34	12.6	0.10	40.5	0.13	98	0.57	78.5	140	0.20	1.01
36	11.6	0.11	45.2	0.17	103	0.55	79.0	140	0.17	1.05
38	12.6	0.12	48.6	0.16	101	0.54	78.0	140	0.18	1.06
40	11.3	0.11	40.3	0.13	96	0.56	75.1	140	0.20	1.03
T (°C)	τ_1 (ns)	a_1	τ_2 (ns)	a_2	τ_3 (ns)	a_3	$<\tau>$ (ns)	τ_M (ns)	f_{Mfree}	χ^2
16	5.2	0.09	19.9	0.14	76	0.13	36.6	113	0.65	0.99
18	4.8	0.11	19.4	0.14	67	0.13	31.2	113	0.62	1.10
20	1.6	0.10	13.8	0.19	64	0.17	29.4	113	0.54	1.06
21	7.2	0.18	27.3	0.14	73	0.14	33.0	113	0.54	1.00
22	2.8	0.11	15.3	0.19	61	0.17	29.5	113	0.53	0.96
23	2.9	0.09	13.9	0.21	57	0.19	28.3	113	0.51	1.05
24	3.9	0.11	16.8	0.20	66	0.18	32.5	113	0.52	1.02
25	8.3	0.16	26.8	0.15	87	0.40	56.5	126	0.29	1.03
26	10.1	0.17	30.8	0.15	102	0.59	73.1	140	0.09	1.04
27	11.9	0.15	45.3	0.16	105	0.60	79.2	140	0.08	1.04
28	11.4	0.11	36.6	0.14	100	0.60	78.0	140	0.14	1.04
29	14.8	0.12	52.0	0.20	113	0.66	88.6	140	0.02	1.00
30	15.5	0.11	46.2	0.14	106	0.65	85.5	140	0.10	1.11
31	15.5	0.11	48.1	0.17	108	0.64	85.8	140	0.09	1.05
32	15.4	0.12	48.8	0.17	109	0.63	85.4	140	0.08	1.07
34	13.8	0.10	45.5	0.15	101	0.58	80.5	140	0.17	1.05
36	16.0	0.13	56.6	0.18	102	0.51	78.3	140	0.18	1.05
38	15.0	0.11	43.5	0.15	101	0.58	79.4	140	0.16	1.09
40	11.7	0.12	48.1	0.19	103	0.54	77.9	140	0.15	1.10

Table SI3.6: Pre-exponential factors and decay times retrieved from the global analysis of the monomer decays for Py$_2$-PNIPAM(25K) using the MFA.

T (^{o}C)	τ_1 (ns)	a_1	τ_2 (ns)	a_2	τ_3 (ns)	a_3	$<\tau>$ (ns)	τ_M (ns)	f_{Mfree}	χ^2
16	13.2	0.05	42.6	0.04	97	0.35	82.4	123	0.56	1.02
19	12.8	0.06	34.2	0.06	94	0.35	76.8	123	0.53	1.11
22	13.4	0.08	37.8	0.07	94	0.35	72.8	123	0.50	1.23
24	12.3	0.10	36.7	0.08	89	0.33	65.5	123	0.49	1.06
25	7.4	0.05	28.8	0.14	93	0.33	66.8	123	0.48	1.28
26	8.0	0.03	20.0	0.14	85	0.34	62.8	123	0.50	1.09
27	8.9	0.04	21.4	0.14	87	0.35	63.9	123	0.47	1.07
28	12.3	0.11	38.4	0.11	96	0.37	69.9	123	0.41	1.06
29	18.4	0.16	69.5	0.14	116	0.58	90.4	150	0.12	1.10
30	16.2	0.11	73.1	0.24	134	0.65	106.7	169	0.00	1.07
31	13.0	0.06	47.8	0.12	115	0.61	97.2	169	0.21	1.07
32	14.0	0.08	75.6	0.27	144	0.65	115.3	169	0.01	1.13
33	13.7	0.07	65.5	0.21	135	0.52	105.9	169	0.20	1.11
34	10.2	0.05	36.2	0.09	112	0.50	93.5	169	0.37	1.03
36	12.1	0.07	57.7	0.14	124	0.43	96.9	169	0.35	1.04
38	11.1	0.07	51.0	0.12	122	0.47	97.3	169	0.34	1.03
40	15.2	0.07	64.1	0.16	129	0.45	101.6	169	0.31	1.06
T (^{o}C)	τ_1 (ns)	a_1	τ_2 (ns)	a_2	τ_3 (ns)	a_3	$<\tau>$ (ns)	τ_M (ns)	f_{Mfree}	χ^2
16	9.9	0.06	32.9	0.04	90	0.29	72.9	123	0.62	1.15
19	0.0	0.07	20.0	0.11	92	0.33	64.4	123	0.49	1.10
22	1.8	0.04	23.9	0.13	94	0.34	68.3	123	0.49	1.26
24	0.6	0.08	17.7	0.14	86	0.31	55.3	123	0.47	1.22
25	0.6	0.07	17.6	0.15	86	0.32	55.5	123	0.46	1.10
26	4.5	0.06	17.4	0.16	85	0.32	55.7	123	0.46	1.21
27	10.3	0.08	25.9	0.11	90	0.36	65.0	123	0.47	1.27
28	11.7	0.13	37.2	0.10	94	0.34	65.7	123	0.43	1.12
29	19.6	0.20	76.1	0.20	119	0.47	86.6	150	0.12	1.28
30	15.7	0.12	62.4	0.16	123	0.65	99.6	169	0.08	1.18
31	16.6	0.08	56.6	0.14	123	0.64	102.4	169	0.14	1.05
32	14.0	0.07	53.9	0.11	118	0.58	99.2	169	0.24	0.98
33	12.0	0.07	57.8	0.16	126	0.52	100.6	169	0.24	1.05
34	17.4	0.10	68.5	0.15	125	0.44	97.7	169	0.31	1.05
36	11.8	0.07	45.4	0.11	118	0.46	94.6	169	0.36	1.06
38	9.9	0.07	45.2	0.11	120	0.47	95.7	169	0.35	1.06
40	15.8	0.06	48.4	0.10	118	0.47	97.2	169	0.37	1.00
T (^{o}C)	τ_1 (ns)	a_1	τ_2 (ns)	a_2	τ_3 (ns)	a_3	$<\tau>$ (ns)	τ_M (ns)	f_{Mfree}	χ^2
16	11.4	0.07	46.4	0.06	102	0.30	79.5	123	0.57	0.99

19	13.5	0.08	35.7	0.05	93	0.28	71.1	123	0.60	1.15
22	13.9	0.10	50.5	0.09	105	0.33	77.4	123	0.48	1.14
24	13.8	0.11	45.6	0.10	101	0.30	71.6	123	0.49	1.23
25	11.5	0.10	31.9	0.09	91	0.29	62.6	123	0.52	1.23
26	13.9	0.13	43.5	0.10	97	0.30	67.0	123	0.48	1.21
27	12.3	0.11	30.0	0.09	86	0.29	59.9	123	0.52	1.05
28	15.4	0.14	53.5	0.10	96	0.30	67.5	123	0.47	0.98
29	16.0	0.16	54.4	0.13	115	0.57	87.5	150	0.14	1.29
30	12.5	0.08	37.4	0.11	114	0.68	95.3	169	0.14	1.08
31	10.5	0.07	46.2	0.12	118	0.62	97.3	169	0.19	0.99
32	16.2	0.08	69.5	0.20	130	0.55	105.2	169	0.17	1.05
33	11.9	0.06	46.8	0.12	118	0.52	96.9	169	0.30	1.11
34	12.2	0.07	46.7	0.09	115	0.49	94.1	169	0.35	1.05
36	19.1	0.08	66.3	0.15	131	0.48	104.7	169	0.29	1.06
38	17.9	0.09	69.8	0.17	133	0.45	103.8	169	0.29	1.07
40	14.5	0.08	58.7	0.13	127	0.48	101.7	169	0.31	0.99

Table SI3.7: Pre-exponential factors and decay times retrieved from the global analysis of the excimer decays for Py$_2$-PNIPAM(14K) using the MFA.

T (°C)		τ_{EE0}		τ_{ED}		χ^2
	f_{Ediff}	(ns)	f_{EE0}	(ns)	f_{ED}	
16	0.43	51.0	0.38	88.5	0.19	1.15
18	0.47	51.0	0.37	88.5	0.16	1.12
20	0.53	51.0	0.35	88.5	0.12	1.09
21	0.47	51.0	0.40	88.5	0.13	1.01
22	0.46	51.0	0.41	88.5	0.13	1.06
23	0.46	51.0	0.42	88.5	0.13	1.04
24	0.42	51.0	0.43	88.5	0.15	1.03
25	0.58	51.0	0.38	88.5	0.03	1.04
26	0.60	51.0	0.33	88.5	0.07	1.01
27	0.60	51.0	0.34	112.0	0.06	1.07
28	0.59	51.0	0.32	112.0	0.09	1.00
29	0.57	51.0	0.31	112.0	0.12	1.08
30	0.59	51.0	0.29	112.0	0.13	1.07
31	0.58	51.0	0.28	112.0	0.14	1.03
32	0.56	51.0	0.28	112.0	0.16	1.03
34	0.57	51.0	0.30	118.0	0.13	1.08
36	0.56	51.0	0.29	118.0	0.15	1.05
38	0.57	51.0	0.28	118.0	0.15	1.16
40	0.57	51.0	0.29	118.0	0.15	1.09
T (°C)	f_{Ediff}	τ_{EE0}	f_{EE0}	τ_{ED}	f_{ED}	χ^2

		(ns)		(ns)		
16	0.49	51.0	0.32	88.5	0.19	1.04
18	0.51	51.0	0.34	88.5	0.15	1.04
20	0.51	51.0	0.33	88.5	0.16	1.11
21	0.48	51.0	0.38	88.5	0.15	1.07
22	0.45	51.0	0.39	88.5	0.16	1.03
23	0.46	51.0	0.40	88.5	0.14	1.12
24	0.46	51.0	0.39	88.5	0.15	1.09
25	0.54	51.0	0.41	88.5	0.04	1.17
26	0.61	51.0	0.34	88.5	0.04	0.99
27	0.59	51.0	0.34	112.0	0.07	1.05
28	0.59	51.0	0.31	112.0	0.10	1.04
29	0.59	51.0	0.29	112.0	0.12	1.06
30	0.59	51.0	0.28	112.0	0.13	1.06
31	0.59	51.0	0.26	112.0	0.15	1.19
32	0.59	51.0	0.26	112.0	0.15	0.97
34	0.58	51.0	0.28	118.0	0.14	1.01
36	0.58	51.0	0.27	118.0	0.15	1.05
38	0.59	51.0	0.27	118.0	0.15	1.06
40	0.59	51.0	0.27	118.0	0.14	1.03
T (°C)	f_{Ediff}	τ_{EE0} (ns)	f_{EE0}	τ_{ED} (ns)	f_{ED}	χ^2
16	0.52	51.0	0.29	88.5	0.20	0.99
18	0.53	51.0	0.28	88.5	0.19	1.10
20	0.59	51.0	0.25	88.5	0.16	1.06
21	0.50	51.0	0.33	88.5	0.17	1.00
22	0.54	51.0	0.31	88.5	0.15	0.96
23	0.51	51.0	0.33	88.5	0.16	1.05
24	0.51	51.0	0.34	88.5	0.14	1.02
25	0.56	51.0	0.39	88.5	0.04	1.03
26	0.60	51.0	0.32	88.5	0.08	1.04
27	0.62	51.0	0.31	112.0	0.07	1.04
28	0.58	51.0	0.31	112.0	0.13	1.04
29	0.59	51.0	0.29	112.0	0.12	1.00
30	0.57	51.0	0.29	112.0	0.13	1.11
31	0.57	51.0	0.28	112.0	0.15	1.05
32	0.56	51.0	0.27	112.0	0.17	1.07
34	0.58	51.0	0.28	118.0	0.14	1.05
36	0.57	51.0	0.28	118.0	0.15	1.05
38	0.59	51.0	0.27	118.0	0.14	1.09
40	0.59	51.0	0.27	118.0	0.14	1.10

Table SI3.8: Pre-exponential factors and decay times retrieved from the global analysis of the excimer decays for Py$_2$-PNIPAM(25K) using the MFA. τ_{ES} was fixed at 3.5 ns for all decays.

| T (^{o}C) | | τ_{EE0} | | τ_{ED} | | | χ^2 |
	f_{Ediff}	(ns)	f_{EE0}	(ns)	f_{ED}	f_{ES}	
16	0.51	51.0	0.39	1	0.00	0.09	1.02
19	0.53	51.0	0.42	1	0.00	0.05	1.11
22	0.56	51.0	0.42	1	0.00	0.03	1.23
24	0.55	51.0	0.43	1	0.00	0.02	1.06
25	0.60	51.0	0.40	1	0.00	0.00	1.28
26	0.58	51.0	0.41	1	0.00	0.00	1.09
27	0.59	51.0	0.41	1	0.00	0.00	1.07
28	0.62	51.0	0.37	1	0.00	0.01	1.06
29	0.65	51.0	0.35	1	0.00	0.00	1.10
30	0.63	51.0	0.31	135	0.03	0.03	1.07
31	0.53	51.0	0.33	135	0.07	0.07	1.07
32	0.60	51.0	0.26	135	0.07	0.07	1.13
33	0.55	51.0	0.28	135	0.10	0.07	1.11
34	0.53	51.0	0.30	135	0.10	0.07	1.03
36	0.53	51.0	0.29	135	0.11	0.07	1.04
38	0.55	51.0	0.28	135	0.10	0.07	1.03
40	0.55	51.0	0.29	135	0.11	0.05	1.06
T (^{o}C)		τ_{EE0}		τ_{ED}			χ^2
	f_{Ediff}	(ns)	f_{EE0}	(ns)	f_{ED}	f_{ES}	
16	0.50	51.0	0.39	1	0.00	0.11	1.15
19	0.60	51.0	0.33	1	0.00	0.07	1.10
22	0.58	51.0	0.38	1	0.00	0.04	1.26
24	0.63	51.0	0.33	1	0.00	0.04	1.22
25	0.63	51.0	0.34	1	0.00	0.02	1.10
26	0.58	51.0	0.31	1	0.00	0.11	1.21
27	0.59	51.0	0.38	1	0.00	0.04	1.27
28	0.61	51.0	0.35	1	0.00	0.04	1.12
29	0.62	51.0	0.38	1	0.00	0.00	1.28
30	0.61	51.0	0.32	135	0.01	0.06	1.18
31	0.56	51.0	0.32	135	0.05	0.07	1.05
32	0.55	51.0	0.30	135	0.06	0.09	0.98
33	0.55	51.0	0.28	135	0.08	0.09	1.05
34	0.54	51.0	0.28	135	0.09	0.08	1.05
36	0.54	51.0	0.28	135	0.10	0.09	1.06
38	0.56	51.0	0.26	135	0.09	0.09	1.06
40	0.54	51.0	0.30	135	0.10	0.05	1.00

T (^{o}C)	f_{Ediff}	τ_{EE0} (ns)	f_{EE0}	τ_{ED} (ns)	f_{ED}	f_{ES}	χ^2
16	0.64	51.0	0.29	1	0.00	0.07	0.99
19	0.62	51.0	0.35	1	0.00	0.03	1.15
22	0.68	51.0	0.32	1	0.00	0.00	1.14
24	0.66	51.0	0.34	1	0.00	0.00	1.23
25	0.64	51.0	0.34	1	0.00	0.02	1.23
26	0.65	51.0	0.35	1	0.00	0.00	1.21
27	0.52	51.0	0.37	1	0.00	0.01	1.05
28	0.64	51.0	0.36	1	0.00	0.00	0.98
29	0.67	51.0	0.32	1	0.00	0.01	1.29
30	0.63	51.0	0.31	135	0.01	0.05	1.08
31	0.59	51.0	0.28	135	0.04	0.09	0.99
32	0.59	51.0	0.27	135	0.07	0.07	1.05
33	0.56	51.0	0.29	135	0.09	0.07	1.11
34	0.55	51.0	0.27	135	0.09	0.08	1.05
36	0.57	51.0	0.28	135	0.10	0.05	1.06
38	0.57	51.0	0.27	135	0.10	0.06	1.07
40	0.57	51.0	0.27	135	0.10	0.06	0.99

Table SI3.9: Fractions of all pyrene species calculated from f_{Mfree}, f_{Mdiff}, f_{Ediff}, f_{EE0}, f_{ED} and f_{ES} for aqueous Py$_2$-PNIPAM(14K) samples.

T (^{o}C)	f_{diff}	f_{free}	f_{E0}	f_{EL}	f_{ES}	f_{agg}
16	0.23	0.48	0.20	0.10	0	0.30
18	0.28	0.41	0.22	0.10	0	0.31
20	0.36	0.32	0.24	0.08	0	0.32
21	0.30	0.37	0.25	0.08	0	0.33
22	0.29	0.37	0.26	0.08	0	0.34
23	0.30	0.34	0.28	0.08	0	0.36
24	0.29	0.33	0.29	0.10	0	0.39
25	0.53	0.08	0.35	0.03	0	0.38
26	0.59	0.01	0.33	0.07	0	0.39
27	0.57	0.06	0.32	0.06	0	0.38
28	0.59	0.00	0.32	0.09	0	0.41
29	0.55	0.03	0.30	0.12	0	0.42
30	0.59	0.00	0.29	0.13	0	0.41
31	0.58	0.00	0.28	0.14	0	0.42
32	0.53	0.05	0.27	0.15	0	0.42
34	0.50	0.12	0.26	0.12	0	0.38
36	0.51	0.09	0.26	0.13	0	0.39
38	0.49	0.13	0.25	0.13	0	0.38

T (^{o}C)	f_{diff}	f_{free}	f_{E0}	f_{EL}	f_{ES}	f_{agg}
40	0.50	0.11	0.25	0.13	0	0.39
T (^{o}C)	f_{diff}	f_{free}	f_{E0}	f_{EL}	f_{ES}	f_{agg}
16	0.24	0.50	0.16	0.09	0	0.26
18	0.27	0.46	0.18	0.08	0	0.27
20	0.31	0.39	0.20	0.10	0	0.30
21	0.29	0.39	0.23	0.09	0	0.32
22	0.28	0.37	0.24	0.10	0	0.34
23	0.29	0.36	0.26	0.09	0	0.35
24	0.30	0.34	0.26	0.10	0	0.36
25	0.46	0.15	0.35	0.04	0	0.39
26	0.58	0.06	0.32	0.04	0	0.36
27	0.54	0.09	0.31	0.06	0	0.37
28	0.56	0.04	0.30	0.10	0	0.39
29	0.59	0.00	0.29	0.12	0	0.41
30	0.59	0.00	0.27	0.13	0	0.41
31	0.59	0.00	0.26	0.15	0	0.41
32	0.59	0.00	0.26	0.15	0	0.41
34	0.51	0.13	0.25	0.12	0	0.37
36	0.51	0.11	0.24	0.14	0	0.38
38	0.52	0.11	0.24	0.13	0	0.37
40	0.51	0.12	0.24	0.12	0	0.36
T (^{o}C)	f_{diff}	f_{free}	f_{E0}	f_{EL}	f_{ES}	f_{agg}
16	0.26	0.49	0.15	0.10	0	0.25
18	0.29	0.46	0.15	0.10	0	0.25
20	0.35	0.41	0.15	0.09	0	0.24
21	0.31	0.38	0.21	0.10	0	0.31
22	0.33	0.38	0.19	0.09	0	0.29
23	0.33	0.35	0.21	0.11	0	0.32
24	0.33	0.36	0.22	0.09	0	0.31
25	0.46	0.19	0.32	0.04	0	0.35
26	0.57	0.05	0.30	0.08	0	0.38
27	0.58	0.05	0.30	0.07	0	0.36
28	0.52	0.09	0.27	0.12	0	0.39
29	0.58	0.01	0.28	0.12	0	0.41
30	0.54	0.06	0.28	0.13	0	0.40
31	0.54	0.05	0.27	0.14	0	0.41
32	0.53	0.05	0.26	0.16	0	0.42
34	0.51	0.11	0.25	0.12	0	0.38
36	0.50	0.11	0.25	0.14	0	0.39
38	0.53	0.10	0.24	0.13	0	0.37

40	0.53	0.09	0.24	0.13	0	0.37

Table SI3.10: Fractions of all pyrene species calculated from f_{Mfree}, f_{Mdiff}, f_{Ediff}, f_{EE0}, f_{ED} and f_{ES} for aqueous Py$_2$-PNIPAM(25K) samples

T (^{o}C)	f_{diff}	f_{free}	f_{E0}	f$_{EL}$	f$_{ES}$	f_{agg}
16	0.31	0.39	0.24	0.00	0.06	0.30
19	0.33	0.37	0.26	0.00	0.03	0.30
22	0.36	0.36	0.27	0.00	0.02	0.29
24	0.36	0.35	0.28	0.00	0.02	0.29
25	0.39	0.35	0.26	0.00	0.00	0.26
26	0.37	0.37	0.26	0.00	0.00	0.26
27	0.39	0.35	0.26	0.00	0.00	0.27
28	0.43	0.30	0.26	0.00	0.01	0.27
29	0.60	0.08	0.32	0.00	0.00	0.32
30	0.63	0.00	0.31	0.03	0.03	0.37
31	0.47	0.13	0.29	0.06	0.06	0.41
32	0.60	0.00	0.26	0.07	0.07	0.40
33	0.49	0.12	0.25	0.08	0.06	0.39
34	0.40	0.23	0.23	0.08	0.06	0.36
36	0.41	0.22	0.22	0.08	0.06	0.36
38	0.43	0.22	0.22	0.08	0.05	0.35
40	0.44	0.20	0.24	0.09	0.04	0.36
T (^{o}C)	f_{diff}	f_{free}	f_{E0}	f$_{EL}$	f$_{ES}$	f_{agg}
16	0.28	0.45	0.21	0.00	0.06	0.28
19	0.38	0.37	0.21	0.00	0.04	0.25
22	0.37	0.36	0.25	0.00	0.03	0.27
24	0.41	0.35	0.21	0.00	0.03	0.24
25	0.41	0.35	0.22	0.00	0.01	0.24
26	0.39	0.33	0.21	0.00	0.08	0.28
27	0.38	0.34	0.25	0.00	0.02	0.27
28	0.41	0.32	0.24	0.00	0.03	0.27
29	0.57	0.08	0.35	0.00	0.00	0.35
30	0.58	0.05	0.30	0.01	0.06	0.37
31	0.52	0.09	0.29	0.05	0.06	0.40
32	0.47	0.15	0.25	0.05	0.07	0.38
33	0.47	0.15	0.24	0.07	0.08	0.38
34	0.43	0.19	0.23	0.07	0.07	0.37
36	0.41	0.23	0.21	0.07	0.07	0.35
38	0.43	0.23	0.20	0.07	0.07	0.34
40	0.41	0.24	0.23	0.08	0.04	0.35
T (^{o}C)	f_{diff}	f_{free}	f_{E0}	f$_{EL}$	f$_{ES}$	f_{agg}

16	0.34	0.46	0.16	0.00	0.04	0.19
19	0.32	0.48	0.18	0.00	0.01	0.20
22	0.42	0.38	0.20	0.00	0.00	0.20
24	0.40	0.39	0.21	0.00	0.00	0.21
25	0.38	0.41	0.20	0.00	0.01	0.21
26	0.41	0.38	0.22	0.00	0.00	0.22
27	0.36	0.39	0.25	0.00	0.01	0.26
28	0.41	0.36	0.23	0.00	0.00	0.23
29	0.60	0.10	0.29	0.00	0.01	0.30
30	0.57	0.09	0.28	0.01	0.05	0.34
31	0.52	0.12	0.24	0.04	0.08	0.36
32	0.53	0.11	0.24	0.06	0.06	0.37
33	0.45	0.19	0.23	0.07	0.06	0.36
34	0.43	0.23	0.21	0.07	0.06	0.34
36	0.47	0.19	0.23	0.08	0.04	0.35
38	0.46	0.19	0.22	0.08	0.05	0.35
40	0.45	0.20	0.22	0.08	0.05	0.34

Table SI3.11: (I_E/I_M) values from steady-state and time resolved fluorescence.

Py$_2$-PNIPAM(14K)				Py$_2$-PNIPAM(25K)			
T (^{o}C)	$(I_E/I_M)^{SS}$	T (^{o}C)	$(I_E/I_M)^{SPC}$	T (^{o}C)	$(I_E/I_M)^{SS}$	T (^{o}C)	$(I_E/I_M)^{SPC}$
10	0.63	16	0.41	16	0.15	16	0.24
13	0.85	18	0.50	20	0.21	19	0.28
16	1.13	20	0.49	25	0.34	22	0.31
19	1.45	21	0.54	28	0.46	24	0.34
20	1.58	22	0.55	29	0.26	25	0.32
21	1.65	23	0.62	30	0.22	26	0.33
22	1.78	24	0.72	31	0.21	27	0.34
24	1.80	25	0.69	32	0.20	28	0.34
25	1.37	26	0.76	33	0.20	29	0.43
26	1.14	27	0.68	34	0.19	30	0.47
27	1.05	28	0.75	37	0.19	31	0.49
28	0.98	29	0.76	40	0.19	32	0.46
31	0.95	30	0.75			33	0.47
34	0.94	31	0.76			34	0.41
40	0.88	32	0.80			36	0.41
		34	0.67			38	0.40
		36	0.73			40	0.42

		T (°C)	$(I_E/I_M)^{SPC}$			T (°C)	$(I_E/I_M)^{SPC}$
		38	0.72				
		40	0.73				
		16	0.37			16	0.23
		18	0.41			19	0.29
		20	0.53			22	0.31
		21	0.54			24	0.34
		22	0.60			25	0.35
		23	0.61			26	0.35
		24	0.66			27	0.33
		25	0.69			28	0.34
		26	0.67			29	0.49
		27	0.67			30	0.44
		28	0.70			31	0.47
		29	0.72			32	0.42
		30	0.73			33	0.43
		31	0.76			34	0.42
		32	0.75			36	0.39
		34	0.66			38	0.36
		36	0.72			40	0.39
		38	0.70				
		40	0.70				
		T (°C)	$(I_E/I_M)^{SPC}$			T (°C)	$(I_E/I_M)^{SPC}$
		16	0.39			16	0.17
		18	0.45			19	0.20
		20	0.51			22	0.23
		21	0.59			24	0.25
		22	0.58			25	0.26
		23	0.68			26	0.28
		24	0.61			27	0.32
		25	0.65			28	0.29
		26	0.73			29	0.41
		27	0.66			30	0.42
		28	0.74			31	0.41
		29	0.74			32	0.42
		30	0.71			33	0.41
		31	0.76			34	0.38
		32	0.80			36	0.40
		34	0.69			38	0.39
		36	0.73			40	0.38

| | | 38 | 0.70 | | |
| | | 40 | 0.72 | | |

Py$_2$-PNIPAM(45K)

T (^{o}C)	$(I_E/I_M)^{SS}$
16	0.07
19	0.10
22	0.13
25	0.19
28	0.27
29	0.20
30	0.13
31	0.12
32	0.12
34	0.12
37	0.10
40	0.10

Table SI3.12: Lifetimes and pre-exponential factors obtained from the global analysis of Py$_2$-PNIPAM(14K) in ethanol with the Birks' scheme.

T (^{o}C)	τ_1 (ns)	τ_2 (ns)	a_{M1}	a_{M2}	a_{free}	a_{E1}	a_{E2}	χ^2
16	42.8	193	0.03	0.78	0.14	-0.33	0.47	1.05
19	43.2	190	0.04	0.74	0.15	-0.32	0.45	1.03
22	42.7	187	0.04	0.78	0.17	-0.31	0.43	1.07
25	40.8	184	0.03	0.78	0.19	-0.33	0.44	1.12
28	40.9	181	0.04	0.77	0.19	-0.34	0.44	1.08
31	40.5	178	0.03	0.80	0.17	-0.34	0.45	1.05
34	38.7	176	0.03	0.80	0.15	-0.33	0.43	1.09
37	38.1	172	0.03	0.79	0.18	-0.36	0.45	1.00
40	37.7	169	0.04	0.77	0.19	-0.18	0.22	1.10

Table SI3.13: Cyclization rate constant (kcy), dissociation rate constant (k-1) and excimer lifetime (τ_E) obtained from the global analysis of Py$_2$-PNIPAM(14K) in ethanol with the Birks' scheme.

T (^{o}C)	k_{cy}	k_{-1}	τ_E
16	0.0015	0.0081	68.7
19	0.0017	0.0087	73.9
22	0.0018	0.0093	76.0
25	0.0016	0.0086	66.5
28	0.0019	0.0089	68.2
31	0.0017	0.0075	60.6

34	0.0019	0.0083	59.8
37	0.0019	0.0086	59.3
40	0.0022	0.0089	60.1

Appendix SI4 – Supporting Information for Chapter 4: Temperature Response of Aqueous Mixtures Pyrene End-Labeled and Unmodified Poly(N-isopropylacrylamide)s Probed by Fluorescence

Analysis of the Fluorescence spectra:

The steady-state fluorescence spectra acquired in this chapter were corrected for light scattering and the excimer emission was separated from the monomer using the same procedure as done in the previous chapter.

Analysis of the fluorescence decays:

The MFA equations were applied in the same manner as described in the previous chapter.

Table SI4.1: Decay times and pre-exponential factors obtained from the triexponential fits of the monomer decays for Py_2-PNIPAM(14K) mixtures.

Initial Temperature Ramp										
T (^{o}C)	τ_1 (ns)	a_1	τ_2 (ns)	a_2	τ_3 (ns)	a_3	$<\tau_N>$ (ns)	$<\tau_W>$ (ns)	PDI	χ^2
22	6.5	0.18	35.7	0.20	111	0.62	76	102	1.33	0.99
23	6.0	0.25	36.6	0.18	110	0.57	71	101	1.43	1.03
24	8.6	0.23	43.0	0.19	111	0.59	75	101	1.34	0.99
25	7.0	0.22	40.1	0.21	111	0.57	73	101	1.38	1.05
26	8.1	0.19	44.7	0.22	112	0.59	78	102	1.31	0.95
27	6.1	0.15	39.4	0.22	111	0.63	80	102	1.29	1.09
28	10.4	0.15	51.7	0.22	114	0.63	84	103	1.22	1.10
29	14.4	0.15	61.6	0.25	116	0.60	87	104	1.19	1.01
30	13.2	0.13	57.8	0.25	116	0.61	87	104	1.19	1.03
31	10.3	0.11	51.7	0.25	115	0.64	88	104	1.19	0.98
32	9.6	0.12	49.3	0.24	116	0.63	87	105	1.21	1.07

T (°C)	τ_1 (ns)	a_1	τ_2 (ns)	a_2	τ_3 (ns)	a_3	$\langle\tau_N\rangle$ (ns)	$\langle\tau_W\rangle$ (ns)	PDI	χ^2
33	15.0	0.14	65.6	0.30	125	0.57	93	110	1.19	0.99
34	18.0	0.11	83.1	0.40	158	0.49	113	134	1.18	0.99
35	9.0	0.07	72.4	0.28	158	0.65	123	143	1.16	1.05
36	13.8	0.06	75.6	0.24	160	0.70	131	148	1.12	0.86
40	4.9	0.08	85.2	0.18	173	0.74	144	163	1.13	1.03

Re-ascending Temperature Ramp

T (°C)	τ_1 (ns)	a_1	τ_2 (ns)	a_2	τ_3 (ns)	a_3	$\langle\tau_N\rangle$ (ns)	$\langle\tau_W\rangle$ (ns)	PDI	χ^2
20	5.2	0.13	35.6	0.17	111	0.70	84	105	1.24	1.08
22	5.9	0.15	38.4	0.18	111	0.67	82	103	1.26	1.06
23	6.4	0.14	34.0	0.18	110	0.69	82	103	1.25	1.03
24	6.9	0.17	37.4	0.17	110	0.67	80	103	1.28	1.03
25	7.3	0.16	35.2	0.17	110	0.67	80	103	1.28	1.09
26	6.9	0.14	38.6	0.20	111	0.66	82	103	1.26	1.07
27	8.1	0.12	43.9	0.20	111	0.68	85	103	1.21	0.96
28	5.5	0.12	42.3	0.21	112	0.67	85	104	1.23	1.15
29	10.5	0.12	51.8	0.22	113	0.67	88	104	1.18	1.04
30	9.5	0.11	50.7	0.21	113	0.68	88	104	1.18	1.10
31	9.1	0.11	47.8	0.22	113	0.68	88	104	1.19	1.08
32	8.1	0.10	46.3	0.22	113	0.68	87	104	1.19	0.98
33	10.6	0.12	59.2	0.28	118	0.60	89	105	1.19	1.04
34	11.5	0.11	58.1	0.27	120	0.62	91	108	1.18	1.11
35	13.1	0.10	69.0	0.36	142	0.55	103	123	1.19	1.08
36	9.7	0.07	64.0	0.30	149	0.63	114	134	1.18	1.10
38	14.6	0.06	69.3	0.27	155	0.66	123	141	1.15	1.18
40	3.9	0.05	55.6	0.20	154	0.75	127	145	1.14	1.14

Table SI4.2: Decay times and pre-exponential factors obtained from the triexponential fits of the

monomer decays for Py$_2$-PNIPAM(25K) mixtures.

Initial Temperature Ramp

T (°C)	τ_1 (ns)	a_1	τ_2 (ns)	a_2	τ_3 (ns)	a_3	$\langle\tau_N\rangle$ (ns)	$\langle\tau_W\rangle$ (ns)	PDI	χ^2
20	10.1	0.07	46.2	0.11	114	0.82	100	110	1.10	1.10
23	15.9	0.14	80.3	0.16	116	0.71	97	109	1.13	1.13
24	5.2	0.11	35.7	0.14	113	0.76	91	108	1.19	1.19
25	9.3	0.15	48.0	0.13	114	0.72	90	108	1.20	1.20
26	4.8	0.13	33.0	0.15	113	0.72	86	107	1.24	1.24
27	5.5	0.13	36.4	0.17	114	0.71	87	107	1.23	1.23
28	6.4	0.14	41.6	0.18	115	0.68	87	108	1.24	1.24

T (°C)	τ_1 (ns)	a_1	τ_2 (ns)	a_2	τ_3 (ns)	a_3	$\langle\tau_N\rangle$ (ns)	$\langle\tau_W\rangle$ (ns)	PDI	χ^2
29	8.7	0.14	50.6	0.19	122	0.66	92	113	1.23	1.23
30	8.2	0.10	59.5	0.23	133	0.67	104	122	1.18	1.18
31	7.6	0.08	58.5	0.22	138	0.70	110	128	1.16	1.16
32	6.5	0.08	58.8	0.21	141	0.71	113	131	1.16	1.16
33	4.3	0.09	57.2	0.20	145	0.71	114	135	1.18	1.18
34	9.2	0.06	63.9	0.19	152	0.74	125	142	1.13	1.13
35	6.1	0.05	67.7	0.18	157	0.77	133	149	1.12	1.12
36	8.9	0.03	67.3	0.15	160	0.81	141	153	1.09	1.09
40			61.7	0.13	169	0.87	155	163	1.06	1.06

Re-ascending Temperature Ramp

T (°C)	τ_1 (ns)	a_1	τ_2 (ns)	a_2	τ_3 (ns)	a_3	$\langle\tau_N\rangle$ (ns)	$\langle\tau_W\rangle$ (ns)	PDI	χ^2
20	4.9	0.07	42.5	0.11	116	0.82	100	112	1.12	1.17
23	4.2	0.10	37.2	0.13	115	0.77	94	111	1.18	1.07
25	8.1	0.11	47.8	0.16	116	0.73	93	110	1.17	1.11
26	4.3	0.12	36.7	0.17	115	0.72	89	109	1.23	1.04
27	8.6	0.13	45.7	0.17	116	0.71	90	109	1.20	1.02
28	8.0	0.12	42.6	0.18	116	0.70	90	108	1.21	1.00
29	14.2	0.12	57.1	0.19	123	0.69	98	114	1.16	1.05
30	7.8	0.09	57.2	0.22	133	0.70	106	123	1.17	1.09
31	4.4	0.10	58.5	0.21	138	0.69	108	128	1.19	1.03
32	8.9	0.07	64.3	0.22	142	0.71	116	132	1.14	1.13
33	12.6	0.05	61.1	0.21	147	0.74	122	137	1.12	1.17
34	3.3	0.07	58.3	0.19	153	0.74	125	144	1.16	1.16
35	5.7	0.02	62.7	0.16	160	0.82	141	153	1.09	1.16
36	6.7	0.02	63.4	0.15	162	0.83	144	155	1.08	1.26
40	11.7	0.02	67.0	0.12	161	0.86	146	155	1.06	1.17

Table SI4.3: Decay times and pre-exponential factors obtained from the exponential fits of the excimer decays for Py$_2$-PNIPAM(14K) mixtures. τ_4, when used, was fixed at 3.5 ns.

Initial Temperature Ramp

T (°C)	τ_1 (ns)	a_1	τ_2 (ns)	a_2	τ_3 (ns)	a_3	a_4	$\langle\tau_N\rangle_E$ (ns)	a_{E-}/a_{E+}	χ^2
22	10.8	-0.58	61.7	1.53	126	0.05		63.7	-0.37	1.20
23	10.9	-0.59	59.2	1.41	92	0.19		63.1	-0.37	1.14
24	11.3	-0.54	58.7	1.39	97	0.15		62.5	-0.35	1.10
25	11.9	-0.55	57.3	1.36	96	0.19		62.0	-0.35	1.00
26	11.6	-0.48	60.1	1.26	112	0.22		67.7	-0.32	1.12
27	12.3	-0.36	60.9	1.06	112	0.30		72.0	-0.26	1.11

T (°C)	τ_1 (ns)	a_1	τ_2 (ns)	a_2	τ_3 (ns)	a_3	a_4	$\langle\tau_N\rangle_E$ (ns)	a_{E-}/a_{E+}	χ^2
28	11.9	-0.30	62.5	0.97	114	0.33		75.5	-0.23	1.01
29	12.2	-0.25	63.7	0.90	116	0.35		78.1	-0.20	0.96
30	12.6	-0.25	62.2	0.83	112	0.42		79.1	-0.20	1.09
31	13.7	-0.26	61.6	0.80	112	0.46		80.0	-0.21	1.14
32	13.8	-0.28	62.9	0.80	113	0.47		81.5	-0.22	1.09
33	14.8	-0.26	63.2	0.84	115	0.43		80.8	-0.21	1.13
34	15.2	-0.27	55.4	0.75	107	0.50	0.02	74.0	-0.23	0.88
35	10.6	-0.21	62.2	0.78	117	0.30	0.12	76.4	-0.15	1.02
36	11.1	-0.20	58.1	0.70	115	0.32	0.18	73.6	-0.16	1.10
40	7.8	-0.04	59.1	0.45	135	0.20	0.38	82.4	-0.06	1.04

Re-ascending Temperature Ramp

T (°C)	τ_1 (ns)	a_1	τ_2 (ns)	a_2	τ_3 (ns)	a_3	a_4	$\langle\tau_N\rangle_E$ (ns)	a_{E-}/a_{E+}	χ^2
20	16.5	-0.35	52.0	0.86	83	0.48		63.2	-0.26	1.1
22	13.5	-0.29	59.4	1.11	97	0.18		64.6	-0.22	1.0
23	14.4	-0.29	57.6	1.06	92	0.23		64.0	-0.23	1.1
24	12.1	-0.25	61.1	1.15	108	0.10		64.9	-0.20	1.1
25	14.3	-0.28	57.8	1.09	100	0.19		64.0	-0.22	1.1
26	15.4	-0.30	57.8	0.98	104	0.31	0.01	68.7	-0.23	0.9
27	15.5	-0.25	61.1	0.93	112	0.29	0.03	73.4	-0.20	1.1
28	16.7	-0.25	61.2	0.87	114	0.36	0.02	76.7	-0.20	1.1
29	14.5	-0.19	66.1	0.85	120	0.28	0.06	79.5	-0.17	1.1
30	16.3	-0.21	59.5	0.68	108	0.47	0.07	79.5	-0.19	1.1
31	17.7	-0.19	62.6	0.73	113	0.42	0.04	80.9	-0.16	1.1
32	17.0	-0.21	64.3	0.75	115	0.40	0.05	81.9	-0.18	1.0
33	23.5	-0.32	54.8	0.74	109	0.56	0.02	78.1	-0.25	1.0
34	15.2	-0.23	66.6	0.79	119	0.38	0.06	83.7	-0.20	1.0
35	13.3	-0.20	65.4	0.74	117	0.34	0.11	81.6	-0.19	1.0
36	12.7	-0.32	64.1	0.73	116	0.35	0.13	80.8	-0.30	1.0
38	13.5	-0.16	63.8	0.68	121	0.26	0.21	79.8	-0.16	1.1
40	14.5	-0.16	59.7	0.60	117	0.29	0.27	78.4	-0.18	1.1

Table SI4.4: Decay times and pre-exponential factors obtained from the exponential fits of the excimer decays for Py_2-PNIPAM(25K) mixtures. τ_4, when used, was fixed at 3.5 ns.

Initial Temperature Ramp

T (°C)	τ_1 (ns)	a_1	τ_2 (ns)	a_2	τ_3 (ns)	a_3	a_4	$\langle\tau_N\rangle_E$ (ns)	a_{E-}/a_{E+}	χ^2
20	12.1	-0.50	57.6	1.33	106	0.16		62.8	-0.33	1.01
23	11.1	-0.61	60.0	1.50	112	0.10		63.4	-0.38	1.03

T (°C)	τ_1 (ns)	a_1	τ_2 (ns)	a_2	τ_3 (ns)	a_3	a_4	$\langle\tau_N\rangle_E$ (ns)	a_{E-}/a_{E+}	χ^2
24	11.3	-0.64	61.2	1.58	136	0.05		63.6	-0.39	1.22
25	11.8	-0.70	60.5	1.62	121	0.08		63.2	-0.41	1.11
26	11.9	-0.73	61.3	1.68	132	0.06		63.6	-0.42	0.98
27	11.6	-0.77	61.6	1.72	136	0.05		63.7	-0.44	1.10
28	12.6	-0.78	60.5	1.68	115	0.10		63.5	-0.44	1.25
29	12.4	-0.66	62.3	1.56	133	0.10		66.6	-0.40	1.04
30	12.9	-0.33	64.2	1.11	136	0.22		76.1	-0.25	1.06
31	14.7	-0.19	62.0	0.84	129	0.35		81.8	-0.16	1.04
32	16.5	-0.19	61.9	0.81	130	0.39		84.0	-0.16	1.15
33	13.6	-0.19	63.5	0.80	133	0.38		85.9	-0.16	1.07
34	10.5	-0.23	62.6	0.73	131	0.38	0.12	85.6	-0.21	1.04
35	11.1	-0.17	59.0	0.66	129	0.31	0.20	81.3	-0.18	1.00
36	7.6	-0.21	57.1	0.57	129	0.26	0.37	79.8	-0.25	1.01
40	3.9	-1.34	49.3	0.26	130	0.14	1.94	77.7		1.22
Re-ascending Temperature Ramp										
T (°C)	τ_1 (ns)	a_1	τ_2 (ns)	a_2	τ_3 (ns)	a_3	a_4	$\langle\tau_N\rangle_E$ (ns)	a_{E-}/a_{E+}	χ^2
20	13.7	-0.72	61.6	1.57	115	0.15		66.1	-0.42	1.07
23	14.1	-0.88	59.3	1.64	101	0.24		64.7	-0.47	1.11
25	13.7	-0.94	62.0	1.84	119	0.11		65.2	-0.49	1.04
26	13.5	-0.98	60.6	1.77	101	0.21		64.9	-0.49	1.07
27	13.5	-0.93	63.2	1.87	134	0.06		65.5	-0.48	1.05
28	13.8	-0.96	61.7	1.83	116	0.12		65.0	-0.49	1.08
29	14.7	-0.79	61.8	1.59	123	0.20		68.9	-0.44	1.11
30	15.3	-0.48	62.8	1.11	129	0.31	0.07	77.2	-0.34	1.12
31	13.1	-0.31	64.0	0.76	129	0.36	0.19	84.8	-0.27	1.11
32	20.5	-0.26	60.6	0.78	128	0.46	0.02	85.9	-0.21	1.15
33	10.2	-0.29	68.2	0.66	137	0.34	0.29	91.2	-0.29	1.30
34	9.5	-0.28	67.5	0.62	138	0.28	0.38	89.7	-0.31	1.17
35	7.5	-0.27	63.7	0.54	135	0.24	0.48	85.7	-0.34	1.04
36	3.8	-3.04	59.1	0.37	136	0.16	3.51	82.7		1.08
40	3.8	-2.88	51.4	0.29	129	0.15	3.44	78.0		1.17

Table SI4.5: Pre-exponential factors and decay times retrieved from the global analysis of the monomer decays for Py$_2$-PNIPAM(14K) mixtures using the MFA equations.

Initial Temperature Ramp

T (°C)	τ_1 (ns)	a_1	τ_2 (ns)	a_2	τ_3 (ns)	a_3	$\langle\tau\rangle$ (ns)	τ_M (ns)	f_{Mfree}	χ^2
22	11.3	0.24	58.6	0.20	1	0.00	32.4	114	0.56	1.18
23	10.8	0.25	59.3	0.21	1	0.00	32.7	114	0.54	1.13
24	11.6	0.26	61.6	0.21	1	0.00	34.0	114	0.54	1.06
25	12.3	0.27	63.8	0.20	1	0.00	34.0	114	0.53	1.08
26	14.9	0.26	94.6	0.59	1	0.00	70.3	140	0.14	1.22
27	16.7	0.22	92.8	0.60	1	0.00	72.5	140	0.18	1.23
28	16.5	0.20	91.8	0.61	1	0.00	73.3	140	0.19	1.13
29	18.3	0.19	93.0	0.61	1	0.00	75.2	140	0.19	1.05
30	17.8	0.19	91.7	0.61	1	0.00	74.4	140	0.20	1.12
31	18.0	0.18	90.6	0.60	1	0.00	73.6	140	0.22	1.18
32	18.4	0.19	91.8	0.58	1	0.00	73.5	140	0.23	1.16
33	17.9	0.18	90.0	0.51	1	0.00	70.9	140	0.31	1.09
34	19.3	0.14	96.5	0.49	1	0.00	79.4	167	0.37	0.95
35	16.5	0.08	91.2	0.39	1	0.00	78.2	167	0.53	1.06
36	14.7	0.07	92.9	0.33	1	0.00	78.4	167	0.60	1.01
40	6.8	0.09	60.8	0.09	1	0.00	34.0	167	0.82	1.14

Re-ascending Temperature Ramp

T (°C)	τ_1 (ns)	a_1	τ_2 (ns)	a_2	τ_3 (ns)	a_3	$\langle\tau\rangle$ (ns)	τ_M (ns)	f_{Mfree}	χ^2
20	15.6	0.16	66.1	0.17	1	0.00	41.4	114	0.66	1.14
22	13.9	0.17	63.5	0.20	1	0.00	40.3	114	0.63	1.08
23	15.4	0.19	67.1	0.19	1	0.00	41.7	114	0.62	1.08
24	13.1	0.19	62.9	0.20	1	0.00	38.6	114	0.61	1.11
25	15.7	0.22	73.2	0.20	1	0.00	42.7	114	0.58	1.17
26	19.7	0.23	100.3	0.66	1	0.00	79.3	140	0.11	1.11
27	22.8	0.19	97.2	0.65	1	0.00	80.3	140	0.15	1.13
28	24.0	0.19	99.2	0.66	1	0.00	82.2	140	0.14	1.20
29	26.3	0.19	99.6	0.67	1	0.00	83.3	140	0.14	1.16
30	24.4	0.17	96.9	0.66	1	0.00	82.1	140	0.17	1.16
31	27.0	0.19	99.3	0.66	1	0.00	83.0	140	0.15	1.14
32	27.4	0.20	99.8	0.66	1	0.00	83.3	140	0.14	1.06
33	24.7	0.18	95.6	0.61	1	0.00	79.2	140	0.21	1.04
34	25.0	0.19	97.6	0.59	1	0.00	79.9	140	0.22	1.14
35	20.1	0.12	94.1	0.59	1	0.00	81.3	167	0.28	1.16
36	18.7	0.10	92.5	0.48	1	0.00	79.7	167	0.42	1.16
38	22.3	0.09	93.5	0.40	1	0.00	80.4	167	0.51	1.17
40	22.6	0.08	97.8	0.35	1	0.00	84.4	167	0.57	1.21
T (°C)	τ_1 (ns)	a_1	τ_2 (ns)	a_2	τ_3 (ns)	a_3	$\langle\tau\rangle$ (ns)	τ_M (ns)	f_{Mfree}	χ^2

T (°C)	τ_1 (ns)	a_1	τ_2 (ns)	a_2	τ_3 (ns)	a_3	$\langle\tau\rangle$ (ns)	τ_M (ns)	f_{Mfree}	χ^2
20	15.6	0.16	68.0	0.19	1	0.00	43.5	114	0.65	1.14
22	15.5	0.17	68.2	0.20	1	0.00	44.3	114	0.63	1.03
23	15.5	0.17	67.1	0.21	1	0.00	43.4	114	0.62	1.08
24	15.0	0.18	68.2	0.21	1	0.00	43.1	114	0.61	1.12
25	16.0	0.19	69.9	0.21	1	0.00	43.9	114	0.60	1.03
26	20.4	0.21	100.4	0.68	1	0.00	81.2	140	0.11	1.19
27	22.6	0.19	97.5	0.66	1	0.00	81.1	140	0.15	1.18
28	24.7	0.18	98.1	0.66	1	0.00	82.4	140	0.16	1.08
29	24.8	0.18	99.4	0.68	1	0.00	83.5	140	0.14	1.14
30	24.6	0.18	98.6	0.68	1	0.00	83.2	140	0.15	1.11
31	26.1	0.19	99.9	0.68	1	0.00	83.5	140	0.13	1.10
32	23.6	0.18	96.5	0.65	1	0.00	80.8	140	0.17	1.05
33	23.6	0.19	95.7	0.60	1	0.00	78.7	140	0.21	1.06
34	24.0	0.15	101.0	0.55	1	0.00	84.3	167	0.30	1.08
35	19.5	0.10	93.6	0.45	1	0.00	80.5	167	0.46	1.22
36	19.4	0.08	92.8	0.38	1	0.00	80.3	167	0.54	1.21
38	20.5	0.07	99.9	0.33	1	0.00	86.4	167	0.60	1.21
40	23.4	0.07	105.0	0.32	1	0.00	90.4	167	0.61	1.18
21	14.2	0.17	65.7	0.19	1	0.00	41.8	114	0.64	1.18
37	20.7	0.08	97.2	0.35	1	0.00	83.3	167	0.57	1.12
39	20.7	0.06	98.7	0.32	1	0.00	85.8	167	0.61	1.17

Table SI4.6: Pre-exponential factors and decay times retrieved from the global analysis of the monomer decays for Py$_2$-PNIPAM(25K) mixtures using the MFA equations.

Initial Temperature Ramp										
T (°C)	τ_1 (ns)	a_1	τ_2 (ns)	a_2	τ_3 (ns)	a_3	$\langle\tau\rangle$ (ns)	τ_M (ns)	f_{Mfree}	χ^2
20	13.6	0.11	71.5	0.12	106	0.27	77.6	120	0.50	1.07
23	9.7	0.10	32.2	0.07	91	0.27	63.6	120	0.56	1.13
24	11.1	0.11	37.1	0.08	95	0.30	67.2	120	0.51	1.25
25	9.0	0.13	40.0	0.10	101	0.32	67.2	120	0.44	1.08
26	7.9	0.11	30.5	0.11	94	0.30	62.1	120	0.48	0.98
27	11.1	0.13	40.3	0.10	99	0.32	67.1	120	0.45	1.20
28	9.1	0.12	35.0	0.11	95	0.29	62.4	120	0.47	1.19
29	13.8	0.15	62.3	0.21	126	0.47	89.5	120	0.18	1.22
30	11.8	0.12	59.8	0.19	131	0.69	103.8	167	0.00	1.21
31	28.4	0.14	113.8	0.63	1	0.00	98.7	167	0.23	1.25
32	28.3	0.12	112.9	0.58	1	0.00	98.0	167	0.29	1.27

T (°C)	τ_1 (ns)	a_1	τ_2 (ns)	a_2	τ_3 (ns)	a_3	$\langle\tau\rangle$ (ns)	τ_M (ns)	f_{Mfree}	χ^2
33	29.4	0.12	116.2	0.56	1	0.00	101.0	167	0.32	1.21
34	21.4	0.09	106.4	0.42	1	0.00	90.9	167	0.49	1.16
35	19.7	0.07	104.8	0.33	1	0.00	89.2	167	0.60	1.22
36	16.6	0.07	102.6	0.26	1	0.00	84.8	167	0.68	1.32
40	59.8	0.13	183.9	0.09	1	0.00	110.2	167	0.78	1.21

Re-ascending Temperature Ramp

T (°C)	τ_1 (ns)	a_1	τ_2 (ns)	a_2	τ_3 (ns)	a_3	$\langle\tau\rangle$ (ns)	τ_M (ns)	f_{Mfree}	χ^2
20	9.8	0.07	35.3	0.06	96	0.24	70.1	120	0.63	1.14
23	7.6	0.08	25.2	0.08	89	0.23	59.9	120	0.61	1.11
25	9.4	0.10	29.8	0.09	90	0.25	60.5	120	0.57	1.10
26	7.7	0.09	24.8	0.10	86	0.25	55.5	120	0.56	1.09
27	11.5	0.12	39.6	0.09	95	0.27	64.1	120	0.51	1.08
28	8.3	0.11	29.1	0.10	91	0.27	58.7	120	0.51	1.09
29	15.1	0.14	67.8	0.21	127	0.46	92.4	120	0.20	1.10
30	24.7	0.16	114.6	0.67	1	0.00	97.2	167	0.16	1.30
31	24.0	0.12	112.1	0.63	1	0.00	97.8	167	0.25	1.15
32	27.4	0.12	113.5	0.59	1	0.00	99.1	167	0.29	1.18
33	30.8	0.13	116.2	0.51	1	0.00	99.2	167	0.36	1.29
34	33.2	0.12	118.2	0.41	1	0.00	99.3	167	0.48	1.18
35	22.6	0.07	103.1	0.24	1	0.00	85.9	167	0.69	1.18
36	19.7	0.06	97.7	0.21	1	0.00	80.9	167	0.73	1.30
40	14.1	0.04	100.2	0.23	1	0.00	86.5	167	0.73	1.18

T (°C)	τ_1 (ns)	a_1	τ_2 (ns)	a_2	τ_3 (ns)	a_3	$\langle\tau\rangle$ (ns)	τ_M (ns)	f_{Mfree}	χ^2
20	7.9	0.08	32.2	0.06	96	0.22	66.8	120	0.65	1.11
23	11.9	0.09	48.2	0.08	103	0.26	73.9	120	0.56	1.04
25	10.6	0.10	36.3	0.08	96	0.26	65.4	120	0.56	1.07
26	6.8	0.08	24.4	0.10	86	0.23	55.8	120	0.58	1.07
27	13.1	0.14	58.6	0.16	115	0.34	78.7	120	0.35	1.00
28	14.9	0.15	64.8	0.19	118	0.31	78.2	120	0.36	1.16
29	14.7	0.15	69.8	0.22	129	0.41	90.6	120	0.23	1.02
30	22.5	0.15	113.0	0.67	1	0.00	96.1	167	0.17	1.20
31	25.1	0.13	114.2	0.64	1	0.00	99.6	167	0.23	1.18
32	29.4	0.12	114.7	0.58	1	0.00	100.1	167	0.29	1.24
33	28.7	0.13	117.0	0.53	1	0.00	99.8	167	0.34	1.20
34	22.9	0.10	108.3	0.41	1	0.00	91.7	167	0.49	1.22
35	17.5	0.07	104.0	0.30	1	0.00	88.2	167	0.63	1.19
36	30.0	0.07	113.2	0.28	1	0.00	96.5	167	0.65	1.21
40	10.6	0.07	106.5	0.27	1	0.00	86.3	167	0.66	1.30

Table SI4.7: Pre-exponential factors and decay times retrieved from the global analysis of the excimer decays for Py_2-PNIPAM(14K) mixtures using the MFA equations. τ_{ES}, when used, was fixed at 3.5 ns.

Initial Temperature Ramp							
T (^{o}C)	f_{Ediff}	τ_{EE0} (ns)	f_{EE0}	τ_{ED} (ns)	f_{ED}	f_{ES}	χ^2
22	0.48	51.0	0.40	88.5	0.13		1.18
23	0.49	51.0	0.39	88.5	0.12		1.13
24	0.46	51.0	0.42	88.5	0.12		1.06
25	0.45	51.0	0.42	88.5	0.13		1.08
26	0.58	51.0	0.36	88.5	0.06		1.22
27	0.56	51.0	0.38	112.0	0.06		1.23
28	0.54	51.0	0.36	112.0	0.10		1.13
29	0.52	51.0	0.35	112.0	0.13		1.05
30	0.51	51.0	0.34	112.0	0.15		1.12
31	0.51	51.0	0.33	112.0	0.16		1.18
32	0.51	51.0	0.31	112.0	0.18		1.16
33	0.49	51.0	0.32	112.0	0.19		1.09
34	0.49	51.0	0.40	112.0	0.12	0.00	0.95
35	0.50	51.0	0.42	135.0	0.05	0.03	1.06
36	0.47	51.0	0.40	135.0	0.05	0.07	1.01
40	0.21	51.0	0.30	135.0	0.02	0.31	1.14
Re-ascending Temperature Ramp							
T (^{o}C)	f_{Ediff}	τ_{EE0} (ns)	f_{EE0}	τ_{ED} (ns)	f_{ED}	f_{ES}	χ^2
20	0.35	51.0	0.46	88.5	0.19		1.14
22	0.36	51.0	0.47	88.5	0.18		1.08
23	0.35	51.0	0.48	88.5	0.17		1.08
24	0.33	51.0	0.48	88.5	0.19		1.11
25	0.33	51.0	0.47	88.5	0.20		1.17
26	0.51	51.0	0.37	88.5	0.12		1.11
27	0.54	51.0	0.39	112.0	0.07		1.13
28	0.53	51.0	0.35	112.0	0.11		1.20
29	0.52	51.0	0.35	112.0	0.13		1.16
30	0.52	51.0	0.34	112.0	0.14		1.16
31	0.50	51.0	0.34	112.0	0.16		1.14
32	0.51	51.0	0.32	112.0	0.16		1.06
33	0.50	51.0	0.32	112.0	0.19		1.04

T (°C)	f_{Ediff}	τ_{EE0} (ns)	f_{EE0}	τ_{ED} (ns)	f_{ED}	f_{ES}	χ^2
34	0.49	51.0	0.31	112.0	0.20	0.00	1.14
35	0.55	51.0	0.36	135.0	0.05	0.04	1.16
36	0.53	51.0	0.37	135.0	0.05	0.05	1.16
38	0.46	51.0	0.38	135.0	0.06	0.09	1.17
40	0.46	51.0	0.36	135.0	0.05	0.13	1.21
20	0.40	51.0	0.45	88.5	0.15		1.14
22	0.38	51.0	0.47	88.5	0.14		1.03
23	0.37	51.0	0.48	88.5	0.14		1.08
24	0.36	51.0	0.49	88.5	0.15		1.12
25	0.35	51.0	0.50	88.5	0.16		1.03
26	0.52	51.0	0.37	88.5	0.10		1.19
27	0.54	51.0	0.38	112.0	0.07		1.18
28	0.52	51.0	0.38	112.0	0.11		1.08
29	0.50	51.0	0.34	112.0	0.12	0.04	1.14
30	0.50	51.0	0.33	112.0	0.13	0.04	1.11
31	0.50	51.0	0.33	112.0	0.15	0.03	1.10
32	0.48	51.0	0.32	112.0	0.16	0.04	1.05
33	0.48	51.0	0.32	112.0	0.19	0.01	1.06
34	0.47	51.0	0.37	112.0	0.12	0.03	1.08
35	0.48	51.0	0.39	135.0	0.05	0.09	1.22
36	0.45	51.0	0.39	135.0	0.05	0.11	1.21
38	0.45	51.0	0.36	135.0	0.04	0.14	1.21
40	0.43	51.0	0.35	135.0	0.05	0.17	1.18
21	0.39	51.0	0.46	88.5	0.15		1.18
37	0.44	51.0	0.38	135.0	0.05	0.13	1.12
39	0.42	51.0	0.38	135.0	0.06	0.15	1.17

Table SI4.8: Pre-exponential factors and decay times retrieved from the global analysis of the excimer decays for Py$_2$-PNIPAM(25K) mixtures using the MFA equations. τ_{ES}, when used, was fixed at 3.5 ns.

Initial Temperature Ramp							
T (°C)	f_{Ediff}	τ_{EE0} (ns)	f_{EE0}	τ_{ED} (ns)	f_{ED}	f_{ES}	χ^2
20	0.66	51.0	0.34	1	0.00	0.00	1.07
23	0.63	51.0	0.37	1	0.00	0.00	1.13

T (°C)	f_{Ediff}	τ_{EE0} (ns)	f_{EE0}	τ_{ED} (ns)	f_{ED}	f_{ES}	χ^2
24	0.65	51.0	0.35	1	0.00	0.00	1.25
25	0.70	51.0	0.29	1	0.00	0.01	1.08
26	0.69	51.0	0.30	1	0.00	0.01	0.98
27	0.68	51.0	0.32	1	0.00	0.00	1.20
28	0.69	51.0	0.31	1	0.00	0.00	1.19
29	0.73	51.0	0.23	135	0.04	0.00	1.22
30	0.68	51.0	0.29	135	0.01	0.01	1.21
31	0.58	51.0	0.36	135	0.06	0.00	1.25
32	0.57	51.0	0.35	135	0.08	0.00	1.27
33	0.58	51.0	0.33	135	0.08	0.00	1.21
34	0.53	51.0	0.36	135	0.11	0.01	1.16
35	0.44	51.0	0.37	135	0.10	0.08	1.22
36	0.35	51.0	0.37	135	0.11	0.16	1.32
40	0.02	51.0	0.36	135	0.17	0.44	1.21

Re-ascending Temperature Ramp

T (°C)	f_{Ediff}	τ_{EE0} (ns)	f_{EE0}	τ_{ED} (ns)	f_{ED}	f_{ES}	χ^2
20	0.72	51.0	0.25	1	0.00	0.03	1.14
23	0.72	51.0	0.24	1	0.00	0.05	1.11
25	0.73	51.0	0.25	1	0.00	0.02	1.10
26	0.72	51.0	0.24	1	0.00	0.04	1.09
27	0.73	51.0	0.27	1	0.00	0.00	1.08
28	0.73	51.0	0.23	1	0.00	0.05	1.09
29	0.79	51.0	0.17	135	0.04	0.00	1.10
30	0.69	51.0	0.30	135	0.01	0.00	1.30
31	0.64	51.0	0.29	135	0.05	0.02	1.15
32	0.60	51.0	0.29	135	0.08	0.02	1.18
33	0.58	51.0	0.30	135	0.12	0.00	1.29
34	0.54	51.0	0.32	135	0.12	0.02	1.18
35	0.40	51.0	0.33	135	0.12	0.14	1.18
36	0.24	51.0	0.33	135	0.13	0.30	1.30
40	0.38	51.0	0.33	135	0.13	0.38	1.18

T (°C)	f_{Ediff}	τ_{EE0} (ns)	f_{EE0}	τ_{ED} (ns)	f_{ED}	f_{ES}	χ^2
20	0.73	51.0	0.20	1	0.00	0.08	1.11
23	0.75	51.0	0.25	1	0.00	0.00	1.04
25	0.74	51.0	0.25	1	0.00	0.01	1.07
26	0.72	51.0	0.23	1	0.00	0.05	1.07
27	0.77	51.0	0.22	135	0.01	0.00	1.00
28	0.76	51.0	0.23	135	0.01	0.00	1.16
29	0.78	51.0	0.18	135	0.04	0.00	1.02

30	0.70	51.0	0.30	135	0.00	0.00	1.20
31	0.65	51.0	0.29	135	0.04	0.02	1.18
32	0.61	51.0	0.29	135	0.07	0.02	1.24
33	0.58	51.0	0.29	135	0.10	0.03	1.20
34	0.53	51.0	0.30	135	0.10	0.07	1.22
35	0.47	51.0	0.31	135	0.09	0.13	1.19
36	0.37	51.0	0.32	135	0.10	0.21	1.21
40	0.31	51.0	0.26	135	0.09	0.34	1.30

Table SI4.9: Fractions of all pyrene species calculated from f_{Mfree}, f_{Mdiff}, f_{Ediff}, f_{EE0}, f_{ED} and f_{ES} for aqueous Py_2-PNIPAM(14K) mixtures.

Initial Temperature Ramp						
T (°C)	f_{diff}	f_{free}	f_{E0}	f_{EL}	f_{ES}	f_{agg}
22	0.30	0.38	0.24	0.08	0.00	0.32
23	0.31	0.36	0.25	0.08	0.00	0.33
24	0.30	0.35	0.27	0.08	0.00	0.35
25	0.30	0.34	0.28	0.09	0.00	0.37
26	0.53	0.09	0.33	0.05	0.00	0.38
27	0.50	0.11	0.34	0.06	0.00	0.39
28	0.48	0.11	0.32	0.09	0.00	0.41
29	0.46	0.11	0.32	0.12	0.00	0.43
30	0.45	0.11	0.30	0.13	0.00	0.43
31	0.44	0.13	0.29	0.14	0.00	0.43
32	0.45	0.13	0.27	0.15	0.00	0.42
33	0.40	0.18	0.26	0.15	0.00	0.41
34	0.38	0.23	0.31	0.09	0.00	0.40
35	0.32	0.37	0.27	0.03	0.02	0.32
36	0.28	0.41	0.24	0.03	0.04	0.31
40	0.12	0.53	0.17	0.01	0.18	0.36
Re-ascending Temperature Ramp						
T (°C)	f_{diff}	f_{free}	f_{E0}	f_{EL}	f_{ES}	f_{agg}
20	0.21	0.41	0.27	0.11	0.00	0.38
22	0.22	0.38	0.29	0.11	0.00	0.40
23	0.22	0.36	0.30	0.11	0.00	0.41
24	0.22	0.34	0.32	0.12	0.00	0.44
25	0.22	0.31	0.33	0.14	0.00	0.46
26	0.48	0.06	0.35	0.11	0.00	0.46

T ($^{\circ}$C)	f_{diff}	f_{free}	f_{E0}	f_{EL}	f_{ES}	f_{agg}
27	0.49	0.09	0.35	0.07	0.00	0.42
28	0.49	0.08	0.32	0.10	0.00	0.43
29	0.48	0.08	0.32	0.12	0.00	0.44
30	0.47	0.10	0.31	0.13	0.00	0.44
31	0.46	0.08	0.31	0.15	0.00	0.46
32	0.47	0.08	0.29	0.15	0.00	0.45
33	0.44	0.11	0.28	0.17	0.00	0.45
34	0.43	0.12	0.27	0.18	0.00	0.44
35	0.45	0.18	0.30	0.04	0.04	0.37
36	0.38	0.28	0.27	0.04	0.03	0.34
38	0.31	0.32	0.26	0.04	0.06	0.36
40	0.29	0.38	0.22	0.03	0.08	0.33
T ($^{\circ}$C)	f_{diff}	f_{free}	f_{E0}	f_{EL}	f_{ES}	f_{agg}
20	0.23	0.43	0.26	0.09	0.00	0.34
22	0.23	0.39	0.29	0.09	0.00	0.37
23	0.23	0.38	0.30	0.09	0.00	0.39
24	0.23	0.36	0.31	0.09	0.00	0.41
25	0.23	0.34	0.33	0.10	0.00	0.43
26	0.49	0.06	0.35	0.10	0.00	0.45
27	0.50	0.09	0.35	0.07	0.00	0.42
28	0.47	0.09	0.34	0.10	0.00	0.44
29	0.47	0.07	0.31	0.11	0.04	0.46
30	0.46	0.08	0.30	0.12	0.04	0.46
31	0.47	0.07	0.30	0.14	0.02	0.46
32	0.44	0.09	0.30	0.14	0.04	0.48
33	0.42	0.11	0.29	0.16	0.01	0.46
34	0.39	0.17	0.31	0.10	0.03	0.44
35	0.34	0.29	0.27	0.03	0.06	0.37
36	0.30	0.34	0.26	0.03	0.07	0.36
38	0.27	0.41	0.22	0.03	0.08	0.32
40	0.26	0.40	0.21	0.03	0.10	0.34
21	0.23	0.41	0.27	0.09	0.00	0.36
37	0.28	0.37	0.24	0.03	0.08	0.36
39	0.25	0.40	0.23	0.03	0.09	0.35

Table SI4.10: Fractions of all pyrene species calculated from f_{Mfree}, f_{Mdiff}, f_{Ediff}, f_{EE0}, f_{ED} and f_{ES} for aqueous Py$_2$-PNIPAM(25K) mixtures.

Initial Temperature Ramp						
T ($^{\circ}$C)	f_{diff}	f_{free}	f_{E0}	f_{EL}	f_{ES}	f_{agg}

20	0.40	0.40	0.21	0.00	0.00	0.21
23	0.35	0.44	0.20	0.00	0.00	0.20
24	0.39	0.40	0.21	0.00	0.00	0.21
25	0.45	0.36	0.19	0.00	0.01	0.19
26	0.42	0.39	0.18	0.00	0.00	0.19
27	0.44	0.36	0.20	0.00	0.00	0.20
28	0.43	0.38	0.19	0.00	0.00	0.19
29	0.63	0.13	0.20	0.03	0.00	0.23
30	0.68	0.00	0.29	0.01	0.01	0.32
31	0.49	0.15	0.30	0.05	0.00	0.36
32	0.46	0.19	0.28	0.07	0.00	0.35
33	0.46	0.22	0.26	0.07	0.00	0.33
34	0.35	0.33	0.24	0.07	0.01	0.31
35	0.27	0.40	0.22	0.06	0.05	0.34
36	0.20	0.43	0.21	0.07	0.09	0.37
40	0.02	0.07	0.34	0.16	0.41	0.91

Re-ascending Temperature Ramp

T (^{o}C)	f_{diff}	f_{free}	f_{E0}	f_{EL}	f_{ES}	f_{agg}
20	0.33	0.55	0.11	0.00	0.01	0.12
23	0.33	0.53	0.11	0.00	0.02	0.13
25	0.37	0.49	0.13	0.00	0.01	0.14
26	0.37	0.48	0.13	0.00	0.02	0.14
27	0.41	0.43	0.15	0.00	0.00	0.15
28	0.41	0.43	0.13	0.00	0.03	0.16
29	0.66	0.16	0.14	0.03	0.00	0.18
30	0.61	0.12	0.27	0.01	0.00	0.27
31	0.53	0.18	0.24	0.04	0.02	0.30
32	0.48	0.20	0.23	0.07	0.02	0.32
33	0.44	0.25	0.23	0.09	0.00	0.31
34	0.36	0.33	0.21	0.08	0.02	0.31
35	0.21	0.47	0.18	0.06	0.08	0.31
36	0.15	0.39	0.20	0.08	0.18	0.46
40	0.17	0.46	0.15	0.06	0.17	0.37

T (^{o}C)	f_{diff}	f_{free}	f_{E0}	f_{EL}	f_{ES}	f_{agg}
20	0.31	0.57	0.08	0.00	0.03	0.12
23	0.38	0.49	0.13	0.00	0.00	0.13
25	0.38	0.48	0.13	0.00	0.01	0.13
26	0.36	0.50	0.11	0.00	0.02	0.14
27	0.54	0.30	0.15	0.01	0.00	0.16
28	0.53	0.29	0.17	0.01	0.00	0.17

29	0.63	0.18	0.14	0.04	0.00	0.18
30	0.61	0.13	0.26	0.00	0.00	0.27
31	0.54	0.16	0.24	0.04	0.02	0.29
32	0.49	0.20	0.23	0.06	0.02	0.31
33	0.45	0.23	0.22	0.08	0.02	0.32
34	0.35	0.33	0.20	0.07	0.04	0.31
35	0.26	0.44	0.17	0.05	0.07	0.29
36	0.22	0.41	0.19	0.06	0.13	0.37
40	0.19	0.37	0.16	0.06	0.21	0.43

Table SI4.11: (I_E/I_M) values from steady-state and time resolved fluorescence.

Py$_2$-PNIPAM(14K)				Py$_2$-PNIPAM(25K)			
Initial Temperature Ramp		Re-ascending Temperature Ramp		Initial Temperature Ramp		Re-ascending Temperature Ramp	
T (^{o}C)	$(I_E/I_M)^{SS}$	T (^{o}C)	$(I_E/I_M)^{SS}$	T (^{o}C)	$(I_E/I_M)^{SS}$	T (^{o}C)	$(I_E/I_M)^{SS}$
15	0.47417	20	0.66542	20	0.13771	20	0.10783
20	0.66223	22	0.7305	25	0.24666	23	0.15322
22	0.73305	23	0.7764	26	0.2663	24	0.16764
23	0.75376	24	0.82239	27	0.29423	25	0.19573
24	0.78644	25	0.8559	28	0.30068	26	0.21361
25	0.76344	26	0.79843	29	0.23303	27	0.23433
26	0.70611	27	0.7165	30	0.18912	28	0.24642
27	0.65157	28	0.68935	31	0.16045	29	0.18973
28	0.64691	29	0.68118	32	0.15555	30	0.16324
29	0.63294	30	0.66804	33	0.09072	31	0.12959
30	0.61571	31	0.66855	34	0.03646	32	0.12636
31	0.60055	32	0.64453	35	0.00827	33	0.07711
32	0.60747	33	0.5995	36	0.00408	34	0.02795
33	0.54269	34	0.46054	40	0	35	0.00862
34	0.31752	36	0.3007			36	0.00742
35	0.18902	38	0.17994			40	0
36	0.12408	40	0.09113				
40	0.04881						

Py$_2$-PNIPAM(45K)	
T (^{o}C)	$(I_E/I_M)^{SPC}$
10	0.02478
15	0.0269
20	0.05959
25	0.11053
26	0.12868

27	0.15424
28	0.18823
29	0.19732
30	0.08548
31	0.05201
32	0.04107
40	0.02498

Figure SI5.1. Plot of k_{cy} versus M_n for pyrene end-labelled linear poly(ethylene oxide). (□) study by Ghiggino et al.[1] and (■) this study.

Figure SI5.2. Plot of k_{cy} versus M_n for pyrene end-labelled linear polystyrene. (□) study by Winnik et al.[2] and (■) this study.
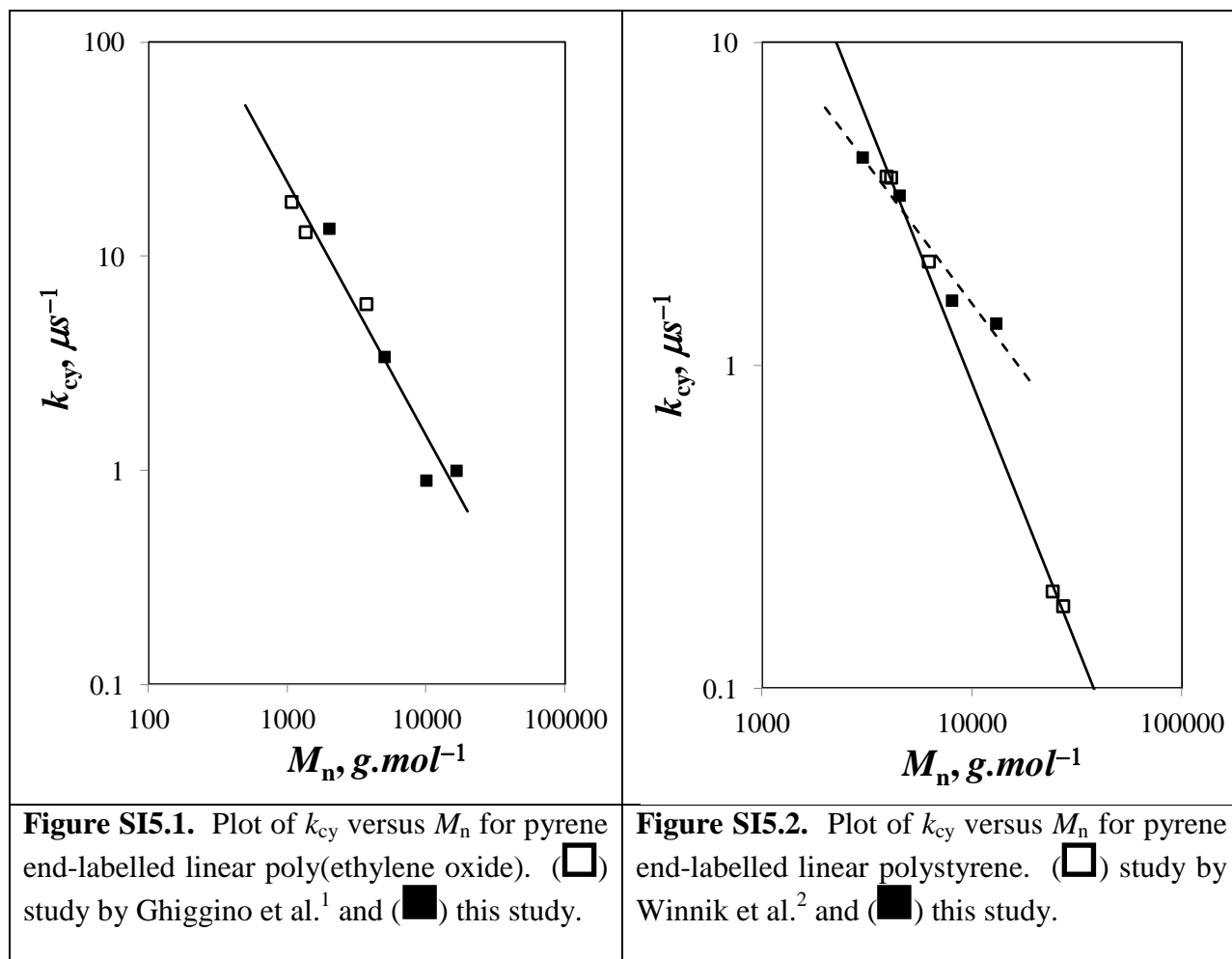
Fluorescence Spectra of Pyrene Labelled Polystyrene
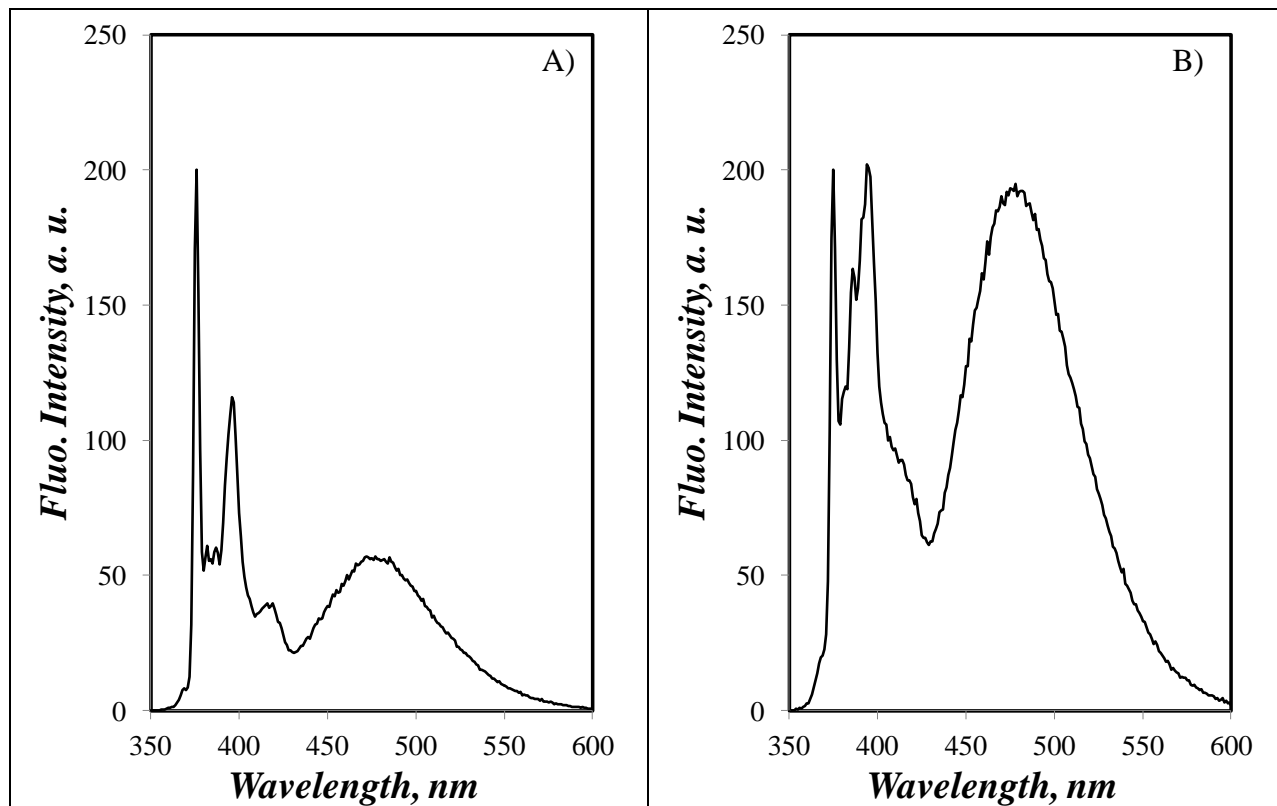
Figure SI5.3. Fluorescence spectra in tetrahydrofuran of A) CoEs-PS-BuPy labeled with 3.1 mol% of pyrene (left; $(I_E/I_M)^{SPC} = 0.27$) and B) CoEt-PS-MPy labeled with 3.2 mol% of pyrene (right; $(I_E/I_M)^{SPC} = 0.81$). [Py] = 2.5×10^{-6} mol.L^{-1}.

The 0-0 transition at 375 nm is allowed for the 1-pyrenebutyl derivative in CoEs-PS-BuPy (Figure S5.3.A) and partially forbidden for 1-pyrenemethyl in CoEt-PS-MPy (Figure SI5.3.B).

Analysis of the Fluorescence Decays

Model Free Analysis

All pyrene monomer and excimer fluorescence decays were fitted globally according to the model free (MF) analysis which has been described in details in a number of publications.[3–7] The different pyrene species encountered with pyrene-labelled macromolecules are Py^*_{diff}, the excited pyrene that diffusively encounters another ground-state pyrene species to form an excimer, Py^*_{free}, the excited pyrene located in a pyrene-poor environment that cannot form an excimer and emits with the natural lifetime of the pyrenyl label (τ_M), $E0^*$, the excimer formed by properly stacked pyrene dimers that emits with a lifetime τ_{E0}, and D^*, the excimer formed by improperly stacked pyrene dimers that emits with a lifetime τ_D that is different from τ_{E0}. All monomer decays were fitted with Equation SI5.1.

$$[Py^*_{diff}]_{(t)} = [Py^*_{diff}]_{(t=0)} \times \sum_{i=1}^{n} a_i \times \exp(-t/\tau_i) + [Py^*_{free}]_{(t=0)} \times \exp(-t/\tau_M)$$

$$\text{(SI5.1)}$$

The pre-exponential factors a_i in the analysis are normalized so that $\sum_{i=1}^{n} a_i = 1$. The lifetime of the pyrene monomer (τ_M) is fixed in the analysis and obtained with a model compound. All pyrene excimer decays except those acquired with the CoA-PS-MPy series were fitted with Equation SI5.2 which assumes that the species $E0^*$ is generated by either direct excitation of a properly stacked pyrene dimer, or diffusive encounter between Py^*_{diff} and a ground-state pyrene

species.[3-6] The species D^* can only be produced via direct excitation of an improperly stacked pyrene dimer.

$$[E^*]_{(t)} = -[Py^*_{diff}]_{(t=0)} \times \sum_{i=1}^{n} a_i \frac{\frac{1}{\tau_i} - \frac{1}{\tau_M}}{\frac{1}{\tau_i} - \frac{1}{\tau_{E0}}} \exp(-t/\tau_i)$$

$$+ \left([E0^*]_{(t=0)} + [Py^*_{diff}]_{(t=0)} \times \sum_{i=1}^{n} a_i \frac{\frac{1}{\tau_i} - \frac{1}{\tau_M}}{\frac{1}{\tau_i} - \frac{1}{\tau_{E0}}} \right) \times \exp(-t/\tau_{E0}) + [D^*]_{(t=0)} \times \exp(-t/\tau_D)$$

(SI5.2)

Integration over time of Equations SI5.1 and SI5.2 yields the $(I_E/I_M)^{SPC}$ ratio whose expression is given in Equation SI5.3.

$$\left(\frac{I_E}{I_M} \right)^{SPC} = \frac{-f_{diff} \times \sum_{i=1}^{n} a_i \frac{\frac{1}{\tau_i} - \frac{1}{\tau_M}}{\frac{1}{\tau_i} - \frac{1}{\tau_{E0}}} \times \tau_i + \left(f_{E0} + f_{diff} \times \sum_{i=1}^{n} a_i \frac{\frac{1}{\tau_i} - \frac{1}{\tau_M}}{\frac{1}{\tau_i} - \frac{1}{\tau_{E0}}} \right) \times \tau_{E0} + f_D \times \tau_D}{f_{diff} \times \sum_{i=1}^{n} a_i \times \tau_i + f_{free} \times \tau_M}$$

(SI5.3)

Interestingly, Equation SI5.3 which has been used in a number of studies[4-7] can be rearranged into a much simpler form shown in Equation SI5.4. The number-average lifetime $<\tau>$ in Equation SI5.4 equals $\sum_{i=1}^{n} a_i \times \tau_i$ and the average rate constant of excimer formation $<k>$ equals $<\tau>^{-1} - <\tau_M>^{-1}$.

$$\left(\frac{I_E}{I_M} \right)^{SPC} = \frac{f_{diff} \times <k> \times \tau_{E0} \times <\tau> + f_{E0} \times \tau_{E0} + f_D \times \tau_D}{f_{diff} \times <\tau> + f_{free} \times \tau_M}$$

(SI5.4)

Setting $f_{\text{free}} = 0$ in Equation S4 yields the $(I_E/I_M)_{f_{free}=0}^{SPC}$ ratio.

In cases where the pyrenyl labels are clustered and cannot rearrange rapidly, both $E0^*$ and D^* can be formed by diffusive encounters and direct excitation.[7] The excimer fluorescence decays are then fitted with Equation SI5.5 which was used for the CoA-PS-MPy series. The rigid amide bond connecting the pyrenyl label to the polystyrene backbone for the CoA-PS-MPy series is certainly responsible for the slow rearrangement of the pyrene pendants which results in the formation of D^* species by diffusive encounters.

$$[E^*]_{(t)} = -[Py_{diff}^*(E0)]_{(t=0)} \times \sum_{i=1}^{n} a_i \frac{\dfrac{1}{\tau_i} - \dfrac{1}{\tau_M}}{\dfrac{1}{\tau_i} - \dfrac{1}{\tau_{E0}}} \exp(-t/\tau_i)$$

$$+ \left([E0^*]_{(t=0)} + [Py_{diff}^*(E0)]_{(t=0)} \times \sum_{i=1}^{n} a_i \frac{\dfrac{1}{\tau_i} - \dfrac{1}{\tau_M}}{\dfrac{1}{\tau_i} - \dfrac{1}{\tau_{E0}}} \right) \times \exp(-t/\tau_{E0})$$

$$- [Py_{diff}^*(D)]_{(t=0)} \times \sum_{i=1}^{n} a_i \frac{\dfrac{1}{\tau_i} - \dfrac{1}{\tau_M}}{\dfrac{1}{\tau_i} - \dfrac{1}{\tau_D}} \exp(-t/\tau_i) + \left([D^*]_{(t=0)} + [Py_{diff}^*(D)]_{(t=0)} \times \sum_{i=1}^{n} a_i \frac{\dfrac{1}{\tau_i} - \dfrac{1}{\tau_M}}{\dfrac{1}{\tau_i} - \dfrac{1}{\tau_D}} \right) \times \exp(-t/\tau_D)$$

$$\text{(SI5.5)}$$

In Equation SI5.5, the concentrations $[Py_{diff}^*(E0)]$ and $[Py_{diff}^*(D)]$ describe those excited pyrene monomer that form the species $E0^*$ and D^* by diffusion, respectively. Integration over time of Equations SI5.1 and SI5.5 yields the $(I_E/I_M)^{SPC}$ ratio given in Equation SI5.6 which takes a form similar to that of Equation SI5.4.

$$\left(\frac{I_E}{I_M}\right)^{SPC} = \frac{\left(f_{diff}^{E0} \times \tau_{E0} + f_{diff}^{D} \times \tau_{E0}\right) \times <k> \times <\tau> + f_{E0} \times \tau_{E0} + f_D \times \tau_D}{\left(f_{diff}^{E0} + f_{diff}^{D}\right) \times <\tau> + f_{free} \times \tau_M}$$

(SI5.6)

The parameters f_{diff}^{E0} and f_{diff}^{D} represent the molar fractions of the species $[Py_{diff}^{*}(E0)]$ and

$[Py_{diff}^{*}(D)]$. Setting $f_{\text{free}} = 0$ in Equation SI5.6 yields the $\left(I_E/I_M\right)_{f_{free}=0}^{SPC}$ ratio.

The results from the MF analysis of the monomer and excimer fluorescence decays are listed in

Tables S1-4.

Birks' Scheme Analysis

The fluorescence decays acquired with the pyrene end-labelled linear chains were also fitted

according to Birks' scheme described in Scheme SI5.1.[8-10]
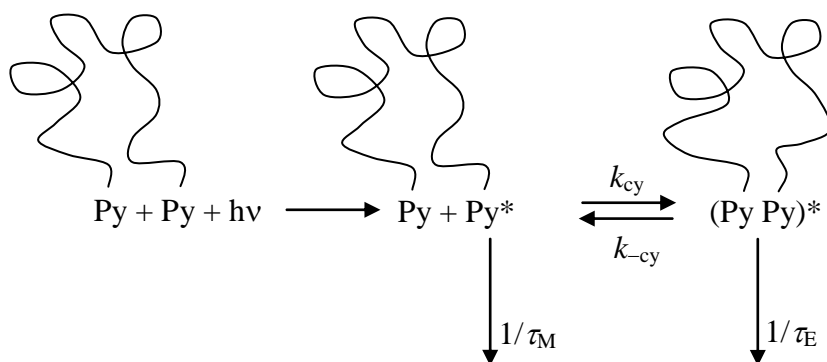
Scheme SI5.1. Excimer formation between the two pyrene-labelled ends of a monodispersed

polymer according to Birks' scheme.

According to Scheme SI5.1, the monomer and excimer fluorescence decays can be fitted by

Equations SI5.7 and SI5.8, respectively.

286

$$[Py^*] = \frac{[Py^*_{diff}]_o}{\sqrt{(X-Y)^2 + 4k_{cy}k_{-cy}}} \left((X - \tau_2^{-1}) \times \exp(-t/\tau_1) - (X - \tau_1^{-1}) \times \exp(-t/\tau_2) \right)$$

$$+ [Py^*_{free}]_o \exp(-t/\tau_M) + [Py^*_S]_o \exp(-t/\tau_S) \qquad\qquad \text{(SI5.7)}$$

$$[E^*] = \frac{k_{cy}[Py^*_{diff}]_o}{\sqrt{(X-Y)^2 + 4k_{cy}k_{-cy}}} \left(-\exp(-t/\tau_1) + \exp(-t/\tau_2) \right) + [Py^*_S]_o \exp(-t/\tau_S)$$

$$\text{(SI5.8)}$$

The parameters X and Y equal $k_{cy} + \tau_M^{-1}$ and $k_{-cy} + \tau_E^{-1}$, respectively, and the expression of the

decay times τ_1 and τ_2 is given in Equations SI5.9 and SI5.10, respectively. Equations SI5.7 and

SI5.8 use the concentrations of pyrenes that form excimer by diffusion, $[Py^*_{diff}]_o$, do not form

excimer because they are attached onto monolabeled chains, $[Py^*_{free}]_o$, and form poorly stacked

excimers, $[Py^*_S]_o$, that emit with a short lifetime τ_S.

$$\tau_1^{-1} = \frac{X + Y + \sqrt{(X-Y)^2 + 4k_{cy}k_{-cy}}}{2} \qquad\qquad \text{(SI5.9)}$$

$$\tau_2^{-1} = \frac{X + Y - \sqrt{(X-Y)^2 + 4k_{cy}k_{-cy}}}{2} \qquad\qquad \text{(SI5.10)}$$

In Equations SI5.7 and SI5.8, the decay times and pre-exponential factors were optimized with respect to the kinetic parameters, k_{cy}, k_{-cy}, and τ_{E0}. This feature enables the experimentalist to fix a given parameter to improve the recovery of the remaining floating parameters.

Fluorescence Blob Model (FBM) Analysis

The pyrene monomer and excimer fluorescence decays of the polystyrene samples randomly labelled with pyrene (CoEs-PS-BuPy, CoEt-PS-MPy, and CoAm-PS-MPy) were fitted globally according to the FBM.[11-13] Within the framework of the FBM, the species Py^*_{diff} describes the slow diffusive motion of the structural units bearing the pyrene labels. The slow diffusive motion is accounted for by the parameters $<n>$, k_{blob}, and $k_e\times[blob]$ which represent the average number of pyrene labels per *blob*, the rate constant of excimer formation between one excited pyrene and one ground-state pyrene located inside a same *blob*, and the exchange of ground-state pyrenes from one *blob* to another, respectively. When two structural units with a pyrene label encounter, they generate the pyrene species Py^*_{k2} which undergoes a rapid rearrangement with a rate constant k_2 resulting in excimer formation. The geometrical constraints imposed by the pyrene-labelled polymer leads to the formation of pyrene pairs which are either properly or improperly stacked and lead to, respectively, excimer ($E0^*$) or dimer (D^*) formation upon direct excitation. The excited dimers emit with a lifetime τ_{E0} and τ_D, respectively. The pyrene species that are located in pyrene-poor domains along the chain cannot form excimer, emit with the natural lifetime of the pyrene monomer τ_M, and are referred to as Py^*_{free}. The fluorescence decays of the pyrene monomer and excimer acquired with the randomly labelled polystyrenes were fitted with Equations SI5.11 and SI5.12.

$$[Py^*]_{(t)} = [Py^*_{diff}]_{(t)} + [Py^*_{k2}]_{(t)} + [Py^*_{free}]_{(t)} = [Py^*_{diff}]_o \exp\left(-\left(A_2 + \frac{1}{\tau_M}\right)t - A_3\left(1 - \exp(-A_4 t)\right)\right)$$

$$+ \left([Py^*_{k2}]_o + [Py^*_{diff}]_o e^{-A_3} \sum_{i=0}^{\infty} \frac{A_3^i}{i!} \frac{A_2 + iA_4}{A_2 + iA_4 - k_2}\right) \exp\left(-\left(k_2 + \frac{1}{\tau_M}\right)t\right)$$

$$- [Py^*_{diff}]_o e^{-A_3} \sum_{i=0}^{\infty} \frac{A_3^i}{i!} \frac{A_2 + iA_4}{A_2 + iA_4 - k_2} \exp\left(-\left(A_2 + iA_4 + \frac{1}{\tau_M}\right)t\right)$$

$$+ [Py^*_{free}]_o \exp\left(-\frac{t}{\tau_M}\right) \Bigg] \tag{SI5.11}$$

$$[E^*]_{(t)} = [E0^*]_{(t)} + [D^*]_{(t)} = k_2 \Bigg(\left([Py^*_{k2}]_o + [Py^*_{diff}]_o e^{-A_3} \sum_{i=0}^{\infty} \frac{A_3^i}{i!} \frac{A_2 + iA_4}{A_2 + iA_4 - k_2}\right)$$

$$\times \frac{\exp\left(-\dfrac{t}{\tau_{E0}}\right) - \exp\left(-\left(k_2 + \dfrac{1}{\tau_M}\right)t\right)}{k_2 + \dfrac{1}{\tau_M} - \dfrac{1}{\tau_{E0}}}$$

$$+ [Py^*_{diff}]_o e^{-A_3} \sum_{i=0}^{\infty} \frac{A_3^i}{i!} \frac{A_2 + iA_4}{A_2 + iA_4 - k_2} \frac{\exp\left(-\left(A_2 + iA_4 + \dfrac{1}{\tau_M}\right)t\right) - \exp\left(-\dfrac{t}{\tau_{E0}}\right)}{A_2 + iA_4 + \dfrac{1}{\tau_M} - \dfrac{1}{\tau_{E0}}} \Bigg)$$

$$+ [E0^*]_o \times \exp\left(-\frac{t}{\tau_{E0}}\right) + [D^*]_o \times \exp\left(-\frac{t}{\tau_D}\right) \tag{SI5.12}$$

The expression of the parameters A_2, A_3, and A_4 used in Equations SI5.11 and SI5.12 is given in Equations SI5.13 – SI5.15 as a function of $<n>$, k_{blob}, and $k_e[blob]$.

$$A_2 = <n> \frac{k_{blob}k_e[blob]}{k_{blob} + k_e[blob]} \qquad \text{(SI5.13)}$$

$$A_3 = <n> \frac{\left(k_{blob}\right)^2}{\left(k_{blob} + k_e[blob]\right)^2} \qquad \text{(SI5.14)}$$

$$A_4 = k_{blob} + k_e[blob] \qquad \text{(SI5.15)}$$

Fitting the monomer and excimer decays using Equations SI5.11 and SI5.12 yields the parameters $<n>$, k_{blob}, and $k_e[blob]$. Fitting the monomer decays using Equation SI5.11 also yields the fractions f_{Mdiff}, f_{Mk2}, and f_{Mfree} which represent the molar fractions of the Py^*_{diff}, $Py^*_{k_2}$, and Py^*_{free} species contributing to the monomer decays, respectively. In a similar manner, fitting the excimer decays with Equation SI5.12 yields the fractions f_{Ediff}, f_{Ek2}, f_{EE0}, and f_{ED} which represent the molar fractions of the species Py^*_{diff}, $Py^*_{k_2}$, $E0^*$, and D^* contributing to the excimer decays, respectively. The fractions f_{Mdiff}, f_{Mk2}, f_{Mfree}, f_{Ediff}, f_{Ek2}, f_{EE0}, and f_{ED} can then be combined to determine the overall molar fractions of each pyrene species present in solution f_{diff}, f_{k2}, f_{free}, f_{E0}, and f_D.

The fraction f_{Mfree} together with $<n>$ and the pyrene content λ_{Py} (see Table 1 in the main text) can be used to determine N_{blob}, the average number of structural units per *blob* given in Equation SI5.16.

$$N_{blob} = \frac{<n>}{\frac{\lambda_{Py}}{(1-f_{Mfree})} \times (x \times M_{Py} + (1-x) \times M)} \qquad \text{(SI5.16)}$$

In Equation SI5.16, M_{Py} and M represent the molar mass of the pyrene labelled and unlabelled monomer. x is the fraction of pyrene-labelled monomers in the polymer.

References

Ghiggino, K. P.; Snare, M. J.; Thistlethwaite, P. J. *Eur. Polym. J.* **1985**, *21*, 265– 272.

Winnik, M. A.; Redpath, T.; Richards, D. H. *Macromolecules* **1980**, *13*, 328-335.

Siu, H.; Duhamel, J. *J. Phys. Chem. B* **2005**, *109*, 1770-1780.

Yip, J.; Duhamel, J.; Bahun, G.; Adronov, A. *J. Phys. Chem. B* **2010**, *114*, 10254-10265.

Chen, S.; Duhamel, J.; Bahun, G.; Adronov, A. *J. Phys. Chem. B* **2011**, *115*, 9921-9929.

Siu, H., Duhamel, J. *J. Phys. Chem. B* **2012**, *116*, 1226-1233.

Keyes-Baig, C.; Duhamel, J.; Wettig, S. *Langmuir* **2011**, *27*, 3361–3371.

Birks, J. B. *Photophysics of Aromatic Molecules*. Wiley: New York, 1970; p 301.

Winnik, M. A. *Acc. Chem. Res.* **1985**, *18*, 73-79.

Chen, S.; Duhamel, J.; Winnik, M. A. *J. Phys. Chem. B* **2011**, *115*, 3289-3302.

Mathew, A.; Siu, H.; Duhamel, J. *Macromolecules* **1999**, *32*, 7100– 7108.

Duhamel, J. *Acc. Chem. Res.* **2006**, *39*, 953-960.

Ingratta, M.; Mathew, M.; Duhamel, J. *Can. J. Chem.* **2010**, *88*, 217-227.

Table SI5.1. Pre-exponential factors and decay times retrieved from the global MF-analysis of the monomer decays for various samples in THF. The a_i pre-exponential factors are not normalized and their sum equals $f_{Mdiff} = 1 - f_{Mfree}$.

Sample	mol%	τ_1 (ns)	a_1	τ_2 (ns)	a_2	τ_3 (ns)	a_3	$<\tau>$ (ns)	f_{Mfree}	χ^2
CoE-PS-MPy $\tau_M = 257$ ns	1.5	18.4	0.21	55.1	0.31	149	0.39	87.2	0.10	1.24
	1.8	16.9	0.22	52.0	0.33	136	0.38	78.0	0.07	1.07
	3.2	13.1	0.23	37.0	0.44	107	0.30	53.1	0.03	1.02
	4.8	11.4	0.38	33.2	0.43	89.8	0.17	34.4	0.02	1.13
	5.1	8.7	0.28	27.7	0.50	75.7	0.21	32.7	0.01	1.12
	6.4	7.2	0.35	22.6	0.49	59.3	0.15	22.7	0.01	1.16
CoA-PS-MPy $\tau_M = 253$ ns	2.5	11.4	0.11	47.1	0.35	119	0.52	81.3	0.03	1.14
	3.7	8.8	0.12	43.3	0.46	106	0.41	65.3	0.01	1.00
	5.0	7.4	0.14	35.9	0.50	85.9	0.36	50.0	0.01	1.10
	5.2	7.3	0.14	36.1	0.54	87.3	0.31	48.2	0.01	1.02
	6.4	7.4	0.19	31.2	0.54	70.8	0.26	37.0	0.00	1.07
CoBuE-PS-BuPy $\tau_M = 200$ ns	2.1	17.7	0.15	52.0	0.31	122	0.47	81.9	0.07	1.11
	3.1	12.5	0.18	39.8	0.40	102	0.39	60.1	0.03	1.05
	4.5	7.6	0.17	27.2	0.48	73.6	0.34	40.0	0.01	1.16
	5.4	10.3	0.27	27.2	0.40	63.3	0.32	34.3	0.01	1.14
	6.0	9.9	0.31	28.8	0.47	66.6	0.22	31.3	0.00	1.07
PS-BuPy2 $\tau_M = 190$ ns	6.9	39.2	0.06	114	0.94			110	0.14	1.30
	4.6	46.0	0.06	131	0.94			125	0.11	1.02
	2.6	45.9	0.02	154	0.98			152	0.19	1.04
	1.6	54.9	0.03	162	0.97			159	0.46	1.14
PEO-MPy2 $\tau_M = 258$ ns	4.4	39	0.29	72	0.71				0.03	1.00
	1.8	67	0.05	149	0.95				0.07	1.33
	0.9	103	0.02	223	0.98				0.09	1.19
	0.6	96	0.02	223	0.98				0.57	1.22
PA-G1-BuPy$_2$	n.a.	17.3	0.72	52.8	0.27			27.0	0.01	1.12
PA-G2-BuPy$_4$		2.4	0.51	7.4	0.45	48.0	0.04	6.7	0.00	1.16
PP-G1-BuPy$_2$	n.a.	1.95	0.27	5.09	0.67	32.0	0.03	4.98	0.03	1.15
PP-G2-BuPy$_4$		1.85	0.53	3.56	0.44	28.3	0.02	3.15	0.01	1.18
PP-G3-BuPy$_8$		1.49	0.64	2.56	0.34	29.1	0.01	2.13	0.00	1.08
PP-G4-BuPy$_{16}$		1.19	0.83	2.46	0.13	25.1	0.01	1.70	0.03	1.11
PP-G4-BuPy$_{16}$-Pure		1.38	0.84	2.93	0.15	38.0	0.01	1.89	0.00	1.19

τ_M = 210 ns								

Table SI5.2. Pre-exponential factors and decay times retrieved from the global MF-analysis of the excimer decays for various samples in THF.

Sample	mol%	τ_{EE0}	f_{Ediff}^{E0}	f_{EE0}	τ_D	f_{Ediff}^{D}	f_{ED}	χ^2
CoE-PS-MPy τ_M = 257 ns	1.5	55.1	0.91	0.08				1.24
	1.8	55.2	0.92	0.08				1.07
	3.2	53.4	0.86	0.14				1.02
	4.8	52.3	0.83	0.17				1.13
	5.1	49.8	0.88	0.12				1.12
	6.4	50.3	0.87	0.13				1.16
CoA-PS-MPy τ_M = 253 ns	2.5	49.3	0.75	0.00	67.4	0.18	0.07	1.14
	3.	40.2	0.49	0.00	63.5	0.46	0.05	1.00
	5.0	37.5	0.47	0.00	61.2	0.48	0.05	1.10
	5.2	38.4	0.44	0.06	62.0	0.49	0.00	1.02
	6.4	43.8	0.64	0.06	64.2	0.28	0.02	1.07
CoBuE-PS-BuPy τ_M = 200 ns	2.1	53.2	0.95	0.00	93.1		0.05	1.11
	3.1	54.0	0.96	0.00	99.4		0.04	1.05
	4.5	53.4	0.96	0.00	77.9		0.04	1.16
	5.4	52.1	0.94	0.00	81.6		0.06	1.14
	6.	53.1	0.94	0.04	95.4		0.02	1.07
PS-BuPy2 τ_M = 190 ns	6.9	55	0.99	0.01				1.30
	4.6	55	0.99	0.01				1.02
	2.6	55	0.99	0.01				1.04
	1.6	55	0.99	0.01				1.14
PEO-MPy2 τ_M = 258 ns	4.4	48	0.90	0.02	3.5		0.08	1.00
	1.8	48	0.97	0.02	3.5		0.01	1.33
	0.9	48	0.92	0.01	3.5		0.07	1.19
	0.6	48	0.92	0.01	3.5		0.06	1.22
PA-G1-BuPy$_2$	n.a.	48.9	0.97	0.03				1.12
PA-G2-BuPy$_4$		42.1	0.59	0.00	57.0	0.38	0.02	1.16
PP-G1-BuPy$_2$	n.a.	53.2	0.98	0.01	4.0		0.01	1.15
PP-G2-BuPy$_4$		52.6	0.90	0.05	4.0		0.05	1.18
PP-G3-BuPy$_8$		52.8	0.88	0.03	4.0		0.09	1.08
PP-G4-BuPy$_{16}$		53.2	0.87	0.07	4.0		0.07	1.11
PP-G4-BuPy$_{16}$- Pure τ_M = 210 ns		52.8	0.82	0.00	4.0		0.18	1.19

Table SI5.3. Molar fractions of all pyrene species calculated from f_{Mfree}, f_{Mdiff} ($=1-f_{Mfree}$), f_{Ediff}^{E0}, f_{EE0}, f_{Ediff}^{D} and f_{ED}.

Sample	mol%	f_{diff}^{D}	f_{diff}^{E0}	f_{free}	f_{E0}	f_{D}	χ^2
CoE-PS-MPy $\tau_M = 257$ ns	1.5		0.84	0.09	0.07		1.24
	1.8		0.85	0.07	0.08		1.07
	3.2		0.84	0.02	0.14		1.02
	4.8		0.82	0.02	0.17		1.13
	5.1		0.88	0.01	0.11		1.12
	6.4		0.87	0.00	0.13		1.16
CoA-PS-MPy $\tau_M = 253$ ns	2.5	0.73	0.17	0.02	0.07	0.00	1.14
	3.7	0.45	0.48	0.01	0.00	0.05	1.00
	5.0	0.47	0.46	0.01	0.00	0.05	1.10
	5.2	0.44	0.49	0.01	0.00	0.06	1.02
	6.4	0.28	0.64	0.00	0.06	0.02	1.07
CoBuE-PS-BuPy $\tau_M = 200$ ns	2.1		0.89	0.07	0.00	0.04	1.11
	3.1		0.93	0.03	0.00	0.04	1.05
	4.5		0.95	0.01	0.00	0.04	1.16
	5.4		0.93	0.01	0.00	0.06	1.14
	6.0		0.94	0.00	0.04	0.02	1.07
PS-BuPy2 $\tau_M = 190$ ns	6.9		0.85	0.14	0.01		1.30
	4.6		0.88	0.11	0.01		1.02
	2.6		0.81	0.18	0.01		1.04
	1.6		0.54	0.46	0.00		1.14
PEO-MPy2 $\tau_M = 258$ ns	4.4		0.88	0.03	0.01	0.08	1.00
	1.8		0.91	0.07	0.02	0.01	1.33
	0.9		0.84	0.08	0.01	0.07	1.19
	0.6		0.41	0.55	0.01	0.03	1.22
PA-G1-BuPy$_2$	n.a.		0.92	0.05	0.03		1.12
PA-G2-BuPy$_4$		0.38	0.59	0.00	0.00	0.02	1.16
PP-G1-BuPy$_2$	n.a.		0.95	0.03	0.01	0.01	1.15
PP-G2-BuPy$_4$	n.a. n.a.		0.90	0.01	0.05	0.05	1.18
PP-G3-BuPy$_8$	n.a.		0.88	0.00	0.03	0.09	1.08
PP-G4-BuPy$_{16}$	n.a.		0.84	0.03	0.06	0.07	1.11
PP-G4-BuPy$_{16}$-Pure $\tau_M = 210$ ns			0.82	0.00	0.00	0.18	1.19

Table SI5.4. $\left(I_E/I_M\right)$ ratios determined from steady-state and time resolved fluorescence.

Sample	mol%	$\left(I_E/I_M\right)^{SS}$	$\left(I_E/I_M\right)^{SPC}$	$\left(I_E/I_M\right)^{SPC}_{fMfree=0}$	χ^2
CoE-PS-MPy $\tau_M = 257$ ns	1.5	1.37	0.36	0.39	1.24
	1.8	1.82	0.44	0.48	1.07
	3.2	3.59	0.85	0.81	1.02
	4.8	5.67	1.39	1.33	1.13
	5.1	6.55	1.42	1.34	1.12
	6.4	10.81	2.21	2.03	1.16
CoA-PS-MPy $\tau_M = 253$ ns	2.5	1.24	0.47	0.46	1.14
	3.7	2.08	0.61	0.60	1.00
	5.0	3.04	0.82	0.81	1.10
	5.2	3.28	0.88	0.85	1.02
	6.4	4.37	1.25	1.17	1.07
CoBuE-PS-BuPy $\tau_M = 200$ ns	2.1	0.71	0.37	0.39	1.11
	3.1	1.20	0.63	0.65	1.05
	4.5	2.26	1.10	1.09	1.16
	5.4	2.70	1.35	1.31	1.14
	6.0	3.19	1.53	1.46	1.07
PS-BuPy2 $\tau_M = 190$ ns	6.9	0.064	0.171	0.219	1.30
	4.6	0.049	0.129	0.154	1.02
	2.6	0.022	0.059	0.076	1.04
	1.6		0.029	0.058	1.14
PEO-MPy2 $\tau_M = 258$ ns	4.4	2.77	0.522	0.598	1.00
	1.8	0.69	0.134	0.152	1.33
	0.9	0.20	0.031	0.035	1.19
	0.6	0.10	0.014	0.035	1.22
PA-G1-BuPy$_2$	n.a.	3.33	1.17	1.49	1.12
PA-G2-BuPy$_4$		13.1	5.62	5.71	1.16
PP-G1-BuPy$_2$	n.a.	12.29	4.36	9.99	1.15
PP-G2-BuPy$_4$	n.a.	36.87	12.3	15.6	1.18
PP-G3-BuPy$_8$	n.a.	40.23	19.8	22.4	1.08
PP-G4-BuPy$_{16}$	n.a.	16.72	6.79	28.27	1.11
PP-G4-BuPy$_{16}$-Pure $\tau_M = 210$ ns	n.a.	101.83	25.7	23.1	1.19

Table SI5.5. Decay times and pre-exponential factors retrieved from the Birks Scheme analysis of the monomer decays of the pyrene end-labelled samples.

Sample	M_n kg/mol	τ_1 (ns)	A_{M1}	τ_2 (ns)	A_{M2}	τ_M (ns)	A_M	τ_s (ns)	A_{MS}	χ^2
PS-BuPy$_2$	3.0	45	0.067	116	0.801	190	0.132	3.5	0	1.22
	4.5	43	0.053	130	0.826	105	0.121	3.5	0	1.00
	8.0	45	0.020	154	0.799	190	0.181	3.5	0	1.04
	13.0	44	0.011	160	0.498	220	0.491	3.5	0	1.17
PEO-MPy$_2$	2.0	38	0.259	72	0.706	258	0.034	3.5	0.000	1.00
	5.0	42	0.020	146	0.663	258	0.058	3.5	0.073	1.23
	10.0	41	0.004	217	0.600	258	0.170	3.5	0.058	1.12
	16.5	40	0.002	215	0.247	258	0.465	3.5	0.078	1.22

Table SI5.6. Decay times and pre-exponential factors retrieved from the Birks Scheme analysis of the excimer decays of the pyrene end-labelled samples.

Sample	M_n kg/mol	τ_1 (ns)	A_{E1}	τ_2 (ns)	A_{E2}	τ_s (ns)	A_{ES}	χ^2
PS-BuPy$_2$	3.0	45	−0.546	116	0.576	3.5	0	1.22
	4.5	43	−0.465	130	0.493	3.5	0	1.00
	8.0	45	−0.404	154	0.435	3.5	0	1.04
	13.0	44	−0.386	160	0.428	3.5	0	1.17
PEO-MPy$_2$	2.0	38	−0.892	72	0.914	3.5	0.055	1.00
	5.0	42	−0.448	146	0.490	3.5	0.042	1.23
	10.0	41	−0.058	217	0.084	3.5	0.121	1.12
	16.5	40	−0.072	215	0.107	3.5	0.126	1.22

Table SI5.7. Kinetic parameters retrieved from the Birks' scheme analysis of the fluorescence decays acquired with the pyrene end-labelled samples.

Sample	M_n kg/mol	k_{cy} (10^6 s^{-1})	k_{-cy} (10^6 s^{-1})	τ_{E0} (ns)
PS-BuPy$_2$	3.0	4.4	3.0	55
	4.5	3.4	4.1	55
	8.0	1.6	3.6	55
	13.0	1.4	4.3	55
PEO-MPy$_2$	2.0	13.5	2.3	48
	5.0	3.4	2.3	48
	10.0	0.9	3.1	48
	16.5	1.0	3.8	48

Table SI5.8. Parameters retrieved from the FBM analysis of the monomer decays of the randomly labelled polystyrenes in THF.

Sample	Mol% Py	k_{blob} (μs^{-1})	$<n>$	$k_e[blob]$ (μs^{-1})	f_{Mdiff}	k_2 (ns^{-1})	f_{Mk2}	τ_M (ns)	f_{Mfree}	χ^2
	1.5	11.8	1.1	4.7	0.72	0.13	0.17	257	0.12	1.30
	1.8	10.8	1.2	3.8	0.75	0.13	0.19	257	0.06	1.13
CoEt-PS-MPy	3.2	10.4	1.8	4.7	0.70	0.13	0.27	257	0.03	1.00
	4.8	10.6	2.6	3.2	0.56	0.13	0.42	257	0.02	1.19
	5.1	10.0	2.8	4.2	0.59	0.13	0.40	257	0.01	1.15
	6.4	8.8	3.9	3.5	0.47	0.13	0.52	257	0.00	1.16
	2.1	9.4	1.1	5.2	0.78	0.12	0.14	200	0.08	1.15
	3.1	10.0	1.5	5.1	0.76	0.12	0.21	200	0.03	1.06
CoEs-PS-BuPy	4.5	9.8	2.2	5.5	0.68	0.12	0.31	200	0.01	1.18
	5.4	10.5	2.4	7.2	0.64	0.12	0.35	200	0.01	1.17
	6.0	9.6	2.9	5.4	0.61	0.12	0.39	200	0.00	1.06
	2.5	7.6	1.4	5.7	0.82	0.13	0.15	253	0.03	1.13
	3.7	6.8	2.0	4.8	0.79	0.13	0.20	253	0.01	1.02
CoAm-PS-MPy	5.0	6.5	2.7	5.0	0.74	0.13	0.25	253	0.01	1.12
	5.2	6.4	2.8	4.6	0.73	0.13	0.26	253	0.01	1.04
	6.4	6.1	3.7	4.6	0.67	0.13	0.33	253	0.00	1.07

Table SI5.9. Parameters retrieved from the FBM analysis of the excimer decays of the randomly labelled polystyrenes in THF.

Sample	Mol% Py	f_{Ediff}	k_2 (ns^{-1})	f_{Ek2}	τ_{E0} (ns)	f_{EE0}	τ_{EL} (ns)	f_{EEL}	χ^2
	1.5	0.77	0.13	0.18	56	0.05	na	na	1.30
	1.8	0.74	0.13	0.19	57	0.07	na	na	1.13
CoEt-PS-MPy	3.2	0.66	0.13	0.26	52	0.08	na	na	1.00
	4.8	0.50	0.13	0.38	53	0.12	na	na	1.19
	5.1	0.52	0.13	0.36	50	0.11	na	na	1.15
	6.4	0.41	0.13	0.45	50	0.14	na	na	1.16
	2.1	0.82	0.12	0.15	54	0.00	94	0.03	1.15
	3.1	0.76	0.12	0.21	55	0.00	92	0.03	1.06
CoEs-PS-BuPy	4.5	0.66	0.12	0.30	54	0.01	77	0.04	1.18
	5.4	0.61	0.12	0.33	52	0.00	77	0.06	1.17
	6.0	0.57	0.12	0.37	53	0.01	77	0.05	1.06
	2.5	0.78	0.13	0.15	52	0.00	92	0.07	1.13
	3.7	0.76	0.13	0.19	52	0.00	107	0.05	1.02
CoAm-PS-MPy	5.0	0.70	0.13	0.24	50	0.00	100	0.06	1.12
	5.2	0.68	0.13	0.25	50	0.00	100	0.07	1.04

	6.4	0.62	0.13	0.30	48	0.00	89	0.08	1.07

Table SI5.10. Overall fractions of pyrene species obtained from the FBM analysis of the monomer and excimer decays for the randomly labelled polystyrenes in THF.

Sample	Mol% Py	f_{diff}	f_{free}	f_{k2}	f_{E0}	f_D
CoEt-PS-MPy	1.5	0.69	0.11	0.16	0.04	0.00
	1.8	0.70	0.06	0.18	0.07	0.00
	3.2	0.65	0.03	0.25	0.08	0.00
	4.8	0.49	0.02	0.37	0.12	0.00
	5.1	0.52	0.01	0.36	0.11	0.00
	6.4	0.69	0.01	0.16	0.04	0.00
CoEs-PS-BuPy	2.1	0.75	0.08	0.14	0.00	0.03
	3.1	0.73	0.03	0.21	0.00	0.03
	4.5	0.65	0.01	0.30	0.01	0.04
	5.4	0.60	0.01	0.33	0.00	0.06
	6.0	0.57	0.00	0.37	0.01	0.05
CoAm-PS-MPy	2.5	0.76	0.02	0.14	0.00	0.07
	3.7	0.75	0.01	0.19	0.00	0.05
	5.0	0.69	0.01	0.24	0.00	0.06
	5.2	0.67	0.01	0.24	0.00	0.07
	6.4	0.62	0.00	0.30	0.00	0.08